

Efficient probabilistic analysis of offshore wind turbines based on time-domain simulations

Von der Fakultät für Bauingenieurwesen und Geodäsie
der Gottfried Wilhelm Leibniz Universität Hannover
zur Erlangung des Grades

DOKTOR-INGENIEUR

- Dr.-Ing. -

genehmigte Dissertation
von

Clemens Janek Hübler M. Sc.

2019

Hauptreferent: Prof. Dr.-Ing. habil. Raimund Rolfes,
Leibniz Universität Hannover
Korreferent: Prof. John Dalsgaard Sørensen, M.Sc., Lic.techn., B.Com.
Aalborg University
Tag der mündlichen Prüfung: 11. Januar 2019

Abstract

Offshore wind energy plays an important role in the successful implementation of the energy transition. However, without subsidies, it is not yet sufficiently competitive compared to other renewables or conventional fossil fuels. This is why offshore wind turbines have to be structurally optimised with regard to economic efficiency. One possibility to significantly increase economic efficiency is to improve the reliability or at least to assess present reliability levels precisely. For an accurate reliability assessment during the design phase, probabilistic analyses based on time-domain simulations have to be conducted. In this thesis, a methodology for a comprehensive probabilistic design of offshore wind turbines with special focus on their substructures is developed and applied. All investigations are based on time-domain simulations. This leads to more accurate results compared to semi-analytical approaches that are commonly used for probabilistic modelling at the expense of higher computing times.

In contrast to previous probabilistic analyses, considering only particular aspects of the probabilistic design, this work defines a comprehensive analysis that can be split up into the following seven aspects: deterministic load model, resistance model (failure modes), uncertainty of inputs, design of experiments, sensitivity analysis, long-term extrapolation/lifetime distribution, and economic effects.

For five of these aspects, scientific innovations are realised, while state-of-the-art approaches are applied for the last two aspects. First, a method is developed in order to efficiently consider soil effects in offshore wind turbine simulations. This method is integrated in a state-of-the-art model for offshore wind turbines to enhance it by considering soil characteristics. At the same time, the number of degrees of freedom is kept constant. Second, the uncertainty of the most important inputs, i.e. environmental conditions, is determined. Theoretical statistical distributions of environmental conditions - like wind speeds - are derived using real offshore measurement data. State-of-the-art approaches are improved by using more sophisticated distributions. This enables a better agreement of theoretical and empirical distributions. Moreover, a variety of environmental conditions - having been neglected so far - is taken into account. Although there is some inherent uncertainty for every input, this uncertainty influences relevant outputs (e.g. reliability) only in some cases. Therefore, third, global sensitivity analyses are applied to determine significant inputs. All other inputs are set to deterministic values to reduce computing times. Especially for non-linear systems, the developed approach is more accurate than commonly used sensitivity analyses in the field of wind energy. Since - due to computational limitations - it is not possible to simulate the entire lifetime of an offshore wind turbine, long-term extrapolations have to be applied. These extrapolations increase the uncertainty of lifetime estimations. If probabilistic inputs are used, this effect is even intensified. Hence, several improved sampling techniques are developed. They enable a significant reduction of the extrapolation-based lifetime uncertainty compared to classic approaches. Finally, the effect of variable, distributed lifetimes on the economic profitability of wind farm projects is investigated. In contrast to state-of-the-art investigations, economic aspects are not included in the engineering model, but independent

economic and engineering models are combined. This enables high-quality results in both disciplines.

Using the methodology for comprehensive probabilistic designs that is developed here, it is demonstrated that probabilistic analyses of wind turbines using time-domain simulations are possible. For this purpose, it is necessary to reduce computing times by applying adequate sensitivity analyses and extrapolation techniques. These approaches are developed in this thesis. Moreover, based on present findings, well-founded recommendations for efficient and realistic probabilistic simulations of offshore wind turbines are given. Finally, since the profitability of wind turbines depends significantly on the service life and lifetimes scatter substantially, deterministic approaches cannot be economically optimised. Hence, probabilistic analyses are valuable.

Keywords: Offshore wind energy; probabilistic analysis; uncertainty; fatigue

Kurzfassung

Für die erfolgreiche Verwirklichung der Energiewende spielt die Offshore-Windenergie eine entscheidende Rolle. Allerdings ist sie ohne Subventionen noch immer kaum konkurrenzfähig gegenüber anderen erneuerbaren Energien oder fossilen Energieträgern. Daher ist eine strukturdynamische Optimierung von Offshore-Windkraftanlagen hinsichtlich ihrer Wirtschaftlichkeit unumgänglich. Eine Möglichkeit, die Wirtschaftlichkeit signifikant zu steigern, ist die Verbesserung oder zumindest genaue Kenntnis der Zuverlässigkeit von Windkraftanlagen. Um Zuverlässigkeiten bereits in der Entwurfsphase präzise zu bestimmen, müssen probabilistische Analysen, die auf Simulationen im Zeitbereich basieren, durchgeführt werden. Die Entwicklung einer umfassenden Methodik für den probabilistischen Entwurf von Offshore-Windkraftanlagen mit dem Fokus auf der Substruktur und deren Anwendung ist der Kern dieser Arbeit. Hierbei ist insbesondere hervorzuheben, dass alle Untersuchungen auf Simulationen im Zeitbereich basieren. Dies erhöht im Vergleich zu den in der Probabilistik oft verwendeten semi-analytischen Ansätzen die Genauigkeit, wobei auch die Rechenzeiten ansteigen.

Im Gegensatz zu bisherigen probabilistischen Ansätzen, die zumeist nur bestimmte Teilaspekte des probabilistischen Entwurfs berücksichtigen, wird hier eine umfassende probabilistische Analyse definiert, die aus den folgenden sieben Teilaspekten besteht: Deterministisches Lastmodell, Widerstandsmodellierung (Fehlermöglichkeiten), Unschärfe in Eingangsgrößen, numerische Versuchsplanung, Sensitivitätsanalyse, Langzeitextrapolation/Lebensdauerverteilung und wirtschaftliche Aspekte.

Wissenschaftliche Neuerungen werden bei fünf der zuvor genannten Punkten erzielt. Für die anderen beiden Teilaspekte werden Ansätze nach dem Stand der Forschung verwendet. Zunächst wird eine effiziente Methode zur Berücksichtigung von Bodeneigenschaften entwickelt. Diese Methode wird in eine Offshore-Windkraftanlagenmodellierung nach dem Stand der Technik eingebunden, um diese hinsichtlich der Berücksichtigung von Bodeneigenschaften zu erweitern. Gleichzeitig wird die Anzahl der Freiheitsgrade nicht erhöht. Der zweite Schritt behandelt die Unschärfe der wichtigsten Eingangsgrößen, der Umgebungsbedingungen. Hierzu werden reale Offshore-Messdaten verwendet, um theoretische Verteilungsfunktionen für Einwirkungsparameter wie Windgeschwindigkeiten abzuleiten. Im Vergleich zu bestehenden Ansätzen werden durch komplexere Verteilungsfunktionen verbesserte Übereinstimmungen mit den empirischen Verteilungen erzielt. Außerdem wird eine Vielzahl von bisher vernachlässigten Umgebungsbedingungen untersucht. Obwohl jede Größe eine gewisse inhärente Unschärfe aufweist, hat die Unschärfe nur in einigen Fällen einen Einfluss auf die relevanten Ergebnisse (z. B. die Zuverlässigkeit). Daher beschäftigt sich der dritte Schritt mit der Entwicklung globaler Sensitivitätsverfahren zur Bestimmung jener Eingangsgrößen, deren Unschärfe relevant ist. Alle anderen Eingangsgrößen können deterministisch behandelt werden, um Rechenzeit zu sparen. Das entwickelte Verfahren zeichnet sich im Vergleich zu in der Windenergie üblichen Ansätzen durch eine hohe Genauigkeit in Bezug auf nichtlineares Systemverhalten aus. Für Windkraftanlagen ist die Langzeitextrapolation von besonderer

Bedeutung, da die Simulation der gesamten Lebensdauer mit heutiger Rechenleistung nicht annähernd möglich ist. Diese Extrapolation stellt eine mögliche Fehlerquelle dar und erhöht die Unschärfe der Lebensdauerberechnung. Da diese Problematik durch die Verwendung von probabilistischen Eingangsgrößen verstärkt wird, werden im vierten Schritt verbesserte Stichprobenverfahren entwickelt. Diese Verfahren sind in der Lage die extrapolationsbedingte Unsicherheit der Lebensdauervorhersage im Vergleich zu klassischen Verfahren deutlich zu reduzieren. Im abschließenden Schritt wird der Einfluss einer nicht konstanten (verteilten) Lebensdauer auf die wirtschaftliche Profitabilität von Windparkprojekten untersucht. Im Gegensatz zu Untersuchungen nach dem Stand der Forschung werden hierfür nicht nur wirtschaftliche Aspekte im Ingenieurmodell berücksichtigt, sondern eigenständige ökonomische und Ingenieurmodelle kombiniert. Dies ermöglicht qualitativ hochwertige Ergebnisse in beiden Bereichen.

Mit Hilfe der hier entwickelten umfassenden Methodik kann gezeigt werden, dass probabilistische Analysen von Windkraftanlagen mit Simulationen im Zeitbereich realisierbar sind. Hierzu müssen Rechenzeiten durch den Einsatz geeigneter Sensitivitäts- und Extrapolationsverfahren verkürzt werden. Entsprechende Verfahren wurden im Rahmen dieser Arbeit entwickelt. Außerdem werden auf Basis der gewonnenen Erkenntnisse Empfehlungen für effiziente und realitätsnahe probabilistische Simulationen von Offshore-Windkraftanlagen gegeben. Abschließend wird die Notwendigkeit von probabilistischen Analysen deutlich, da Lebensdauern hohe Streuungen aufweisen und die Profitabilität von Windkraftanlagen signifikant von der Gesamtlaufzeit abhängt. Somit sind deterministische Betrachtungen wirtschaftlich gesehen nicht optimal.

Schlagworte: Offshore-Windenergie; probabilistische Analyse; Unschärfe; Ermüdung

Contents

List of Figures	III
List of Tables	V
List of Papers	VII
Notation	IX
1 Introduction	1
1.1 Motivation	1
1.2 State of the art	4
1.2.1 Reliability assessment	4
1.2.2 Probabilistic analysis of offshore wind turbines	11
1.2.3 Deterministic modelling of offshore wind turbines	15
1.2.4 Resistance models and failure modes	19
1.2.5 Uncertainty in input parameters	20
1.2.6 Design of probabilistic experiments	22
1.2.7 Sensitivity analysis	24
1.2.8 Long-term extrapolation	27
1.2.9 Economic effects	31
1.3 Research gap and objectives	32
1.3.1 Research gap	32
1.3.2 Objectives	32
1.4 Outline and connection of publications	33
1.4.1 Outline	33
1.4.2 Connection of publications	34
2 Deterministic model design	37
2.1 Research context	37
2.2 Methods	37
2.3 Results	38
2.4 Outlook	38
2.5 Paper A	39
3 Aleatory uncertainty of input parameters	61
3.1 Research context	61
3.2 Methods	62
3.3 Results	62

3.4	Outlook	63
3.5	Paper B	63
4	Sensitivity analysis	79
4.1	Research context	79
4.2	Methods	79
4.3	Results	80
4.4	Outlook	80
4.5	Paper C	81
5	Long-term extrapolation	97
5.1	Methodologies for fatigue assessment of offshore wind turbines	97
5.1.1	Research context	97
5.1.2	Methods	98
5.1.3	Results	99
5.1.4	Outlook	99
5.1.5	Paper D	99
5.2	Validation of improved sampling concepts for fatigue design	114
5.2.1	Research context	114
5.2.2	Methods	114
5.2.3	Results	114
5.2.4	Outlook	115
5.2.5	Paper E	115
6	Economic effects	137
6.1	Research context	137
6.2	Methods	137
6.3	Results	138
6.4	Outlook	138
6.5	Paper F	139
7	Summary and outlook	161
7.1	Summary	161
7.2	Limitations and outlook	162
	Bibliography	165

List of Figures

1-1	Annual installed wind power in the European Union in GW with onshore and offshore percentages according to the wind report 2017 by the European Academy of Wind Energy (EAWWE) [52].	2
1-2	Weighted average levelised costs of electricity in $\frac{\text{€}}{\text{kWh}}$ for different types of energy in 2016 according to the International Renewable Energy Agency (IRENA) [82].	2
1-3	Illustration of generic failure probabilities with assumed independence of statistically distributed effects and resistances.	5
1-4	Illustration of a generic deterministic design using a safety factor approach (cf. “Level 1 reliability methods: semi-probabilistic methods” in Section 1.2.1). Deterministic values are marked with k , design values with d	6
1-5	Various methods with increasing levels of complexity and growing computational costs (level 1 to level 4) that can be used to determine or ensure the reliability of a structure (following Madsen et al. [110]). FORM and SORM stands for first- and second-order reliability methods, respectively, and MCS for a Monte Carlo simulation. $\boldsymbol{\mu}$ and $\boldsymbol{\sigma}$ are the mean and standard deviation vector of all inputs.	7
1-6	Visualisation of probabilistic structural analyses. Distributions of (physical) inputs ($p(\mathbf{x})$) and disturbance variables ($p(\mathbf{e})$, not taken into account in this thesis, cf. Section 1.2.5) are used to evaluate the deterministic “black box” model N times. The uncertainty proceeds through the model and yields distributions of outputs ($p(\mathbf{y})$).	12
1-7	Probabilistic modelling schemes.	15
1-8	Illustration of various soil models for a monopile foundation. The complexity of the soil model and the number of DoF increase from the left (clamped structure) to the right (FE model). From left to right: clamped structure, apparent fixity length, soil matrix, distributed springs, FE model.	18
1-9	Generic examples to illustrate the procedure (e.g. systematic or random) and performance (e.g. space filling) of various sampling concepts: (a) systematic sampling, full factorial design (b) standard MCS with clusters due to limited sampling (c) LHS for a better resolution of the data space (d) quasi-random sampling using Sobol’ sequence (e) importance sampling for more samples in relevant regions of the data space (f) mass function that is used for the importance sampling (i.e. more samples for high values of the mass function)	24
1-10	Flowchart presenting the short-term damage calculation procedure based on strain measurements or simulated strains according to Hübler et al. [78] (FA: fore-aft, StS: side-to-side).	27

1-11 Generic, exemplary time series that illustrates the picked maxima of various peak extraction methods: (a) taking the global maximum of the time series (b) subdividing the time series in blocks and using the maximum of each block (c) extracting all peaks above a given threshold.	30
---	----

List of Tables

1-1 Reliability classes (RC) according to Eurocode 0 [43]. 7

List of Papers

A	HÜBLER, C., HÄFELE, J., GEBHARDT, C. G., AND ROLFES, R. Experimentally supported consideration of operating point dependent soil properties in coupled dynamics of offshore wind turbines. <i>Marine Structures</i> 57 (2018), 18-37.	40
B	HÜBLER, C., GEBHARDT, C. G., AND ROLFES, R. Development of a comprehensive database of scattering environmental conditions and simulation constraints for offshore wind turbines. <i>Wind Energy Science</i> 2(2) (2017), 491-505.	64
C	HÜBLER, C., GEBHARDT, C. G., AND ROLFES, R. Hierarchical four-step global sensitivity analysis of offshore wind turbines based on aeroelastic time domain simulations. <i>Renewable Energy</i> 111 (2017), 878-891. . . .	82
D	HÜBLER, C., GEBHARDT, C. G., AND ROLFES, R. Methodologies for fatigue assessment of offshore wind turbines considering scattering environmental conditions and the uncertainty due to finite sampling. <i>Wind Energy</i> 21(11) (2018), 1092-1105.	100
E	HÜBLER, C., WEIJTJENS, W., GEBHARDT, C. G., ROLFES, R., AND DEVRIENDT, C. Validation of improved sampling concepts for offshore wind turbine fatigue design. <i>Energies</i> 12(4), (2019), 603.	116
F	HÜBLER, C., PIEL, J.-H., STETTER, C., GEBHARDT, C. G., BREITNER, M. H., AND ROLFES, R. Influence of Structural Design Variations on Economic Viability of Offshore Wind Turbines: an Interdisciplinary Analysis. <i>Renewable Energy</i> , under review (minor revision).	140

Notation

Latin symbols

Symbol	Unit	Name
C	N s	Damping matrix
<i>D</i>	1	Damage
e	1	Vector of disturbance variables
<i>e</i>	1	Disturbance variable
<i>E</i>	1 / N mm ⁻²	Effect or expected value or Young's modulus
<i>f</i>	1	Model function
F	N	External force vector
<i>g</i>	1	Limit state function
I	1	Identity matrix
<i>I</i>	1	Number of stress amplitudes
K	N m ⁻¹	Stiffness matrix
M	kg	Mass matrix
<i>M</i>	1	Number of iterations
<i>n</i>	1	Number of cycles
<i>N</i>	1	Number of inputs/model evaluations or endurance limit
<i>p</i>	1	Probability density function
<i>P_f</i>	1	Failure probability
<i>R</i>	1	Resistance
<i>S</i>	1 / m ³	Sensitivity index or section modulus
<i>SF</i>	1	Safety factor
u	m	Displacement vector
<i>V</i>	1	Variance
x	1	Vector of physical inputs
<i>x</i>	1	Physical input
y	1	Output vector
<i>y</i>	1	Output
<i>z</i>	m	Height

Greek symbols

Symbol	Unit	Name
γ	1	Partial safety factor
Δ	1	Variation or amplitude
ϵ	1	Strain
μ	1	Mean vector of inputs
μ	1	Mean of an input
σ	1	Standard deviation vector of inputs
σ	Nmm ⁻²	Stress
Φ	1	Mode (shape) matrix

Indices

Symbol	Name
<i>cor</i>	Corrected
<i>d</i>	Design
<i>f</i>	Load
<i>i</i>	General index
<i>j</i>	Second general index
<i>k</i>	Characteristic
<i>L</i>	Fixed-interface
<i>m</i>	Material/resistance
<i>n</i>	Consequence
<i>OAT</i>	One-at-a-time
<i>R</i>	Constraint
<i>T</i>	Total

Abbreviations

Abbreviation	Name
ACER	Average conditional exceedance rate
AIC	Akaike information criterion
API	American Petrol Institute
APV	Adjusted present value
BIC	Bayesian information criterion
BSH	Bundesamt für Schifffahrt und Hydrographie
CAPEX	Capital expenditures
CDF	Cumulative density function
DLC	Design load case
DMCS	Damage distribution based Monte Carlo simulation
DNV	Det Norske Veritas
DNV GL	Det Norske Veritas and Germanischer Lloyd
DOE	Design of (probabilistic) experiments
DoF	Degree of freedom
DOWEC	Dutch offshore wind energy converter
EAWC	European Academy of Wind Energy
EC	Environmental condition

EU	E uropean U nion
FA	F ore- a ft
FAST	F atigue, a erodynamics, s tructures, and t urbulence
FE	F inite e lement
FINO	F orschungsplattformen i n N ord- und O stsee
FLS	F atigue l imit s tate
FORM	F irst- o rd(er) r eliability m ethod
FOSM	F irst- o rd(er) s econd m oment
GL	G ermanischer L loyd
HAWC2	H orizontal a xis w ind turbine c ode 2 nd generation
IEC	I nternational E lectrotechnical C ommission
IRENA	I nternational R enewable E nergy A gency
IS	I mportance s ampling
ISO	I nternational O rganization for S tandardization
ISOA	I ncomplete s econd- o rd(er) a pproach
IWES	I nstitut für W indenergie und E nergiesystemtechnik
JCSS	J oint C ommittee of S tructural S afety
KS	K olmogorov- S mirnov
LASSO	L east a bsolute s hrinkage and s election o perator
LHS	L atin h ypercube s ampling
MBS	M ulti- b ody s ystem
MCS	M onte C arlo s imulation
MLE	M aximum l ikelihood e stimation
MSE	(l east) M ean s quare e rror
MSL	M ean s ea l evel
NESS	N orth E uropean S torm S tudy
OAT	O ne- a t- a - t ime
OC3	O ffshore C ode C omparison C ollaborative
OC4	O ffshore C ode C omparison C ollaborative C ontinuation
OWI-lab	O ffshore W ind I nfrasturcture A pplication L ab
OWT	O ffshore w ind turbine
PDF	P robability d ensity f unction
POT	P eak- o ver- t hreshold
PRA	P robabilistic r isk a ssessment
PSA-OWT	P robabilistic s afety a ssessment of o ffshore w ind turbines
RBMCS	R educed b in M onte C arlo s imulation
RC	R eliability c lass
SA	S ensitivity a nalysis
SCF	S tress c oncentration f actor
SIS	S tochastic i mportance s ampling
SORM	S econd- o rd(er) r eliability m ethod
SOTM	S econd- o rd(er) t hird m oment
StS	S ide- t o- s ide
TTH	T estzentrum T ragstrukturen H annover
ULS	U ltimate l imit s tate
US	U nited S tates of A merica

1 Introduction

The present thesis is motivated by the need of innovation and progress in the field of offshore wind energy. Additional developments are required to turn offshore wind energy into a seminal technology in order to achieve the goals set for the deployment of renewable energies. In this context, the reliability of offshore wind turbines (OWTs) is an essential factor for cost reductions and safety reasons. To assess and optimise the reliability of OWTs, probabilistic analyses for the design¹ are required. However, till now, probabilistic analyses of OWTs are rare, time-consuming, and based on highly simplified models. This research gap is addressed by the present thesis.

This first chapter starts with a short general motivation, followed by an introduction to the state of the art. Subsequently, the research gap is mapped out and objectives of this thesis are specified. Lastly, the outline of this thesis is given and the interconnection of the included publications is illustrated.

1.1 Motivation

The significance of renewable energies for the global energy production with regard to a reduction of greenhouse gas emissions and a sustainable utilisation of resources increases continuously. In Germany, this importance is even more pronounced due to the nuclear phase-out after the catastrophe in Fukushima in March 2011 in addition to the energy transition in general. The German government aims at reducing greenhouse gas emissions by at least 55 % below 1990 levels by 2030 and by at least 80 % by 2050 [153]. Furthermore, the share of renewable energy in final energy consumption shall be at least 30 % by 2030 and 60 % in 2050 [153]. Wind energy is a pillar for the achievement of these goals, as it already accounts for a major proportion of the energy in gross power generation with more than 12 % overall and about 40 % of the renewable energy gross power generation in Germany [56]. Furthermore, annual growth rates are still about 10 % in Germany [150] and the European Union (EU) [52]. Figure 1-1 illustrates the ongoing growth of wind energy.

Offshore wind energy has several advantages compared to onshore wind energy, e.g. higher power outputs, steadier and less turbulent wind conditions, and less challenges regarding public acceptance. Nevertheless, the share of offshore wind energy is still quite low with about 2 % of the total gross power generation in Germany and the European Union [52, 150]. The offshore wind energy market is massively growing as shown in Fig. 1-1. In 2017, 20 % of wind power installations in the EU were offshore [52]. The main reason for the small overall share are significantly higher levelised costs of electricity for offshore wind energy with about $0.15 \frac{\text{€}}{\text{kWh}}$ compared to $0.065 \frac{\text{€}}{\text{kWh}}$ for onshore wind energy [82]. This is displayed in Fig. 1-2. Hence, although the first bids for subsidy-free wind farm projects have been

¹In this thesis, probabilistic analyses are always used for design purposes. However, it is not limited to probabilistic design but deals with probabilistic analyses in general. Most probabilistic methods covered here are application-independent and not design-specific.

made recently, the reduction of costs is essential. These bids are at least partly a “bet on the future”, on technological improvements of the next years. Therefore, reductions have to be realised to fasten up the expansion of offshore wind energy and to include it into the process of energy transition.

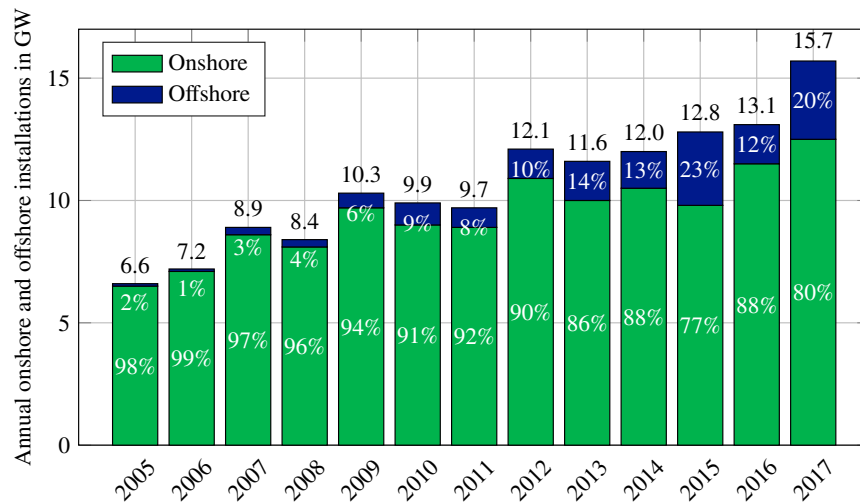


Figure 1-1: Annual installed wind power in the European Union in GW with onshore and offshore percentages according to the wind report 2017 by the European Academy of Wind Energy (EAWWE) [52].

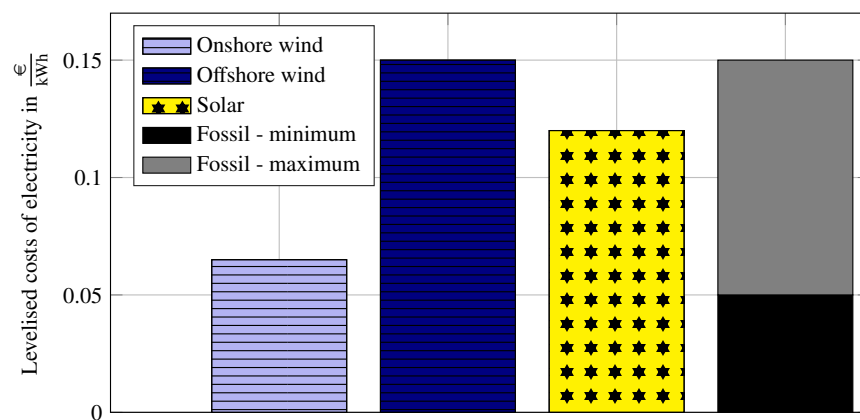


Figure 1-2: Weighted average levelised costs of electricity in $\frac{\text{€}}{\text{kWh}}$ for different types of energy in 2016 according to the International Renewable Energy Agency (IRENA) [82].

In contrast to onshore wind turbines, substructures and foundations of OWTs account for a significant part of their overall costs [121]. Therefore, new concepts, like floating substructures for greater water depths, are under development. Nevertheless, today, nearly all new installed substructures are monopiles (nearly 90%) or jackets (about 10%) [71]. Improvements and structural optimisations of these types of substructures with respect to costs will be expedient - at least for the next decade - to substantially decrease overall costs of offshore wind energy.

For these optimisations, it is indispensable to accurately model the dynamic behaviour, environmental conditions (ECs), reliability, etc. There are several standards and guidelines that define how OWTs and their substructures should be designed and modelled² [37, 53, 84].

Offshore wind turbines have to be designed with a certain reliability level specified in current standards [37, 84]. The topic of reliability is of further interest for OWTs. As OWTs are unmanned structures with no residents in the closer surroundings, reliability is more an economic than a safety aspect. Hence, costs of offshore wind energy can be decreased significantly, if the required reliability is regarded as an economic variable instead of a fixed value, as stated in current standards. However, this is not a straightforward task. First, this approach needs coupled techno-economic models that are not yet available. Second, probabilistic models are needed, as all inputs - like environmental conditions or material parameters - are uncertain. Nevertheless, it is state of the art to model wind turbines using deterministic time-domain approaches and to consider safety factors to ensure a certain reliability or to use simplified, less accurate semi-analytical probabilistic approaches.

As a consequence, several aspects regarding the improvement of OWT designs by means of probabilistic analyses are evident. Four of them are the key topics of this thesis.

First, an adequate modelling of wind turbines meeting all requirements of current standards is needed. On the one hand, this model has to represent the turbine behaviour accurately, since only a high accuracy justifies the higher computational costs compared to state-of-the-art semi-analytical models. On the other hand, computing times have to be still manageable, since probabilistic analyses demand a significant amount of model evaluations. In this work, an existing simulation code is enhanced by an effective soil model³ to meet these requirements (cf. Section 2). This enhancement enables more accurate modelling of the dynamic behaviour compared to common approaches that neglect soil-structure interaction [145, 209, 220]. Other improvements of state-of-the-art codes that might be necessary for the next generation of wind turbines with growing dimensions, for example, geometric or material non-linearities, are not considered in this work.

Second, the uncertainty of all significant parameters⁴ has to be characterised. In this work, only physical (aleatory) uncertainties are considered. Other types of uncertainties - like model or statistical uncertainties (epistemic uncertainty) - are not taken into account (cf. Section 1.2.5). For all “important” inputs, underlying theoretical statistical distributions - representing the inherent, physical uncertainty - are determined. In some cases, literature values are utilised, whereas for other parameters, distributions⁵ are derived using available raw data (i.e. empirical distributions). Compared to previous research [15, 51, 68], more

²Information on coupled aero-hydro-servo-elastic OWT modelling in the time domain is given in Section 1.2.3.

³In this thesis, the term “soil model” is used quite broadly. It is neither limited to geotechnical models nor it is restricted to real soil-structure interaction with two-way coupling. Here, “soil model” comprises all methods that are somehow capable of modelling the connection of soil and structure by including soil characteristics in the structural turbine model.

⁴“Parameters” is used synonymously with “inputs” here. Examples are wind speeds, steel densities, the number of rotor blades, structural damping ratios, etc. This is consistent with the common use in structural engineering. This definition is given here, because in a probabilistic context, definitions do not agree (the term “parameter” denotes statistical parameters of distributions, e.g. the mean value, while inputs are called “variables”).

⁵The expression “distribution” refers to “theoretical statistical distribution functions” or distribution functions in general. If only empirical distribution functions are meant, this is stated explicitly.

sophisticated theoretical distributions are utilised (cf. Section 3) that lead to a more accurate representation of the real empirical distributions. Since computing times of probabilistic analyses can be decreased, if the number of probabilistic inputs is reduced, non-influential or non-significant parameters are set to deterministic values. To identify those inputs that are influential (i.e. the uncertainty of these parameters influences important outputs, for example, lifetimes or maximum stresses), global sensitivity analyses are applied. In this context, a new stepwise global sensitivity method is developed (cf. Section 4) that is characterised by a good compromise between accuracy and computing time.

Third, the development of a general methodology to determine lifetime distributions and accompanying economic effects within acceptable computing times and accuracy is required. Improved sampling concepts are developed (cf. Section 5.1) to reduce the number of required model evaluations for a well-founded fatigue lifetime estimation. In contrast to other improved sampling concepts [127, 185], not only simulation data is used for validation purposes, but the general validity is tested using measurement data (cf. Section 5.2).

And fourth, by applying this lifetime calculation scheme to OWTs and by combining it with a techno-economic model, economic effects of uncertain lifetimes of various substructure designs are assessed (cf. Section 6). This combined, interdisciplinary model is capable of evaluating the economic efficiency of wind turbine designs. This is a major improvement compared to state-of-the-art concepts that commonly optimise with respect to the structural weight or capital expenditures [62, 96, 105].

After all, the comprehensive probabilistic modelling presented in this thesis enables a significant progress in OWT reliability modelling. Unlike most probabilistic approaches [122, 175, 178, 191], here, all analyses are conducted in the time domain leading to more realistic results. Moreover, experimental and field measurement data is used frequently to validate concepts and to achieve more realistic results. For example, for the soil model (cf. Section 2), large-scale measurements are used, the theoretical statistical distributions in Section 3 are derived using offshore measurements of environmental conditions, and in Section 5.2, in situ strain measurements of offshore wind turbines are used for validation purposes.

1.2 State of the art

In this section, an overview of the state of the art in probabilistic modelling is given. While some sections focus on offshore wind turbines, most parts - especially definitions and methods - are generally valid for probabilistic modelling of structures. Since, the significance of probabilistic analyses is partly based on reliability assessments, the first part covers reliability aspects - based on semi-probabilistic and probabilistic approaches. On that basis, the concept of probabilistic analyses is presented and state-of-the-art approaches for OWTs are discussed. Furthermore, intermediate steps of a full probabilistic analysis are clarified. The following sections cover the state of the art of the various steps of a probabilistic analysis with respect to OWTs.

1.2.1 Reliability assessment

Probabilistic analyses are strongly related to reliability assessments. Therefore, before presenting the state of the art in probabilistic modelling of OWTs, this connection is described. At first, it has to be defined what is meant by reliability and reliability level.

Then, a clear distinction between reliability analysis and probabilistic analysis is given. Lastly, existing reliability methods are presented. For further reading it is referred to standard textbooks in structural reliability, e.g. Madsen et al. [110] or Melchers and Beck [116].

Definition: reliability

In general, the reliability of a system is defined as:

$$\text{reliability} = 1 - \text{probability of failure.} \quad (1.1)$$

In this context, the probability of failure (P_f) is the probability that loads or effects (E) are larger than the corresponding resistances (R):

$$P_f = \int \int p(g(E, R) < 0) dE dR. \quad (1.2)$$

Here, p is the probability density function (PDF) of the limit state function $g(E, R) = R - E$. Figure 1-3 illustrates generic probability density functions of effects and resistances.

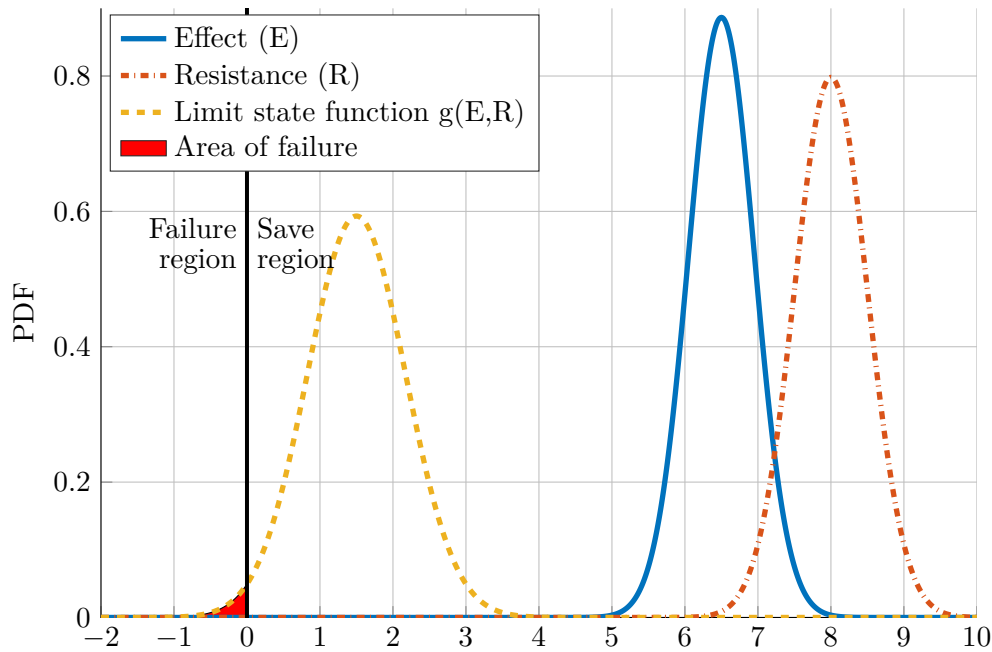


Figure 1-3: Illustration of generic failure probabilities with assumed independence of statistically distributed effects and resistances.

For deterministic inputs (see Fig. 1-4), this design practice would lead to failure probabilities of zero. However, in reality, structures do fail with a certain probability. The reason for this possible failure are all kinds of uncertainties. Examples for these uncertainties are physically stochastic inputs (e.g. material uncertainties), model or measurement uncertainties, or statistical uncertainties. For the different kinds of uncertainties, there are various classifications [12, 92, 116] that are presented in detail in Section 1.2.5. In this work,

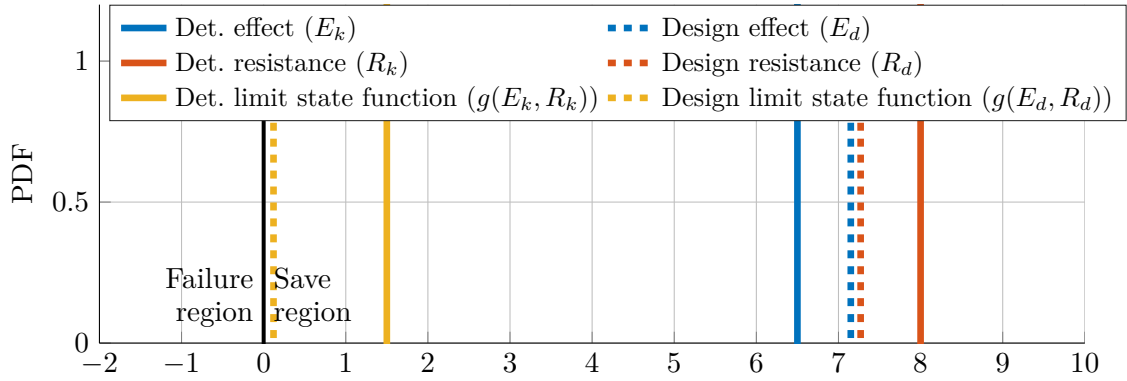


Figure 1-4: Illustration of a generic deterministic design using a safety factor approach (cf. “Level 1 reliability methods: semi-probabilistic methods” in Section 1.2.1). Deterministic values are marked with k , design values with d .

only physical (aleatory) uncertainty is taken into account. In any case, neither effects nor resistances are actually deterministic, but statistically distributed (cf. Fig. 1-3).

To incorporate the different types of uncertainties, several methods of reliability analysis - presented in the following subsections - are available. Frequently, four groups of methods are differentiated according to their complexity [43, 110, 116, 173]. This classification is illustrated in Fig. 1-5. However, there are also slightly different definitions. For example, the ISO standard (International Organization for Standardization) [86] defines in this context three so-called levels of verification: semi-probabilistic, reliability-based, and risk-informed.

In general, the topic of structural reliability is discussed in many basic textbooks [110, 116] and is addressed by several standards [43, 86, 92]. More specific for wind turbines, an overview of reliability methods applied to wind turbines is given, for example, by Jiang et al. [91]. All reliability analyses are used to fulfil a design criterion. This means that they are intended to guarantee that designed structures fail with a probability that is lower or equal to the desired maximum failure probability (reliability level). Hence, the initial challenge is the selection of an adequate reliability level.

Reliability level

The reliability level of a structure defines the desired maximal failure probability. For OWTs, the selection of a suitable reliability level, is an important but not straightforward topic. In the first place, reliability always has a safety aspect, as failing structures can endanger people and the environment. However, as OWTs are unmanned structures with no residents in the closer surroundings, this aspect is less relevant for OWTs. Besides, it is an economic factor, since neither frequently failing nor massively overdesigned structures are economically optimised. It is possible to determine an optimal target reliability by applying level 4 reliability analyses (cf. Fig. 1-5). In this case, advanced Monte Carlo simulation (MCS) considering economic effects is required. Since such analyses are complex and computationally expensive, commonly, a “suitable” target reliability is defined. For structures in general, this is done, for example, in Eurocode 0 [43] or in the Joint Committee of Structural Safety (JCSS) standard [92]. The value for the target reliability level depends on so-called “consequence classes” defining how risky a failure of this structure is concerning human

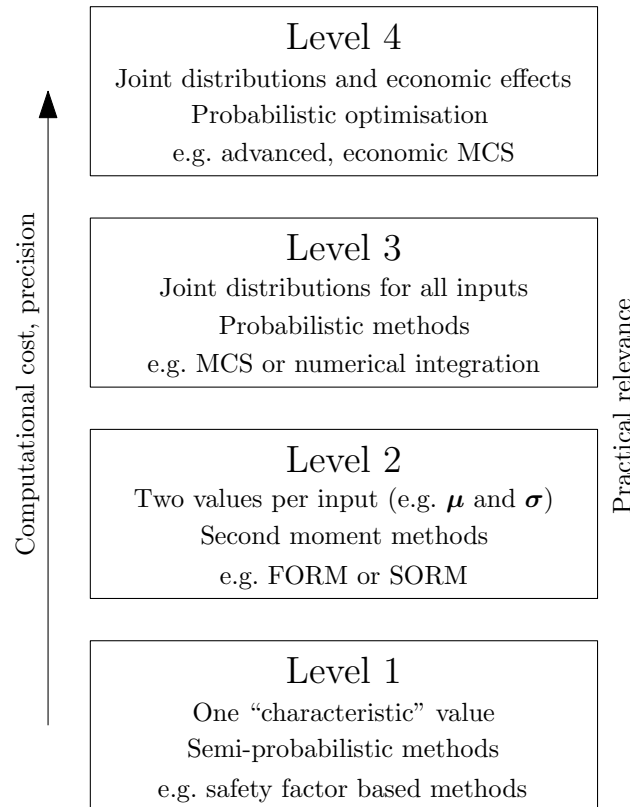


Figure 1-5: Various methods with increasing levels of complexity and growing computational costs (level 1 to level 4) that can be used to determine or ensure the reliability of a structure (following Madsen et al. [110]). FORM and SORM stands for first- and second-order reliability methods, respectively, and MCS for a Monte Carlo simulation. μ and σ are the mean and standard deviation vector of all inputs.

lives and economic consequences. Additionally, it can depend on the cost for increasing the reliability and on the reference period. The approach in Eurocode 0 [43] is summarised in Table 1-1.

Table 1-1: Reliability classes (RC) according to Eurocode 0 [43].

Reliability class	Maximal failure probability	
	Reference period 1 year	Reference period 50 years
RC 1	1.33×10^{-5}	4.83×10^{-4}
RC 2	1.30×10^{-6}	7.23×10^{-5}
RC 3	9.96×10^{-8}	8.54×10^{-6}

For OWTs, there has been a long debate which target reliability is appropriate and which reference period should be utilised [69]. Frequently, the same consequence classes as for onshore wind turbines were applied, although different boundary conditions apply. On the one hand, the accessibility of OWTs is limited leading to higher repair costs [201]. Therefore, a higher reliability level could be applied. On the other hand, OWTs are unmanned structures

with no residents close to them. Hence, the reliability of OWTs is mainly an economic aspect with less relevance for the public leading to lower target reliability levels [69, 204]. In the past, inconsistent values were applied. Det Norske Veritas [37] proposes an annual failure probability of 10^{-4} . This value is chosen by Muskulus and Schafhirt [131] for their probabilistic analyses as well. Sørensen and Toft [178] recommend significantly higher failure probabilities (i.e. lower safety levels) of 2×10^{-4} to 10^{-3} for one year. Tarp-Johansen [191] calibrates safety factors with an annual failure probability of about 2×10^{-4} . It becomes apparent that target failure probabilities were not consistent and varied between 10^{-4} to 10^{-3} . This changed with the new standards by Det Norske Veritas and Germanischer Lloyd (DNV GL) regarding support structures of wind turbines [40] and floating wind turbines [41]. Both recommend a nominal annual failure probability of 10^{-4} and a maximal annual failure probability 5×10^{-4} . This maximal annual failure probability is consistent with the recommendation in the draft version of the International Electrotechnical Commission (IEC) standard for onshore wind turbines [85]. Due to the fact that OWTs are unmanned structures, all proposed values indicate very low reliability classes (below RC 1). For manned OWTs, nominal annual failure probabilities are decreased to 10^{-5} [41].

Reliability assessment versus probabilistic analyses

Before presenting the state of the art in reliability analyses, a distinction between reliability analysis and probabilistic analysis is made.

Reliability analyses are objective-orientated. They are used to demonstrate that design criteria are fulfilled. Hence, the aim of such an analysis is to guarantee a failure probability equal or smaller than a desired reliability level. This can be done by various methods discussed in the following subsections. Most commonly, level 1 reliability methods (semi-probabilistic methods) are used [53, 84]. Level 1 reliability methods (see next subsection) do not consider uncertainties directly. Failure probabilities are not calculated, but deterministic inputs and safety factors are applied.

On the contrary, probabilistic analyses are more general procedures (method-orientated). Although they can be used for reliability assessments as well, their focus does not have to be the reliability itself. The general idea is to consider uncertainties directly using statistical distributions of input parameters. The statistical uncertainty proceeds through the model and leads to statistically distributed outputs like lifetime distributions. A more detailed description of probabilistic analyses follows in Section 1.2.2.

Level 1 reliability methods: semi-probabilistic methods

Semi-probabilistic reliability analyses (level 1) are still most commonly used and are recommended by current standards. Therefore, the derivation of partial safety factors based on these target reliabilities is briefly discussed. Partial safety factors aim at guaranteeing that failure probabilities are equal or lower than the target reliability. Therefore, the characteristic (deterministic) loads and resistances are multiplied with partial safety factors to increase loads (decrease resistances) and to get so-called design values. So, a conservative design on the safe side is achieved. For ultimate load design, this state-of-the-art method is illustrated by Eq. 1.3 and Fig. 1-4:

$$\gamma_n E_d = \gamma_n \gamma_f E_k \leq \frac{1}{\gamma_m} R_k = R_d \quad (1.3)$$

with E_d and E_k being design and characteristic loads, respectively and R being resistances with the same indices. γ represents partial safety factors for loads (f), resistances (m), and the consequence of failure of the specific component (n). Values for these safety factors are given in current standards [53, 83]. Different values for these factors are recommended for different types of analysis (ultimate, fatigue, etc.) and design situations (normal, abnormal, etc.). Neither the (calculation) basis nor the degree of conservatism of these factors is always known. To enable economic designs, safety factors have to be derived carefully for the specific structure and reliability level. This means that safety factors have to be adjusted accurately using probabilistic analyses, for example, level 3 or 4 reliability methods. The ISO standard [86] recommends to only use semi-probabilistic methods, if failure consequences, reliability classes, failure modes, and material properties can be fairly standardised, as in this case, safety factors can be sensibly adjusted using more advanced methods.

Level 2 reliability methods: second moment methods

Second moment methods (level 2) are the linking element between semi-probabilistic methods (level 1) and probabilistic methods (level 3; discussed in the next subsection). Together with level 3 methods, the ISO standard [86] defines them as reliability-based design procedures. While semi-probabilistic methods do not yield any information regarding the present failure probability and probabilistic methods can be very time-consuming, level 2 methods are a compromise between accuracy and efficiency. Overviews are given, for example, by Melchers and Beck [116] or Spaethe [182]. Two kinds of second moment methods can be distinguished: There are statistical moment-based methods - like the first-order second moment (FOSM) method - and first- or second-order reliability methods (FORM/SORM). In any case, second moment methods model uncertain parameters by using two values (i.e. the first ($\boldsymbol{\mu}$) and the second ($\boldsymbol{\sigma}^2$) statistical moment). Correlations can be taken into account by correlation coefficients, while the distributions of the parameters are assumed to be normal.

Methods based on statistical moments have the lowest computing times. The limit state function $g(R, E)$ is approximated by a Taylor series. Depending on the number of terms of the Taylor series that are kept and of statistical moments that are considered, different methods are available. For the FOSM method, only the linear term and the first two moments are used [29]. Hence, the limit state function (g) of the input vector (\mathbf{x}) is approximated at the mean vector ($\boldsymbol{\mu}$) of the N inputs:

$$g(\mathbf{x}) \approx g(\boldsymbol{\mu}) + \sum_{i=1}^N \frac{\partial g(\boldsymbol{\mu})}{\partial x_i} (x_i - \mu_i). \quad (1.4)$$

For the quadratic approximation of the Taylor series:

$$g(\mathbf{x}) \approx g(\boldsymbol{\mu}) + \sum_{i=1}^N \frac{\partial g(\boldsymbol{\mu})}{\partial x_i} (x_i - \mu_i) + \frac{1}{2} \sum_{i=1}^N \sum_{j=1}^N \frac{\partial^2 g(\boldsymbol{\mu})}{\partial x_i \partial x_j} (x_i - \mu_i)(x_j - \mu_j), \quad (1.5)$$

there are, for example, the second-order third moment⁶ (SOTM) approach [73] or special “incomplete second-order approaches” (ISOA) [102].

The reliability methods like FORM or SORM [50, 70, 146] pursue a similar concept of

⁶Although a third moment method is strictly speaking not a level 2 reliability method, as three values per input are used, normally, third moment methods are still counted as level 2 methods.

approximating the limit state function with a Taylor series. However, contrary to moment-based methods, not the mean value of the input parameters is used to evaluate the limit state function, but the “most probable point”. This point has to be found by an optimisation procedure. Therefore, reliability methods need M times more evaluations of the limit state function than moment-based methods. Here, M is the number of iterations needed to find the “most probable point”. Depending on the problem, the computational effort of these methods can be close to moment-based methods. However, for probabilities close to 0.5, the computational cost can even exceed the effort of MCS [89].

In the field of wind energy, there are several examples using probabilistic approximations: Márquez-Domínguez and Sørensen [112] use FORM to calibrate fatigue design factors for OWTs. Kelma et al. [99] approximate loads by applying one-dimensional regressions with quadratic terms based on time-domain simulations. This enables fast evaluations of the limit state function at the expense of accuracy.

Level 3 reliability methods: probabilistic methods

Probabilistic methods (level 3) are probably the most straightforward approach. According to the ISO standard [86], they also represent reliability-based design procedures. Their methodological basis is MCS. This means that several simulations for effects and resistances are conducted. The failure probability is the amount of cases where effects are higher than resistances divided by the overall number of cases. Although this concept is easy to understand and to implement, it is not very frequently used due to several challenges. First, it can be time-consuming to compute enough cases to approximate failure probabilities or the limit state function itself. Second, for small failure probabilities, the number of calculations has to be even higher to get reliable values for the failure probability [67], as the fitted distribution in the tails does not necessarily agree with the distribution around the mean value. This means that the empirical distribution might, for example, be well approximated by a normal distribution around the mean value, but extreme values (i.e. tails) are better fitted by an extreme value (Gumbel) distribution. And third, effects and resistances cannot be treated independently, as one and the same input can influence effects and resistances. Consequently, special sampling methods like importance sampling [35, 106, 152] were developed to reduce the amount of required samples. Importance sampling concentrates samples on “important” regions of the data space. For example, more samples are generated for parameter constellations that might lead to failures ($g(\mathbf{x}) \approx 0$). Other advanced sampling concepts for small failure probabilities and variations of importance sampling are, for example, line sampling [33], subset simulation [139], or enhanced Monte Carlo simulation [135]. Another concept of limiting the overall numerical effort is to reduce the computing time of each model evaluation by replacing the full simulation model by a meta-model. For meta-models [18, 20], the limit state function is evaluated several times (generating so-called training data), so that the design space is covered as good as possible. Then, a mathematical meta-model for the limit state function - based on the training data - replaces the complex structural model. As the evaluation of the meta-model (e.g. linear regression, Gaussian process regression, etc.) is much faster than of the original model, it is evaluated instead of the complex structural model. It has to be noted that the quality of the approximation depends significantly on the training data.

For wind turbine applications, probabilistic methods are not widespread. This is due to limitations regarding computing times. Moreover, probabilistic results are no longer unambiguous (i.e. one single value) but distributed. This makes the assessment of the findings - especially for industry - more complex. Morató et al. [122] apply a Gaussian process regression as a meta-model for stresses and moments to approximate the reliability of OWT support structures. Muskulus and Schafhirt [131] calculate failure probabilities of OWTs using importance sampling. Furthermore, Müller and Cheng [127] compute probabilistic fatigue damages based on MCS with quasi-random sampling. Other aforementioned advanced sampling methods have not been used in OWT modelling yet.

Level 4 reliability methods: probabilistic optimisations

Although Veldkamp [204] conducted an optimisation of partial safety factors (i.e. reliability) with regard to costs already in 2006, probabilistic optimisations (level 4) - for example, advanced economic MCS - are still not state of the art. These methods take economic aspects into account when optimising the reliability. This means that reliability levels are no longer set to constant values but are considered as a variable in the optimisation process with regard to economic efficiency. In the PSA-OWT (probabilistic safety assessment of offshore wind turbines) project [69], it is proposed to use such level 4 reliability analyses to find the optimal safety level. On the one hand, very low reliability levels lead to economically inefficient structures, since the high failure probability causes follow-up costs. On the other hand, too high reliability levels are not economically efficient as well. The reason are high costs that result from making the structure very reliable. Hence, the best reliability level can only be found by optimising it with respect to the economic efficiency. In Section 1.2.9, there is a more detailed discussion of economic effects regarding OWT reliability.

For level 4 methods, the definition of the ISO standard [86] is slightly different. The highest level of verification according to the ISO standard is risk-informed design optimisation. This means that it also refers to advanced probabilistic optimisations, but focuses not only economic aspects. Risk-informed methods should cover the whole spectrum of risks from loss of human lives to environmental aspects all the way to monetary losses. Hence, the economic optimisation is only part of it.

1.2.2 Probabilistic analysis of offshore wind turbines

Definition: probabilistic analyses

Without a doubt, deterministic models have the great advantage of small computing times. Moreover, they lead to unambiguous, undistributed results. That is why they are still most commonly used. However, such approaches do not provide any information on statistical distributions of the model outputs (e.g. lifetime) resulting from uncertainties. To compute output distributions ($p(\mathbf{y})$), full probabilistic analyses are necessary.

The general concept of probabilistic analyses is to replace deterministic input values⁷ (\mathbf{x}) by variables that are statistically distributed ($p(\mathbf{x})$). Furthermore, statistical disturbance

⁷“Inputs” include all physical variables that are used in the “black box” model. These inputs can be load parameters (e.g. wind speeds) but also resistance or system parameter (e.g. yield strength of steel) and exhibit aleatory uncertainty.

variables⁸ (\mathbf{e}) can be introduced. Then, the uncertainty proceeds through the model. This leads to statistically distributed (i.e. uncertain) outputs. Examples can be forces, stresses, lifetimes, etc. Augusti et al. [8] summarise probabilistic structural analyses as follows: It is “to determine the probabilistic properties of the output random process [...] from the probabilistic properties of the data given as random quantities and from the values of the data given as deterministic quantities. Another source of uncertainties in the output process lies in the [...] mathematical (analytical or numerical) model of reality” (Augusti et al., 1984, pp. 3-4). This quite generally applicable definition is visualised in Fig. 1-6. The deterministic model can be regarded as a “black box” with uncertain inputs. (Physical) inputs (e.g. wind speeds) and model parameters (e.g. the uncertainty of the dynamic model) are sampled using their distributions. The “black box” model is evaluated several times and yields a distribution of the outputs (e.g. lifetimes).

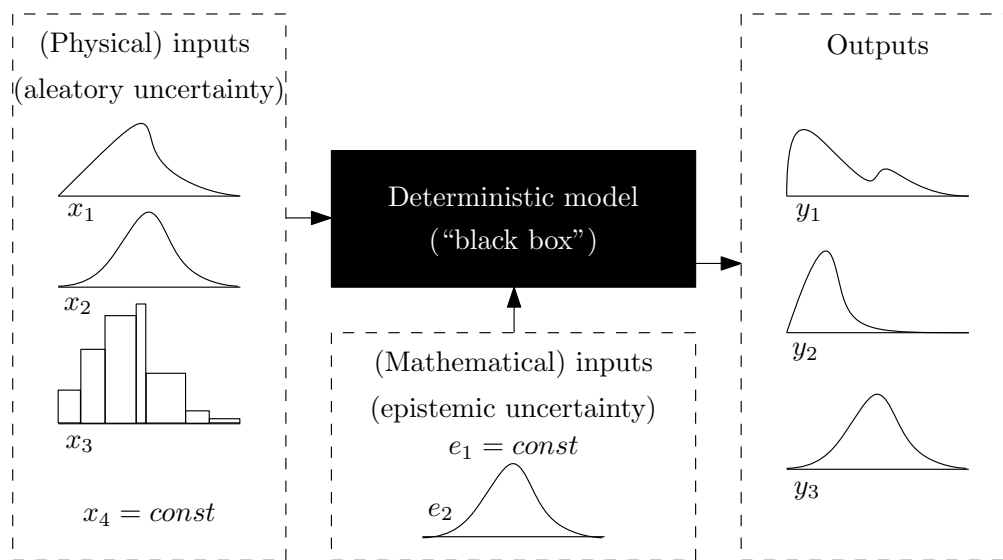


Figure 1-6: Visualisation of probabilistic structural analyses. Distributions of (physical) inputs ($p(\mathbf{x})$) and disturbance variables ($p(\mathbf{e})$, not taken into account in this thesis, cf. Section 1.2.5) are used to evaluate the deterministic “black box” model N times. The uncertainty proceeds through the model and yields distributions of outputs ($p(\mathbf{y})$).

Simplified models

One application of probabilistic analyses is the derivation of distributions for important outputs. These outputs are, for example, modal properties or lifetimes. Another application - in the context of reliability analyses - is the calculation of failure probabilities to determine the risk associated with a structure. Failure probabilities can be used to calibrate safety factors for level 1 reliability analyses. In this context, the work of Tarp-Johanson, Sørensen, Márquez-Domínguez, and Ronold et al. has to be mentioned [112, 151, 174, 179, 190, 191].

⁸“Statistical disturbance variables” are all non-physical inputs, i.e. mathematical model parameters with epistemic uncertainty, for example, model uncertainty.

All of them adjust safety factors for wind turbines (or their components) on the basis of simplified statistical models. Model uncertainties (sometimes also called model errors) are considered in addition to aleatory uncertainties on the load and resistance side. The statistical approaches are applied to semi-analytical, simplified limit state equations of load effects (load responses). When using these simplified models, an analysis in the time domain is not conducted. Therefore, dynamic effects resulting from uncertainties are not taken into account by these approaches.

To approximate dynamic effects, some new simplified models - mainly calibrated using time-domain simulations - have been proposed recently. An approximation of the dynamic response of the turbine with uncertain input parameters is executed by Kim and Lee [100]. They use a static analysis in combination with a so-called “peak-response factor”, which was calibrated in advance. This enables an approximation of a dynamic time-domain analysis, while computing times remain small. So, uncertainties in several input parameters can be taken into account. Further probabilistic reliability analyses of the full wind turbine system are performed, for example, by Morató et al. [122] and Abdallah et al. [1]. They apply Kriging meta-models based on time-domain simulations to reduce the computational cost. Hence, although their meta-models are relatively accurate approximations, the work is still based on simplified models that are not capable of representing all non-linear and unsteady effects. Moreover, the accuracy of these simplified models highly depends on the training data.

Component models

In contrast to fully coupled aero-hydro-servo-elastic time-domain models for OWTs, where probabilistic analyses are still extremely rare, for component models, probabilistic modelling is relatively widespread. The reliability of the foundation of a monopile using uncertain soil parameters is investigated, for example, by Schmoor and Achmus [164] or Carswell et al. [23]. Both do not simulate the turbine itself, but use equivalent loads at mudline. Further probabilistic analyses of foundation piles are conducted by Schmoor et al. [165]. This study takes model uncertainties being calibrated using large-scale experiments into account. A probabilistic investigation of the transition piece of a monopile is executed by Lee et al. [105]. Probabilistic analyses of turbine blades for onshore and offshore wind turbines are conducted, for example, by Hu et al. [74] and Bacharoudis et al. [9]. In both cases, the analysis is based on meta-models to decrease the computational effort. This is necessary in these cases, as finite element (FE) models with many degrees of freedom (DoF) are used for the blades. Furthermore, there are several probabilistic approaches that derive distributions for modal parameters of the entire wind turbine. An example is the work of Zaaijer and Vugts [216]. Kallehave et al. [96] add an optimisation process regarding eigenfrequencies to their probabilistic analysis. Finally, one rare example of the consideration of polymorphic uncertainty (aleatory and epistemic uncertainty; cf. Section 1.2.5) using imprecise probability in wind energy is the recent work of Caboni et al. [22]. Caboni et al. optimise the aerodynamic airfoil design and consider polymorphic uncertainty in a single key parameter in the airfoil model by using imprecise probabilistic methods. More precisely, they use traditional probability methods that are combined with evidence theory to create a range of probabilistic distributions (i.e. imprecise distributions). They conclude that the use of imprecise probability methods leads to slightly different designs that are more robust against uncertainties.

Time-domain models

As mentioned before, probabilistic analyses of fully coupled time-domain models for OWTs are still quite rare. However, due to increasing computing power and a more pronounced focus on turbine reliabilities, recently, there have been some applications. The first comprehensive probabilistic time-domain analysis of offshore wind turbines - without using meta-models - was conducted by Cheng [25] in 2002. As computing times at that time were even more challenging for time-domain simulations, the focus of his work is the load extrapolation for ultimate loads. Fatigue loads are not considered by Cheng. Based on this work, Veldkamp [204] carried out another full probabilistic time-domain analysis of OWTs. As an addition to Cheng's work, his focus is on fatigue loads. Special emphasis is given to the model uncertainty of the fatigue model. Cheng and Veldkamp both apply several simplifications to manage computing times. Soil variability is not considered at all. As the uncertainty of the soil can be significant [69], this is a clear simplification. Furthermore, only monopile substructures are analysed. Modern alternatives for greater water depths like jackets or tripods with more complicated structural models are omitted. Moreover, the selection of the probabilistic subset is based on their expert knowledge, not being an objective measure. Another current probabilistic analysis using time-domain simulations is conducted by Muskulus and Schafhirt [131]. Here, the calculation of wind and wave loads is uncoupled to keep computing times manageable. Furthermore, the amount of stochastic variables is relatively small. In contrast to previous studies, a soil model and some soil uncertainty are included. For OWTs with floating substructures, the first probabilistic study using time-domain simulations is done by Müller and Cheng [127]. They use quasi-random sampling to reduce the computational effort. Still, only three environmental conditions are treated probabilistically. Thence, there is a need for a holistic probabilistic analysis⁹ using coupled time-domain simulations.

Probabilistic simulation framework

For a holistic probabilistic analysis, several steps are needed that are related to the classical probabilistic risk assessment (PRA). Although there are several slightly different methodologies for PRA in literature [173, 183, 207], the steps are more or less the same. An example based on Sørensen [173] is shown in Fig. 1-7a. Based on these PRA concepts, holistic probabilistic simulation schemes can be defined. The general structure of such a scheme is shown in Fig. 1-7b and is elucidated in section 1.4.1. On the one hand, compared to PRA schemes, a holistic probabilistic simulation framework does not focus on risks and their consequences. Therefore, steps like the analysis of failure consequences, risk assessment, and risk treatment are not directly included but incorporated by investigating economic effects. On the other hand, the "analysis of probability / uncertainty analysis" is further divided into the determination of uncertainties and the design of experiments. Furthermore, for OWT applications, an additional long-term extrapolation is required for a holistic probabilistic modelling.

⁹"Holistic probabilistic analysis" means that the analysis does not only cover particular aspects. For example, probabilistic analyses without sensitivity analyses or an uncertainty assessment of inputs are possible, if the relevant information is taken from literature. In a holistic concept, these aspects are included, so that a holistic analysis does not rely on literature values/previous research.

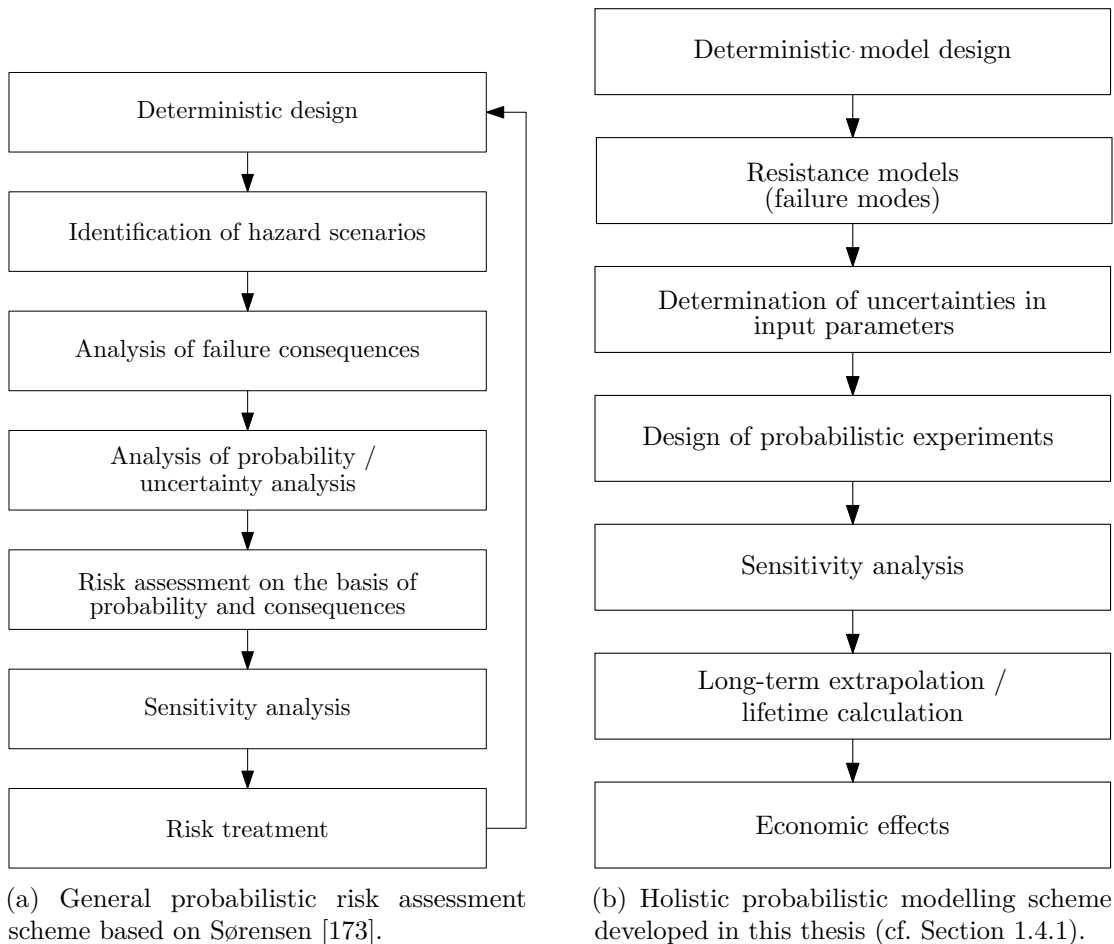


Figure 1-7: Probabilistic modelling schemes.

1.2.3 Deterministic modelling of offshore wind turbines

Wind turbine models

Wind turbines in general and OWTs in particular are complex structures exhibiting a pronounced dynamic behaviour. The interaction of non-linear structural behaviour with aerodynamics and soil characteristics has to be taken into account. Furthermore, the electric system, especially the control system of turbines, interacts with the structure. In case of OWTs, hydrodynamic effects have to be considered as well. Therefore, wind turbine models tend to be sophisticated and coupled aero-elastic models. This means that the turbine is not split up into several component models being solved independently, but dependencies and interactions are taken into account by utilising an overall model. In the past, static approaches, frequency-domain solutions, or semi-analytical models have been used. However, current standards require coupled aero-elastic time-domain simulations for the certification of wind turbines [53, 84]. Normally, these coupled time-domain simulations are based on deterministic inputs, but consider the stochastic nature of turbulent wind and irregular waves making their evaluation more time-consuming. These models are called quasi- or pseudo-deterministic or just deterministic. Over the past years, several time-

domain simulation codes meeting the requirements of the standards and being based on finite elements, multi-body systems (MBS), and modal approaches have been developed. The codes were initially designed for onshore turbines. With the growth of offshore wind energy, codes were adapted for offshore applications. Some of the most important codes are “Bladed” [17], FAST (Fatigue, aerodynamics, structures, and turbulence) [94], and HAWC2 (Horizontal axis wind turbine code 2nd generation) [104]. Overviews of the most common codes and details regarding differences of codes are given, for example, by Böker [16]. FAST occupies a special position for research purposes, as the entire source code is open source and can be adapted and enhanced by everyone.

To adapt onshore wind turbine models for offshore applications, the substructure (e.g. monopile) has to be included and hydrodynamic loads have to be considered. FE and MBS models of substructures, in particular of jackets, have many DoF. Hence, to keep computing times manageable, a reduction of DoF is almost indispensable. Therefore, in most cases, reduction techniques are applied. A rudimentary approach is a static reduction adapted from Guyan [57], which rearranges the structural equation so that external forces of the lower part of the equation system are zero:

$$\begin{pmatrix} \mathbf{K}_{11} & \mathbf{K}_{12} \\ \mathbf{K}_{21} & \mathbf{K}_{22} \end{pmatrix} \begin{pmatrix} \mathbf{u}_1 \\ \mathbf{u}_2 \end{pmatrix} = \begin{pmatrix} \mathbf{F} \\ \mathbf{0} \end{pmatrix}. \quad (1.6)$$

Here, \mathbf{K}_{ij} are sub-matrices of the stiffness matrix, \mathbf{u} and \mathbf{F} are the displacement and external force vectors, respectively, and $\mathbf{0}$ is the zero vector.

More sophisticated reduction methods, preserving modal parameters, are based on the work of Craig Jr. and Bampton [30]. The general idea is to apply the Ritz transformation:

$$\Phi^T \mathbf{M} \Phi \ddot{\mathbf{u}} + \Phi^T \mathbf{C} \Phi \dot{\mathbf{u}} + \Phi^T \mathbf{K} \Phi \mathbf{u} = \Phi^T \mathbf{F}, \quad (1.7)$$

where \mathbf{M} , \mathbf{C} , and \mathbf{K} are mass, damping, and stiffness matrices, respectively. The matrix Φ consists of constraint modes (Φ_R), fixed-interface normal modes (Φ_L), and the identity matrix (\mathbf{I}):

$$\Phi = \begin{pmatrix} \mathbf{I} & \mathbf{0} \\ \Phi_R & \Phi_L \end{pmatrix}. \quad (1.8)$$

Such a modal reduction according to Craig Jr. and Bampton [30] is used, for example, in HAWC2 and FAST [172, 209]. In FAST, this enables a reduction from thousand DoF to about 10 DoF for the substructure [172]. The main limitation of all these reduction schemes is that the linearity of the equations of motion is required. Hence, non-linearities, for example, resulting from large deformations, cannot be covered. This is not so relevant in the current context, but might become an important shortcoming, if wind turbine dimensions continue to increase.

One main challenge in OWT modelling - independent of the code - is the scarcity of real field measurement data of OWTs to validate models. Hence, it is hardly possible to assess the accuracy of existing models and to quantify existing model uncertainties. Validations using field measurement data are not available, so that so far, validations have mainly been performed against experimental data with scaled structures [148, 149]. Alternatively, codes were cross-verified in several extensive studies [95, 144, 145, 159]. For these verification campaigns, a 5 MW reference turbine was defined being mainly based on data of the REpower 5M machine [21] and the Dutch offshore wind energy converter (DOWEC) 6 MW turbine

[101]. Specifications of this reference turbine and corresponding substructures are defined in various technical reports [95, 101, 211]. Furthermore, consistent load cases are freely available and can serve as a reference [210].

Soil model

For OWTs, soil-structure interaction is an important topic that has to be considered in some way. However, sophisticated soil models based on FE approaches have many DoF making them unsuitable. An alternative are so-called p-y methods. These methods are based on the Winkler approach [214] and model foundation piles using beam elements that are supported by uncoupled non-linear springs. This leads to significantly fewer DoF than FE approaches. Nonetheless, in contrast to applications in the oil and gas industry, where the use of non-linear soil models is state of the art [14, 119], for OWTs, it is still quite common to neglect soil-structure interaction in coupled time-domain simulations. One rare example of the use of a non-linear soil model in coupled OWT simulations with jacket substructures is the work of Alati et al. [4]. Commonly, OWTs - especially with jacket substructures - are assumed to be clamped to the seabed [69, 145, 209]. This simplification is, *inter alia*, reasoned by the applied reduction schemes for the substructure (e.g. Craig-Bampton reduction [30]). Since reduction schemes are not necessary in the oil and gas industry, non-linear soil models are - as stated before - state of the art for these applications. For OWTs, the reduction of the substructure - for example, to its first 10 modal DoF - is conducted only once at the beginning of the time-domain simulation. Hence, a non-linear soil-structure interaction in each time step is impossible. This means that p-y methods cannot be applied. To combine reductions of the substructure and considerations of soil characteristics, a soil model has to be included in the reduction scheme itself. So far, this has not been common practice. This leads to the first research focus of this thesis: the enhancement of state-of-the-art OWT models by an effective soil model (cf. Section 2). Therefore, in the following, the state of the art in soil modelling for OWTs is presented.

There is a wide variety of soil models for OWTs. An illustration of some approaches (non-exhaustive) is shown in Fig. 1-8. The complexity of the soil model and the number of DoF increases from the left (clamped structure) to the right (FE model). The simplest approach is to neglect the soil and to assume the structure to be clamped to the seabed [69, 145, 209]. However, it was shown that the dynamic behaviour cannot be modelled accurately using this simplified approach [95].

A relatively rudimentary approach is the so-called apparent fixity length. Here, still, a clamped pile foundation is modelled. However, the rigid connection is not at the seabed, but at a fictive point below the surface. This approach is described by Zaaier [217] using values for the distance of the fictive point below mudline taken from Barltrop and Adams [11]. Although the apparent fixity approach enables some kind of soil consideration, the dynamic behaviour - for example, the first eigenfrequency - is not modelled correctly [59]. Therefore, a different apparent fixity approach is used, *inter alia*, in the OC3 project [140]. The distance below the seabed is determined iteratively by matching the first eigenfrequency of the substructure. This leads to a better representation of the dynamic behaviour, but still, higher eigenfrequencies, etc. cannot be matched using the apparent fixity approach. More detailed models use uncoupled or coupled springs at the seabed, so-called soil matrices or super-elements [45, 59, 76, 140, 217]. These models are of special interest in this thesis.

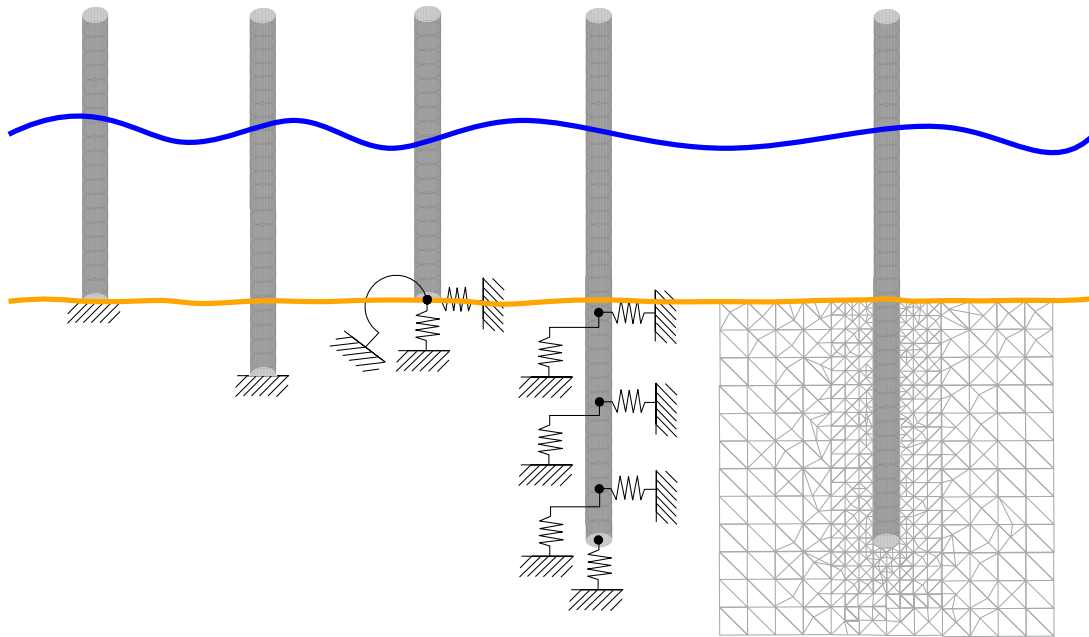


Figure 1-8: Illustration of various soil models for a monopile foundation. The complexity of the soil model and the number of DoF increase from the left (clamped structure) to the right (FE model). From left to right: clamped structure, apparent fixity length, soil matrix, distributed springs, FE model.

On the one hand, they are mostly compatible with reduction schemes for the substructure. On the other hand, the matrix-based approach yields a more realistic soil representation than previously mentioned concepts. The matrix-based models can be improved by taking non-linear load-stiffness correlations into account. For example, Dubois et al. [45] enhance the classical spring model by assuming load-dependent spring stiffnesses, or Hübler et al. [76] define operating point dependent soil stiffnesses.

The most common type of soil models for pile foundations are distributed, non-linear springs like p-y curves as recommended by the American Petroleum Institute (API) standard [6]. Compared to soil matrices, a better representation of the real soil behaviour is possible. In return, the number of DoF is higher and a compatibility with substructure reduction schemes is precluded. For standard p-y curves - originally based on the work of Murchison and O'Neill [129] - the simulation results do not accurately match the simulation results of FE models or experimental results. This is shown, for example, by Hald et al. [64] and Lesny and Wiemann [107]. The comparison with experimental data shows that especially for large pile diameters, p-y curves of the API standard [6] are not valid [64]. For small or initial loads, stiffnesses are underestimated, whereas for ultimate loads, too high soil stiffnesses are predicted. Therefore, different p-y curves are proposed, for example, by Kallehave et al. [97] and Sørensen et al. [180, 181]. Kallehave et al. modify the initial stiffness of the soil to achieve more realistic results. Sørensen et al. focus on the soil stiffness under extreme loads. Amar Bouzid [5] and Thieken et al. [193] assess the modified p-y curves and conclude that none of them are satisfying. That is why Thieken et al. [192] develop a significantly different p-y model. It is based on completely new “basic p-y curves” taking both the underestimation for small loads and the overestimation of the soil stiffness for

high loads into account. Afterwards, the “basic p-y curves” are iteratively adjusted to consider interaction effects of the deflection line with the bedding resistance as well as the pile tip effect. Experimental investigations of the performance of the various p-y models in a dynamic context are missing, although the dynamic soil behaviour is relevant for coupled OWT simulations.

For special purposes, models with spring-damper combinations [200] or spring-slider combinations [13] can be used, if the focus is on damping.

The most accurate models at the expense of high computing times and a large amount of DoF are FE models [2, 32]. Despite their good representation of the real soil-structure interaction, using FE models in coupled time-domain simulations for OWTs is impractical, since the number of DoF of the soil model would exceed the number of overall DoF.

In this thesis, the focus regarding soil modelling is not on new and accurate models, but on an efficient consideration of soil-structure interaction in probabilistic, coupled time-domain simulations for OWTs. Since computing time is a limiting factor for probabilistic time-domain simulations, for efficient soil modelling, the number of DoF and compatibility with the overall turbine model, especially if reduction methods are applied, are top priorities. Thus, p-y curves and FE models are not suitable. Super-element approaches are most relevant [45, 59, 76, 140, 217] in this context. The possible inclusion of these matrix-based approaches in the Craig-Bampton reduction was shown by Häfele et al. [59] and Hübler et al. [76]. The drawback of state-of-the-art linearised super-element approaches is the missing load dependency. This shortcoming is resolved here (see Section 2) by linearising the non-linear soil behaviour at the present load level (i.e. operating point). The use of non-linear soil matrices, as proposed by Dubois et al. [45], is not possible, since non-linear matrices cannot be included in standard reduction schemes. For the proposed load-dependent, linearised approach, a limited accuracy compared to, for example, FE models is accepted to fasten up probabilistic time-domain simulations.

1.2.4 Resistance models and failure modes

In the previous section, the deterministic wind turbine model is described. This model is capable of simulating acting loads. However, to calculate failure probabilities according to Eq. 1.2, not only loads or effects (E) have to be known, but resistances (R) are needed as well. Therefore, the most important failure modes have to be identified. Resistance models and failure modes are not the focus of this thesis (cf. Section 1.1). Hence, state-of-the-art approaches are utilised. For OWTs, these approaches and the most important failure modes that have to be considered are stated in current standards. The IEC [84] gives some general remarks. Ultimate limit states (ULS), fatigue limit states (FLS), stability (buckling), and maximal deflections (for example, to prevent blade-tower strikes) are the failure modes of interest. Further details regarding failure modes and how to model them are given in standards like the Germanischer Lloyd (GL) or Det Norske Veritas (DNV) standard for offshore wind energy [37, 53]. These standards provide details for the design of steel structures, concrete structures, or grouted joints. Since this thesis focuses on monopile and jacket substructures, which are both made of steel, the focus is particularly on the welded connections (not looking at grouts). Additionally, guidance for the foundation design is given, as failures due to geotechnical reasons are considered to be significant as well. As these two standards just provide general guidance for OWT design, there is a lack of details

for some failure modes. Therefore, references to specialised standards [38, 184] concerning resistances of steel structures for ULS and FLS, respectively, and to standards [42] regarding pile foundations are given.

Here, resistances are modelled as being mainly based on material and geometric parameters. All standards assume deterministic values for these parameters. However, not only loads are uncertain, but resistances scatter or are vaguely known as well. This uncertainty is quite high especially for fatigue resistances. This is the reason why Veldkamp [204] places special emphasis on the probabilistic modelling of the fatigue resistance. Muskulus and Schafhirt [131] introduce uncertainties to resistances by using distributed values for the yield strength of steel. In the PSA-OWT project [69], the variety of the soil resistance is considered and can exceed the assumed uncertainty in loads. Hence, a probabilistic consideration of geotechnical limit states can be of special interest.

1.2.5 Uncertainty in input parameters

Theory

After having built up models for loads and resistances, the third step according to the scheme in Fig. 1-7b is the determination of uncertainties in inputs. Therefore, at first, a short definition of uncertainty is given. In literature, there are various definitions [12, 92, 116]. One approach is a more theoretical, philosophical differentiation of two types: aleatory and epistemic [12, 116]. Aleatory uncertainty is random physical variability or scattering of parameters. It is irreducible. Examples are alternating wind speeds due to changing weather conditions or spatial and temporal variations in soil conditions. Epistemic uncertainty covers, for example, lack of knowledge and incomplete, ambiguous or dubious information. Hence, epistemic uncertainty is reducible. Examples are measurement inaccuracies or model uncertainties. While probabilistic approaches are used to model aleatory uncertainty, for epistemic uncertainty, different methods like Bayesian statistics or set-theoretical models can be applied [12]. If a combination of aleatory and epistemic uncertainties occurs, imprecise probability can be used to represent both types of uncertainties independently. Another, more practical, engineering way to classify uncertainties is the differentiation in physical, statistical, and model uncertainty [92]. This classification can be extended by adding, for example, measurement uncertainty [173] or phenomenological, decision and prediction uncertainty and human factors [116].

In any case, in wind energy research, mostly the random physical variability of parameters (aleatory uncertainty) is considered. Furthermore, some researchers additionally take model uncertainties into account. Nevertheless, nearly exclusively, probabilistic approaches are applied, even if model uncertainty is considered [131, 178]. One rare example of the use of imprecise probabilities is the work of Caboni et al. [22]. The consideration of model uncertainties is problematic or at least challenging, as first, classical probabilistic models are only of limited suitability (model uncertainties represent epistemic uncertainty). Second, the determination of actual model uncertainties for wind turbine models is nearly impossible due to limited data for model validations (discussed in Section 1.2.3). Frequently, it is abstained from explicitly considering model uncertainty, as there is an essential lack of profound analyses of it. Hence, a consideration would always be biased in some way. So, the rest of this section focuses on aleatory uncertainty, and in this thesis, only aleatory uncertainty is applied.

Uncertain/deterministic parameters

To find theoretical statistical distributions for all relevant inputs that are not considered to be deterministic, there are two main challenges. The first challenge is to determine those parameters that have to be treated in a probabilistic manner and those that can be set to fixed, deterministic values. Generally, two approaches can be used. The first one is a sensitivity analysis. In this case, theoretically, all parameters are considered as probabilistic inputs in the first place. Using sensitivity analyses, the amount of probabilistic inputs (probabilistic subset) is reduced. Sensitivity analyses are discussed in Section 1.2.7 in detail. The second approach is the use of technical expertise¹⁰. To some extent, technical expertise has to be used in any case, since full sensitivity analyses are hardly practical. However, most studies considering uncertainties in a fully coupled wind turbine model in the time domain reduce the set of probabilistic parameters by utilising their technical expertise only. For example, Veldkamp [204, 205] sets several parameters to deterministic values by stating their influences to be negligible or their variations to be small. Negro et al. [136] investigate where major uncertainties are present using technical expertise. Their focus is on model uncertainties. Sørensen and Tarp-Johansen [177] optimise wind turbines with respect to costs on the basis of a probabilistic reliability model. For this model, they state several parameters to be uncertain. These examples of only using expert knowledge to set up a probabilistic subset clarify the need for a more comprehensive uncertainty analysis based on sensitivity analyses that is conducted in Section 4.

Statistical distributions

The second challenge is to define theoretical statistical distributions for identified, significant probabilistic parameters. In specific fields, like wind or wave parameters, various investigations of uncertainties and their statistical distributions are available. To model the uncertainty in wind parameters, Cheng [25] and Veldkamp [204] use their technical expertise to state ranges or distributions, respectively. Furthermore, there are several wind databases available. Ernst and Seume [47] and the PSA-OWT project [68] use data of the German research platform FINO1 (“Forschungsplattformen in Nord- und Ostsee”) to derive distributions for wind speeds, turbulence intensities, and wind shear power law exponents. Bierbooms [15] uses the NESS (North European Storm Study) database [141] to deduce wind and wave distributions that include interaction effects. Morgan et al. [123] evaluate different kinds of theoretical statistical distributions for wind speeds on the basis of offshore measurements in the United States of America (US). Schmidt et al. [162] derive combined distributions for wind and waves including their directions on the basis of FINO1 measurements. Häfele et al. [60, 61] take data from the FINO3 platform for their distributions of dependent wind and wave parameters. Stewart et al. [185, 186] set up a comprehensive database for wind and wave conditions around the US using buoy measurement data. Distributions for soil properties are proposed by Zaaijer [217] on the basis of his expert knowledge and literature research. He divides the uncertainty into spatial and time (changes over lifetime) uncertainties. For most parameters, he only proposes boundary values but no distributions. Distributions for soil conditions are proposed, for example, by Kim and Lee [100]. They use

¹⁰The terms “technical expertise” and “expert knowledge” are quite vague. They cover knowledge based on research and industry experience, non-citable literature, unpublished preliminary studies, but also assumptions, etc. This means that they include all kinds of not further defined or stated sources of “knowledge”.

their technical expertise to state distributions. Carswell et al. [24] review current standards like the DNV standard [36] and available literature [10, 142, 167] regarding distributions for soil parameters. Material properties are often considered to be deterministic. Therefore, only a few authors deal with probabilistic material properties [69, 178, 213]. These authors do not use data to derive distributions but technical expertise and current standards. Zaaier [217] deals with some geometrical uncertainties (e.g. manufacturing tolerances). Although aleatory uncertainty is mainly considered here, some examples for model uncertainty are given as well. Fatigue model parameters are quite uncertain and might even be regarded as determining [131, 205]. Here, for example, Veldkamp [204, 205] gives recommendations based on expert knowledge. Furthermore, model uncertainties of the structural dynamics and the climate statics are stated, for example, by Tarp-Johansen et al. [190]. Again, values are just based on expert knowledge. Hence, it is apparent that for model uncertainties, well-founded investigations for wind turbines are missing. Thus, the use of stochastic variables for model uncertainties is subjective, and in this work, it is abstained from applying them.

Determination of distributions

Although a variety of theoretical statistical distributions for uncertain inputs for OWT models is available in literature, a comprehensive compilation is missing. The different sources - presented in the last subsection - may be incompatible. For example, wave distributions of deep water sites cannot be combined with wind distributions of nearshore sites. Hence, for some applications or for parameters that have not been sufficiently covered in literature yet, the derivation of theoretical statistical distributions from raw data (i.e. empirical distribution) itself is a suitable alternative to literature values. In this thesis, a database with theoretical distributions for several wind and wave parameters is set up (cf. Section 3). Compared to state-of-the-art approaches [15, 51, 68], more sophisticated theoretical distributions are utilised. For example, multi-modal and non-parametric distributions are taken into consideration, which improves the agreement of theoretical and empirical distributions. Furthermore, data quality and/or relevance is improved (e.g. wind measurements at about hub height) compared to other approaches [186]. And lastly, a larger number of environmental conditions at the same site (e.g. wind shear, ocean currents, etc.) are included. This reduces the challenge of incompatible data sources.

If theoretical distributions are derived using raw data, distribution fitting is needed. Approaches consisting of distribution fitting and testing the goodness of the fit are illustrated, for example, by Morgan et al. [123]. Relevant methods for the fitting are, for example, maximum likelihood estimation (MLE) or least mean square errors (MSEs). For the evaluation of the goodness, tests like the Kolmogorov-Smirnov test (KS test) or the calculation of the coefficient of determination can be used. If extreme values shall be extracted, additional extrapolation methods like the peak-over-threshold (POT) method are necessary [47]. Extrapolations methods will be evaluated in Section 1.2.8 in more detail.

1.2.6 Design of probabilistic experiments

Knowing the distributions of all significant, probabilistic parameters¹¹, the next challenge is to generate samples in an efficient manner. This procedure is called “design of probabilistic

¹¹“Significant parameters” are those parameters that are selected (based on expert knowledge) or determined (based on sensitivity analyses) to be treated probabilistically. This means that the uncertainty of these parameters significantly influences the considered output.

experiments” (DOE). Efficient sampling methods are relevant for nearly all disciplines using simulations. Therefore, there is still ongoing fundamental research [168, 171]. These quite theoretical considerations go beyond the scope of the present work. Hence, state-of-the-art approaches - presented next - are utilised. Although purely theoretical considerations regarding sampling methods are not covered by this work, more advanced sampling methods are part of this thesis. However, these advanced, new sampling methods are not part of the DOE itself, but are used for the long-term extrapolation in Section 1.2.8. Therefore, they are partly dependent on the application and on the extrapolation scheme.

In general, the aim of a sampling process is to generate a set of samples that is as small as possible by conserving all important information of the input parameters. This means that samples have to represent (but not reproduce) distributions of the input parameters and achieve a good resolution of the data space. Two types of sampling methods can be distinguished. First, there are systematic methods like linear or quadratic sampling or full factorial designs (cf. Fig. 1-9 (a)) that are mainly used for optimisation purposes [46]. Second, there are stochastic and quasi-random methods that can be used for sensitivity, robustness, or reliability analyses. The plain MCS [106, 117, 152] that has its origin in the 1940s (cf. Fig. 1-9 (b)) is probably the most common stochastic sampling method. It is based on the law of large numbers and generates samples totally randomly. Uniformly distributed random samples can be transformed to match statistical distributions of (correlated) parameters afterwards. Using MCS, random samples are only equally distributed for high numbers of samples. Otherwise, random clusters show up and the data space resolution is getting worse. That is the reason for latin hypercube sampling (LHS) [114, 152]. It is an enhancement of MCS that divides the data space into “stripes”, so-called hypercubes, with equal probabilities. In each hypercube, one random sample is created. This reduces the effect of clustering (cf. Fig. 1-9 (c)). An overview of enhancements of LHS reducing the correlation among inputs or guaranteeing a better data space filling than classical LHS is, for example, presented by Viana [208]. To avoid correlations and clustering that might occur due to the random sampling process, alternatively, quasi-random sampling methods can be applied (cf. Fig. 1-9 (d)). These sampling techniques are based on quasi-random sequences like the Sobol’ [170] or the Halton sequence [65]. For the calculation of small failure probabilities, very high numbers of samples are necessary. Therefore, approaches reducing the number of samples to an acceptable level are needed. A definition of “acceptable level” cannot be given, as it depends on the application, available resources, etc. One relevant method in this context is importance sampling (IS) [35, 106, 152] that is illustrated in Fig. 1-9 (e). Here, samples are mainly generated in the region of interest (e.g. high loads and low resistances that are potentially leading to failures). This is achieved by changing or replacing the probability distribution with an alternative distribution, the so-called mass function (cf. Fig. 1-9 (f)). This mass function can be chosen arbitrarily, but this selection influences the performance of IS significantly and an optimal mass function concentrates samples where they are needed ($g(E, R) \approx 0$). The potential use of a mass function is the reason why - at the beginning of this section - it is stated that samples have to represent but not reproduce statistical distributions. For structural reliability analysis, IS is proposed, for example, by Melchers [115] or Hannus [66]. Other sampling methods that are suitable for small failure probabilities are, for example, subset simulation [139] or enhanced MCS [135].

For OWTs and their components, mainly MCS is used [23, 164, 204]. However, recently, other sampling methods have been applied as well. Müller and Cheng [127] use quasi-random

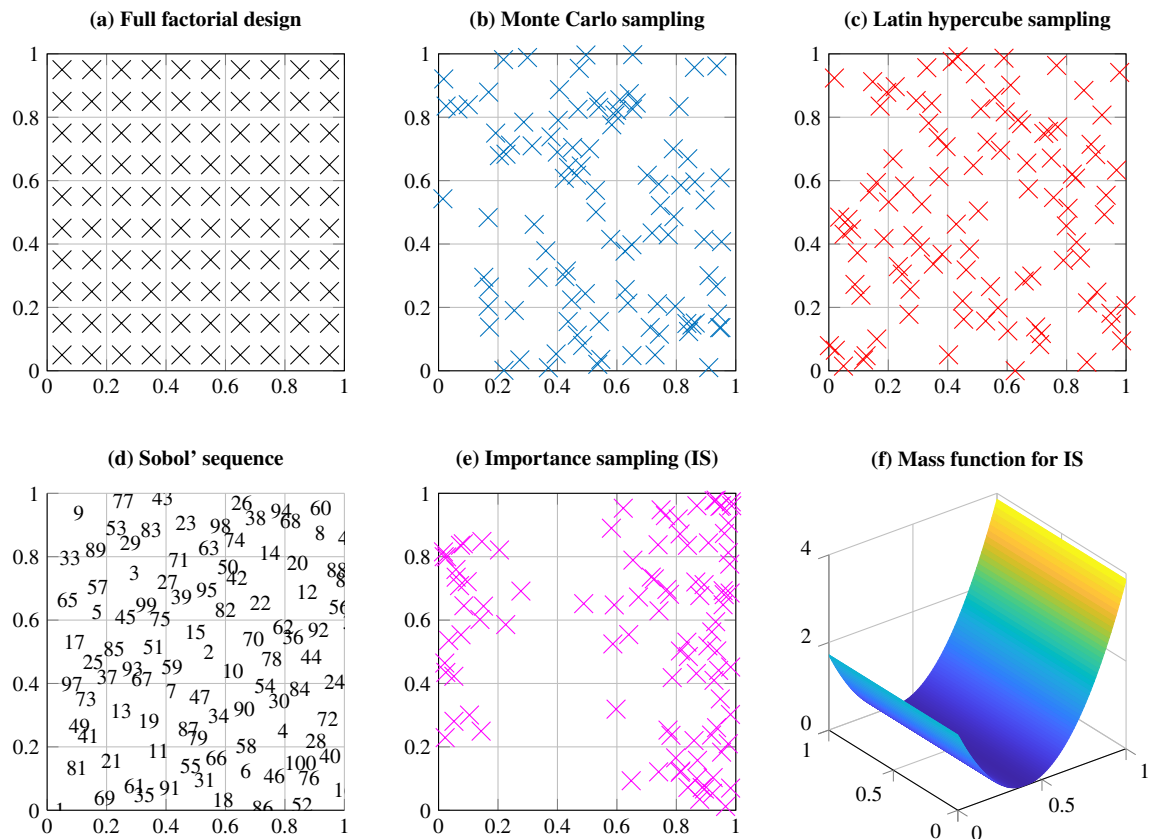


Figure 1-9: Generic examples to illustrate the procedure (e.g. systematic or random) and performance (e.g. space filling) of various sampling concepts: (a) systematic sampling, full factorial design (b) standard MCS with clusters due to limited sampling (c) LHS for a better resolution of the data space (d) quasi-random sampling using Sobol' sequence (e) importance sampling for more samples in relevant regions of the data space (f) mass function that is used for the importance sampling (i.e. more samples for high values of the mass function)

sampling based on the Sobol' sequence. Importance sampling is utilised by Muskulus and Schafhirt [131] and Stieng and Muskulus [187] to reduce sample sizes for their time-consuming time-domain simulations.

As mentioned before, in addition to sampling for probabilistic analyses, for lifetime damage extrapolations, several load situations have to be simulated as well. Therefore, an additional advanced sampling of “load cases” is needed. This topic is discussed in more detail in Section 1.2.8 and improved sampling concepts are developed and validated in Section 5.1 and 5.2.

1.2.7 Sensitivity analysis

Figure 1-7 shows that sensitivity analyses can be conducted before and after the probability determination. The aims of both types of sensitivity analyses are different. Homma and Satelli [72] define the aim of sensitivity analyses as follows: “Sensitivity analysis (SA) of a model output aims to quantify the relative importance of each input model parameter in determining the value of an assigned output variable” (Homma and Satelli, 1996, p. 1).

Bearing that in mind, two objectives of a sensitivity analysis can be highlighted. The first one is to reduce the amount of parameters that have to be regarded as stochastic. Inputs without significant influence can be treated deterministically. If this is the aim of the sensitivity analysis, it has to be conducted before the uncertainty analysis (Fig. 1-7b). The second objective is to identify subdomains of the full input domain (i.e. input subsets) where outputs are most sensitive. These subdomains are the best starting points for optimisations. Hence, this sensitivity analysis has to be conducted after the uncertainty analysis (Fig. 1-7a). The methodology for both is the same.

In any case, two types of sensitivity analyses have to be distinguished. On the one hand, there are local methods based on derivatives. These methods are quite efficient concerning computing time. However, derivatives ($\partial y_i / \partial x_j$) are only valid at one position of the full data space. For non-linear problems, it is not possible to make general statements based on local methods [158]. On the other hand, there are global methods. These methods can be used to analyse the entire data space. However, most global methods are much more time-consuming. Although state-of-the-art turbine models neglect many non-linearities, for OWTs, the function mapping inputs to outputs is still fairly non-linear so that local methods are only partially suitable. Hence, in this thesis, the focus is on global sensitivity analyses. A good overview is given by Saltelli et al. [158] and reviews are presented, for example, by Iooss and Lemaître [87] or Tian [194].

In the area of global sensitivity analyses, there is a wide range of approaches from rudimentary and straightforward to sophisticated ones. A first overview of the general model behaviour can be achieved by graphical methods like scatter plots, cobweb plots, etc. [157]. One of the most frequently used approaches in structural engineering is the one-at-a-time (OAT) sampling [155]. Here, all parameters except one are kept fixed. The “free” parameter is varied. In most cases, the maximum and the minimum of this parameter are tested. A sensitivity index ($S_{OAT,i}$) for the OAT method can, for example, be defined as follows:

$$S_{OAT,i} = \frac{f(x_1, x_2, \dots, x_i + \Delta x_i, \dots, x_N) - f(x_1, x_2, \dots, x_i - \Delta x_i, \dots, x_N)}{2\Delta x_i}, \quad (1.9)$$

where f is the model function, x_1 to x_N are the N input factors and Δx_i is the variation in the i^{th} input factor. OAT sampling has the advantage of small computing times. It can be used to identify those parameters that are influential [87] and it never detects uninfluential ones as significant [155]. The opposite - never detecting influential inputs as non-significant - is not the case. There are several reasons why OAT sampling should not be used. Saltelli et al. [155, 158] criticise missing interactions between parameters and the inefficiency for higher numbers of parameters. Alternatives, like the elementary effects method [125], regressions, or variance-based methods [72, 169] are given. The elementary effects method is basically a OAT sampling method. By changing the algorithm so that the variation of the parameters does not always start from the same point (mean value of all parameters), the elementary effects method overcomes some shortcomings of the classical OAT sampling. By correlating input parameters with outputs, a regression analysis can be conducted. The correlation between inputs and outputs can be used as a measure of global sensitivity. There are several correlation coefficients available. For example, the standard regression coefficient, the Pearson correlation coefficient, or the Spearman rank-order correlation are used [46, 87]. For an automatic selection of influential parameters, so-called subset selection methods were developed. A good overview of different methods, like best-subset selection, forward

selection, or backward elimination and of different selection criteria, like F-test, Akaike information criterion (AIC) [3], or Bayesian information criterion (BIC) [166], that can replace correlation coefficients is given, for example, by Miller [118]. More sophisticated subset selection methods, so-called shrinkage and selection methods, are the non-negative garrote method by Breiman [19] and the least absolute shrinkage and selection operator (LASSO) by Tibshirani [195]. If all interaction effects among inputs and all non-linearities shall be taken into account and if higher computing times are accepted, variance-based methods are a good choice [72, 169]. Variance-based methods enable a computation of so-called “total effects” that include all interactions:

$$S_{Ti} = \frac{E_{\mathbf{x}_{\sim i}}(V_{x_i}(y|\mathbf{x}_{\sim i}))}{V(y)} = 1 - \frac{V_{\mathbf{x}_{\sim i}}(E_{x_i}(y|\mathbf{x}_{\sim i}))}{V(y)}. \quad (1.10)$$

Here, $V(y)$ is the unconditional variance of the output $y = f(x_1, x_2, \dots, x_i, \dots, x_N)$. $E_{\mathbf{x}_{\sim i}}(V_{x_i}(y|\mathbf{x}_{\sim i}))$ can be interpreted as the expected variance that is left, if all factors except the i^{th} factor are fixed. $V_{\mathbf{x}_{\sim i}}(E_{x_i}(y|\mathbf{x}_{\sim i}))$ is the expected reduction of the variance, if all factors except the i^{th} factor are fixed.

As the calculation of total sensitivities is time-consuming, slightly different numerical methods were developed to improve this computation [72, 90, 156, 169]. Furthermore, there are stepwise approaches proposed, for example, by Mokhtari et al. [120] that combine regression methods with variance-based approaches to reduce computing times. On this basis, in Section 4, a new stepwise sensitivity method is developed. By combining OAT, a subset selection, and a variance-based approach, computation costs compared to pure variance-based approaches [72, 169] are approximately halved. Furthermore, it is shown by Hübler et al. [77] that the accuracy of this new stepwise approach is better compared to most state-of-the-art simplifications (e.g. OAT analyses or regressions). Only meta-model-based concepts achieve similar accuracies and could be included in the new stepwise approach to enhance it.

The field of global sensitivity analysis is extensive. Nevertheless, examples of sensitivity analyses in offshore wind energy, even for parts of a turbine, are rare. In most cases, the term “sensitivity analysis” is used for an investigation of different parameter constellations [23, 31, 131] or local methods are used [7]. For onshore turbines, Robertson et al. [147] use the elementary effects approach to conduct a comprehensive global sensitivity analysis of wind parameters. For offshore applications, a “real” global sensitivity analysis can be found in the work of Ziegler et al. [219]. Ziegler et al. investigate fatigue loads for different site conditions. In addition to simple OAT variations, they use scatter plots to analyse randomly generated samples. In the PSA-OWT project [69], linear regressions with Pearson correlation coefficients and coefficients of determination are used. The sensitivity of eigenfrequencies of OWTs to changing environmental conditions, material, and geometrical parameters is investigated. Velarde et al. [203] use linear regressions. They evaluate the sensitivity of various ECs with regard to ULS and FLS loads of a gravity-based foundation of an OWT. Stieng and Muskulus [187] analyse the global sensitivity of the failure probability of an entire OWT. They apply a simplified, uncoupled time-domain model and investigate the sensitivity of four parameters using a rank correlation. Hübler et al. [77] compare the accuracy and computational efficiency of different global sensitivity methods for OWTs. They utilise a coupled time-domain model, but limit their investigations to a single load case.

Nonetheless, only with a reduced number of uncertain parameters, probabilistic time-domain

simulations are possible nowadays. To perform a well-founded reduction, global sensitivity analyses are indispensable. Since there is a lack of “real” global sensitivity analyses for OWTs, this topic is addressed in Section 4.

1.2.8 Long-term extrapolation

Current standards require aero-elastic time-domain simulations for the certification of wind turbines [53, 84]. Using these simulations, it has to be proved that requirements regarding failure modes (cf. Section 1.2.4) are met. This means that ULS and FLS proofs have to be fulfilled. However, simulations for a lifetime of 20 years for FLS or even 50 years for ULS are not manageable. Therefore, long-term extrapolations have to be applied. Using an adequate long-term extrapolation, a certain amount of 10-minute simulations is sufficient to approximate FLS and ULS loads with an appropriate accuracy. Effects like time-dependent material properties (e.g. ageing, corrosion) are not considered by these extrapolation approaches or just in a simplified form. In the following, state-of-the-art methods for the FLS extrapolation are summarised. Subsequently, although ULS is not the focus of this thesis, some approaches for the ULS extrapolation are presented.

Fatigue limit state

For FLS, in a first step, short-term (10-minute) values have to be calculated, as fatigue cannot be measured or simulated directly. In a second step, short-term values have to be extrapolated to lifetime values.

On the one hand, for short-term damages, the procedure is fairly standardised. Recommendations are given by the standards [53, 84]. An illustrative overview of fatigue values based on measurements can be found in Hübler et al. [78] and is presented in Fig. 1-10.

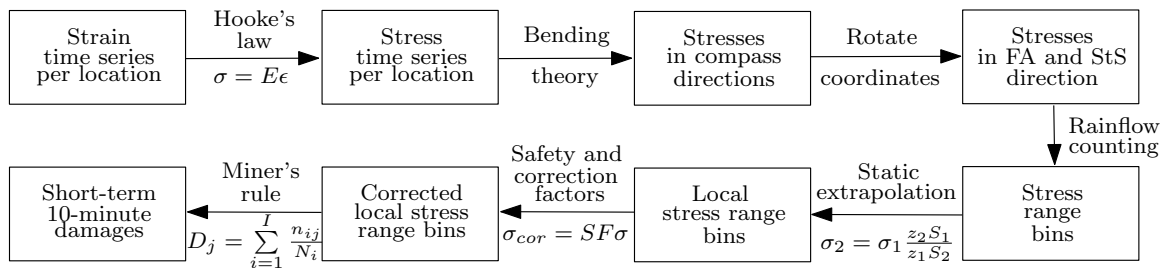


Figure 1-10: Flowchart presenting the short-term damage calculation procedure based on strain measurements or simulated strains according to Hübler et al. [78] (FA: fore-aft, StS: side-to-side).

The required steps are the following: At first, time series of stresses at all relevant locations (e.g. blade root, mudline, welded connections, etc.) have to be determined using either simulated forces and moments or measured strains. As stresses vary around the circumference of the considered location, a directional dependence has to be taken into account. In this context, several approaches are used: rotation of coordinates so that all stresses are in fore-aft or side-to-side direction [78], use of several points around the circumference [38], etc. Second, rainflow counting [44, 137] is applied to stress time series. Rainflow counting

determines the number of stress cycles for different stress ranges. Strictly speaking, rainflow counting should only be applied to cycles with zero mean. Therefore, for cycles with non-zero mean values, corrections like the Goodman correction [54] can be applied. Third, since stresses are significantly higher at details like notches, welds, holes, etc., hot spot stresses have to be calculated. Therefore, so-called "stress concentration factors" (SCF) - being defined in standards [38, 48] - are applied to nominal stresses to correct them for increased stresses at hot spots. Lastly, the conservative linear damage accumulation according to the Palmgren-Miner rule and S-N curves (stress range versus maximum number of allowed cycles) according to standards [38, 48] are utilised to determine the produced fatigue damage of the considered short-term (10-minute) period:

$$D_{10min} = \sum_{i=1}^I \frac{n_i}{N_i}, \quad (1.11)$$

where n_i is the number of cycles associated with the stress amplitude $\Delta\sigma_i$, N_i is the endurance (number of cycles) for the same stress amplitude, and I is the number of considered stress range bands/bins.

On the other hand, the extrapolation of short-term to long-term (i.e. lifetime) damages is neither extensively investigated nor standardised. Although there are some requirements in standards [53, 84], they remain fairly vague. For fatigue calculations, for different ECs, the data space should be divided into bins. In each bin, at least six simulations of 10 minutes have to be conducted. For wind speeds, bins with a resolution of less or equal than 2 m s^{-1} are required. For wave conditions, it is only stated that number and resolution have to be sufficient. Bins for other ECs like turbulence intensities are not suggested. Hence, to reduce computing times, in academia, commonly, only wind speed bins are used [131, 204, 220] and all other ECs are assumed to be constant in each bin. In industry, a finer binning and bins for more ECs are normally used. This grid-based approach is numerically inefficient [55] and leads to a high computation effort [185] that is hardly practical in academia and quite expensive in industry. Recently, Müller and Cheng [126] have shown that constant ECs in each wind speed bin cannot reproduce the scattering in offshore fatigue measurements. Furthermore, Zwick and Muskulus [220] show that using six simulations per bin and exclusively wind speed bins (minimum requirements according to standards) leads to highly uncertain approximations of lifetime damages. This effect is intensified, if scattering ECs within each bin are included, as it is done by Häfele et al. [60]. The authors show that even for 2048 overall simulations, distributed to bins according to the statistical occurrence distribution of the wind speed, the error in the damage at an X-joint of the OC4 (Offshore Code Comparison Collaboration Continuation) jacket is more than 10% with a probability of 5% (95th percentile). This is why it is necessary to use better extrapolation methods. A straightforward approach is the use of bins for several ECs (not only wind speed) and a high resolution, as conducted by Stewart [185]. This grid-based approach is normally used in industry, but in an academic context, it leads to hardly manageable computing times. Moreover, Graf et al. [55] and Chian et al. [26] demonstrated that it is numerically inefficient for high input space dimensions. Therefore, there is a current research focus on methods reducing the computational effort while preserving a high accuracy. There are two possibilities to achieve this aim: meta-models and advanced sampling techniques. Meta-modelling for fatigue damages is applied, for example, by Zwick and Muskulus [221]. They

reduce the number of simulations by a factor of seven without adding a significant amount of additional uncertainty by applying a multivariate linear regression. Toft et al. [199] use, *inter alia*, a central composite design as meta-model for fatigue damages. Again, the increase in uncertainty due to the meta-model is small compared to the uncertainty introduced by the finite number of simulated random seeds. Murcia et al. [130] apply polynomial meta-models to calculate fatigue loads of an OWT under uncertain ECs. Müller et al. [128] estimate fatigue damages by applying an artificial neural network regression. Moreover, Huchet et al. [79–81] use an adaptive Kriging meta-model that reduces the required time-domain simulations by a factor of 7 and more. Finally, Stewart [185] evaluates different meta-models. He concludes that genetic programming is more suitable than linear regressions. Since meta-models always introduce some additional model uncertainty, advanced sampling techniques are an alternative. Here, Stewart [185] assesses the performance of a so-called “probability sorting method” that focuses sampling on the most frequently occurring bins. This has the advantage that bins that do not occur in reality - e.g. a calm sea during a storm - are not simulated. This approach is similar to the approach by Häfele et al. [61]. Häfele et al. generate samples according to the dependent probability distribution functions of all considered ECs. Hence, only frequently occurring conditions are taken into account. Müller and Cheng [127] apply quasi-random sampling based on Sobol’ sequences. This is intended to achieve a better space filling design compared to random sampling. However, the problem of all these approaches is that a low occurrence probability does not necessarily imply an insignificant contribution to the overall lifetime damage. For this reason, Stieng and Muskulus [188, 189] apply a sparse version of the state-of-the-art grid-based approach that only uses grid points with a significant influence on the lifetime damage. The challenge of this approach is to identify the most important grid points. For this purpose, Stieng and Muskulus conduct a computationally expansive preliminary study using a full grid. Hence, their approach can be improved with respect to the computing time. In this thesis, alternative sampling concepts are developed and validated in Section 5.1 and 5.2.

Ultimate limit state

The best possible situation to determine ultimate loads is the availability of real ULS wind data. For example, Larsen and Petersen [103] measured ULS loads for a 300-year storm. However, this favourable situation cannot be assumed. Especially in the design phase, ULS loads cannot be measured. Normally, wind data of several years is available that does not include 50-year storms. Even if such an event occurs, the challenge is to recognise it. Therefore, current standards [53, 84] define design load cases (DLCs) that have to be simulated. First, these DLCs are based on extreme ECs, like 50-year storms. Second, fault conditions and other special events have to be simulated. And lastly, for blades, extreme loads at normal operation have to be extrapolated, since the highest loads (i.e. ultimate loads) can also occur at rated wind speed and not only under extreme environmental conditions [25].

Regarding the first type of DLCs (extreme ECs): If extreme ECs are not available, a common approach is to use maxima of smaller time periods, like one year or four weeks. Annual maxima have the advantage that seasonal effects are covered as described by Schmidt and Hansen [161]. However, in many cases the amount of annual maxima is far too small [163]. Therefore, Schmidt et al. propose 4-week maxima [160, 163]. These maxima are fitted with

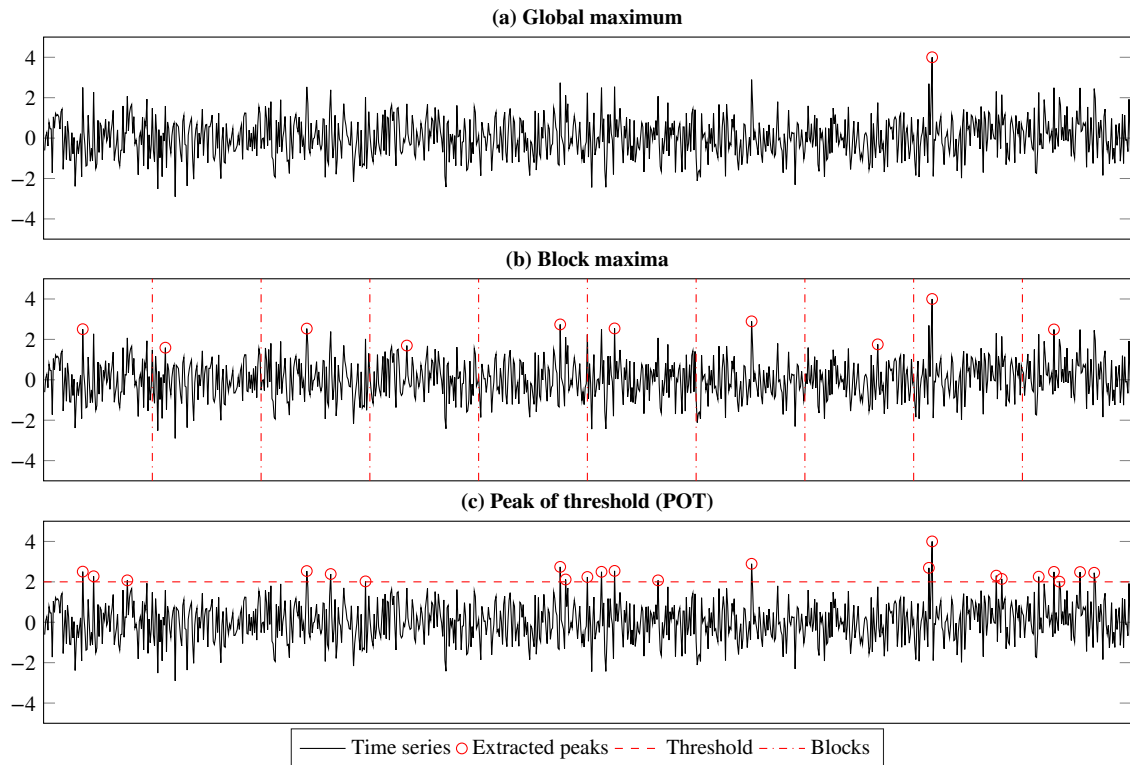


Figure 1-11: Generic, exemplary time series that illustrates the picked maxima of various peak extraction methods: (a) taking the global maximum of the time series (b) subdividing the time series in blocks and using the maximum of each block (c) extracting all peaks above a given threshold.

an extreme value distribution type-I (i.e. Gumbel distribution) that can easily be shifted to other reference periods. So, annual distributions can be computed. The ULS wind speeds are calculated as the 98th quantile of the annual extreme value distribution.

DLCs for fault conditions and other special events need separate treatment, since they are nearly completely turbine- and controller-dependent. Moreover, the ability of state-of-the-art simulation codes to model these events accurately is limited [212].

For extreme loads during normal operation, several methods extracting maximum loads from time series at different wind speeds are available. Cheng [25] and Toft et al. [197] present the three most common approaches for wind turbines: global maxima, block maxima, and POT that are illustrated in Fig. 1-11. These methods have to be combined with a weighted integration over all significant wind speeds to get a long-term distribution. Applications of these standard extrapolation methods can be found, for example, in Moriarty et al. [124] or Lott and Cheng [109]. Still, all these methods lead to quite uncertain results as shown by van Eijk et al. [202]. An alternative to these three more common methods is the average conditional exceedance rate (ACER) method by Naess and Gaidai [132, 133]. For the ACER method, conditional up-crossings (i.e. peaks) are used. This means that peaks are not selected independently but depending on previous values. This enables - in contrast to POT, etc. - the use of statistically dependent data without further data processing. Peaks that are too close to each other - meaning that there is just one physical maximum - are already

identified by the ACER algorithm and do not have to be sorted out in the post-processing. ACER is applied to wind speeds by Naess and Haug [134] and Karpa and Naess [98] and to the ULS design of wind turbines by Ernst and Seume [47] and Toft et al. [196].

To avoid the extrapolation of extreme loads that is necessary for the previously presented methods (e.g. POT, ACER, etc.), sampling-based approaches can be used. Sampling-based methods do not rely on an approximated long-term distribution, but actually simulate all relevant conditions that can lead to ultimate loads. However, for classical MCS, computing times are still far too high. Hence, advanced sampling methods are needed to waive extrapolation. One example is the recently developed stochastic importance sampling (SIS) by Choe et al. [27]. It is based on classical importance sampling (cf. Section 1.2.6), but accounts for the different behaviour of stochastic simulations (turbulent wind and irregular waves). Choe et al. [28] demonstrate that extreme loads of wind turbines can be determined without any extrapolation, if SIS is applied.

Normally, ULS simulations are conducted deterministically. This means that, although different stochastic representations (random seeds) of the turbulent wind field and irregular waves are simulated, ECs are kept fixed to deterministic values. For example, constant wind shear exponents are assumed [124]. The use of probabilistic inputs for ULS simulations can lead to different results, where extreme loads during normal operation are more relevant. This is discussed, for example, by Hübler et al. [75].

1.2.9 Economic effects

For OWTs, economic effects of the structural design are of special importance. This has several reasons. First, for OWTs, the reliability is less related to public safety than for other structures in civil engineering (e.g. bridges), since human life is not endangered directly. Therefore, OWT reliability is mainly an economic factor. Second, in comparison to other structures in civil engineering, OWTs are “high-volume production”. Thence, previous experience can be used for structural optimisations of many future turbines leading to more pronounced economic effects. Therefore, for OWTs, structural optimisations regarding the economic efficiency are of major interest.

In general, these optimisations can be performed based on deterministic or probabilistic models. Probabilistic models yield more realistic results due to the stochastic nature of environmental conditions acting on OWTs. For this reason, in this thesis, probabilistic models are utilised. As discussed before, deterministic models are still state of the art in OWT modelling. In any case, for optimisations regarding the economic efficiency, some kind of combined techno-economic model is needed. This means that economic effects have to be taken into account. So far, in structural optimisations of OWTs, it has been state of the art to use the structural weight as cost indicator [62, 96, 105, 138]. Even if cost models - instead of mass considerations - are applied, these models approximate costs by empirical formulations taking into account material, production, and installation costs [49, 111]. Effects on the economic viability of entire OWT projects are normally not considered. For example, interest payments or the risk of defaults on loans are not included. Moreover, target reliabilities or lifetimes are set to deterministic values (cf. level 1 to 3 reliability methods; Section 1.2.1). Hence, analyses of the trade-off between lifetime and costs are not possible. A first approach that takes variable lifetimes in engineering models for OWTs into account is presented by Ziegler et al. [218]. However, they focus on the trade-off between variable lifetimes and the structural mass and do not consider

complex economic effects. Nowadays, the missing consideration of economic effects is still typical for engineering approaches. This lack of probabilistic, interdisciplinary approaches is addressed in Section 6, where a combined probabilistic techno-economic model is proposed.

1.3 Research gap and objectives

1.3.1 Research gap

For further developments in the offshore wind energy sector, structural reliability is an important topic. To improve cost efficiency, the reliability of current and future turbines has to be sufficiently high and best possibly known. In this context, the safety factor approach - as it is state of the art - is not optimal. It is neither economic nor does it provide any information on the present reliability level. Therefore, although deterministic simulations definitively have their advantages - especially regarding computing times and seemingly unambiguous results - benefits of probabilistic concepts are indubitable. Hence, probabilistic simulation approaches for OWTs are an important field of research.

For probabilistic OWT simulations, mainly simplified and analytical models have been utilised so far. Essential research in the field of probabilistic wind turbine simulation using semi-analytical models is done by Sørensen [112, 174–176, 179, 198], Tarp-Johansen [190, 191] and Ronold et al. [151]. However, although these semi-analytical models are commonly used for safety factor calibrations [112, 179] and are quite sophisticated in a probabilistic context (e.g. some of them include system reliability effects), regarding the aero-elastic model itself, they are less accurate than time-domain simulations. Furthermore, current standards even require coupled aero-hydro-servo-elastic time-domain simulations [53, 84]. As a consequence, future probabilistic approaches should also be based on coupled time-domain simulations.

Up to now, not many probabilistic approaches have used coupled time-domain simulations and the existing approaches all have their limitations. Some examples are Cheng [25], Veldkamp [204], Muskulus and Schafhirt [131], or Müller and Cheng [127]. However, since computing times are a limiting factor for probabilistic time-domain simulations, all approaches remain simplified so far. For example, Cheng [25] and Veldkamp [204] both neglect soil-structure interaction and apply a set of probabilistic parameters that is only based on expert knowledge. Veldkamp [204] and Muskulus and Schafhirt [131] use a strongly reduced set of load cases for their fatigue calculations. Furthermore, aerodynamic and hydrodynamic effects are decoupled by Muskulus and Schafhirt [131]. Finally, complex economic effects are neglected by all of these authors, while Veldkamp [204] considers at least some simplified economic effects. All of this points out that there is a significant research gap in the field of probabilistic time-domain simulations of OWTs. This research gap is addressed by this thesis.

1.3.2 Objectives

With the research gap regarding probabilistic time-domain simulations of OWTs in mind (cf. Section 1.3.1), the overall objective of this thesis can be formulated:

Development and establishment of probabilistic analyses using coupled offshore wind turbine simulations in the time domain.

The idea of probabilistic time-domain analyses aims - in general - at the following improvements compared to state-of-the-art methods (i.e. deterministic approaches and simplified probabilistic concepts):

- More realistic simulations including complex OWT behaviour and aleatory input uncertainty
- Reduction of safety factors and/or calibration of them
- Assessment of inherent, physical uncertainties
- Determination of failure probabilities and lifetime distributions

Since probabilistic time-domain analyses are not straightforward, a number of interim goals are defined for this thesis:

- Effective OWT modelling using coupled time-domain simulations
- Comprehensive knowledge of the aleatory uncertainty of input parameters
- Reduction of computing times using efficient long-term extrapolations
- Integrated analysis using an interdisciplinary techno-economic approach

The first goal is the development of an effective soil model to improve state-of-the-art OWT models. The second one is the derivation of statistical distributions of physically uncertain parameters. Moreover, significant inputs (i.e. those parameters that have to be treated probabilistically) and non-significant ones (i.e. those inputs that can be set to deterministic values) are identified. The third aim is about improved sampling methods to reduce the computational effort of fatigue damage calculations. And finally, the last intermediate objective is the assessment of economic effects of structural design changes.

1.4 Outline and connection of publications

1.4.1 Outline

In accordance with Fig. 1-7b, seven steps are part of a complete probabilistic modelling scheme. In this thesis, five of the seven steps are investigated in detail. These five steps, corresponding to the defined interim goals/main aspects (cf. Section 1.1 and 1.3.2), also reflect the structure of this thesis.

- Deterministic model design (Section 2)
 - Development of an adequate soil model for OWT simulations in the time domain (Paper A)
- Aleatory uncertainty of input parameters (Section 3)
 - Creation of a database for statistically distributed environmental conditions for probabilistic OWT modelling based on real offshore measurements (Paper B)
- Sensitivity analysis (Section 4)
 - Hierarchical global sensitivity analysis to reduce the number of probabilistic inputs (Paper C)

- Long-term extrapolation (Section 5)
 - Determination and reduction of uncertainties in fatigue damages due to limited samples by improved sampling techniques (Paper D)
 - Validation of proposed improved sampling techniques using strain measurement data (Paper E)
- Economic effects (Section 6)
 - Investigation of economic effects of statistically distributed lifetimes and variable costs of OWT substructures (Paper F)
- Summary and outlook

1.4.2 Connection of publications

This thesis includes six journal publications (five have already been published (A-E) and one is under review with minor revision (F)). All publications cover one aspect of the full probabilistic analysis. The only exception are Papers D and E that both treat the long-term extrapolation. As a whole, they make up a comprehensive probabilistic study. Hence, the connection of the publications is described in the following.

Paper A (cf. Section 2) lays the foundation for the probabilistic analysis. In this publication, an effective soil model for the deterministic wind turbine model is developed. This work is slightly different from the others, since it has no direct connection to probabilistic modelling. Nevertheless, it is essential for the subsequent probabilistic modelling. As quite a large number of simulations is required for probabilistic analyses, the deterministic model itself (cf. Fig. 1-6) has to be very efficient. Consequently, the developed soil model in Paper A incorporates soil characteristics in the wind turbine model with high efficiency but at the expense of accuracy. The limited accuracy compared to state-of-the-art soil models is influenced by the subsequent use in probabilistic analyses.

Paper B (cf. Section 3) is the first publication dealing with a probabilistic topic. According to Fig. 1-6, besides the deterministic model, probabilistically distributed inputs are required. These distributions are provided by this second publication. Hence, it lays the probabilistic foundation for the subsequent steps. Surely, probabilistic inputs could also be taken from literature, but the provided data has the advantage of a good agreement of empirical and theoretical statistical distributions and of a single data source.

In addition to the determination of statistical distributions for probabilistic inputs, it is also important to select the “significant” parameters that are treated probabilistically and those that are fixed at deterministic values. This is done in Paper C (cf. Section 4), but without using literature recommendations (not available yet) or pure expert knowledge. Instead, sensitivity analyses are conducted. These analyses are based on simulations that are executed using the deterministic model of Paper A. The probabilistic input data is part of Paper B.

Papers D and E cover the long-term extrapolation of fatigue damages (i.e. the derivation of the lifetime distribution). Since state-of-the-art calculation methods are very ineffective in a probabilistic context, new methods are developed and validated. For the improved long-term extrapolation, again, simulations are executed using the deterministic model of Paper A. Those inputs that are most significant according to the findings of Paper C are

modelled using statistical distributions of Paper B.

Finally, economic aspects - being the last step of the proposed modelling scheme in Fig. 1-7b - are modelled probabilistically in Paper F. This work is based on the previous findings and comprises an entire probabilistic framework including a state-of-the-art deterministic model, probabilistic inputs according to Paper B and C, and a state-of-the-art fatigue extrapolation. The soil model according to Paper A and the improved fatigue extrapolation of Paper D and E are not applied here to be consistent with the state of the art. However, they could easily replace the utilised standard approaches to reduce computing times or increase accuracy.

2 Deterministic model design

To enable probabilistic analyses of OWTs using coupled time-domain simulations, at first, a deterministic time-domain model for OWTs is required. On the one hand, this model has to represent reality accurately. On the other hand, computing times have to be manageable, as probabilistic analyses can require thousands of model evaluations. In this thesis, the state-of-the-art model FAST [93] is used. However, FAST normally neglects soil-structure interaction, as standard soil models (see Section 1.2.3) are not compatible with the applied Craig-Bampton reduction [30] of FAST. Therefore, an efficient soil model that can be combined with a Craig-Bampton reduction is developed here to enhance FAST. Probabilistic aspects, for example the model uncertainty of the developed soil model, are not considered.

2.1 Research context

As discussed in Section 1.2.3 in detail, there is a large variety of soil models for OWT foundations. The more complex ones with many degrees of freedom (e.g. FE models) are not suitable for coupled time-domain simulations, but are used for detailed soil-structure interaction investigations. In time-domain coupled simulations, soil modelling ranges from soil neglect (i.e. clamped structures) to non-linear p-y curves. Different approaches are compared, for example, in the OC3 (Offshore Code Comparison Collaboration) project [95]. However, the most common soil models (i.e. p-y curves) cannot be used, if reduction schemes - like the Craig-Bampton reduction [30] - are applied. Still, to limit computing times, some kind of reduction is nearly indispensable for substructures with many DoF like jackets. Hence, alternative soil models are needed in order not to model jacket substructures as clamped to the seabed, as it is frequently done [145, 209]. Probably, the most suitable approach is the reduction of the complete soil-structure interaction to a super-element (e.g. soil matrix). Soil matrices are proposed, for example, by Zaijer [217], Dubois et al. [45], Häfele et al. [59], or in the OC3 project [140]. The advantage of these super-element formulations is that they do not necessarily add any DoF to the system (i.e. do not increase computing times). Furthermore, they do not have to be linearised, but can be formulated as a function of applied loads [45]. However, only if they are linearised, it is possible to combine them with a Craig-Bampton reduction [59]. Since computing times have to be manageable for probabilistic analyses, in this thesis, the linearised approach of Häfele et al. [59] is enhanced by including operating point dependent soil matrices.

2.2 Methods

To include soil behaviour in coupled time-domain simulations without increasing computing times significantly, the super-element approach of Häfele et al. [59] is used as a basis. Condensed soil-structure interaction matrices are included in the overall stiffness matrix of the substructure. Therefore, no additional DoF are added. Soil matrices are included

as flexible boundary conditions. P-y curves are linearised and condensed to compute soil matrices. In contrast to Häfele et al. [59], linearisations of the p-y curves are conducted not only for initial stiffnesses but for different loads. Loads are approximated a priori using a non-linear response surface linking loads and the most important ECs. This enables operating point dependent soil matrices. Furthermore, not only p-y curves according to standards [6] but also adapted versions [64, 181, 192] are investigated. For this purpose, dynamic soil-structure interaction experiments are conducted on a large scale to assess the performance of various p-y curves in a dynamic context.

2.3 Results

The present enhancement of the approach by Häfele et al. [59] creates a flexible super-element concept. Soil matrices can be used for all kinds of substructures (monopiles, jackets, etc.) with and without reduction schemes applied. Moreover, the derivation procedure of soil matrices is not regulated. This means that different p-y curves, FE models (e.g. for suction bucket foundations), or experimental results can be used to set up soil matrices.

Dynamic experimental investigations show that the suitability of p-y curves for transient OWT simulations is limited, since they cannot accurately represent the dynamic soil-structure behaviour.

Finally, when using the new soil-structure interaction approach in coupled time-domain simulations for OWTs, it is important to choose condensed p-y curves carefully. Soil modelling can significantly influence the overall OWT behaviour. The operating point (i.e. linearisation point of p-y curves) should be taken into account at least for load-sensitive p-y curves like the approach by Thieken et al. [192]. Nonetheless, a rough load approximation for the operating point is sufficient for most applications.

2.4 Outlook

In the context of efficient soil modelling, some recommendations for future research can be derived from the present work. First and most important, current p-y curves should be reconsidered. New p-y curves for dynamic applications might be advisable. Second, since p-y curves cannot describe the dynamic soil-structure interaction accurately, the use of more advanced soil models (e.g. FE models) can be an alternative. Here, the influence of the computing time should be considered. Only if many simulations with the same soil matrices are conducted, the use of FE soil models can be efficient. Third, future research could consider non-linear soil matrices, as proposed by Dubois et al. [45]. This is not a straightforward task, since Craig-Bampton reductions are not compatible with non-constant soil matrices. Nevertheless, for high-accuracy simulations, it might be valuable to adjust soil matrices at least for large load changes. Finally, regarding probabilistic simulations, it can be concluded that an inclusion of soil super-elements is a significant improvement compared to clamped substructures. More detailed models - in most cases even operating point matrices - are not essential, as inherent uncertainties exceed differences in soil modelling.

2.5 Paper A: Experimentally supported consideration of operating point dependent soil properties in coupled dynamics of offshore wind turbines

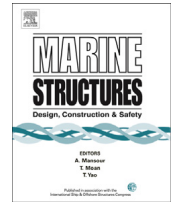
The following paper is published in *Marine Structures*, Volume 57 (2018), pages 18-37 (<https://doi.org/10.1016/j.marstruc.2017.09.002>). The main work was done by the author of this thesis. Jan Häfele contributed the fundamentals (Section 2 of Paper A) based on previous work [59]. Cristian Gebhardt and Raimund Rolfes contributed with advisory and supporting work. Special thanks go to “Fraunhofer-Institut für Windenergie und Energiesystemtechnik” (IWES) Hannover and to “Testzentrum Tragstrukturen Hannover” (TTH) for preparing the test pit and installing piles.



ELSEVIER

Contents lists available at ScienceDirect

Marine Structures

journal homepage: www.elsevier.com/locate/marstruc

Experimentally supported consideration of operating point dependent soil properties in coupled dynamics of offshore wind turbines



Clemens Hübler*, Jan Häfele, Cristian Guillermo Gebhardt, Raimund Rolfes

Institute of Structural Analysis, Leibniz Universität, Hannover, Germany

ARTICLE INFO

Article history:

Received 23 November 2016

Received in revised form 15 August 2017

Accepted 20 September 2017

Keywords:

Soil-structure interaction

Dynamic soil experiments

Offshore wind turbine

FAST

p-y curves

Component-mode synthesis

ABSTRACT

The consideration of soil properties is necessary to predict the time domain dynamic behavior of offshore wind turbines. Accurate soil-structure interaction models are in essence very expensive in terms of computing time and therefore, not directly applicable to transient calculations of wind energy converters. In this work, the incorporation of dynamic soil properties is addressed. The basic model, previously developed by the authors, is based on a linearized approach using stiffness and mass matrices representing the soil-structure interaction. This approach already leads to significant reductions of the eigenfrequencies compared to clamped boundary conditions which are still commonly used. Here, the basic approach is enhanced by two aspects. Firstly, different numerical soil models, based on nonlinear springs, to calculate the matrices are compared to experimental results for embedded piles at conditions similar to the North Sea. Comparisons of numerically and experimentally determined eigenfrequencies of the piles show that nonlinear spring models are only suitable for dynamic analyses to a limited extent. Secondly, a piecewise defined response surface, which enables a linearization of the nonlinear soil behavior at different approximated operating points, is introduced. This approximation proves to be sufficiently accurate in the current setting. By analyzing two full offshore wind turbine examples in time domain, a monopile substructure and a jacket substructure anchored by piles, further shifts of the eigenfrequencies, being caused by the load-dependent mechanical properties of the soil, are determined by considering the operating point.

© 2017 Elsevier Ltd. All rights reserved.

1. Introduction

Time domain simulations are entailed in design and certification of offshore wind turbines. Standards and guidelines require ultimate and fatigue limit state verifications. In this connection, fully coupled aero-hydro-servo-elastic simulation codes for the whole offshore wind turbine including the substructure are state of the art. One major challenge is the consideration of effects of the soil on the dynamic behavior of the whole turbine in the aforementioned coupled models. The behavior of the soil is highly nonlinear and its stiffness strongly depends, inter alia, on the acting loads. This applies to all kinds of anchorages like piles or suction buckets. Still, in this work only pile foundations are considered. The spectrum of soil-

* Corresponding author.

E-mail address: c.huebler@isd.uni-hannover.de (C. Hübler).

structure interaction models for pile foundations reaches from very complex and nonlinear finite element models [6,14] to simplified but still nonlinear static p-y curves [4,39]. Furthermore, there exist other nonlinear models based on CPTs cone penetration tests [2]; or spring-damper combinations with varying complexity [36]. However, these sophisticated, nonlinear soil-structure interaction models are commonly not coupled with the whole wind turbine, but loads - for example calculated with previously run turbine simulations - are just applied at mudline. The high number of degrees of freedom required by all sophisticated soil-structure interaction models and the complexity of offshore wind turbines are the reasons for this decoupled procedure. To illustrate this problem: For jacket structures in the oil and gas industry, wind loads and controller actions can be neglected or are not existent and fewer load cases have to be calculated. Therefore, in the oil and gas industry nonlinear soil models in combination with time domain simulations are used for example by Ref. [7] or [28]. For transient, coupled wind turbine simulations with noticeable demands for numerical efficiency in their current form due to high computational cost for a single simulation and the large number of simulations that is required to satisfy the certification standards, these models are only partly suitable. That is why, nowadays in transient simulations, offshore wind turbines are often modeled as clamped to the seabed, for instance, see Ref. [9]. These authors outline the implementation of a structural dynamics module for offshore wind turbines with space-frame substructures into the current FAST framework (an aeroelastic simulation code by the National Renewable Energy Laboratory, NREL) where the soil is considered to be rigid [26]. use nonlinear spring models in wind turbine simulations even for optimization purposes. However, the authors only analyze eigenfrequencies, and no time domain simulations are conducted. The work of [3] is one of the few recent cases that incorporates a nonlinear soil model in time domain simulations of offshore wind turbines and studies seismic responses. However, this leads to very high computing times, as a full FE model of the substructure is needed, and the substructure cannot be condensed. Hence, only a few load cases can be simulated in an adequate time.

A promising approach to enhance time domain simulations of offshore wind turbines by considering soil properties effectively with reasonable computing times is a two-step approach by Ref. [19]. This approach is based on linear 6×6 stiffness and mass matrices representing the soil-structure interaction and allows an effective consideration of soil characteristics in transient, coupled simulations of offshore wind turbines, even if the substructure is - as in common practice - condensed with reduction methods like a Craig-Bampton reduction, for instance. However, as the matrices are linear, the nonlinear behavior of the soil is not taken into account. A linearization is carried out at the zero-deflection point of the piles. This means that no loads are applied to the pile head and therefore, the pile is not deflected. As the soil stiffness reduces with higher pile deflections due to increasing loads, disregarding the operating point (i.e. the load conditions) is a simplification, though it is much less serious than assuming clamped boundary conditions.

The contribution of the present work comprises two aspects. The approach developed by Ref. [19]; named “basic approach” throughout this work, uses nonlinear springs (i.e. p-y curves) of the American Petroleum Institute [4] to determine the soil matrices. However, in literature, other p-y curves are available as well. On the one hand [39], and approaches developed by Refs. [33,34] are supposed to give better approximations of the soil stiffness for ultimate loads. On the other hand [25], give a changed formulation for p-y curves being more suitable for small and initial loads [27]. introduce a new formulation for initial stiffnesses and reduce the internal friction angle in order to get better results for small and ultimate loads [35]. compare different p-y curves with a calibrated FE model. On the basis of their findings that none of the p-y curves leads to sufficient results, completely new p-y curves are developed that are supposed to be more suitable for all load conditions. In this work, firstly, large-scale experiments to determine the dynamic soil properties of embedded piles are presented. These results are then compared to numerical results obtained with different p-y models. An assessment, based on the experimental results, of the nonlinear spring models in the current dynamic context is possible, although it has to be kept in mind that p-y curves are initially derived from static conditions. Still, due to the lack of alternatives, they are used for dynamic applications as well. Secondly, an enhancement of the basic approach concerning the linearization is presented. As the method requires linearized interaction matrices, the present refined approach linearizes at the actual operating point and no longer at the zero-deflection point. This improvement allows the incorporation of variable soil stiffnesses for different environmental conditions. Even for the different piles of a jacket substructure, the soil stiffness can vary. In order to determine the acting loads at a specific operating point effectively, response surfaces (RSs) linking the environmental conditions to the loads at mudline are utilized.

The present paper is structured as follows: Firstly, a short overview of the basic two-step soil consideration approach is given. For detailed explanations, it is referred to [19]. Subsequently, different nonlinear spring models for calculating the stiffness matrices are introduced. Experimental results of the dynamic behavior of soil-pile combinations are presented and discussed. These results are then compared to numerical results using the different nonlinear spring models in order to evaluate the suitability of these models. A new approach to determine loads at the operating point, using response surfaces, is described afterwards, and some results of the load approximation by the response surface method are presented. In this connection, results of coupled time domain simulations of an offshore wind turbine with jacket substructure and monopile substructure are given, whereas the operating point is neglected in the first place. The calculations are conducted with the aero-hydro-servo-elastic simulation code FAST. Then, further examples illustrate the effect of using different p-y models on the interaction matrices and on the overall turbine behavior. Furthermore, differences between the use of the zero-deflection point and the response surface method for the consideration of the operating point are pointed out. Lastly, conclusions are drawn, pointing out limitations and giving an outlook on future work.

2. Fundamentals

2.1. Effective consideration of soil-structure interaction in coupled analyses of offshore wind turbines

The basis of the present work is a methodology for numerically efficient consideration of soil characteristics in fully coupled wind turbine simulations described by Ref. [19]. This approach is based on a reduction method by Ref. [8] and is briefly outlined in this section. The interested reader is referred to the original work for further information.

It is presumed that the equations of motion were derived in the general form:

$$\mathbf{M}\vec{u} + \mathbf{C}\dot{\vec{u}} + \mathbf{K}\vec{u} = \vec{F}. \quad (1)$$

\mathbf{M} is the mass matrix, \mathbf{C} the damping matrix, \mathbf{K} the stiffness matrix, \vec{u} the displacement vector along all degrees of freedom and \vec{F} comprises the corresponding external forces. The vector \vec{u} is partitioned into subvectors of boundary and interior displacements \vec{u}_R and \vec{u}_L , respectively:

$$\vec{u} = \begin{pmatrix} \vec{u}_R \\ \vec{u}_L \end{pmatrix}. \quad (2)$$

2.2. The partition yields

$$\begin{pmatrix} \mathbf{M}_{RR} & \mathbf{M}_{RL} \\ \mathbf{M}_{LR} & \mathbf{M}_{LL} \end{pmatrix} \begin{pmatrix} \vec{u}_R \\ \vec{u}_L \end{pmatrix} + \begin{pmatrix} \mathbf{C}_{RR} & \mathbf{C}_{RL} \\ \mathbf{C}_{LR} & \mathbf{C}_{LL} \end{pmatrix} \begin{pmatrix} \dot{\vec{u}}_R \\ \dot{\vec{u}}_L \end{pmatrix} + \begin{pmatrix} \mathbf{K}_{RR} & \mathbf{K}_{RL} \\ \mathbf{K}_{LR} & \mathbf{K}_{LL} \end{pmatrix} \begin{pmatrix} \vec{u}_R \\ \vec{u}_L \end{pmatrix} = \begin{pmatrix} \vec{F}_R \\ \vec{F}_L \end{pmatrix}. \quad (3)$$

The stiffness matrix \mathbf{K} in Eq. (1) is singular due to rigid body motions. In the next step, the displacements at points of interest are allocated to \vec{u}_R and \vec{u}_L :

$$\vec{u}_R = \vec{u}_{int}, \quad (4)$$

$$\vec{u}_L = \begin{pmatrix} \vec{u}_I \\ \vec{u}_{base} \end{pmatrix}, \quad (5)$$

where \vec{u}_{int} comprises the displacements at the interface between substructure and tower, \vec{u}_I the displacements of all interior nodes, except the nodes at the interface between structure and soil (base nodes), and \vec{u}_{base} the base node displacements. It follows:

$$\mathbf{M}_{LL} = \begin{pmatrix} \mathbf{M}_I & \mathbf{M}_{I,base} \\ \mathbf{M}_{base,I} & \mathbf{M}_{base} \end{pmatrix}, \quad (6)$$

$$\mathbf{K}_{LL} = \begin{pmatrix} \mathbf{K}_I & \mathbf{K}_{I,base} \\ \mathbf{K}_{base,I} & \mathbf{K}_{base} \end{pmatrix}. \quad (7)$$

\mathbf{M}_{base} and \mathbf{K}_{base} contain the terms from the structural system assembly $\mathbf{M}_{base,ij}$ and $\mathbf{K}_{base,ij}$. The soil terms from the mass and stiffness matrices $\mathbf{M}_{soil,i}$ and $\mathbf{K}_{soil,i}$ are assembled at the level of the main diagonal blocks. The modified matrices \mathbf{M}_{base}^* and \mathbf{K}_{base}^* read

$$\mathbf{M}_{base}^* = \begin{pmatrix} \mathbf{M}_{base,11} + \mathbf{M}_{soil,1} & \cdots & \mathbf{M}_{base,1n} \\ \vdots & \ddots & \vdots \\ \mathbf{M}_{base,n1} & \cdots & \mathbf{M}_{base,nn} + \mathbf{M}_{soil,n} \end{pmatrix} \quad (8)$$

$$\mathbf{K}_{base}^* = \begin{pmatrix} \mathbf{K}_{base,11} + \mathbf{K}_{soil,1} & \cdots & \mathbf{K}_{base,1n} \\ \vdots & \ddots & \vdots \\ \mathbf{K}_{base,n1} & \cdots & \mathbf{K}_{base,nn} + \mathbf{K}_{soil,n} \end{pmatrix}. \quad (9)$$

Some substitutions yield.

$$\begin{pmatrix} \mathbf{M}_{RR} & \mathbf{M}_{RL} \\ \mathbf{M}_{LR} & \mathbf{M}_{LL}^* \end{pmatrix} \begin{pmatrix} \vec{u}_R \\ \vec{u}_L \end{pmatrix} + \begin{pmatrix} \mathbf{C}_{RR} & \mathbf{C}_{RL} \\ \mathbf{C}_{LR} & \mathbf{C}_{LL} \end{pmatrix} \begin{pmatrix} \dot{\vec{u}}_R \\ \dot{\vec{u}}_L \end{pmatrix} + \begin{pmatrix} \mathbf{K}_{RR} & \mathbf{K}_{RL} \\ \mathbf{K}_{LR} & \mathbf{K}_{LL}^* \end{pmatrix} \begin{pmatrix} \vec{u}_R \\ \vec{u}_L \end{pmatrix} = \begin{pmatrix} \vec{F}_R \\ \vec{F}_L \end{pmatrix}. \quad (10)$$

In the next step, a Ritz transformation is applied in order to reduce the size of \vec{u}_L where the transformation matrix Φ maps \vec{u}_L onto the generalized coordinates \vec{q}_m :

$$\begin{pmatrix} \vec{u}_R \\ \vec{u}_L \end{pmatrix} = \Phi \begin{pmatrix} \vec{u}_R \\ \vec{q}_m \end{pmatrix}. \quad (11)$$

For this purpose, a Component-Mode Synthesis is utilized, where the matrix Φ contains constraint modes Φ_R and fixed-interface normal modes Φ_L :

$$\Phi = \begin{pmatrix} \mathbf{I} & \mathbf{0} \\ \Phi_R & \Phi_L \end{pmatrix}, \quad (12)$$

In this equation, \mathbf{I} is the identity matrix, and $\mathbf{0}$ is the zero matrix.

To calculate Φ_R , the homogenous (all derivatives with respect to time set to zero), static (all boundary DOFs set to unit displacement) case is considered in Eq. (10), leading to:

$$\Phi_R = -\mathbf{K}_{LL}^{*-1} \mathbf{K}_{LR}. \quad (13)$$

The matrix of fixed-interface normal modes Φ_L is obtained by solving the eigenvalue problem.

$$\mathbf{K}_{LL}^* \Phi_L = \Omega_m^2 \mathbf{M}_{LL}^* \Phi_L. \quad (14)$$

The approach of the Component-Mode Synthesis is to use Φ_m which depicts a truncated subset of Φ_L neglecting the modes corresponding to higher frequencies. This procedure is valid as long as the excitation frequency is distinctly within the range of covered eigenfrequencies in Φ_m . Applied to Eq. (10), the following is obtained:

$$\begin{pmatrix} \mathbf{M}_{BB} & \mathbf{M}_{Bm} \\ \mathbf{M}_{mB} & \mathbf{I} \end{pmatrix} \begin{pmatrix} \vec{u}_R \\ \vec{q}_m \end{pmatrix} + \begin{pmatrix} \mathbf{0} & \mathbf{0} \\ \mathbf{0} & 2\xi\Omega_m \end{pmatrix} \begin{pmatrix} \vec{u}_R \\ \vec{q}_m \end{pmatrix} + \begin{pmatrix} \mathbf{K}_{BB} & \mathbf{0} \\ \mathbf{0} & \Omega_m \end{pmatrix} \begin{pmatrix} \vec{u}_R \\ \vec{q}_m \end{pmatrix} = \begin{pmatrix} \vec{F}_R + \Phi_R^T \vec{F}_L \\ \Phi_m^T \vec{F}_L \end{pmatrix}, \quad (15)$$

with

$$\mathbf{M}_{BB} = \mathbf{M}_{RR} + \mathbf{M}_{RL} \Phi_R + \Phi_R^T \mathbf{M}_{LR} + \Phi_R^T \mathbf{M}_{LL}^* \Phi_R, \quad (16)$$

$$\mathbf{M}_{mB} = \Phi_m^T \mathbf{M}_{LR} + \Phi_m^T \mathbf{M}_{LL}^* \Phi_R, \quad (17)$$

$$\mathbf{M}_{Bm} = \mathbf{M}_{mB}^T, \quad (18)$$

$$\mathbf{K}_{BB} = \mathbf{K}_{RR} + \mathbf{K}_{RL} \Phi_R. \quad (19)$$

In this equation, a viscous damping was introduced that affects each mode. Damping effects on the interface nodes are neglected. Ω_m is the diagonal matrix of eigenvalues corresponding to the truncated subset of eigenvectors in Φ_m . ξ is the critical viscous damping affecting the fixed-interface normal modes. ξ can be easily considered as a diagonal matrix as well, if different damping values for each mode are desirable.

As $\det(\Omega_m^2)$ and $\det(\mathbf{K}_{BB})$ are each greater than zero, the stiffness matrix in Eq. (15) is regular, and rigid body motions are removed from the system. This obviates the need to apply kinematic boundary conditions.

2.3. Application to state-of-the-art bottom-fixed substructure concepts

The proposed method is applicable to most state-of-the-art substructure concepts. However, in particular two types are of special interest, as they are important for practical applications in offshore wind engineering. These are monopiles and jackets.

Up to now, the most used substructures are monopiles for economic reasons. In general, this substructure type is relatively soft. Moreover, the effect of soil-structure interaction is high, as it is a single pile being rammed into the seabed. As it is nearly coaxial to the vertical center axis of the entire structure, the foundation is affected by a large overturning bending moment. These physical effects are supposed to lead to a point, where the monopile concept reaches its limits: For high water depths or turbines with high power, the structure gets too soft, and resonance problems due to rotor motion or wave excitation might occur. In such cases, jackets become a more reasonable alternative, as the loads are distributed on commonly three (for newer concepts) or four foundation piles. Additionally, the vertical forces at the base nodes are not aligned with the jacket center axis which implies that the bending moment on the piles is significantly lower compared to the monopile concept. Moreover, a state-of-the-art jacket, which fulfills fatigue and ultimate limit state proofs according to common standards and guidelines, is a relatively stiff structure and in this case, the structural response is dominated by the physical behavior of the upper

structural parts or the foundation. Therefore, the soil-structure interaction is very crucial for the structural behavior of jacket foundations, though the soil stiffness is usually lower compared to a monopile foundation.

2.4. Condensation of the interaction matrices

For the present consideration of soil properties in time domain calculations, the key points are the stiffness and mass matrices of the soil. The basic approach does not specify how to compute these matrices. Nevertheless, it is state of the art to use static p-y (lateral, nonlinear spring models) and T-z curves (axial, nonlinear spring models) to determine the stiffnesses in case of pile foundations, though these curves were developed for static loads. Current guidelines recommend to calculate the spring stiffnesses for the p-y and T-z curves according to [4]. However, the calculated stiffnesses are differing a lot from experimental results, as it is shown for instance by Refs. [2] and [16]. Experimental results are limited to static and cyclic effects. So far, to the authors' knowledge, dynamic experiments on a large scale have only been conducted for seismic excitations (e.g. Ref. [29]) and not for natural oscillations or wind turbine specific excitations. In case of seismic excitations, more sophisticated p-y curves are used that consider cyclic and damping effects as well. However, these seismic p-y curves are not suitable for the present approach, as linearized soil matrices are needed. Furthermore, seismic loads are not comparable to those for wind turbines. Experimental results of dynamic soil tests conducted by the authors and comparisons with numerical results computed with different static p-y curves are presented in the next section. Other methods to calculate the nonlinear spring stiffnesses, which are supposed to handle some shortcomings of the API approach, were developed by Refs. [25,27,34] and [35]; just to mention a few of them. For the axial stiffnesses, cone penetration test (CPT) based methods have already been included in current guidelines [5].

The present approach uses soil matrices instead of nonlinear springs. Still, these curves can be used for the derivation of the interaction matrices. The procedure is the following: A pile is discretized with Timoshenko beam elements in an FE solver (e.g. ANSYS). Nonlinear spring elements are distributed in all spatial coordinate directions along its length. A selection of the different p-y methods is used by the authors. As the system will be linearized only once at the beginning, an operating point has to be chosen before starting a time domain simulation. The choice of the operating point is important, as increasing pile deflections and acting loads reduce the stiffnesses significantly. For example, according to the [4]; the following equation for the lateral stiffness, visualized in Fig. 1, applies:

$$E_{py} = \frac{\partial}{\partial y} \left[A p_u \tanh \left(\frac{kz}{A p_u} y \right) \right] = \frac{kz}{\cosh^2 \left(\frac{kz}{A p_u} y \right)}, \quad (20)$$

where E_{py} is the secant soil-spring stiffness, p_u is the maximum subgrade reaction, y is the lateral pile deflection, k is the increase in initial soil stiffness with depth, A is a calibration factor for static or cyclic loading and z is the depth below the seabed.

Other lateral as well as axial nonlinear spring models also predict smaller stiffnesses for higher loads. Hence, an effective way of choosing an operating point and determining the loads at mudline for this operating point is desirable and presented in section "Operating Point Analysis". After having selected an operating point, the entire dynamic pile-spring system behavior is linearized at the chosen operating point. Subsequently, it is condensed in the pile head or at the uppermost point. The static condensation due to [15] is applied for this purpose. As the p-y and T-z curves do not specify a torsional stiffness k_ψ , a rudimentary approach according to [13] is used to calculate the initial torsional stiffness. However, studies carried out by the

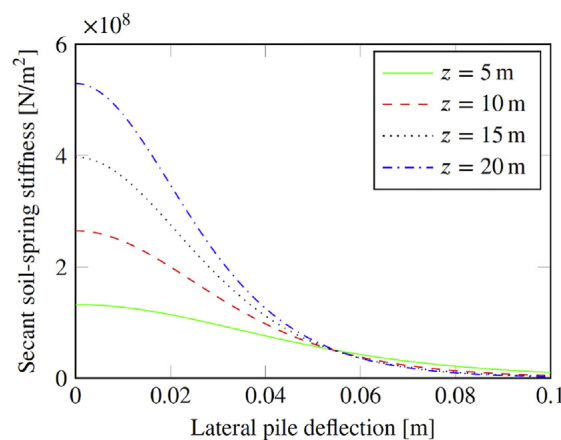


Fig. 1. Plot of the secant soil-spring stiffness according to the [4] for an exemplary monopile with an embedded length of $L = 20$ m and a diameter of $d = 6$ m for different depths z and lateral deflections.

authors have shown that the torsional stiffness does not have a major impact on the overall turbine behavior. The presented procedure yields the stiffness matrix as follows:

$$\mathbf{K}_{soil} = \begin{pmatrix} k_x & 0 & k_{xz} & 0 & -k_{x\theta} & 0 \\ 0 & k_y & k_{yz} & k_{y\phi} & 0 & 0 \\ k_{zx} & k_{zy} & k_z & -k_{z\phi} & -k_{z\theta} & 0 \\ 0 & k_{\phi y} & -k_{\phi z} & k_\phi & 0 & 0 \\ -k_{\theta x} & 0 & -k_{\theta z} & 0 & k_\theta & 0 \\ 0 & 0 & 0 & 0 & 0 & k_\psi \end{pmatrix}. \quad (21)$$

The coordinate system is the following: x is in wind direction, y is to the left (looking in x direction) and z is upwards (c.f. Fig. 10). The corresponding rotational DOFs with respect to x , y , and z are ϕ , θ , and ψ .

The mass matrix has the same form. For the mass matrix, only the pile weight is considered and no added masses due to the surrounding soil. This is a simplification. However, this work focusses on soil stiffnesses, and added masses are not a straightforward problem. Furthermore, Table 1 suggests that the influence of the mass matrix can be disregarded in many cases. Values for the mass matrix, which do not incorporate added soil masses, can be found in Ref. [19]. However, these values are in general several orders higher, if added masses are included.

For a pile foundation and the present approach, the soil model is energy-conservative, and there is no axial-lateral coupling. Therefore, the matrix in Eq. (21) becomes symmetric and simplifies to:

$$\mathbf{K}_{soil} = \begin{pmatrix} k_x & 0 & 0 & 0 & -k_{x\theta} & 0 \\ 0 & k_y & 0 & k_{y\phi} & 0 & 0 \\ 0 & 0 & k_z & 0 & 0 & 0 \\ 0 & k_{y\phi} & 0 & k_\phi & 0 & 0 \\ -k_{x\theta} & 0 & 0 & 0 & k_\theta & 0 \\ 0 & 0 & 0 & 0 & 0 & k_\psi \end{pmatrix}. \quad (22)$$

Exemplary values for the pile stiffnesses calculated, using the proposed procedure and utilized for the calculations in the section “Time Domain Results with Initial Soil Stiffnesses”, are given in Table 2.

The same reduction scheme can also be adapted for other foundation types like suction buckets. In this case, if soil models without energy conservation are applied, unsymmetrical stiffness matrices arise (e.g. $k_{x\theta} \neq k_{\theta x}$), and if lateral and axial coupling terms are included, all the entries in Eq. (21) are nonzero (e.g. $k_{xz} \neq 0$; see Ref. [20]).

3. Dynamic soil tests and model assessments

3.1. Experiments for embedded piles

In the last section, several different p - y curves, which can be used to compute linearized soil matrices, were introduced. However, in literature there is no consensus concerning the suitability of these models. There are some comparisons of the different p - y models with FE models and/or experiments in order to find the most accurate p - y model. However, these studies mainly consider static loads or in a few cases cyclic loads. An example is the work of [35]. For the calculation of the stiffness matrices, the dynamic behavior, even if it is linearized, is of interest as well. Therefore, in this work, the different p - y models are compared to dynamic measurements of large-scale pile tests. Axial T- z models are not compared here, as the differences

Table 1

Maximum and mean shear forces (\mathbf{H}) and bending moments (\mathbf{M}) at mudline of an OC3 monopile calculated using FAST and the “basic soil-structure interaction approach”. All input values are the same (standard load case at rated wind speed), only the entries of the mass matrices are two orders higher (e.g. $\mathbf{m}_{x,case 1} = 7 \times 10^4$ and $\mathbf{m}_{x,case 2} = 7 \times 10^6$).

Case	H_{max} [MN]	H_{mean} [MN]	M_{max} [MNm]	M_{mean} [MNm]
1	1.4360	0.68981	97.661	78.581
2	1.4426	0.68982	97.658	78.610

Table 2

Soil stiffness parameters for an exemplary pile foundation of a jacket substructure regarded in the section “Time Domain Results with Initial Soil Stiffnesses” calculated with the presented approach in this section and spring models according to [4].

k_x [Nm^{-1}]	k_y [Nm^{-1}]	k_z [Nm^{-1}]	k_ϕ [Nm]
3.56×10^8	3.56×10^8	2.91×10^9	1.2×10^{10}
k_θ [Nm]	k_ψ [Nm]	$k_{x\theta}, k_{\theta x}$ [N]	$k_{y\phi}, k_{\phi y}$ [N]
1.2×10^{10}	2.45×10^{10}	1.62×10^9	1.62×10^9

in vertical soil models can frequently be neglected [20], and the identification of axial modes has emerged as being complicated. For the classic p-y approaches, it has to be kept in mind that they were not initially developed for dynamic applications. Nevertheless, due to the lack of alternatives, it is state of the art to use them in transient wind turbine simulations. As the development of new dynamic p-y curves is out of the scope of this work and the use of static p-y curves is requested by the standards, classic curves are investigated here. In the following, firstly, the experiments are described. Secondly, the numerical modeling is explained and lastly, results comparing experiments and numerical calculations are given.

As part of the IRPWind project and in cooperation with Fraunhofer IWES Hannover, six steel piles, as they are used for jackets, were tested on a large scale in a well-defined, sandy and water-saturated environment in a new geotechnical test pit, with the dimensions 10 m × 14 m × 9 m, at the Test Center Support Structures in Hanover. The piles have different diameters and lengths as indicated in Table 3 and were rammed into the sand. It has to be mentioned that the tested structures are jacket piles. Monopiles have significantly smaller L/d ratios. The sand conditions were investigated within the project using different methods (Cone penetration tests, soil samples and wave propagation tests). Results of the cone penetration tests are shown in Figs. 2 and 3. Fig. 2 displays the CPT raw data: cone resistances versus depth. For Fig. 3, relative densities are calculated using cone resistances and an empirical correlation method according to [30]. Fig. 4 shows the relative densities that are determined with soil samples. Results are comparable and a relative density of about 0.74 was determined. Hence, the sand is dense sand. The soil conditions are similar to conditions in the North Sea. Some additional information on the sand itself are given in Table 4. For further information concerning the soil preparation and testing, the interested reader is referred for example to [11]. The pile driving process was interrupted every meter, and dynamic tests were performed. The dynamic tests were conducted about half an hour after the pile driving was stopped due to limitations in the overall testing time. Surely, some long-term settling effects of the soil, being less pronounced for sand where most of the settling occurs immediately, are not covered perfectly. The first test took place after the pile had been driven in 3 m. Tests with an embedded length of less than 3 m are not possible, as the stability of the pile is not sufficient, and an inclination of the pile could occur.

The tests consist of several excitations at different heights and in all three directions with an impact hammer, and four triaxial accelerometers (20 g, 100 mV/g) attached to the piles were used to measure the decay process of the pile vibration with a sampling frequency of 2 kHz. The positions of the accelerometers were changed while the pile was driven into the soil to keep them above the ground. That is why changing sensor positions is the only possibility to achieve a fairly uniform

Table 3

Jacket pile dimensions with d , L , L_{tot} and t being the pile diameter, embedded and total length and wall thickness respectively.

	d in mm	L in m	L_{tot} in m	L/d	t in mm
Pile1	273.0	5.7	6.9	20.9	5.0
Pile2	273.0	6.7	7.9	24.5	5.0
Pile3	355.6	5.7	6.9	16.0	6.3
Pile4	355.6	6.7	7.9	18.8	6.3
Pile5	355.6	5.3	6.5	14.9	6.3
Pile6	355.6	6.7	7.9	18.8	6.3

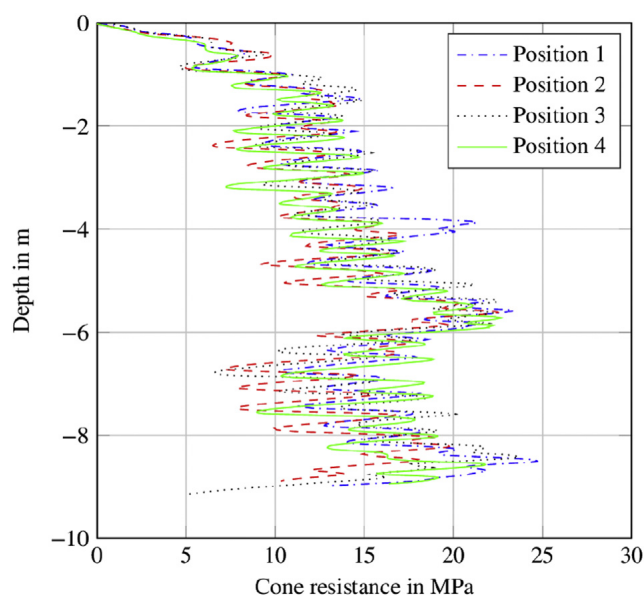


Fig. 2. Results of the cone penetration tests: cone resistance versus depth for four different positions in the test pit.

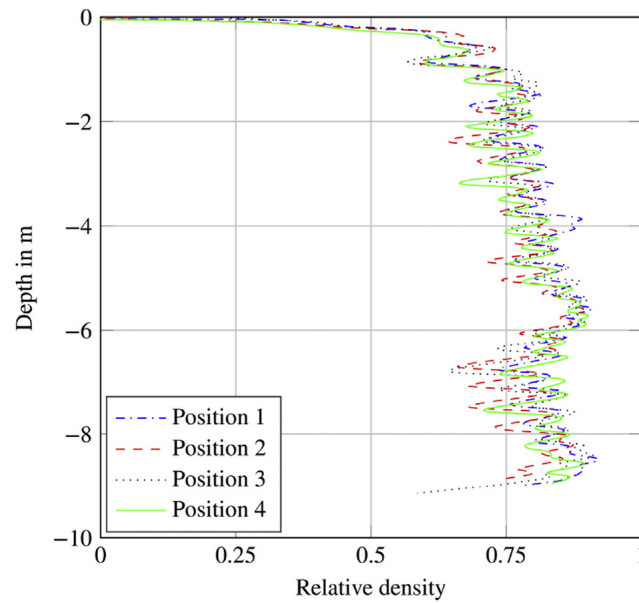


Fig. 3. Post-processed results of the cone penetration tests: relative density calculated using cone resistances and an empirical correlation method according [30] versus depth.

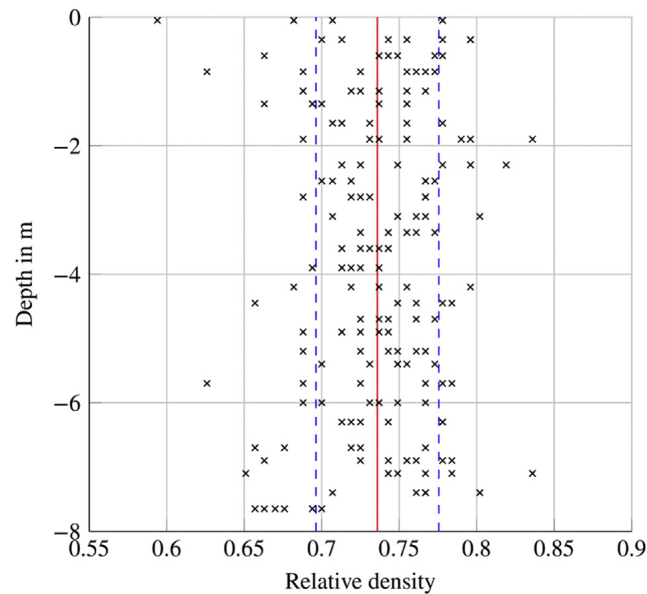


Fig. 4. Relative densities determined using soil samples in different depths and positions. Mean value and one sigma interval are marked (solid and dashed lines respectively).

distribution of the sensors for all embedded lengths. In total, more than 300 decay tests of the six piles with different embedded lengths and excitations were conducted.

The measured time signals of the accelerometers are analyzed using system identification methods. Here, system identification through data driven stochastic subspace identification (SSI), firstly introduced by Ref. [37]; is conducted. The automation of the system identification is done using a triangulation-based extraction of model parameters (TEMP) based on the work of [17]. The SSI combined with the TEMP method, initially developed for structural health monitoring applications [18], identifies automatically eigenfrequencies, mode shapes and damping values of the piles at different embedded lengths. However, some input parameters of the TEMP have to be chosen carefully. These parameters are, inter alia, the maximum, relative frequency difference between two solutions (f_{crit}) or the minimum number of model orders in a path (\hat{P}_{crit}). For further details, it is referred to [17].

Table 4
Properties of the sand utilized for the experiments.

Property	Unit	Value
Grain diameter 10th percentile (D_{10})	mm	0.22
Grain diameter 30th percentile (D_{30})	mm	0.29
Grain diameter median (D_{50})	mm	0.36
Grain diameter 60th percentile (D_{60})	mm	0.40
Coefficient of uniformity (C_u)	–	1.82
Coefficient of curvature (C_c)	–	0.96
Specific gravity (G_s)	–	2.65
Minimum porosity (n_{min})	–	0.31
Maximum porosity (n_{max})	–	0.46

This work focusses on the eigenfrequencies that are compared to those numerically calculated later on. Mainly, three eigenfrequencies of the piles were identified accurately: The first and the second bending mode and a radial or “breathing” mode of the piles. The radial mode has a relatively constant frequency over all embedded lengths of about 140 Hz to 145 Hz for the large pile diameter and of 175 Hz to 180 Hz for the small one. The first bending eigenfrequency increases from about 7 Hz for an embedded length of 3 m to about 60 Hz for $L = 6.7$ m. The second bending eigenfrequency varies between 45 Hz and 210 Hz for the different embedded lengths and diameters. The experimentally determined eigenfrequencies for different embedded lengths are shown in Fig. 5. It has to be mentioned that for the second bending mode, the pile diameter has a much greater influence and not in all cases it was possible to identify this mode properly.

For the sake of completeness, some results of the damping identification are depicted in Fig. 6. Increasing and relatively high damping values for higher embedded lengths for the first bending mode become noticeable. This increase can be

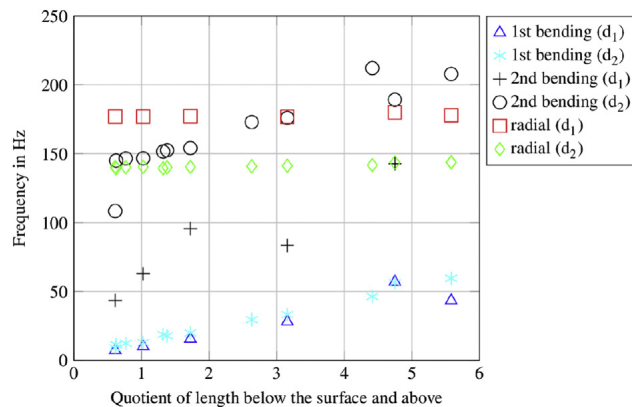


Fig. 5. Experimentally determined eigenfrequencies of the piles with smaller diameter d_1 and larger diameter d_2 for different embedded lengths.

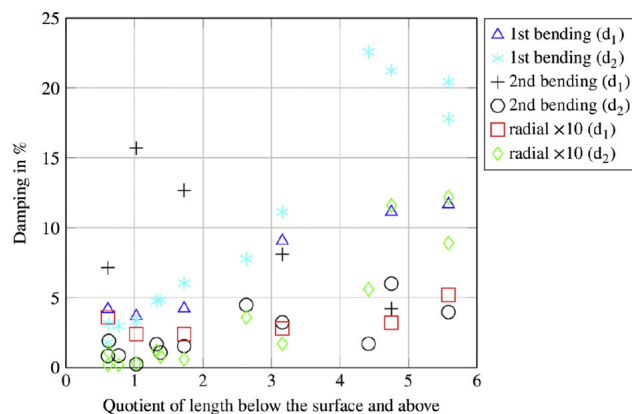


Fig. 6. Experimentally determined damping in % of the critical damping of the piles with smaller diameter d_1 and larger diameter d_2 for different embedded lengths. Damping values of the radial modes are scaled with a factor of ten for reasons of clarity.

explained by the geometrical damping of the soil. However, the second bending mode can be more damped for smaller embedded lengths. Here, nonlinear and material effects overlay the geometric effects. Radial damping values are fairly small being the reason for a scaled presentation (factor of ten) in Fig. 6. Due to the difficult determination of damping values, the results have to be interpreted with caution. In the following, the damping is not further considered, as the damping measurements exhibit large scattering, and the static p-y models used here do not model damping.

3.2. Numerical results for embedded piles

In addition to the experiments, numerical calculations were conducted. The piles are modeled with linear Timoshenko beam elements in ANSYS. The surrounding soil is represented by uncoupled spring elements in all spatial coordinate directions along the embedded length of the pile. The stiffnesses of the p-y and T-z curves are computed according to the different nonlinear soil models. This is the same procedure as for the computation of the stiffness matrices (c.f. section “Condensation of the Interaction Matrices”). The basic formulations of the utilized approaches are summarized in the following.

For the [4] approach, the calculation procedure of the secant soil-spring stiffness E_{py} is given in Eq. (20). The approaches according to [33,34,39] and [25] all propose a modification of the increase in the initial soil stiffness with depth (k) [39]. and [25] propose the following changes of k depending on the pile diameter D :

$$k_{Wiemann} = k \left(\frac{D_{ref}}{D} \right)^{\frac{4(1-a)}{4+a}} \quad (23)$$

with the reference values $D_{ref} = 0.61$ m and $a = 0.5$ to 0.6 and

$$k_{Kallehave} = \frac{1}{z} k z_{ref} \left(\frac{z}{z_{ref}} \right)^m \left(\frac{D}{D_{ref}} \right)^{0.5} \quad (24)$$

with $z_{ref} = 2.5$ m and $m = 0.6$. The reference diameter remains unchanged ($D_{ref} = 0.61$ m).

The changes being proposed by Refs. [33,34] focus on errors occurring under ultimate loads [34]. formulates:

$$k_{Sørensen,2012} = \frac{1}{z} a \left(\frac{z}{z_{ref}} \right)^b \left(\frac{D}{D_{ref}} \right)^c \left(\frac{E_s}{E_{s,ref}} \right)^d \quad (25)$$

Here, $a = 1$ MPa is a reference stiffness. For the dimensionless coefficients, the following values are recommended: $b = 0.3$, $c = 0.5$ and $d = 0.8$. For the reference values $z_{ref} = 1$ m, $D_{ref} = 1$ m and $E_{s,ref} = 1$ MPa are proposed Formerly et al., 2010 suggested:

$$k_{Sørensen,2010} = \frac{1}{z} a \left(\frac{z}{z_{ref}} \right)^b \left(\frac{D}{D_{ref}} \right)^c \phi'^d \quad (26)$$

The reference values and constants are the following: $b = 0.6$, $c = 0.5$, $d = 3.6$, $z_{ref} = 1$ m, $D_{ref} = 1$ m and $a = 50$ MPa. ϕ' is the internal friction angle [35]. do not modify the k value, but develop completely new basic p-y curves incorporating, inter alia, the soil unit weight γ' and the passive earth pressure coefficient K_{phg}

$$p_{Thieken}^{Basic} = \frac{11}{16} \gamma' z^{1.5} K_{phg} \left(1 + 2 \tan(\phi') \right) D^{0.5} \quad (27)$$

These basic p-y curves are subsequently adapted iteratively by considering interaction effects of the deflection line with the bedding resistance and pile tip effects.

The excitations with the impact hammer in the experiments do not lead to significant displacements of the pile in the soil. Hence, it is only a marginal simplification to assume initial soil conditions in lateral direction (linearization at the zero-deflection point).

The described model is used to compute the first and second bending eigenfrequencies of piles with the same geometry as in the experiments and for different embedded lengths. “Breathing” modes cannot be calculated with the utilized beam model. The use of, for example, shell models, which are capable to simulate radial modes, is not expedient, as p-y curves are generally applied to beam models, only.

3.3. Comparison of experimental and numerical results

To evaluate the different soil models, the measured and the calculated bending eigenfrequencies are compared. Fig. 7 shows the normalized first bending frequencies of the piles with the larger diameter for different embedded lengths. The frequencies are normalized with the experimental values. Results of the piles with the smaller diameter (not shown here) are comparable. The results of the soil models differ a lot and mostly do not fit the experiments well. The standard model of the API predicts frequencies that are about 10% lower than the experimental values. This is a significant deviation, considering the fact that eigenfrequencies are fairly insensitive to changing soil conditions. For example a significant increase of the internal friction angle from $\phi' = 39^\circ$ (experimental value) to $\phi' = 41^\circ$ only leads to deviations of the first bending eigenfrequency of about 2–3%. The approaches of [33,34] show even higher deviations. This can be explained by the purpose of these approaches. They focus on extreme loads. The same applies to [39]. However, as the pile diameters of the test piles are smaller than the reference diameter of Wiemann and the model is intended for large diameters, this model is only partly applicable here. The model of [25] fits the experiments best. For this approach, the focus is on initial conditions, as they are present here. However, in some cases even this model shows differences of about 25% [35]. try to get better approximations for initial and ultimate limit state conditions with their new approach. However, it is clear that for initial conditions the eigenfrequencies are overestimated. It has to be mentioned that the approach of Thielen et al. is much more sensitive to changing loads which is analyzed in more detail in the last section (see Fig. 15). Therefore, for this approach, it might be a significant simplification to assume initial conditions, as the hammer excitations introduce some loads, even if these loads are fairly small. However, for loads greater than zero, the soil becomes significantly softer for this approach (c.f. Fig. 8) and therefore, the calculated eigenfrequencies are getting closer to the measured ones. For all other approaches, the effect of loads greater than zero, if

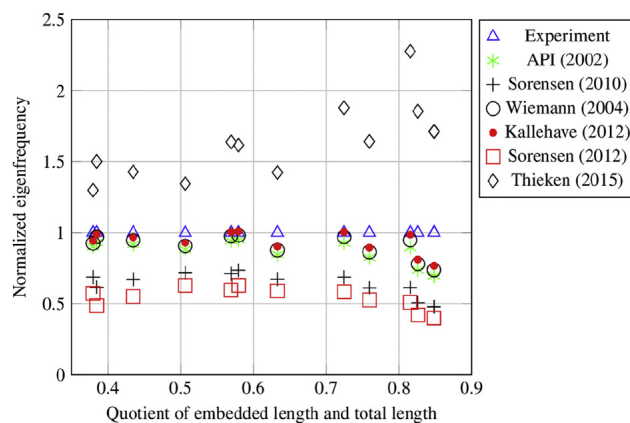


Fig. 7. Normalized eigenfrequencies of the piles with larger diameter for different embedded lengths calculated with different soil models.

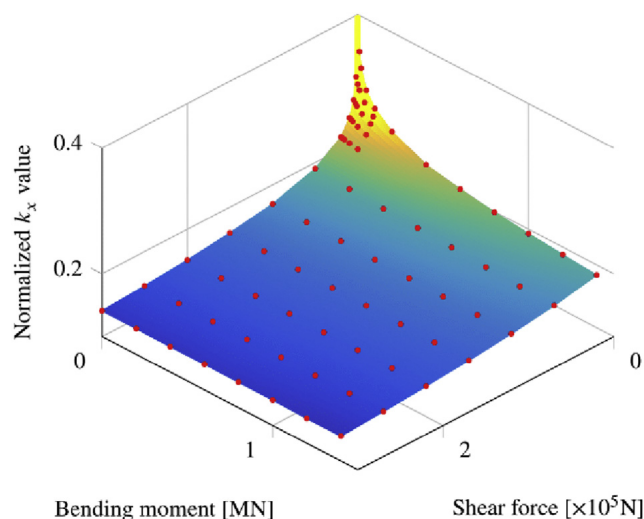


Fig. 8. Normalized stiffness term k_x (normalized with $k_{x0} = f(H = 0, M = 0)$) as a function of the shear force (H) and the bending moment (M) at mudline. For reasons of clarity, the vertical axis only shows values up to $k_x = 0.4$. The initial stiffness $k_{x0} = f(H = 0, M = 0) = 1$ is not plotted.

present, leads to greater differences compared to the experimental results. However, as neither the loads at mudline nor the displacements were measured, a quantitative assessment of this effect is not possible.

For the second bending mode, the identification is not that clear. Therefore, it is abstained from judging the soil models on this basis as well. However, the numerical calculations fit the experiments even worse in case of the second bending mode (not shown here), and the errors are changing for different embedded lengths which is not the case regarding the first bending mode.

After all, the comparisons of experiments and numerical models show that none of these soil models can really predict the dynamic behavior of the piles, as deviations of up to 25% even for the “best” model occur.

It has to be pointed out that all investigated p-y curves were initially developed for static loads, but are currently used in dynamic wind turbine applications. Dynamic p-y curves, as for seismic applications [29], have not yet found application in offshore wind energy. Still, the fact of being developed for static loads explains, at least partly, the deviations between the numerical and experimental results. However, if models are chosen carefully according to their intended load conditions, model errors can be reduced. Models that focus on initial conditions can deliver the best results for these conditions. Whether models that focus on ultimate loads are best suitable for high load conditions or not cannot be investigated with the present data, as the experiments conducted only apply small loads. Still, it would be valuable to investigate ultimate load conditions.

For the following numerical investigations, the model of [25] is considered in detail, as it fits the experimental results best. Furthermore, the API model (2002) is analyzed, as this model is proposed by the standards, and the model by Ref. [35]; as it is quite sensitive to changing loads and has shown promising results in numerical comparisons [35].

4. Operating point analysis

4.1. Method

The second contribution of this work is the incorporation of the operating point. So far, the nonlinear soil-structure interaction behavior is linearized at the zero-deflection point of the pile which means that no loads are applied at the pile head and initial soil stiffnesses are assumed. However, the soil stiffness depends on the acting loads at mudline. Fig. 8 illustrates this dependency by displaying the normalized stiffness term k_x as a function of the shear force (H) and the bending moment (M) at mudline. The values of k_x are calculated using the procedure from section “Condensation of the Interaction Matrices” and the spring model according to [35]; as this model shows the strongest dependency between loads and soil stiffnesses which is advantageous for illustration purposes. For other spring models, the dependencies are comparable, but less pronounced. Similar figures showing the dependencies of different stiffness values on the acting loads can be found in Ref. [10]. These authors are using a different method of computing soil matrices, but the results are comparable.

So, it was clarified that the consideration of the operating point is influencing the soil stiffness. However, more important is the overall wind turbine behavior, for example the maximum loads. Therefore, comparisons of time domain simulations with clamped boundary conditions (state of the art; c.f. approach (1) in Fig. 9), initial soil stiffnesses ([19]; c.f. approach (2)) and operating point dependent soil stiffnesses (this work; c.f. approaches (3) to (5)) are done in the next step. For the

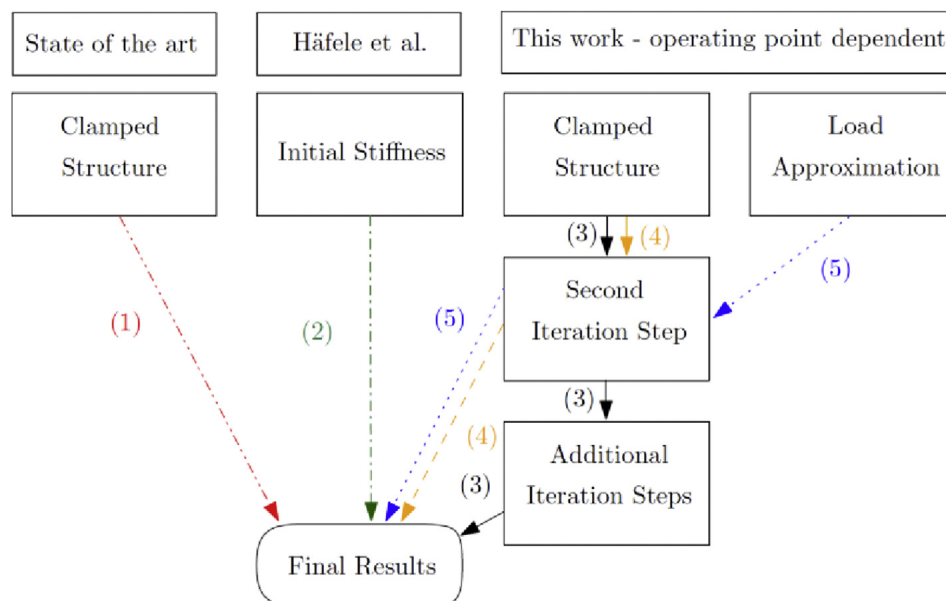


Fig. 9. Illustration of different possibilities to incorporate the operating point in time domain simulations (c.f. Table 5).

operating point dependent simulations, previously calculated loads at the operating point are needed. Here, different possibilities to determine these loads ((3) to (5)) are presented and subsequently, the results are compared. The general procedure of the different approaches is illustrated in Fig. 9.

Here, approach (1) and (2) do not consider load-dependent soil stiffnesses. Concept (3) determines the loads at the operating point most precisely, but it uses a quite time-consuming iterative procedure. At first, a fully coupled time domain simulation of the wind turbine with a clamped structure (1) or with initial soil stiffnesses (2) is conducted. The results of this first simulation (the calculated loads) are used to linearize the soil stiffnesses at an updated operating point. A second time domain calculation follows with soil stiffnesses linearized at the updated operating point. As the loads - calculated in this second step - might be different from the previously calculated ones, the operating point is updated again and a third step follows. This iterative procedure is repeated until the loads are no longer changing significantly. Although, the loads are calculated precisely using this procedure, several time domain simulations are needed which makes it inefficient. Therefore, a more detailed analysis of the load dependence of the soil stiffness is valuable. Fig. 8 indicates that there is a significant change of the soil stiffness, if initial stiffnesses are compared to operating points with loads greater than zero. However, small changes of operating loads (e.g. $H = 2 \times 10^5$ N, $M = 1$ MN $\pm 10\%$) do not change the soil stiffness significantly. This fact leads to the assumption that there is no need of several iteration steps. It might be sufficient to conduct a first calculation with a clamped structure (1) for a rough approximation of the loads. The results of this calculation are used for a second coupled simulation that considers the linearized soil stiffness for the present loads (4). Still, the overall computation time is doubled. To limit the number of time domain simulations to one, an approximation of the loads at the operating point which replaces the “clamped calculation” (1) and links environmental conditions to the loads at mudline is introduced (5). The last procedure is by far the fastest (nearly the same computing time as with approaches that do not consider operating points at all), but the loads are only roughly approximated. For these five methods, results of time domain simulations are summarized in Table 5.

It is apparent that there are significant differences between clamped boundary conditions (1), initial soil stiffnesses (2) and stiffnesses at operating points (3–5). Hence, the operating point should be incorporated. However, there is no need for several iteration steps, as the results are already converged after two steps (compare (3) and (4)). Furthermore, even rough approximations of the loads at the operating point (5) lead to the same results as the converged solution (3). Therefore, in this work, an approximate but effective approach is proposed which links environmental conditions to the loads at mudline that are decisive for the soil stiffness.

For the approximation approach, it has to be specified first what is meant in terms of environmental conditions in the present case. Regressions and variance-based sensitivity analyses using coupled time domain simulations with probabilistic input parameters are performed by Ref. [21]. They show that wind speeds and wave heights have a major influence on the acting loads at mudline. Therefore, these two parameters are related with the environmental condition. Furthermore, the direction of wind and waves can be even more important, as the four piles undergo different loads in case of a jacket substructure. That is why, for jackets, the third condition parameter is the direction. It is assumed that the wind and wave direction are the same, as it is recommended by common regulations [22], though studies have shown that this is frequently not the case [32]. The sensitivity analyses show that all other environmental conditions are less significant. This does not mean that the scattering of all other parameters is not influential, but for the approximation of the loads at mudline less influential parameters are neglected in the first place.

Secondly, it has to be determined which loads are decisive for the soil stiffness. As it is well-known for p-y curves, the overturning moment and the horizontal shear force are important for the lateral stiffness, whereas the vertical force is the determining factor for the axial soil stiffness. Since the loads at mudline vary periodically, and time-variant stiffnesses are beyond the scope of this work, it was decided that the maximum values of the loads are decisive for the stiffness. This simplification is due to the fact that the use of a Craig-Bampton reduction of the substructure to its first mode shapes allows only constant soil stiffnesses, as the reduction is performed just once at the beginning of the time domain simulation. The choice of maximum values leads to minimum stiffnesses. For the vertical force, the minimum (most negative) and the maximum are considered as both, compression and tension, can be of interest.

Thirdly, a correlation between the conditions and the decisive loads has to be identified. Coupled time domain calculations of the whole wind turbine and a clamped substructure using the simulation code FAST and for wind speeds between $v_w = 0$ ms⁻¹ and $v_w = 40$ ms⁻¹, for wave heights between $h_s = 0$ m and $h_s = 14$ m and wind and wave directions between $\alpha = -45^\circ$ and $\alpha = 45^\circ$ were computed. The use of a clamped structure is justified by the results in Table 5. The relevant results

Table 5

Maximum and mean shear forces (**H**) and bending moments (**M**) at mudline of an OC3 monopile calculated using FAST and different soil models: (1) clamped structure, (2) linearization of the soil behavior at the zero-deflection point (c.f. [19]), (3) linearized at iteratively calculated loads (converged solution), (4) linearized at loads calculated with clamped structure (two iteration steps) (5) Load approximation plus single step.

Case	H_{max} [MN]	H_{mean} [MN]	M_{max} [MNm]	M_{mean} [MNm]
(1) Clamped	1.38	0.690	93.9	78.3
(2) Initial Stiffness	1.44	0.690	97.7	78.6
(3) n Iteration steps	1.45	0.690	101	78.9
(4) 2 Iteration steps	1.45	0.690	101	78.9
(5) Single Step	1.45	0.690	101	78.9

of these calculations are the maximum loads at mudline for the given, varying environmental conditions. Other directions do not have to be considered due to the symmetry of jackets with four legs. Fig. 10 illustrates the configuration of the jacket by showing a horizontal cut through the jacket on mean sea level (MSL).

The results of the time domain simulations using FAST, for example the maximum overturning moments at mudline, are used as grid points for response surfaces. The challenge is to define functions that can be well fitted to the grid points using a least square algorithm. Fig. 11 illustrates the situation. It shows the maximum horizontal shear forces at mudline in leg 1 of the OC4 jacket substructure for different wind speeds. Each data point is the result of a fully coupled time domain simulation. There is a discontinuity at the cut-off wind speed resulting from the simplified shut-down procedure at cut-off wind speed which is not considered in detail here. For each time domain simulation in FAST, the turbine is either running or shut off which leads to this discontinuity. Fig. 11 clarifies that the data space can be divided into sections in order to apply polynomial approaches. The characteristics of the results are dependent on the turbine controller leading to highly nonlinear discontinuous functions. Hence, the data space is divided into three sections depending on the wind speed that is correlated with the controller actions. In the first section (below rated wind speed), the blade-pitch control system is inactive. After reaching rated wind speed, the controller starts to pitch the blades. For wind speeds higher than the cut-off wind speed (third section), the blades are pitched out completely (pitch angle of 90°), and the turbine is shut off.

Based on this segmentation, polynomials of a maximum degree of three are fitted with good agreement in all three dimensions (wind speed, wave height and direction). For most sections, polynomial degrees of one or two are sufficient. For example, Fig. 11 suggests for the wind speed above cut-off a linear fit. The coefficients of the polynomials were calculated using a linear regression for each section and force. Here, the effect of higher polynomial degrees was judged using the adjusted coefficient of determination. A degree as low as possible without losing significant accuracy was selected. The corresponding coefficients of an exemplary response surface for a jacket are summarized in Table 6, and a plot of another (two-dimensional) response surface for a monopile and the whole data space is shown in Fig. 12.

The presented approach of linking the decisive loads to the most important environmental conditions using multi-dimensional, piecewise polynomial response surfaces enables an estimation of the loads at mudline in advance without

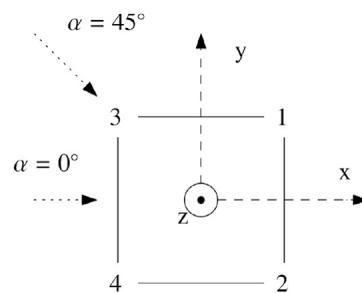


Fig. 10. Horizontal cut through the jacket on MSL with coordinate system (dashed), leg numbering and inflow wind angle (dotted).

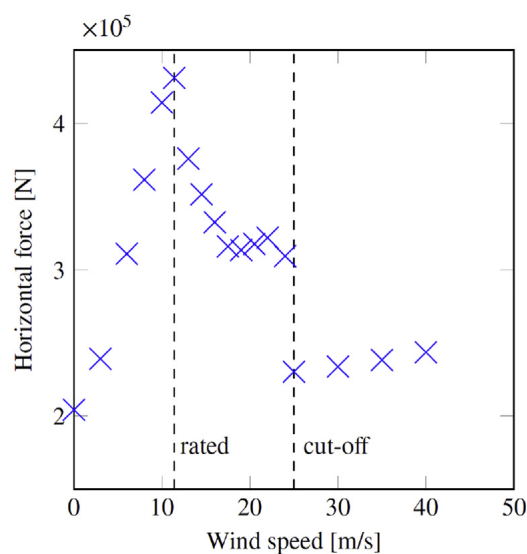


Fig. 11. Illustration of maximum horizontal shear forces at mudline in leg 1 of the OC4 jacket for different wind speeds and with $h_s = 6$ m and $\alpha = 0^\circ$ calculated in time domain simulations using FAST.

Table 6

Coefficients for the three-dimensional response surface of the overturning moment at mudline in leg 1 of the jacket with $11.4 \text{ ms}^{-1} \leq v_w = 25 \text{ ms}^{-1}$. For reasons of simplicity, units are omitted, but all coefficients are in SI units.

Linear regression model $M = c_0 + c_x \alpha + c_v v_w + c_h h_s + c_{xv} \alpha v_w + c_{zh} \alpha h_s + c_{vh} v_w h_s + c_{v2} v_w^2 + c_{h2} h_s^2$	
Coefficient of	Estimate
c_0	2.8063×10^6
c_x	1.9605×10^3
c_v	-2.0918×10^5
c_h	1.0630×10^5
c_{xv}	1.3382×10^1
c_{zh}	8.0765×10^1
c_{vh}	-2.3423×10^3
c_{v2}	5.3624×10^3
c_{h2}	5.9823×10^3
Adjusted coefficient of determination : $R^2_{\text{adjusted}} = 0.996$	

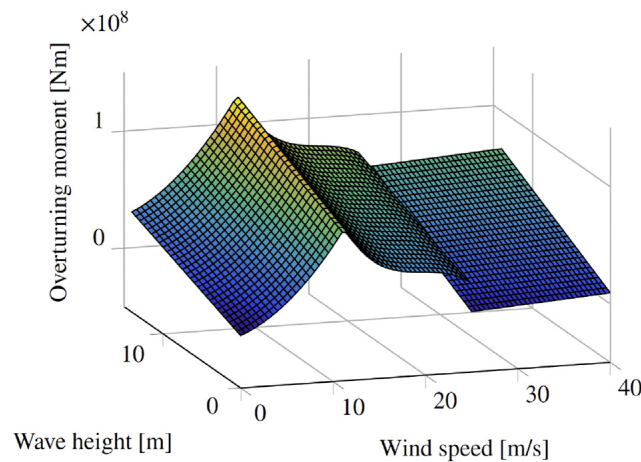


Fig. 12. Response surface of the overturning moment at mudline for a monopile foundation and all three sections.

further coupled time domain simulations. Of course, it is only an estimate with the mentioned simplifications. Nonetheless, to determine the load-dependent soil stiffness for a given operating point, such a reduced model is adequate, as slightly changing loads are not influencing the soil stiffness and the overall turbines results significantly (c.f. Fig. 8 and Table 5).

4.2. Results of the load approximation using a response surface

An effective way to relate loads at mudline to the environmental conditions was presented. In this section, results of load approximations using the response surface method are presented clarifying that - despite all simplifications - this approach gives sufficiently accurate approximations. Therefore, it is an appropriate way to determine the soil stiffness beforehand. In order to analyze the applicability of the method of relating loads to environmental conditions, loads computed with coupled transient simulations using FAST are compared to loads approximated with the response surface method. Firstly, only grid points are used. These are the data points that are used to generate the response surface itself. Secondly, the loads are compared for other points in all different conditions. Lastly, some other environmental conditions (not used for the construction of the response surface) are changed as well in order to check whether these three variables are sufficient.

Table 7

Relative difference between approximated shear forces and values computed with time domain calculations for different environmental conditions for an OC3-monopile in %. The wind and wave direction ($\alpha = 0^\circ$) is not relevant for the symmetric monopile.

v_w in ms^{-1}	h_s in m	$F_{xy,max}$ in N		
		Approx. with RS	Calculation using FAST	Diff.
11	7	2.400×10^6	2.404×10^6	0.15%
16	10	2.851×10^6	2.846×10^6	0.18%
1.5	1	2.578×10^5	2.653×10^5	2.83%
50	14	3.668×10^6	3.683×10^6	0.41%

Table 8

Relative difference between approximated bending moments and values computed with time domain calculations for an OC4-jacket and by applying different environmental conditions in %. $\alpha = 0^\circ$, $v_w = 25 \text{ms}^{-1}$ and $h_s = 8 \text{m}$ are fixed.

T_p in s	ρ_L in kgm^{-3}	l_{water} in m	$M_{xy,max}$ in Nm		
			Approx. with RS	Calculation using FAST	Diff.
10	1.225	50	2.07×10^6	2.13×10^6	2.81%
14	1.225	50	2.07×10^6	1.78×10^6	14.31%
10	1.225	55	2.07×10^6	2.09×10^6	0.95%
10	1.3	50	2.07×10^6	2.17×10^6	4.49%

Table 7 shows that, in general, response surface approximations for grid points as well as for other points show less than 3% deviation of the time domain simulations for the monopile and less than 5% for the jacket (not shown). For extrapolated values (for example for $v_w = 50 \text{ms}^{-1}$), the difference is still less than 5%. Therefore, if other environmental conditions are kept fixed, the proposed approximation proves to be sufficiently accurate.

However, if other environmental conditions are changed, the approximation is less precise. In this study, the air density (ρ_L), the wave peak period (T_p) and the water depth (l_{water}) are selected to be other important environmental conditions and are varied. Some results of the approximation with changing conditions are summarized in Table 8. Errors of mainly below 5% show that the approximation is still sufficiently exact for the purpose of this work, even in case of changing environmental conditions. However, it should be reconsidered to include T_p as an additional parameter in the response surface estimation, as it leads to deviations of up to 15%. There are similar results for the monopile, but the errors due to T_p are even up to 20% (not shown). The high influence of the wave peak period, especially for the monopile, can be explained by resonance effects of the wave loads and the structure itself. Due to the larger diameter, monopiles are more strongly affected by wave loads. For more precise approximations, the wave peak period has to be included in the calculation procedure of the response surface, as well. However, this is not performed in this study. Fairly rough approximations are sufficient for the consideration of the operating point, as soil stiffnesses are not that sensitive to the changing loads around the operating point (c.f. Fig. 8 and Table 5). Furthermore, the wave peak period is highly correlated with the wave height (e.g. Ref. [12]). Hence, it is not absolutely necessary to consider it as a fourth parameter, but for example a dependency of the wave height is an effective alternative.

5. Numerical results of coupled simulations

5.1. Time domain results with initial soil stiffnesses

Results of coupled time domain calculations of a whole offshore wind turbine using FAST are shown exemplarily in order to illustrate the effectiveness of the basic approach. In this section, neither the operating point is taken into account nor the different soil models discussed in connection with the experiments. For the OC4-Jacket [24] as the substructure and different configurations of soil-structure interaction, the design load case 5.7 is applied. This load case, according to [38]; has a fully enabled wind turbine with turbulent wind ($v_w = 18 \text{ms}^{-1}$) and irregular waves ($h_s = 6 \text{m}$). Results are compared for the bottom fixed or clamped situation, an apparent fixity length approach according to [40] and the condensed stiffness matrix for the pile foundation according to [19]. For the condensed stiffness matrices, initial conditions are applied, and the [4] p-y curves are utilized. The use of the operating point and other p-y curves will be discussed in the next section.

For the OC3-Monopile [23], the same three configurations of soil-structure interaction are compared. Additionally, results of different simulation codes and soil-structure interaction models, summarized in the OC3-report [23], are depicted. The load case is an operating load case (load case 5.2 of the OC3-report) with a fully enabled turbine, turbulent wind ($v_w = 11 \text{ms}^{-1}$) and irregular waves ($h_s = 6 \text{m}$).

Fig. 13 shows exemplary power spectral densities (PSDs) for load case 5.7 of the jacket foundation. It depicts the jacket shear force at mudline and indicates a shift of the second bending eigenfrequencies from about 1.2 Hz to about 0.9 Hz for the flexible foundation and to about 0.8 Hz for the apparent length approach. The shift of natural frequencies for the apparent length approach is slightly higher than for the stiffness matrix approach. The approach of an apparent length of six times the diameter according to [40] seems to overestimate the effect of a flexible foundation for a jacket structure considering the employed type of soil and penetration depth.

The power spectral density for load case 5.2 and the monopile foundation is shown in Fig. 14. Here, the good accordance of the present approach with other codes from the OC3-report is noticeable. All codes from the OC3-report and the basic model show the same merged peaks between about 1.2 Hz and 1.8 Hz. Pronounced peaks are not existent. The apparent fixity length approach is overestimating the flexibility again. Comparisons with other codes are only possible for monopile foundations. For jackets, the use of a substructure reduction scheme like the Craig-Bampton reduction is necessary in most cases. Therefore, other soil models like linearized p-y curves are no longer practical, and to the authors' knowledge, nearly no results of coupled time domain simulations of the whole turbine with a jacket substructure and soil-structure interaction are available.

In summary, it can be concluded that the selected version of apparent fixity length overestimates the effect of flexibility. The basic soil-structure interaction approach [19] is comparable to results of other codes of the OC3-report that are only

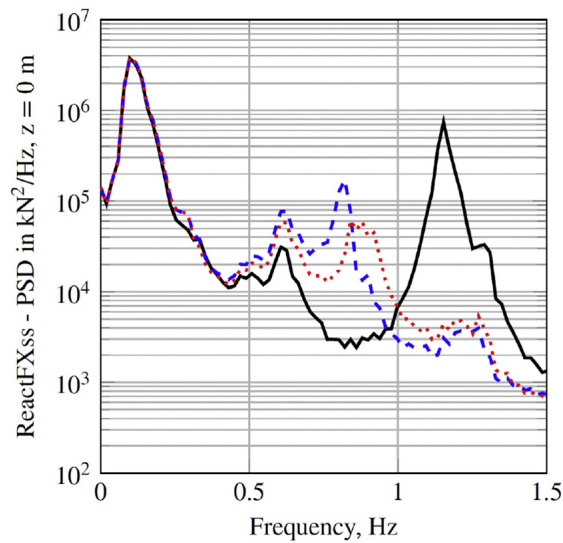


Fig. 13. Power spectral densities of the shear force at mudline from design load case 5.7 for an OC4-jacket: clamped (—), apparent length (---), basic approach according to [19] (.....).

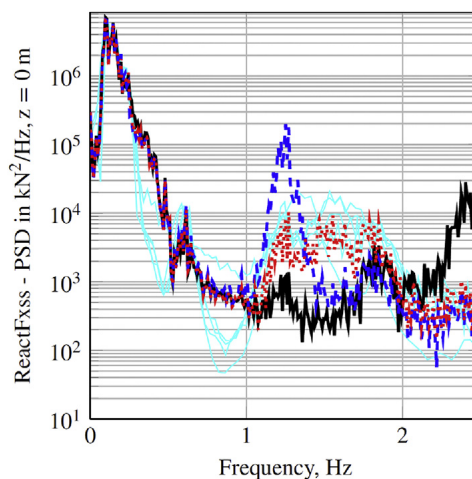


Fig. 14. Power spectral densities of the shear force at mudline from design load case 5.2 for an OC3-monopile: clamped (—), apparent length (---), basic approach according to [19] (.....), other codes from OC3-report (—).

available for monopile foundations. The clamped situation clearly represents the stiffest configuration of soil-structure interaction and is a massive simplification.

This analysis makes clear that the presented approach to model soil effects leads to reasonable results. For further results and a verification of this approach by means of additional code to code comparisons, it is referred to [19].

5.2. Time domain results with operating point consideration

Results of time domain simulations of jackets with pile foundations and of monopiles were presented and discussed in the last section. However, the results do not incorporate an estimation of the operating point so far which is a major enhancement compared to the basic approach. Furthermore, so far, the soil matrices were computed only by using the p-y and T-z curves based on the [4]. However, the experimental results pointed out that the API models do not achieve the best results for dynamic applications. This section focuses on the changing overall turbine behavior resulting from different operation points and various soil models. Again, an OC3-Monopile [23] and an OC4-Jacket [24] with the corresponding soils are investigated.

Before analyzing the overall behavior of the turbine by comparing the results of fully coupled time domain simulations, a study concerning the impact of the operating point and the lateral soil models on the stiffness matrices is conducted. The effect of the axial soil models can be neglected in most cases [20] and it is, therefore, not regarded in this work. This does not mean that the vertical stiffness is not influential at all, but the differences of axial soil models are less pronounced and

therefore, do not change the overall turbine behavior significantly. So, the values of k_x - exemplarily chosen to represent the lateral soil stiffness - are compared for three different load cases to show the load dependence of the soil stiffness and for several lateral soil models to show the differences between the models. The load conditions are the initial stiffness (no loads applied), an operational load case ($v_w = 8 \text{ ms}^{-1}$ $h_s = 6 \text{ m}$) and a 50-year storm load case ($v_w = 42 \text{ ms}^{-1}$ $h_s = 10.5 \text{ m}$) of [31]. The results are shown in Fig. 15. The initial stiffnesses of the API model are used to normalize the values.

Two points are apparent: There are remarkable differences between the soil models, as already known from the experiments. Therefore, a reflection about the usage of the right model is essential, as the intended application area of the models is different (c.f. section “Comparison of Experimental and Numerical Results”). Some differences between the models can be explained by these deviating application areas. Furthermore, this load dependency leads to another feature. The stiffness decreases with increasing loads. For the [4] approach, there is a stiffness reduction (c.f. Fig. 1), but still, the overall change in soil stiffness is only about 5% as shown in Fig. 15, and therefore, does not significantly affect the overall turbine behavior. However, for other models, especially for Thieken, the stiffness differences are more pronounced leading to considerably changing stiffness matrices. For the model according to [25]; which was identified to be most suitable for dynamic applications in the tested conditions, the load dependency is considerable as well (about 15%).

It was demonstrated that different load levels and soil models significantly influence the stiffness matrices and the eigenfrequencies of the tested piles. However, the effects on the overall behavior of wind turbines are of greater interest. Since it is not possible to generalize the changes of the stiffness matrices, coupled simulations are necessary to investigate overall effects. In Fig. 16, power spectral densities for an OC3-Monopile under extreme environmental conditions are presented. Three soil models are chosen: Firstly, the API model, as it is still recommended by the standards. Secondly, the model by

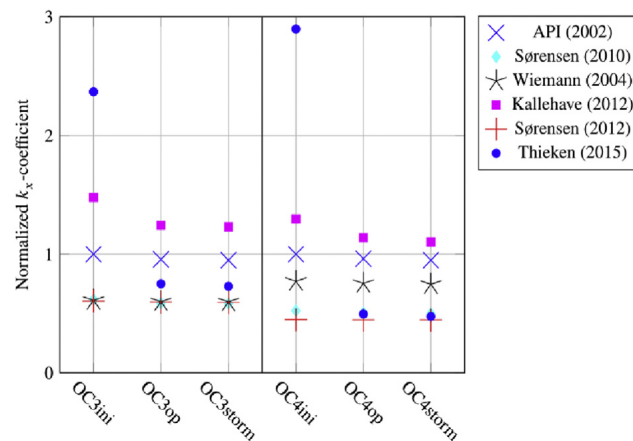


Fig. 15. Normalized k_x coefficients for different lateral soil models and load cases. The X signs for the initial conditions (OC3ini and OC4ini) represent the normalizing values.

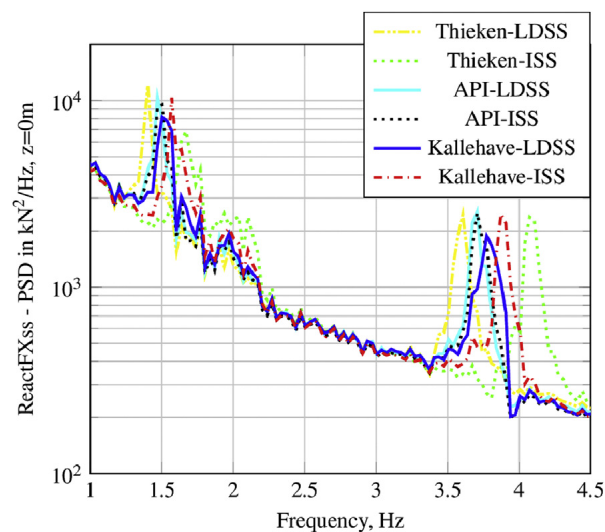


Fig. 16. Power spectral densities for OC3-Monopile with different lateral soil models each evaluated with initial soil stiffness (ISS) and load-dependent soil stiffness (LDSS).

Thieken et al. as it exhibits the highest load dependence and lastly, the model by Kallehave et al. as it matches the experiments best. For all three models, two time domain calculations were conducted with the same extreme environmental conditions, but the soil behavior is either linearized at the zero-deflection point (initial stiffness) or at the operating point (loads applied).

Two features are visible. Eigenfrequencies of the entire wind turbine depend highly on the soil model. The discrepancy of the natural frequency of Thieken and API with initial loads at about 4 Hz is approximately 10%. The eigenfrequencies of Kallehave are just in between. Furthermore, the effect of the load level and therefore, of the response surface application highly depends on the soil model applied. For the API model, the effect of changing loads can be neglected, whereas for Kallehave it is significant, and for Thieken it is even more pronounced than the discrepancies between the models themselves.

It can be summarized that the lateral soil model has to be chosen with care and according to the load conditions and the intended application area of the soil model. It depends on the soil model, whether an estimation of the operating point with the response surface method is essential or initial conditions can be assumed as in the basic model by Ref. [19].

6. Conclusions

The basic approach by Ref. [19] is an effective method to consider effects of the soil in coupled time domain simulations of offshore wind turbines. It is very flexible and can be used for different kinds of substructures and anchorages, even if the substructure is condensed with a Craig-Bampton reduction, as it is common practice. This approach, which is based on preliminary calculated mass and stiffness matrices, is enhanced here. The approach is independent of the computation method of the matrices. One way to compute the matrices is the use of nonlinear spring models representing the soil, so-called p-y curves. P-y curves are important for different types of substructures, for example monopiles and jackets, as both are exposed to significant horizontal forces and moments at mudline. The first focus of this work is on different spring models that can be found in literature. The models are analyzed in detail using experimental investigations of jacket piles on a large scale. Additional experiments assessing the applicability of p-y models for monopiles with smaller L/d ratios would be valuable, as results might be slightly different. By comparing eigenfrequencies of numerical calculations with experimental ones, large differences between the models themselves and to the experimental results are apparent. It is abstained from utilizing other modal parameters, e.g. mode shapes, since their detection is more error-prone than it is for eigenfrequencies. For the calculation of eigenfrequencies, the p-y model by Ref. [25] proved to be most suitable in the present case. As only eigenfrequencies and no real load conditions were tested, all results have to be treated with caution.

The second focus of the work is on the load dependence of the soil stiffness. The consideration of the operating point is a major enhancement of the basic approach, as it enables a load-dependent consideration of soil characteristics. The presented use of response surfaces is an effective way to incorporate the operating point.

Firstly, it was shown that a rough approximation of the loads at the operating point using results of time domain simulations with clamped structures is sufficient and no iterative procedure is needed (c.f. Table 5). Then, the use of a multi-dimensional, piecewise polynomial response surface approximating the acting loads at the operating point proved to be sufficiently precise. Thirdly, coupled time domain calculations of wind turbines with substructures, which are modeled as clamped to the seabed, and of substructures anchored with (mono-) piles and modeled with the basic approach and initial soil stiffnesses were conducted. The results were compared, and significant shifts of the eigenfrequencies are recognizable. Afterwards, comparisons of the stiffness matrices of pile foundations of jacket substructures and a monopile modeled using different p-y curves were made. Time domain simulations of wind turbines with these varying matrices were analyzed. It is very important to point out that there are huge discrepancies between different soil models as already seen in the experiments.

The present approach of considering soil characteristics is effective, but still very flexible. However, if higher computing times are manageable, even more accurate results can be achieved by some small modifications. The response surface can be enhanced with further environmental conditions (e.g. T_p), or it can be replaced by an a priori (and iterative) calculation of the acting loads (e.g. procedure (3) or (4) in Fig. 9). Furthermore, more sophisticated soil models can be applied to compute the soil matrices, as the use of static p-y curves can lead to uncertain results due to the great differences between the numerical models and the measured values. The use or development of specific dynamic p-y curves, as for seismic applications, might be valuable. Furthermore, the present approach is restricted to time-invariant load-dependent soil matrices. This means that in case of changing loads over time (time-variant loads), for example transient load cases, the load-dependent soil matrices remain time-invariant and are not recalculated in each time step. While the substructure is condensed using a Craig-Bampton reduction, it is not possible to apply time-variant soil matrices. Nevertheless, for unreduced substructures, which is frequently the case for monopiles, other soil models with time-variant stiffnesses are possibly slightly more accurate.

In future work, a detailed experimental investigation on a large scale of different soil models, including dynamic p-y curves, for different load conditions should be conducted, as it could help to reduce model errors and to give the maximum possible guidance on the selection of the most suitable model.

Acknowledgements

We gratefully acknowledge the financial support of the German Federal Ministry for Economic Affairs and Energy (research project Gigawind life, FKZ 0325575A), the European Commission (research projects IRPWind and Innwind.EU, funded from the European Union's Seventh Framework Programme for research, technological development and

demonstration under grant agreement numbers 609795 and 308974) and the “niedersächsisches Ministerium für Wissenschaft und Kultur (NMWK)” (research project Ventus Efficiens, FKZ ZN3024) that enabled this work.

References

- [2] Achmus M, Müller M. Evaluation of pile capacity approaches with respect to piles for wind energy foundations in the north sea. In: 2nd int symp front offshore geotech. Perth: University of Western Australia; 2010.
- [3] Alati N, Failla G, Arena F. Seismic analysis of offshore wind turbines on bottom-fixed support structures. *Phil Trans R Soc A* 2015;373:1–24.
- [4] American Petroleum Institute (API). Recommended practice for planning, designing and constructing fixed offshore platforms – working stress design. Recommended practice rp 2a-WSD. 2002.
- [5] American Petroleum Institute (API). Errata and Supplement 3—API recommended practice 2a-WSD, recommended practice for planning, designing, constructing fixed offshore platforms – working stress design. 2007.
- [6] Augustesen AH, et al. Numerical modelling of large-diameter steel piles at Horns Rev. In: *Int conf civ, struct, env eng comput*; 2009 [Funchal, Portugal].
- [7] Bienen B, Cassidy M. Advances in the three-dimensional fluid–structure–soil interaction analysis of offshore jack-up structures. *Mar Struct* 2006;19:110–40.
- [8] Craig Jr RR, Bampton MCC. Coupling of substructures for dynamic analyses. *AIAA J* 1968;6(7):1313–9.
- [9] Damiani R, Song H, Robertson A and Jonkman, J (2013). “Assessing the Importance of Nonlinearities in the Development of a Substructure Model for the Wind Turbine CAE Tool FAST”, *ASME Int Conf Ocean, Offshore Arc. Eng. Am Soc Mech Eng.*
- [10] Dubois. Advanced incorporation of soil-structure interaction into integrated load simulation. In: *Proc int offshore polar eng conf*; 2016 [Rhodos, Greece].
- [11] Foglia A, Kohlmeier M, Wefer M. Physical modeling and numerical analyses of vibro-driven piles with evaluation of their applicability for offshore wind turbine support structures. In: *Proc nord geotech meet*; 2016 [Reykjavik].
- [12] Germanischer Lloyd. Guideline for the certification of offshore wind turbines. *Offshore Standard*; 2012.
- [13] Georgiadis M, Saekou S. Piles under axial and torsional loads. *Comput Geotech* 1990;9:291–305.
- [14] Grabe J, Mahutka KP, Dührkop J. Monopilegründungen von Offshore-Windenergieanlagen - zum Ansatz der Bettung. *Bautechnik* 2005;82(1):1–10.
- [15] Guyan RJ. Reduction of stiffness and mass matrices. *AIAA J* 1965;3(2):380.
- [16] Hald T, Mørch C, Jensen L, Bakmar CL, Ahle K. Revisiting monopile design using py curves. Results from full scale measurements on Horns Rev. In: *Proc eur offshore wind conf*; 2009 [Stockholm, Sweden].
- [17] Häckell M, Rolfes R. Monitoring a 5MW offshore wind energy converter-Condition parameters and triangulation based extraction of modal parameters. *Mech Syst Sig Proc* 2013;40(1):322–43.
- [18] Häckell MW, Rolfes R, Kane MB, Lynch JP. Three-tier modular structural health monitoring framework using environmental and operational condition clustering for data normalization: validation on an operational wind turbine system. *Proc IEEE* 2016;104(8):1632–46.
- [19] Häfele J, Hübler C, Gebhardt CG, Rolfes R. An improved two-step soil-structure interaction modeling method for dynamical analyses of offshore wind turbines. *Appl Ocean Res* 2016;55:141–50.
- [20] Hübler C, Häfele J, Ehrmann A, Rolfes R. Effective consideration of soil characteristics in time domain simulations of bottom fixed offshore wind turbines. In: *Proc int offshore polar eng conf*; 2016 [Rhodos, Greece].
- [21] Hübler C, Gebhardt CG, Rolfes R. Hierarchical four-step global sensitivity analysis of offshore wind turbines based on aeroelastic time domain simulations. *Renew Energ* 2017;111:878–91.
- [22] International Electrotechnical Commission. Wind turbines - Part 3: design requirements for offshore wind turbines, vol. 2009. Standard IEC-61400–61403; 2009.
- [23] Jonkman J, Musial W. Offshore code comparison collaboration (OC3) for IEA task 23 offshore wind technology and deployment. Tech Rep NREL/TP-5000-48191. National Renewable Energy Laboratory; 2010.
- [24] Jonkman J, et al. Offshore code comparison collaboration continuation (OC4), phase I – results of coupled simulations of an offshore wind turbine with jacket support structure. In: *Proc int offshore polar eng conf*; 2012 [Rhodos, Greece].
- [25] Kallehave D, Thilsted CL, Liingaard MA. Modification of the API py formulation of initial stiffness of sand. In: *Offshore site investigation and geotechnics: integrated technologies - present and future*; 2012 [London, UK].
- [26] Kallehave D, Byrne B, Thilsted C, Mikkelsen K. Optimization of monopiles for offshore wind turbines. *Phil Trans R Soc A* 2015;373:1–15.
- [27] Kirsch F, Richter T, Coronel M. Geotechnische Aspekte bei der Gründungs bemessung von Offshore-Windenergieanlagen auf Monopfählen mit sehr großen Durchmesser. *Stahlbau* 2014;83(2):61–7.
- [28] Mirzadeh J, Kimiaei M, Cassidy M. Effects of irregular nonlinear ocean waves on the dynamic performance of an example jack-up structure during an extreme event. *Mar Struct* 2016;49:148–62.
- [29] Nagggar MHE, Bentley KJ. Dynamic analysis for laterally loaded piles and dynamic p-y curves. *Can Geotech J* 2000;37(6):1166–83.
- [30] Puech A, Foray P. Refined model for interpreting shallow penetration CPTs in sands. In: *Offsh tech conf*; 2002.
- [31] Schmidt B, Hansen M. Analyse mehrjähriger Messzeitreihen zur Ermittlung designrelevanter Lastparameter für Offshore-Windenergieanlagen. In: *Dwv-seminar zeitabhängige messgrößen*; 2014 [Hannover, Germany].
- [32] Schmidt B, Hansen M, Marx S. Directional dependence of extreme load parameters for offshore wind turbines. In: *Proc int offshore polar eng conf*; 2015 [Kona, Big Island, Hawaii, USA].
- [33] Sørensen SPH, Ibsen LB, Augustesen AH. Effects of diameter on initial stiffness of py curves for large-diameter piles in sand. In: *Eur conf numer meth geotech eng*; 2010 [Trondheim, Norway].
- [34] Sørensen SPH. Soil-structure interaction for nonslender, large-diameter offshore monopiles. PhD thesis. Aalborg Universitet; 2012.
- [35] Thieken K, Achmus M, Lemke K. A new static p-y approach for piles with arbitrary dimensions in sand. *Geotechnik* 2015;38(4):267–88.
- [36] Van Buren E, Muskulus M. Improving pile foundation models for use in bottom-fixed offshore wind turbine applications. *Energy Procedia* 2012;24:363–70.
- [37] Van Overschee P, De Moor B. Subspace algorithms for the stochastic identification problem. *Decis Control* 1991;2:1321–6.
- [38] Vorpahl F, Popko W. Description of the load cases and output sensors to be simulated in the OC4 project under IEA wind Annex30. Tech Report. Fraunhofer IWES; 2013.
- [39] Wiemann J, Lesny K, Richwien W. Evaluation of the pile diameter effects on soil-pile stiffness. In: *Proc ger wind energy conf*; 2004 [Wilhelmshaven, Germany].
- [40] Zaaier M. Foundation modelling to access dynamic behaviour of offshore wind turbines. *Appl Ocean Res* 2006;28:45–57.

3 Aleatory uncertainty of input parameters

Since input parameters are not set to deterministic values in probabilistic analyses, statistical data of these parameters is a basic prerequisite. However, there are two challenges. First, it has to be defined which parameters should be considered as uncertain and thus be statistically distributed and which ones can be set to deterministic values. Due to computational limitations, today, it is unrealistic to include all possible parameters in a probabilistic analysis. This challenge is addressed in Section 4. Second, in many cases, neither raw data nor empirical or theoretical statistical distributions are available for the considered site, turbine, etc. In this case, research databases in literature, being created for “standard” conditions, are a well-founded starting point. Such a database is set up here.

3.1 Research context

For probabilistic analyses of OWTs and even for deterministic approaches, considering various wind speeds, the knowledge of empirical or theoretical EC distributions is fundamental. Therefore, there are several databases for offshore ECs created and/or used in literature. Some examples are the widely known UPWIND database [51], a database for the US by Stewart et al. [186], and databases based on FINO data by Hansen et al. [69] and Häfele et al. [61]. Nonetheless, all these databases have some more or less severe limitations. The design basis of Stewart et al. [186] is only for deep water sites off the coasts of the US. Hence, it cannot be used for shallow water conditions in the North Sea. Moreover, wind speeds are not measured at hub height but at buoys only some metres above mean sea level (MSL). Similarly, for the UPWIND design basis [51], wind speeds are given at a reference height of 10 m and not at hub height. Furthermore, for conditional parameters (e.g. wave height H_s), only scatter plots are given. In the PSA-OWT project [69], data of the research platform FINO1 in the North Sea is used. Here, wind speeds are measured at hub height, but shadow effects can occur, if sensors are positioned behind the measuring mast. Häfele et al. [61] use data of FINO3. Due to several sensors at each height, shadow effects are reduced. Häfele et al. analyse only five ECs. Furthermore, most researches do not use dependent distributions and just apply “standard” distributions. For example, multi-modal distributions are only considered by Häfele et al.

Even if statistical distributions of probabilistic inputs are known precisely, another important factor for accurate OWT simulations are simulation constraints. Here, two of these constraints - simulation lengths and run-in time (i.e. the time at the beginning of each simulation that has to be discarded due to initial transients) - are discussed. Recommendations in standards remain fairly vague [53, 84]. For ULS calculations, normally, 1 h simulation length is recommended, while 10-minute simulations are proposed for FLS. For run-in times, 5 s or more are advised. This leads to varying values in literature [61, 95, 206]. To harmonise utilised simulation lengths based on well-founded analyses, several authors investigate the simulation lengths required for floating OWTs [58, 63, 185, 186]. For floating OWTs, it is concluded that a simulation length of 10 min is sufficient, if adequate algorithms are applied

(e.g. merging time series to reduce the effect of unclosed cycles in the rainflow counting for FLS). For bottom fixed structures, these investigations have not been performed so far. Regarding run-in times, there are even less well-founded recommendations. Haid et al. [63] propose 60s and the utilisation of initial conditions for floating OWTs. However, no details are given so that it is not clear why this value is recommended. Zwick and Muskulus [220] analyse the required run-in time for bottom fixed OWTs by checking the rotor speed to reach a steady state, although this procedure cannot guarantee that all initial transients are damped out. They conclude that run-in times up to 200s depending on the wind speed are needed. After all, there is a lack of well-founded recommendations for simulation constraints especially for bottom fixed OWTs.

3.2 Methods

Due to the present limitations of existing databases, in this thesis, a new database, is set up with the intention to resolve at least some shortcomings. For this purpose, raw data of three measurement masts in the German North and Baltic Sea (FINO1-3) is used. This data has the advantage that it is of high quality, for various ECs, for a relatively long measurement period, and based on wind measurements at hub height. Raw data is post-processed (missing data is handled and outliers are removed). Afterwards, ECs that cannot be measured directly (e.g. wind shear exponent) are calculated. In the next step, MLE is used to fit theoretical statistical distributions to the post-processed data. Since a large amount of raw data is available, the statistical uncertainty of the fits is fairly small in most cases and is not further considered. To enable an accurate and realistic representation of the real data, dependent, “advanced” distributions are used. This means that multi-modal and non-parametric distributions are considered as well. Furthermore, ECs cannot be considered as independent. Therefore, for example, for different wind speeds, changing distributions for the turbulence intensity are defined. The goodness of fits is assessed by applying KS and χ^2 tests and the best fitting distributions are selected.

Regarding simulation constraints, convergence studies of fatigue damages and ultimate loads with respect to simulation length and run-in time are conducted independently. These studies are based on several thousand probabilistic simulations with various lengths and run-in times. For ULS, the overall length of all simulations is kept constant (e.g. 600 ten-minute simulations and 100 one-hour simulations; c.f. Haid et al. [63]). For FLS, in accordance with the findings of Stewart [185], several simulations are merged (e.g. merging of six 10-minute simulations to one 1-hour simulation).

3.3 Results

The developed database consists of statistical distributions for three different sites and thirteen ECs. Dependent, “advanced” distributions are defined leading to accurate fits. The open-source character of the database makes it a possible basis for future probabilistic simulations. Furthermore, the database reveals some interesting facts regarding ECs. One example is the bimodal shape of the wind shear exponent PDF that includes a broad range of negative values. A second example are relatively low turbulence intensities compared to standards [84] and other databases [51].

For the investigated bottom fixed OWT, simulation lengths of 10 min are sufficient for ULS

and FLS calculations. This matches findings for floating OWTs. In probabilistic analyses, the use of 10-minute simulations is recommended, since it enables the simulation of more different EC combinations (i.e. six 10-minute simulations instead of one 1-hour simulation). For run-in times, it is shown that minimum values depend on the structure, wind speed, and load case (ULS/FLS). Some recommendations are given, although it has to be kept in mind that run-in times highly depend on the simulation code, damping values, etc.

3.4 Outlook

Although the present database for ECs and simulation constraints is a good starting point for future probabilistic analyses, its value can be significantly increased, if it is enlarged. For example, additional sites (including deep water sites for floating OWTs) and more long-term data (for the investigation of extreme events) should be added. This includes statistical distributions for extreme events like extreme turbulence intensities that are also relevant for turbine design (c.f. DLC 1.3 in the IEC standard [84]). Moreover, the inclusion of more ECs could be beneficial. One example is the change of wind direction over height (wind veer) that has not been considered so far, but could be determined using the present FINO data. Furthermore, only aleatory uncertainty (random variations of ECs) is covered. However, as, for example, the amount of raw data is limited, epistemic uncertainty (e.g. uncertainty due to incompleteness, statistical uncertainty) occurs as well. To cover epistemic uncertainty, in future, the present database could be updated to include imprecise probability data (e.g. using left and right bounds of cumulative density functions (CDFs) in a p-box approach). Lastly, recommendations regarding run-in times are a valuable help for designers and researchers, since in most cases, no convergence studies are conducted in advance. Nevertheless, the validity of these recommendations is limited (e.g. code or damping dependencies). Therefore, similar investigations for other codes, etc. would increase the benefit of the present contribution.

3.5 Paper B: Development of a comprehensive database of scattering environmental conditions and simulation constraints for offshore wind turbines

The following paper is published in *Wind Energy Science*, Volume 2 (2017), pages 491-505 (<https://doi.org/10.5194/wes-2-491-2017>). The main work was done by the author of this thesis. Cristian Gebhardt and Raimund Rolfes contributed with advisory and supporting work. Special thanks go to “Bundesamt für Schifffahrt und Hydrographie” (BSH) and the various operators and funders of the FINO platforms for providing the raw data.

Wind Energ. Sci., 2, 491–505, 2017
<https://doi.org/10.5194/wes-2-491-2017>
© Author(s) 2017. This work is distributed under
the Creative Commons Attribution 3.0 License.



Development of a comprehensive database of scattering environmental conditions and simulation constraints for offshore wind turbines

Clemens Hübler, Cristian Guillermo Gebhardt, and Raimund Rolfes

Institute of Structural Analysis, Leibniz Universität Hannover, Appelstr. 9a, 30167 Hanover, Germany

Correspondence to: Clemens Hübler (c.huebler@isd.uni-hannover.de)

Received: 17 May 2017 – Discussion started: 8 June 2017

Revised: 4 September 2017 – Accepted: 23 September 2017 – Published: 26 October 2017

Abstract. For the design and optimisation of offshore wind turbines, the knowledge of realistic environmental conditions and utilisation of well-founded simulation constraints is very important, as both influence the structural behaviour and power output in numerical simulations. However, real high-quality data, especially for research purposes, are scarcely available. This is why, in this work, a comprehensive database of 13 environmental conditions at wind turbine locations in the North and Baltic Sea is derived using data of the FINO research platforms. For simulation constraints, like the simulation length and the time of initial simulation transients, well-founded recommendations in the literature are also rare. Nevertheless, it is known that the choice of simulation lengths and times of initial transients fundamentally affects the quality and computing time of simulations. For this reason, studies of convergence for both parameters are conducted to determine adequate values depending on the type of substructure, the wind speed, and the considered loading (fatigue or ultimate). As the main purpose of both the database and the simulation constraints is to compromise realistic data for probabilistic design approaches and to serve as a guidance for further studies in order to enable more realistic and accurate simulations, all results are freely available and easy to apply.

1 Introduction

Although the share of offshore wind energy in overall energy production has been steadily growing over the last years, the cost of offshore wind energy is still high compared to other renewable energies (Kost et al., 2013). In order to achieve potential cost reductions of about 30 % in the next 10 years (Prognos AG and Fichtner, 2013), a realistic and accurate simulation of offshore wind turbines and their substructures is beneficial. On the one hand, for realistic simulations, the knowledge of scattering environmental conditions is a central point. In this context, scattering conditions are non-constant parameters that exhibit stochastic variations and aleatoric uncertainties, and therefore should be modelled as statistically distributed. On the other hand, carefully chosen simulation constraints, like the simulation length or the time of initial transients, are essential to obtain accurate results. Here, the simulation length is defined as the usable time for the post-

processing. The time of initial transients is the time that is removed from each simulation to exclude initial transients resulting from starting a calculation with a set of initial turbine conditions (like rotor speed). Simulation length plus initial transient time make up the overall length.

Regarding the first point, current guidelines (IEC, 2009) already define that simulations should mirror the changing environmental conditions at the precise site of a wind turbine. However, for academic research, real site data are rarely available, and, even for industrial purposes, data quality might be poor for some parameters or long-term data might be missing. As a result, various research projects have characterised environmental conditions at specific sites or entire areas and published statistical distributions as a reference. Probably the most frequently used example is the UP-WIND design basis (Fischer et al., 2010). Further examples are the work of Stewart et al. (2015), the PSA-OWT project (Hansen et al., 2015), and the investigations by Häfele et al.

(2017). All these reference conditions have some limitations. The design basis of Stewart et al. (2015) is only for deep-water sites off the coasts of the United States of America. The wave state of deep-water sites is not comparable to shallow-water conditions in the North Sea, as significant wave heights generally increase with the water depth (Hansen et al., 2015). Additionally, wind speeds are not measured at hub height and therefore have to be extrapolated, which increases uncertainties. For the UPWIND design basis, the wind speed is just given at a reference height of 10 m and not at hub height as well. Furthermore, no statistical distributions for conditional parameters (e.g. the wave height H_s depends on the wind speed v_s) are given, only scatter plots. In the PSA-OWT project, data of the research platform FINO1 in the North Sea are used. Here, the wind speed is measured at hub height, but shadow effects can occur if sensors are positioned behind the measuring mast. Häfele et al. (2017) use data of the research platform FINO3, which has several sensors at each height to reduce shadow effects. However, only five environmental parameters (wind speed and direction, wave height, period and direction) are analysed, and the data period is only 5 years. Hence, the need for a comprehensive database, covering several sites and the most important parameters, becomes obvious in order to enable future research that is based on realistic data. Missing conditions are, for example, the turbulence intensity, the wind shear, or ocean currents.

As to the second point, simulation constraints are frequently chosen based on experience, literature values, or recommendations in current standards. However, considering the simulation length and time of initial transients, recommendations in the guidelines are mainly fairly vague (GL, 2012; IEC, 2009). Simulation lengths of 10 min for fatigue calculations (FLS), and 1 h or less for ultimate loads (ULS) are frequently recommended. For the initial transients, it is advised to discard lengths of 5 s or more. Literature values partly differ significantly. To reduce the effects of initial transients, the first 20, 30, or 60 s are discarded, for example (Vemula et al., 2010; Jonkman and Musial, 2010; Hübler et al., 2017), and simulation lengths of 10 min and 1 h are common practice (Jonkman and Musial, 2010; Popko et al., 2012; Cheng, 2002). However, longer simulation lengths are partly used as well, especially in the oil and gas industry or for floating substructures (DNV, 2013). Still, all these recommendations are not underpinned with detailed analyses. For floating offshore wind turbines, such investigations were conducted for the simulation length by Stewart et al. (2015), Stewart et al. (2013) and Haid et al. (2013). It is shown that simulation lengths of 10 min are sufficient for ULS and FLS loads. The observation that ULS and FLS loads tend to be higher for longer simulations is not for physical reasons but due to unclosed cycles in the rainflow counting for the FLS case and a result of the averaging technique in the case of ULS loads. Both can be handled by adapting the algorithms. Concerning the time of initial transients, Haid et al. (2013) recommend 60 s and the utilisation of initial conditions. This

recommendation is based on an analysis which has not been further specified. For a jacket foundation, Zwick and Muskulus (2015) conducted a study investigating lengths of simulations and initial transients and also concluded that 10 min is sufficient, as long as 10 min time series are merged before the rainflow counting is applied. The required time of initial transients is determined by checking the rotor speed to reach a steady state. However, the initial conditions are not applied, and a steady speed does not guarantee that all transients are damped out. Therefore, the need for well-founded guidance on simulation lengths and times of initial transients for bottom-fixed substructures becomes clear. For the simulation length, useful preliminary work is available, but it is limited to jacket substructures. Concerning initial transients, extensive studies are rare and do not concentrate on the convergence of the relevant loads (FLS and ULS). Furthermore, scattering environmental conditions are not taken into account. This is a simplification especially in the case of the initial transients, as this variation might lead to more pronounced resonance effects (e.g. rarely occurring low wave peak periods that are close to the natural frequency of the structure; see Sect. 2.4) and therefore to more pronounced initial transients.

After all, the listed shortcoming in state-of-the-art modelling assistance motivated the current work that focuses on the following aspects:

1. deriving an open-access database for various scattering environmental conditions at different sites to enable more realistic modelling;
2. giving well-founded guidance on simulation length requirements and the time needed to exclude initial transients, when these realistic conditions are applied, to improve accuracy of numerical simulations.

In order to address these topics, firstly, a database for all significant environmental conditions is derived from real data of the FINO research platforms. In this work, the data source is introduced, the analysis is described, and the resulting distributions and some interesting findings are presented. Secondly, required simulation lengths and times of initial transients are determined. For this purpose, the probabilistic simulation approach and the simulation model are explained. Then, studies of convergence are conducted for the simulation length and the time of initial transients. A monopile and a jacket substructure, FLS and ULS loads, and different wind speeds are considered. Recommendations are summarised. Lastly, the benefits and limitations of the current approach are summarised, and a conclusion is drawn.

2 Comprehensive database

2.1 Raw data

Environmental conditions can vary significantly among various turbine sites. As these states affect loads, and therefore

Table 1. Environmental conditions (wind speed v_s , significant wave height H_s , wave peak period T_p , and turbulence intensity TI) of the K13 shallow-water site (UPWIND design basis; Fischer et al., 2010). The wind shear exponent is $\alpha = 0.14$, and wind and wave directions are usually set to zero, but scatter plots are available.

v_s (m s^{-1})	2	4	6	8	10	12	14	16	18	20	22	24	26
TI (%)	29.2	20.4	17.5	16.0	15.2	14.6	14.2	13.9	13.6	13.4	13.3	13.1	13.0
H_s (m)	1.07	1.10	1.18	1.31	1.48	1.70	1.91	2.19	2.47	2.76	3.09	3.42	3.76
T_p (s)	6.03	5.88	5.76	5.67	5.74	5.88	6.07	6.37	6.71	6.99	7.40	7.80	8.14



Figure 1. Positions of the three FINO platforms in the North and Baltic Sea, adapted from OpenStreetMap.

the design of offshore wind turbines, precise data of specific turbine location are valuable. Real site data are scarce, which is the reason for the previously mentioned reference databases (Fischer et al., 2010; Hansen et al., 2015; Stewart et al., 2015; Häfele et al., 2017). These databases define conditional, statistical distributions for some of the most important environmental conditions: wind speed and direction, wave height, direction, and peak period. However, other conditions are fixed for each wind speed or are set completely constant. The states of the frequently used UPWIND design basis are summarised in Table 1 as an example.

In this study, scattering conditions are derived directly from offshore measurement data. The raw data are taken from the three FINO platforms, and conditional distributions for the following 13 environmental parameters are determined: wind speed and direction, wave height, peak period and direction, turbulence intensity, wind shear exponent, speed and direction of the sub- and near-surface current, and air and water density. The FINO measurement masts are located in the North Sea and Baltic Sea and are operated on behalf of the German Federal Ministry for the Environment, Nature Conservation, Building and Nuclear Safety (BMUB).¹ for details. The locations of the three FINO sites are marked in Fig. 1.

¹Raw data of the FINO platforms are freely available for research purposes. See <http://www.fino-offshore.de/en/>

For all three sites, maximum, minimum, mean, and standard deviation values of the wind speed, measured at different heights between 30 and 100 m above mean sea level, are available for 10 min intervals. Wind speeds are measured with cup and ultrasonic anemometers. In this study, cup anemometers are used, as these sensors are available at more different heights. For FINO1 and 2, the anemometers are positioned on jibs in secondary wind directions to reduce shadow effects. For FINO3, three anemometers are installed around the mast to minimise shadow effects. Sensors at different heights allow a detailed analysis of shear effects. Wind direction, air pressure, temperature, and humidity are measured at different heights as well. Buoys in the immediate vicinity of the research platforms (about 150 m) measure the wave conditions. Mean values of significant wave heights, wave directions, wave peak periods and water temperatures are measured every 30 min. Furthermore, acoustic Doppler current profilers (ADCPs) close to the platforms measure ocean current velocities and directions at different water depths using the Doppler effect of sound waves. The platforms FINO1, 2, and 3 have been measuring continuously since 2004, 2007, and 2009 respectively, resulting in 7 to 13 complete years of measurement data, and enabling at least some long-term predictions. Data of incomplete years are not taken into account in order not to introduce bias due to seasonal effects.

2.2 Conditional distributions

In this work, raw data of the FINO measurement masts are used to set up a database for correlated, scattering environmental conditions. As the post-processing of raw data is time-consuming and it is unnecessary to repeat it each time environmental conditions are used, conditional probability distributions (i.e. $P(Y = y|X = x)$, with X being the independent random variable, Y the dependent one, and P the probability function) for environmental conditions are derived to make the database easy to use. Firstly, post-processing is carried out to identify sensor failures (missing data) and measurement failures (outliers). Missing data are not interpolated but instead left out, in order not to introduce any bias. As sufficient data of proper signal quality are available (e.g. more than 350 000 data points for the wind speed even for FINO3), this approach is practicable. Wind speed data are synchronised with the wind direction data. This enables a selection of the anemometer in front of the mast for FINO3. For FINO1 and 2, wind speed values are discarded if the jib is located directly in the tower shadow. The turbulence intensity (TI) can be computed as the quotient of the standard deviation of the wind speed in a 10 min interval (σ_v) and the mean wind speed in this interval (v_s) according to Eq. (1):

$$TI = \frac{\sigma_v}{v_s}. \quad (1)$$

For the wind shear, Eq. (2) applies according to the standard of IEC (2005):

$$v_s(z) = v_s(z_0) \times \left(\frac{z}{z_0}\right)^\alpha, \quad (2)$$

where z is the height above mean sea level, z_0 is a reference height, $v_s(z)$ and $v_s(z_0)$ are wind speeds at the specified heights, and α is the wind shear exponent. At the FINO platforms, the wind speed is measured at eight different heights. Therefore, it is possible to determine the wind shear exponent for every 10 min interval by assuming $z_0 = 90$ m and applying a non-linear regression. The air density can be calculated using Avogadro's law in Eq. (3) and the measurements of humidity (ϕ), air pressure (p_{humid}), and temperature in degrees Celsius (T_{air}):

$$\rho_{\text{air}} = \frac{p_{\text{humid}}}{R_{\text{humid}} T_{\text{air}}}. \quad (3)$$

As humid air can be regarded as a mixture of ideal gases, the following equation applies for R_{humid} :

$$R_{\text{humid}} = \frac{R_{\text{dry}}}{1 - \phi \frac{p_{\text{sat}}}{p_{\text{humid}}} \left(1 - \frac{R_{\text{dry}}}{R_{\text{vapour}}}\right)}, \quad (4)$$

where $R_{\text{dry}} = 287.1 \text{ J kg}^{-1} \text{ K}^{-1}$ is the specific gas constant for dry air, $R_{\text{vapour}} = 461.5 \text{ J kg}^{-1} \text{ K}^{-1}$ for water vapour, and

p_{sat} is the saturation vapour pressure that can, for example, be calculated using the August–Roche–Magnus formula:

$$p_{\text{sat}} = 6.1094 \text{ hPa} \times e^{\frac{17.625 \times T_{\text{air}}}{T_{\text{air}} + 243.04}}. \quad (5)$$

For the water density, a semi-analytical approach by Millero and Poisson (1981) of the following form is applied:

$$\rho_{\text{water}} = A(T_{\text{water}}) + B(T_{\text{water}})S + C(T_{\text{water}})S^{1.5} + DS^2, \quad (6)$$

where S is the salinity; T_{water} is the water temperature at the surface; A , B , and C are polynomial functions of the water temperature; and D is a constant. As constant salinity is assumed, the water density is a function of the water temperature. For all wave parameters, 3 h mean values are calculated, as wave conditions stay stationary for a duration of about 3 h (GL, 2012). For the speeds and directions of sub- and near-surface currents, measured current values (v_m and θ_m) have to be converted in order to separate sub- and near-surface components. According to, for example, IEC (2009), the following two equations apply for sub- and near-surface currents respectively:

$$v_{\text{SS}}(z) = v_{\text{SS}}(0 \text{ m}) \left(\frac{d-z}{d}\right)^{\frac{1}{7}} \quad (7)$$

and

$$v_{\text{NS}}(z) = \begin{cases} v_{\text{NS}}(0 \text{ m}) \left(\frac{20 \text{ m} - z}{20 \text{ m}}\right) & \text{for } z \leq 0 \\ 0 & \text{for } z > 0. \end{cases} \quad (8)$$

Here, $v_{\text{SS}}(z)$ and $v_{\text{NS}}(z)$ are the sub- and near-surface current speeds at a position z below the water surface, and d is the water depth. For reasons of clarity, the following notation is introduced: $v_{\text{SS}}(z) = v_{\text{SS},z}$. The velocity profiles are shown in Fig. 2. Obviously, the near-surface current does not exist below a reference depth of 20 m. Hence, it is possible to use measurement data of a depth of 20 m (or more) to directly get the sub-surface direction ($\theta_{\text{SS},20} = \theta_{m,20}$) and to calculate the speed, for example for FINO2 ($d = 25$ m):

$$v_{\text{SS},0} = v_{\text{SS},20} \left(\frac{25 \text{ m} - 20 \text{ m}}{25 \text{ m}}\right)^{-\frac{1}{7}}. \quad (9)$$

For the near-surface current, measurements close to the surface (e.g. $v_{m,2}$) can be used. However, these measurements include sub- and near-surface components, as shown in Fig. 3.

Therefore, the sub-surface component at 2 m has to be calculated using Eq. (7), and the sub-surface direction is assumed to be constant over depth ($\theta_{\text{SS},20} = \theta_{\text{SS},2} = \theta_{\text{SS},0}$). Then, trigonometrical relationships can be applied to calcu-

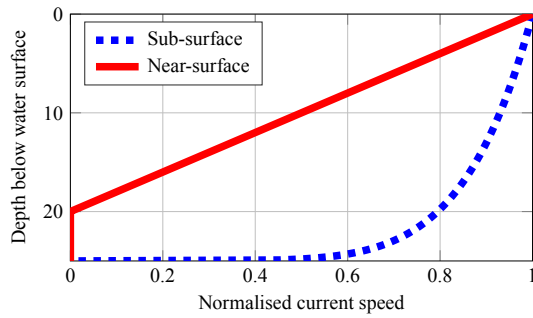


Figure 2. Velocity profiles of the sub- and near-surface currents according to Eqs. (7) and (8) respectively, with a water depth of 25 m and normalised speeds ($v_{SS,0} = v_{NS,0} = 1$).

late the near-surface current at 2 m:

$$v_{NS,2} = \sqrt{v_{SS,2}^2 + v_{m,2}^2 - 2v_{SS,2}v_{m,2}\cos(\theta_{m,2} - \theta_{SS,2})}, \quad (10)$$

$$\theta_{NS,2} = \theta_{m,2} + \arcsin\left(\frac{v_{SS,2}\sin(\theta_{m,2} - \theta_{SS,2})}{v_{NS,2}}\right). \quad (11)$$

Lastly, the reference near-surface current $v_{NS,0}$ is given by

$$v_{NS,0} = v_{NS,2} \left(\frac{20\text{ m}}{20\text{ m} - 2\text{ m}}\right). \quad (12)$$

A depth-independent near-surface direction is assumed, and therefore $\theta_{NS,0} = \theta_{NS,2}$.

After having post-processed the measurement raw data, maximum likelihood estimations are applied to the processed data of the regarded 13 environmental conditions in order to fit several statistical distributions. In addition to unimodal distributions, and if several distinct peaks are distinguishable, multimodal distributions are fitted as well, as it is assumed that the peaks are due to physical phenomena. However, as multimodal approaches have more degrees of freedom, they always fit the data better, even in the case of a physically unimodal shape. Therefore, they have to be chosen with care in order not to fit physically unimodal distributions with multimodal approaches.

Considering the example of wind speed and wave height, it is self-evident that some environmental parameters are conditioned by others, and dependencies have to be defined. For example, the case of a calm sea during a storm is very unlikely. Analysing scatter plots of the environmental inputs and taking a literature review into account, the dependencies in Table 2 are defined, although it is possible to define them differently (see Stewart, 2016), as mainly the correlation is significant, and the determination of cause and effect is secondary.

One of the most common ways to include dependencies in statistical distributions is to split up the data of the dependent parameters into several bins of the independent parameters (e.g. Stewart, 2016; Johannessen et al., 2002; Li et

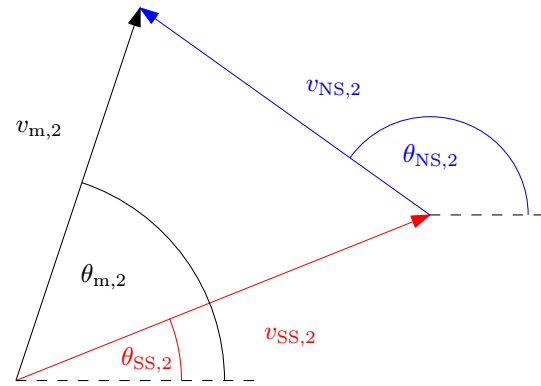


Figure 3. Vectorial analysis of ocean current components at a depth of 2 m (measured values (m), near- and sub-surface components (NS and SS)).

al., 2015). To illustrate this approach, for example, the wave peak period is fitted in several bins of 0.5 m wave height (e.g. $P(T_p) = P(T_p|1.5\text{ m} \leq H_s < 2\text{ m})$). The bin widths for the dependent parameters are summarised in Table 2 as well. For highly correlated parameters, an alternative to the binning procedure is to model only the deviation between the parameters. Here, the direction of the near-surface current that is highly dependent on the wind direction is an example. Therefore, by modelling the deviation Δ_{NS} according to Table 2, the following applies:

$$\theta_{NS} = \Delta_{NS} + \theta_{wind} \quad (13)$$

Visual inspections and objective criteria using Kolmogorov–Smirnov tests (KS tests) and chi-squared tests (χ^2 tests) are used to select the best fitting distribution for each environmental condition. Although the KS test is less powerful than other statistical tests, it is still used due to its suitability for small samples (occurring, for example, for dependent variables and high wind speeds), where χ^2 tests are not applicable. For one parameter, it is attempted to choose only one distribution for all bins and sites in order to keep the database easy to use. However, as noted in Table 2, in some cases several distributions are selected to increase the accuracy of the fits.

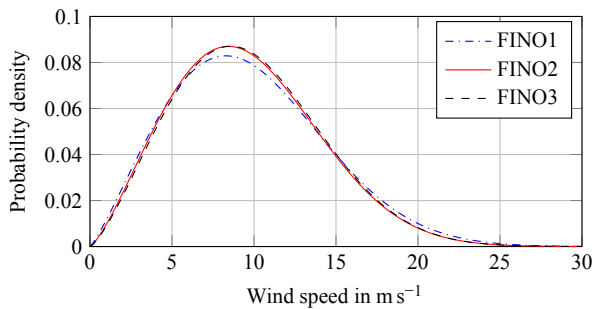
Directional parameters like θ_{wind} are treated differently, as classical, parametric distributions can hardly fit several peaks in continuous distributions ($0^\circ = 360^\circ$). Therefore, a non-parametric kernel density estimation (KDE) is used to fit directional parameters.

2.3 Resulting distributions

In order to establish a full database, statistical distribution and their parameters for all 13 environmental conditions, the three sites and all bins (if necessary) have to be provided. Furthermore, for non-parametric distributions the underlying data are needed. The main ideas are explained here; however,

Table 2. Dependencies, statistical distributions, and bin widths for environmental conditions derived from FINO1–3 data.

Parameter	Statistical distributions	Dependencies	Bin sizes
Wind speed (v_s)	Weibull	–	–
Wind direction (θ_{wind})	Non-parametric KDE	Wind speed	2 m s^{-1}
Turbulence intensity (TI)	Weibull, gamma	Wind speed	2 m s^{-1}
Wind shear exponent (α_{PL})	Bimodal normal	Wind speed	2 m s^{-1}
Air density (ρ_{air})	Bimodal log-normal	–	–
Significant wave height (H_s)	Gumbel, Weibull	Wind speed	2 m s^{-1}
Wave peak period (T_p)	Bimodal Gumbel	Wave height	0.5 m
Wave direction (θ_{wave})	Non-parametric KDE	Wave height and wind direction	1.0 m and 30°
Water density (ρ_{water})	Trimodal normal	–	–
Near-surface current (v_{NS})	Weibull	–	–
Sub-surface current (v_{SS})	Weibull, Gumbel	–	–
Deviation NS direction (Δ_{NS})	Bimodal normal	(Wind direction and NS direction)	–
SS direction (θ_{SS})	Non-parametric KDE	–	–

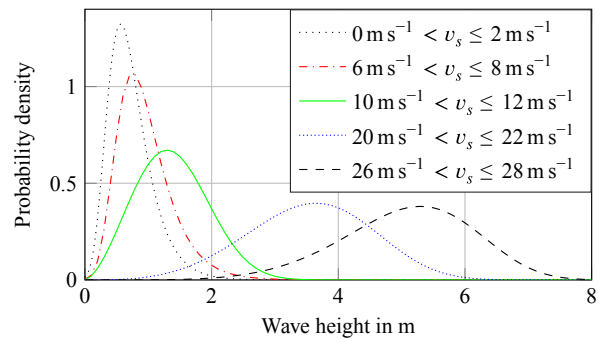
**Figure 4.** Weibull distributions for the wind speeds for all three sites.

due to the comprehensiveness of the data, detailed and additional information is provided in an easily applicable form, in the Supplement. At this point, only two examples are shown in Figs. 4 and 5.

2.4 Special findings

In this section, some noteworthy findings of this database, mainly resulting from the consideration of scattering, are pointed out. Three examples are presented: the importance of wave peak periods, the high scattering of wind shear exponents, and the behaviour of the turbulence intensity.

Wave loads are of particular importance if the wave frequency is close to the first natural frequency of the structure. Standard offshore wind turbines have first bending frequencies of about 0.25 to 0.3 Hz (Jonkman and Musial, 2010; Popko et al., 2012) corresponding to eigenperiods of less than 4 s. If state-of-the-art databases are used (see Table 1), there will be no resonance. However, real data suggest that resonance effects are problematic even for higher wind speeds, as wave peak periods of less than 4 s occur (see Fig. 6).

**Figure 5.** Distribution of the significant wave height for different wind speeds and the FINO1 site. For $v_s \leq 10 \text{ m s}^{-1}$, Gumbel distributions are applied. For higher wind speeds, Weibull distributions fit the data more accurately.

Concerning the wind shear exponent, in the standards and most current databases (e.g. GL, 2012; Fischer et al., 2010), constant values for all wind speeds are proposed. However, this assumption is a massive simplification. Ernst and Seume (2012) showed that the wind shear exponent significantly depends on the wind speed. Here, it is shown (see Fig. 7) that it does not only vary between wind speeds but also scatters remarkably within each bin as well, and might even be negative.

For the turbulence intensity, this database reveals that state-of-the-art approaches are mainly conservative, as too high turbulence intensities are assumed. This is shown in Fig. 8, where the turbulence intensity for all three sites is compared to a standard database (Fischer et al., 2010) and to current standards (IEC, 2009). All three sites exhibit similar mean turbulence intensities and 90th percentile values ($Q_{0.9}$). For the comparison with literature values, the 90th percentile is of importance, as standards require simulations with this percentile value. However, even for the 90th per-

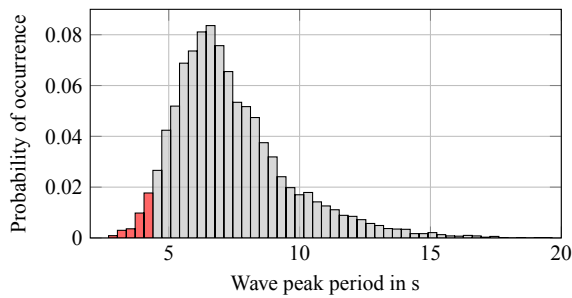


Figure 6. Probability distribution of the wave peak period for $v_s = 11\text{--}13\text{ m s}^{-1}$ for the FINO3 site.

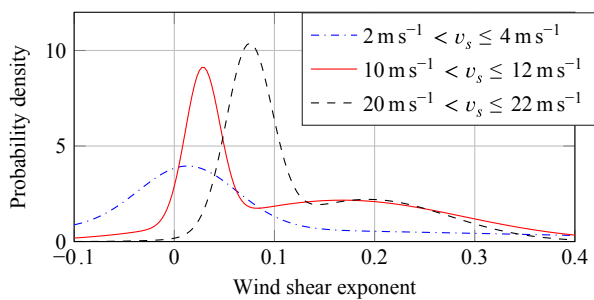


Figure 7. Distribution of the wind shear exponent for different wind speeds for the FINO2 site.

centile, the UPWIND database is very conservative. The least conservative case (category C) in IEC (2009) fits the $Q_{0.9}$ values relatively well, but it predicts slightly higher turbulence intensities for wind speeds above about 10 m s^{-1} . Considering the fact that using the 90th percentile is a conservative assumption and that the measurements include some wake effects due to wind farms near to all measurement masts, it can be concluded that state-of-the-art assumptions for turbulence intensities are probably unnecessarily conservative. The wake effects are depicted in Fig. 9, where turbulence intensity measurements of FINO1 from 2011 to 2016 are shown. In this period, the wind farm Alpha Ventus was operating on the east side of FINO1. Therefore, west wind leads to free stream conditions and east wind to wake conditions. Obviously, free stream conditions lead to even lower turbulence intensities, whereas wake conditions increase the turbulence, especially for smaller wind speeds, as also detected by Hansen et al. (2012).

3 Simulation assistance

In the previous section, a comprehensive database for scattering environmental offshore conditions was developed. However, even with realistic input parameters the accuracy of numerical simulations is significantly influenced by constraints like their lengths and the time eliminated to exclude ini-

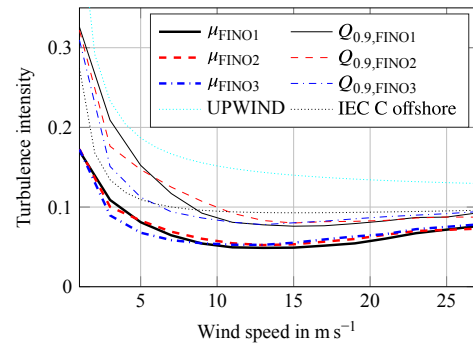


Figure 8. Turbulence intensity (mean value and 90th percentile ($Q_{0.9}$)) for different wind speeds compared to the literature.

tial transients. Therefore, in this section, efficient simulation lengths and times of initial transients for varying wind speeds and different types of loading and substructures are determined. This is achieved by analysing the convergence of relevant quantities (i.e. FLS and ULS loads). Before conducting these studies, the overall probabilistic simulation approach is explained, as it differs from the approach in the standards. Subsequently, the utilised simulation model and the chosen environmental conditions are briefly presented.

3.1 Probabilistic simulation approach

For the design of offshore wind turbines, several design load cases (DLC1.1 to 8.3) have to be simulated according to the standards (IEC, 2009). These load cases cover ultimate and fatigue loads during power production, idling and fault conditions, and several special cases like start-up or shut-down. Stochastic inputs for turbulent wind and irregular wind are included. Nevertheless, the DLCs remain quasi-deterministic, as environmental conditions like turbulence intensities and wind shear do not scatter. In order to guarantee safe designs despite the deterministic approach, several ULS load cases, covering extreme environmental conditions (e.g. DLC1.3 for turbulence or DLC1.5 for wind shear), are needed.

In this work, statistically scattering environmental conditions are applied, and therefore a probabilistic simulation approach is used. This probabilistic approach differs from the deterministic load-case-based approach. For the probabilistic approach or “real-life” approach, it is not necessary to simulate any load cases of extreme environmental conditions (e.g. DLC1.3 to 1.6), but the use of scattering conditions leads directly to simulations that represent the real lifetime of the turbine (without fault, start-up, or other special situations). Hence, simulations (e.g. 10 000 simulations) cover a realistic period of power production and idling, leading to about 2.3 months of turbine lifetime (for 10 000 simulations). As environmental conditions scatter, effects like high turbulences, extreme wind shear, high waves, small wave periods,

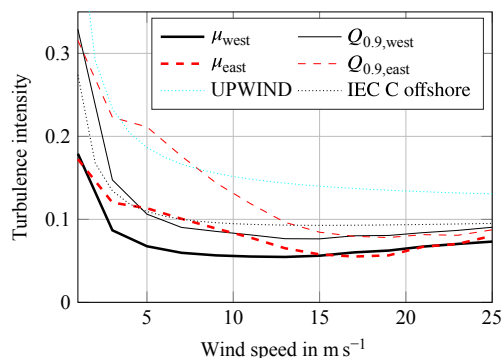


Figure 9. Shadow effects on the turbulence intensity for FINO1 and free stream (western) and wake (eastern) conditions.

and others are covered and do not have to be considered separately. Load cases are not simulated explicitly, but are covered implicitly by conducting probabilistic simulations.

That is why the two approaches do not differ significantly for FLS. The “real-life” approach covers DLC 1.2 and 6.4. For ULS, the “real-life” approach covers all power production cases (DLC 1.1–1.6) and DLC 6.1 by applying scattering environmental conditions. As the “real-life” approach cannot simulate 20 years of turbine lifetime (or even a return period of 50 years), a load extrapolation, as required for DLC 1.1, is needed in order to calculate an ULS design. However, this extrapolation is not needed here, as it does not influence the investigated simulation constraints.

As common in academia, only power production and idling is simulated. Fault cases, start-up, etc. are not taken into account due to several reasons. Firstly, at least for the jacket, fault cases are less relevant (Vemula et al., 2010). Secondly, these load cases are very controller and design dependent and need special treatment (e.g. there is no need of removing initial transients for start-up load cases). Thirdly, this work is not intended to calculate exact fatigue damages or ultimate loads for the whole turbine lifetime, as no turbine design or optimisation is done. The exclusion of some load cases does not affect the recommendations on simulation constraints that are given for power production and idling conditions. As there is no need of exact FLS and ULS lifetime loads in this study, an assessment of the probabilistic approach concerning accordance with the standards is neither conducted nor needed, but this would be valuable for further applications of probabilistic approaches.

3.2 Simulation setup

As environmental conditions vary for various turbine sites, a database being used for the studies of convergence has to be chosen. The basis developed in this work is appropriate, and the FINO3 site is chosen. Some conditions, like air and water density, are kept fixed, as it was shown that their variation

is of minor importance (Hübler et al., 2017). An attempt is made to keep the convergence study as simple as possible, and to focus on the most relevant parameters. Hence, for the probabilistic approach, statistically scattering values according to the determined distributions of wind speed and direction, wave height, direction and period, turbulence intensity, and wind shear exponent are used in all simulations. In addition, the following assumptions are made for all simulations:

- The turbulent wind field is computed according to the Kaimal model and using the software TurbSIM (Jonkman, 2009) with a different wind seed for each simulation.
- Irregular waves are calculated according to the JON-SWAP spectrum using varying wave seeds for all simulations.
- Soil conditions of the OC3 model (Jonkman and Musial, 2010) are applied.
- The current, second-order and breaking waves, wave spreading effects, marine growth, local vibration effects of braces, joint stiffnesses, and degradation effects are neglected.

The time domain simulations of the convergence study are conducted using the aero-servo-hydro-elastic simulation framework FASTv8 (Jonkman, 2013). A soil model (Häfele et al., 2016) applying linearised soil-structure interaction matrices enhances this code. The NREL 5 MW reference wind turbine (Jonkman et al., 2009) with two different substructures is investigated: Firstly, the OC3 monopile (Jonkman and Musial, 2010) and secondly, the OC4 jacket (Vorpahl et al., 2013). The outcomes of the FAST simulations are, inter alia, time series of forces, moments, and stresses for each element of the substructure.

Since the convergence of fatigue and ultimate loads is investigated in the next step, the calculation concept of these two loads is briefly explained.

For the jacket, the procedure of the fatigue analysis in accordance with DNV (2010) is the following: for each connection of each joint (K joints, Y joint, butt welds, etc.), eight hotspot stresses around the circumference of the intersection have to be calculated using the time series. The needed stress concentration factors (SCFs) depending on the joint geometry are calculated according to Appendix B of DNV (2010). The fatigue damage is calculated with a fatigue limit of 52.6 MPa at 10^7 cycles. This corresponds to the DNV-GL S-N curve 90 (for cathodic protection) as used in the original design (Vemula et al., 2010). For all stresses, rainflow counting evaluates the stress cycles. As recommended by the current standards, the conservative damage accumulation according to the Palmgren–Miner rule is assumed using a slope of the S–N curve of 3 before and 5 after the fatigue limit for both substructures. The separated fatigue calculation (and summation over all simulations) for each connection of each

joint is necessary, as damages in each connection and joint are different for each simulation, and the highest values do not always occur in the same joint (for example due to the probabilistic variation of the wind direction). Finally, the decisive damage for the jacket is the highest accumulated value of all connections of all joints.

For the monopile, the fatigue procedure is similar, but is done according to European Committee for Standardization (2010b), where a detail of 71 MPa for transverse butt welds and an additional reduction due to the size effect ($t > 25$ mm) is recommended. Differing from the recommendations in European Committee for Standardization (2010b), the same slopes of the S–N curves as for the jacket are used.

For the ULS analysis, maximum stresses are decisive and extracted from the time series. For the monopile, European Committee for Standardization (2010a) is used to analyse the plastic limit state, cyclic plasticity limit state, and buckling limit state (LS1–3). For the jacket, NORSOK N-004 is applied for tubular members and joints, which takes combined axial, shear, bending, and hydrostatic loadings into account. In both cases, the yield stress is 355 MPa.

Additionally, ultimate limit state proofs for the foundation piles are performed including axial and lateral soil proofs according to GEO2 (DIN 1054, 2010) and a plastic limit state proof (LS1) for the steel pile below mudline. Especially for the monopile, the last proof might be decisive as the bending moment frequently reaches its maximum below mudline. For all ULS proofs, utilisation factors, being the percentage of the maximum loads, are the outcomes.

3.3 Simulation length

The simulation length significantly influences the overall computing time of the load assessment. However, there is no conclusive consensus concerning the length needed. Current standards recommend, for example, 10 min or 1 h calculations. The offshore oil and gas industry prefers simulation lengths of 6 h to cover all low-frequency hydrodynamic effects.

The use of 10 min simulations can potentially reduce the computing time by a factor of about 36 compared to 6 h simulations. Hence, a study of convergence for bottom-fixed offshore wind turbines is conducted here. For floating wind turbines, it is referred to Stewart (2016), who showed that for floating structures all physical effects can be covered with 10 min simulations.

The presented outcomes of this study focus on the monopile substructure, but a jacket is analysed as well and results (not shown) are generally comparable. For several wind speed bins, 500 simulations with a total length of 10 h are conducted. As the initial transient behaviour is analysed subsequently, a clearly sufficient time, being discarded to exclude the initial transients, of 4 h is chosen. With elimination of these 4 h of initial transients, the total length of 10 h reduces to a maximum available length (simulation length) of

6 h for the convergence study. In a first step, the convergence of FLS loads is analysed. Afterwards, the ULS case is investigated.

The procedure to calculate the mean fatigue damage for each wind speed bin is the following: from the basis of the 500 ten-hour simulations having different random seeds and varying environmental conditions, 500 cases are selected (with replacement). For each simulation, the fatigue damage is calculated and weighted with the simulation length. The mean value of all cases is calculated. This procedure is repeated 10 000 times (bootstrapping) to assess the associated uncertainty.

Figure 10 displays the normalised mean fatigue damages for different wind speeds and simulation lengths between 10 min and 6 h. The values are normalised with the 6 h values, and error bars show the $\pm\sigma$ confidence intervals (68 %) that are estimated using a bootstrap procedure with 10 000 resamplings.

It is apparent that due to scattering environmental conditions and the limited number of simulations the uncertainty is relatively high. A detailed investigation of the fatigue load uncertainty, when scattering environmental conditions are applied, is valuable but out of the scope of this work (see Sect. 4). Nevertheless, from Fig. 10 it is apparent that there are no pronounced trends for changing simulation lengths. A slight increase in fatigue loads for higher simulation lengths might be suspected given the fact that such behaviour was observed for floating substructures by Stewart (2016). In order to focus on the simulation length effects, the variation of environmental conditions is neglected in a second step (only varying random seeds). This reduces the uncertainty, making it possible to clearly identify a slight increase in FLS loads of about 5 % for higher simulation lengths (see Fig. 11, non-merged case). However, as shown by Stewart (2016) for floating substructures, the increasing fatigue loads are not due to any physical effect (all important low-frequency effects of waves are already covered by 10 min simulations), but can be explained by the effect of unclosed cycles in the rainflow counting. Cycles that are not completed at the end of the simulation are approximated by counting them as half cycles. The longer the simulation, the less influential this approximation is, as the number of half cycles compared to the number of full cycles reduces. A quite straightforward approach to reduce the problem of half cycles is to merge several shorter simulations (e.g. 10 min simulations) into a longer one (e.g. 6 h simulation). This means fatigue damages are not calculated for each time series separately but rather for longer time series consisting of several shorter ones that are just appended to each other. It is possible to either append different 10 min time series to each other or each time series is duplicated and appended several times to itself. If scattering environmental conditions are assumed, in some simulations, fairly different load levels occur. In these cases, load levels of the simulations might not fit, and additional cycles can be introduced by merging different time series, leading to

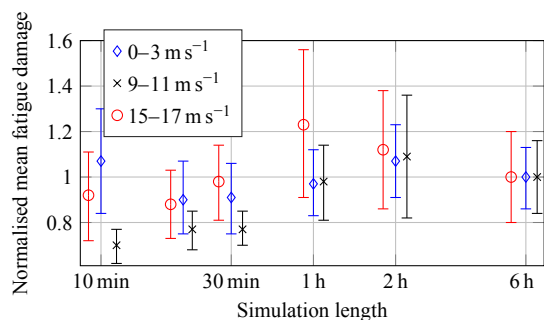


Figure 10. Normalised mean fatigue damage (500 simulations) for increasing simulation lengths and different wind speeds.

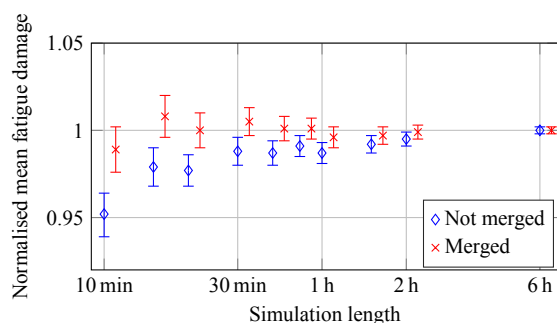


Figure 11. Normalised mean fatigue damage (500 simulations) for increasing simulation lengths and $v_s = 9\text{--}11\text{ m s}^{-1}$. Environmental conditions are kept constant to demonstrate the effect of merging time series more clearly.

unreasonably increased fatigue damages. Merging each time series with itself guarantees fitting load levels. A downside of this is that the computing time of the post-processing is slightly increased. The effect of merging several shorter simulations with themselves to generic and repetitive 6 h time series (e.g. each 10 min time series is duplicated 36 times and is appended to itself to create a 6 h time series) is demonstrated in Fig. 11. It can be seen that the simulation error of about 5 % too low FLS loads for non-merged 10 min simulations can be compensated for by merging time series in the post-processing.

For the ULS loads, the calculation procedure is similar. From the basis of the 500 ten-hour simulations, 500 cases are selected (with replacement). The maximum value of all simulations is taken as decisive utilisation factor. This procedure is repeated 10 000 times (bootstrapping) to assess the associated uncertainty.

The convergence is shown in Fig. 12. Obviously, ULS loads are higher for longer simulations. Again, this increase is not due to any physical phenomenon, but a result of different overall computing times. Clearly, 500 ten-minute simulations should not be compared to 500 six-hour simulations but

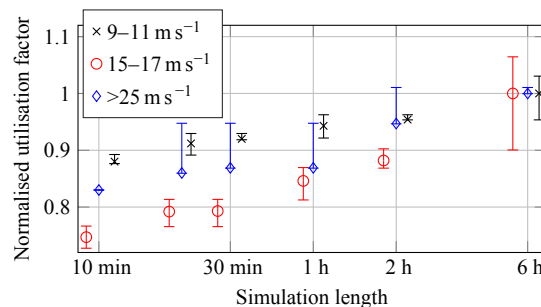


Figure 12. Normalised mean ULS utilisation factor (500 simulations) for increasing simulation lengths and different wind speeds.

instead to about 14 six-hour simulations (Haid et al., 2013). Therefore, in a second step, the ULS calculation procedure is slightly adapted. Now, 500 cases are only selected for 10 min simulations. For all other simulation length, the number of cases is reduced to keep the overall simulation length constant at 5000 min (i.e. 250 cases for 20 min simulation, for example). This comparison is displayed in Fig. 13 and makes clear that ULS loads do not depend on the simulation length but instead on the overall computing time. A second fact being visible in Fig. 13 are the higher uncertainties for longer simulation lengths. Since 10 min simulations lead to a higher number of cases than 6 h simulations for the same total length (i.e. 500 and 14), shorter simulations better cover rare cases, and therefore scattering environmental conditions leading to less uncertainty.

After all, the investigations of this section suggest that simulations of 10 min length are sufficient independent of the type of load or investigated substructure, or wind speed. At this point, it has to be noted that only two types of substructures are analysed and environmental conditions typical for the North Sea. For significantly different substructures or locations, the validity might be limited. Notwithstanding the above, for ULS loads, the same overall time has to be compared in order to achieve reliable results. By keeping the simulation length short, more simulations can be conducted in the same overall computing time leading to a better convergence of ULS loads. For FLS loads, simulation errors due to the simulation length can be reduced by merging the time series.

3.4 Initial transients

For the analysis of the simulation length, the first 4 h of each simulation were discarded to guarantee a steady-state operation of the turbine. However, removing 4 h of initial transients and only using 10 min of simulation is computationally very expensive. Therefore, the convergence of FLS and ULS loads with respect to the time of initial transients is analysed. As initial conditions, like an initial rotor speed, influence the initial transient behaviour (Haid et al., 2013), initial

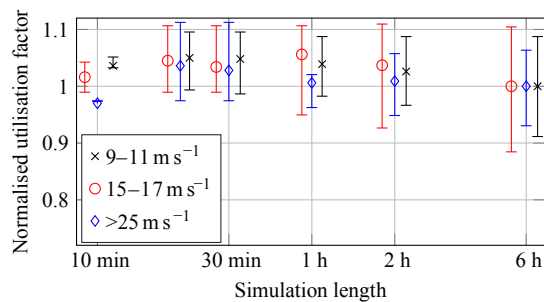


Figure 13. Normalised mean ULS utilisation factor for increasing simulation lengths (constant overall length of 500×10 min, leading to 500 to 14 simulations) and different wind speeds.

rotor speeds and blade pitches depending on the wind speed are set here. These initial conditions are quasi-static states determined using prior simulations.

As the initial transient behaviour is affected by the type of substructure and the load condition, the time that has to be removed is analysed in each wind speed bin for FLS and ULS loads and for both types of substructures separately. Commonly, time series are investigated to estimate times of initial transients (Zwick and Muskulus, 2015). Although this is a straightforward approach, here it is considered to not be expedient. For a fatigue assessment, the convergence of the fatigue damage has to be analysed, and for the ULS analysis, maximum loads or utilisation factors have to be considered.

For each wind speed bin, 10 000 simulations for the monopile and 500 for the jacket were conducted according to the simulation setup in Sect. 3.2. This means that each simulation has its own random seed for irregular waves and turbulent wind, and in addition, different wind speeds and directions, wave heights, directions and periods, turbulence intensities and wind shear exponents according to the FINO3 data are applied. The high and unequal number of simulations is needed to exclude effects of the number of simulations, mentioned in the previous section and addressed in Sect. 4, as well as possible. For the monopile, each simulation at operating conditions is 900 s long (600 s simulation length plus 300 s of initial transients) and 1800 s at idling conditions. When the turbine is idling, the aerodynamic damping is lower, leading to more pronounced initial transients. For the jacket, all simulations are 720 s long. Using this simulated database, it is possible to analyse the effect of different initial simulation times removed on the fatigue damage and utilisation factors in order to determine optima. The analysed simulation length is kept constant at 600 s, while the removed length varies between 0 and 300 s (1200 s for idling; 120 s for the jacket).

Figure 14 displays the convergence of the fatigue damage of the monopile substructure at operating conditions. Here, 300 s or 120 s values are used as a reference, the so-called “converged value”. The 10 h simulations in Sect. 3.3 were

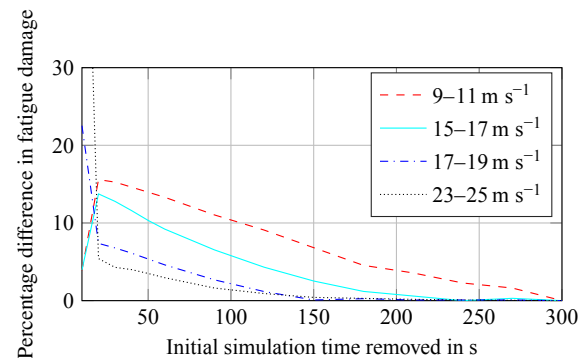


Figure 14. Initial transient behaviour of the operating wind turbine with a monopile substructure for different wind speeds. Percentage difference in the fatigue damage compared to the “converged” value (300 s).

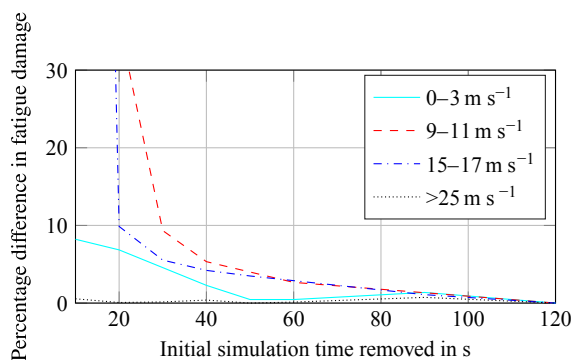
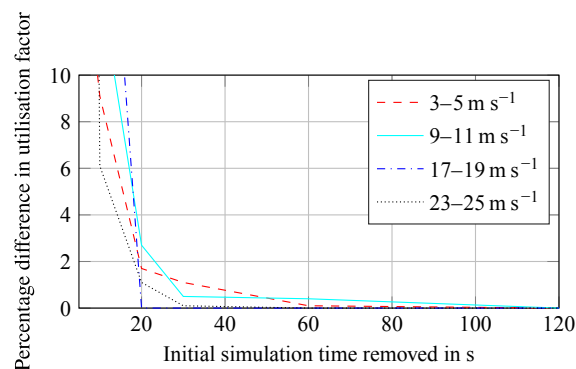
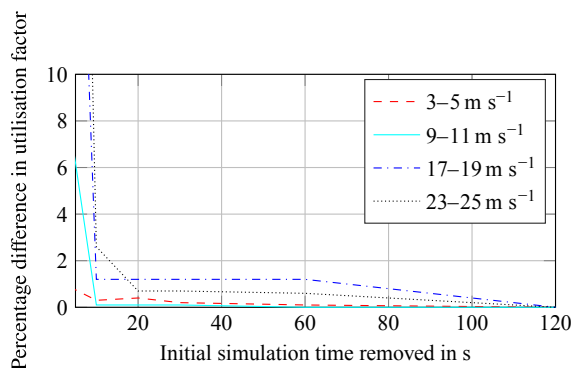
used to determine these values, where the error due to initial transients can be neglected and is much smaller than the error due to the number of simulations. For idling conditions (not shown), the initial transient behaviour takes longer, as the aerodynamic damping is lower. For the same reason, the transients are shorter for higher wind speeds. For the jacket substructure displayed in Fig. 15, the transients decay much faster in all wind speed bins. As jackets are less influenced by wave loads, being not always aligned with the wind, the aerodynamically marginally damped side-to-side modes are less excited, leading to a shorter transient behaviour. This interpretation is supported by the fact that for the jacket, idling conditions, where the hydrodynamic behaviour dominates, have shorter initial transients.

The convergence of ULS utilisation factors for both substructures is shown in Figs. 16 and 17. It becomes apparent that initial transients are short independent of the type of substructure and wind speed. The cycles with high amplitudes occurring at the beginning of each simulation are damped out within a few seconds, and hence are not influencing the ULS behaviour. More problematic are less damped cycles with smaller amplitudes leading to the previously presented, higher times of initial transients for FLS loads.

The recommended times that should be discarded to exclude initial transients for both substructures, being always a compromise between computing time and accuracy (here, errors below 5%), are summarised in Table 3. It has to be mentioned that the general validity is limited, as these times of initial transient might vary, for example, for different aero-elastic codes, numerical solvers, time constants of the aero-elastic models, or substantially different substructures. For example, jackets for 10 MW turbines might behave differently due to larger diameters of legs and braces increasing wave effects. However, for similar applications (e.g. FASTv8, NREL 5 MW turbine, OC3 monopile, or OC4 jacket) that are not rare in academia (e.g.

Table 3. Recommended times that should be discarded to exclude initial transients for simulations with OC4 jacket and OC3 monopile substructures for different wind speeds to achieve errors below 5 %.

v_s in m s^{-1}	Case	< 3	3–5	5–7	7–9	9–11	11–13	13–15	15–17	17–19	19–21	21–23	23–25	> 25
Monopile Jacket	FLS	720 s	240 s	240 s	240 s	240 s	240 s	240 s	150 s	120 s	60 s	60 s	60 s	360 s
		40 s	30 s	50 s	40 s	50 s	50 s	50 s	50 s	50 s	50 s	60 s	50 s	50 s
Monopile Jacket	ULS	< 10 s	< 10 s	< 10 s	< 10 s	10 s	10 s	10 s	10 s	10 s	10 s	10 s	10 s	< 10 s
		< 10 s	20 s	20 s	20 s	20 s	20 s	20 s	20 s	20 s	20 s	20 s	20 s	< 10 s

**Figure 15.** Initial transient behaviour of the wind turbine with a jacket substructure for different wind speeds. Percentage difference in the fatigue damage compared to the “converged” value (120 s).**Figure 17.** Initial transient behaviour of the wind turbine with a jacket substructure for different wind speeds. Percentage difference in the utilisation factor (ULS) compared to the “converged” value (120 s).**Figure 16.** Initial transient behaviour of the wind turbine with a monopile substructure for different wind speeds. Percentage difference in the utilisation factor (ULS) compared to the “converged” value (120 s).

Zwick and Muskulus, 2015 or Morató et al., 2017), the given values represent a well-founded guidance for simulation set-ups. Furthermore, these results should sensitise the research community to the problem of initial transients especially in the case of fatigue. For fatigue, the time of initial transients might be higher than frequently presumed in the literature. This is due to weakly damped cycles with small amplitudes that cannot directly be identified when looking at time series.

4 Benefits and limitations

The benefit of the current work is twofold. Firstly, a comprehensive database for scattering environmental conditions was set up, which is freely available and easy to use. Secondly, two simulation constraints (simulation length and time of initial transients) were analysed, and well-founded recommendations are given.

The main advantages over existing databases are the following: the database covers several different sites situated in different oceans. It has to be admitted that the sites are fairly similar, as they are all in shallow-water conditions. Additionally, the database contains statistical distribution for much more environmental conditions than existing ones. As was shown, for example, by Hübler et al. (2017) that not only main conditions like the wind speed are influencing the dynamic behaviour of offshore wind turbines, knowledge of additional parameters is beneficial. Current databases consist frequently of raw data that need to be post-processed, which is a time-consuming process. Here, on the one hand, easily applicable statistical distributions are given. On the other hand, the complexity of dependent environmental conditions is still covered by utilising conditional distributions and multimodal and non-parametric approaches. In contrast to many existing databases, the raw data are of good quality.

For example, wind speeds are measured at heights comparable to hub heights of current turbines, and there is no need for extrapolations, as is the case for buoy measurements. Still, more data would be valuable in order to achieve more reliable distributions in high-wind-speed bins that rarely occur. After all, the developed database is capable of improving offshore wind turbine modelling by providing more realistic inputs for simulations in academia, where real site data are scarce. One example of improved offshore wind turbine modelling is given in Sect. 3.3 and 3.4. The inclusion of probabilistic inputs leads to a significant and realistic increase in fatigue damage scattering requiring high numbers of simulations. Hence, deterministic inputs underestimating this scattering can lead to biased fatigue values. Detailed analyses of the effect of scattering environmental conditions on fatigue damage, and therefore of the needed number of simulations, are part of upcoming work of the authors.

Concerning the second benefit, the simulation constraints, it has to be kept in mind that not only realistic modelling but also small simulation errors are important in order to model accurately. In this context, the chosen simulation length and time of initial simulation transients matter. So far, these values are frequently chosen without profound knowledge. Some approaches to gain a deeper insight into these constraints (Stewart, 2016; Zwick and Muskulus, 2015) concentrate on simulation lengths or specific types of substructures and are not taking realistically scattering environmental conditions into account. In this work, the scattering of the conditions is addressed and different bottom-fixed substructures are analysed. This enables recommendations for simulation lengths and times of initial transients depending on the wind speed, the type of substructure, and the considered load case (ULS or FLS). However, the general validity of the current results has to be slightly restricted, as only one design of each type of substructure was investigated. Therefore, the initial transient behaviour might be slightly different for significantly different designs. Furthermore, for the time being removed to exclude initial transients, the values might also differ between different simulation codes and are only tested for the FASTv8 code. Different numerical solver or time constants of the aero-elastic models might also influence the time of initial transients. Nevertheless, even in these cases, firstly, the given recommendations can be regarded as a well-founded starting point for further investigations. Secondly, and even more important, they clarify the challenge of a well-founded choice.

5 Conclusions

This work aims to help future simulation work to be more realistic and accurate. In order to achieve this objective, a freely available and comprehensive database for scattering environmental conditions was set up. This database consists of conditional statistical distribution for many parameters and can

be applied without further post-processing. All needed information (statistical distribution and their parameters) is given in the Supplement. In academia, this database enables simulations with probabilistic environmental conditions making them more realistic. For industry purposes, this work might lead to a reconsideration of the current practice. This study shows that the use of deterministic values that are either only dependent on the wind speed (e.g. turbulence intensity) or even totally constant (e.g. wind shear) does not represent realistic offshore conditions. However, for a well-founded reconsideration of the current practice, a detailed assessment of probabilistic approaches compared to deterministic load-case-based ones is needed.

Additionally, scientifically sound recommendations are given for the choice of simulation lengths and times to be removed to exclude initial transients. Simulation lengths of 10 min are generally sufficient, and can even help to reduce uncertainties. However, in the case of FLS loads, times series should be merged, and for ULS situations, the overall computing time has to be kept constant. Recommendations concerning the initial transients have to be handled with care due to limitations of the general validity. The values are summarised in Table 3 and can help to improve the accuracy of simulations, and to reduce computing times. It should be noted that a partly significantly longer initial transient behaviour compared to values in the literature was detected. Literature values are mainly based on educated guesses so far.

An enlargement of the current database to include additional offshore sites, other types or designs of substructures, or investigations for other simulation codes and numerical solver would be definitely valuable to increase the general validity. Furthermore, even for the utilised FAST code, additional investigations concerning the amount of eigenmodes representing the substructure would be beneficial, as a reduction of retained eigenmodes might reduce the time of initial transients.

Data availability. The raw data are taken from the FINO platforms – operated on behalf of the Federal Ministry for the Environment, Nature Conservation, Building and Nuclear Safety (BMUB) – and are freely available for research purposes (<http://www.fino-offshore.de/en/>). The derived database, consisting of statistical distribution for 13 partly dependent environmental conditions and three offshore sites, is freely available. All needed information concerning the statistical distribution and their parameters is given in the Supplement.

The Supplement related to this article is available online at <https://doi.org/10.5194/wes-2-491-2017-supplement>.

Competing interests. The authors declare that they have no conflict of interest.

Acknowledgements. We gratefully acknowledge the financial support of the Lower Saxony Ministry of Science and Culture (research project VENTUS EFFICIENS, FKZ ZN3024) and the European Commission (research project IRPWIND, funded from the European Union's Seventh Framework Programme for research, technological development, and demonstration under grant agreement number 609795) that enabled this work. This work was supported by the compute cluster which is funded by Leibniz Universität Hannover, the Lower Saxony Ministry of Science and Culture (MWK), and the German Research Foundation (DFG).

The publication of this article was funded by the open-access fund of Leibniz Universität Hannover.

Edited by: Michael Muskulus

Reviewed by: two anonymous referees

References

- Cheng, P. W.: A reliability based design methodology for extreme responses of offshore wind turbines, DUWIND Delft University Wind Energy Research Institute, the Netherlands, 2002.
- Det Norske Veritas (DNV): Fatigue design of offshore steel structures, Recommended practice DNV-RP-C203, available at: <https://rules.dnvgl.com/docs/pdf/DNV/codes/docs/2010-04/RP-C203.pdf> (last access: October 2017), 2010.
- Det Norske Veritas (DNV): Design of floating wind turbine structures, Offshore Standard DNV-OS-J103, available at: <http://rules.dnvgl.com/docs/pdf/DNV/codes/docs/2013-06/OS-J103.pdf> (last access: October 2017), 2013.
- DIN – Normenausschuss Bauwesen: Subsoil – Verification of the safety of earthworks and foundations – Supplementary rules to DIN EN 1997-1, DIN 1054, available at: <https://www-1perinorm-1com-100000boj285b.shan02.han.tib.eu/document.aspx> (last access: October 2017), 2010.
- Ernst, B. and Seume, J. R.: Investigation of site-specific wind field parameters and their effect on loads of offshore wind turbines, *Energies*, 5, 3835–3855, 2012.
- European Committee for Standardization: Eurocode 3: Design of steel structures – Part 1–6: Strength and stability of shell structures, EN 1993-1-6, Brussels, Belgium, 2010a.
- European Committee for Standardization: Eurocode 3: Design of steel structures – Part 1–9: Fatigue, EN 1993-1-9, Brussels, Belgium, 2010b.
- Fischer, T., de Vries, W., and Schmidt, B.: Upwind Design Basis, Endowed Chair of Wind Energy (SWE) at the Institute of Aircraft Design Universität Stuttgart, Germany, 2010.
- Germanischer Lloyd (GL): Guideline for the Certification of Offshore Wind Turbines, Offshore Standard, Hamburg, Germany, 2012.
- Häfele, J., Hübler, C., Gebhardt, C. G., and Rolfes, R.: An improved two-step soil-structure interaction modeling method for dynamical analyses of offshore wind turbines, *Appl. Ocean Res.*, 55, 141–150, 2016.
- Häfele, J., Hübler, C., Gebhardt, C. G., and Rolfes, R.: Efficient Fatigue Limit State Design Load Sets for Jacket Substructures Considering Probability Distributions of Environmental States, The 27th International Ocean and Polar Engineering Conference, 25–30 June 2017, San Francisco, USA, 167–173, 2017.
- Haid, L., Stewart, G., Jonkman, J., Robertson, A., Lackner, M., and Matha, D.: Simulation-length requirements in the loads analysis of offshore floating wind turbines, 32nd International Conference on Ocean, Offshore and Arctic Engineering, 9–14 June 2013, Nantes, France, 1–10, ASME, 2013.
- Hansen, K. S., Barthelmie, R. J., Jensen, L. E., and Sommer, A.: The impact of turbulence intensity and atmospheric stability on power deficits due to wind turbine wakes at Horns Rev wind farm, *Wind Energy*, 15, 183–196, 2012.
- Hansen, M., Schmidt, B., Ernst, B., Seume, J., Wilms, M., Hildebrandt, A., Schlurmann, T., Achmus, M., Schmoor, K., Schumann, P., Kelma, S., Goretzka, J., Rolfes, R., Lohaus, L., Werner, M., Poll, G., Böttcher, R., Wehner, M., Fuchs, F., and Brenner, S.: Probabilistic Safety Assessment of Offshore Wind Turbines, Leibniz Universität Hannover, Hannover, Germany, 2015.
- Hübler, C., Gebhardt, C. G., and Rolfes, R.: Hierarchical Four-Step Global Sensitivity Analysis of Offshore Wind Turbines Based on Aeroelastic Time-Domain Simulations, *Renew. Energ.*, 111, 878–891, 2017.
- International Electrotechnical Commission (IEC): Wind turbines – part 1: Design requirements, International standard IEC 61400-1, Geneva, Switzerland, 2005.
- International Electrotechnical Commission (IEC): Wind turbines – part 3: Design requirements for offshore wind turbines, International standard IEC 61400-3, Geneva, Switzerland, 2009.
- Johannessen, K., Meling, T. S., and Hayer, S.: Joint distribution for wind and waves in the northern north sea, *Int. J. Offshore Polar*, 12, 1–8 2002.
- Jonkman, B. J.: TurbSim user's guide: Version 1.50, National Renewable Energy Laboratory, Golden, Colorado, USA, 2009.
- Jonkman, J.: The New Modularization Framework for the FAST Wind Turbine CAE Tool, 51st AIAA Aerospace Sciences Meeting, including the New Horizons Forum and Aerospace Exposition, 7–10 January 2013, Dallas, Texas, USA, 1–26, 2013.
- Jonkman, J., Butterfield, S., Musial, W., and Scott, G.: Definition of a 5 MW Reference Wind Turbine for Offshore System Development, National Renewable Energy Laboratory, Golden, Colorado, USA, 2009.
- Jonkman, J. M. and Musial, W.: Offshore Code Comparison Collaboration (OC3) for IEA Task 23 Offshore Wind Technology and Deployment, National Renewable Energy Laboratory, Golden, Colorado, USA, 2010.
- Kost, C., Mayer, J. N., Thomson, J., Hartmann, N., Senkpiel, C., Philipps, S., Nold, S., Lude, S., and Schlegl, T.: Stromgestehungskosten erneuerbare Energien, Fraunhofer-Institut für solare Energiesysteme ISE, Freiburg, Germany, 2013.
- Li, L., Gao, Z., and Moan, T.: Joint distribution of environmental condition at five european offshore sites for design of combined wind and wave energy devices, *J. Offshore Mech. Arct.*, 137, 031901, <https://doi.org/10.1115/1.4029842>, 2015.
- Millero, F. J. and Poisson, A.: International one-atmosphere equation of state of seawater, *Deep-Sea Res. Pt. A*, 28, 625–629, 1981.

C. Hübler et al.: Development of a database of scattering environmental conditions

505

- Morató, A., Sriramula, S., Krishnan, N., and Nichols, J.: Ultimate loads and response analysis of a monopile supported offshore wind turbine using fully coupled simulation, *Renew. Energ.*, 101, 126–143, 2017.
- Popko, W., Vorpahl, F., Zuga, A., Kohlmeier, M., Jonkman, J., Robertson, A., Larsen, T. J., Yde, A., Saeterstro, K., Okstad, K. M., Nichols, J., Nygaard, T. A., Gao, Z., Manolas, D., Kim, K., Yu, Q., Shi, W., Park, H., and Vásquez-Rojas, A.: Offshore Code Comparison Collaboration Continuation (OC4), Phase 1 – Results of Coupled Simulations of an Offshore Wind Turbine With Jacket Support Structure, *The Twenty-second International Offshore and Polar Engineering Conference*, International Society of Offshore and Polar Engineers, 17–22 June 2012, Rhodes, Greece, 337–346, 2012.
- Prognos AG and Fichtner: *Kostensenkungspotenziale der Offshore-Windenergie in Deutschland*, Stiftung Offshore-Windenergie, Berlin, Germany, 2013.
- Stewart, G. M.: *Design Load Analysis of Two Floating Offshore Wind Turbine Concepts*, PhD thesis, University of Massachusetts, Massachusetts, USA, 2016.
- Stewart, G. M., Lackner, M., Haid, L., Matha, D., Jonkman, J., and Robertson, A.: *Assessing fatigue and ultimate load uncertainty in floating offshore wind turbines due to varying simulation length*, *Safety, Reliability, Risk and Life-Cycle Performance of Structures and Infrastructures*, CRC Press, London, UK, 239–246, 2013.
- Stewart, G. M., Robertson, A., Jonkman, J., and Lackner, M. A.: *The creation of a comprehensive metocean data set for offshore wind turbine simulations*, *Wind Energy*, 19, 1151–1159, 2015.
- Vemula, N. K., de Vries, W., Fischer, T., Cordle, A., and Schmidt, B.: *Design Solution for the UpWind Reference Offshore Support Structure – Deliverable D4.2.5 (WP4: Offshore Foundations and Support Structures)*, Rambøll Wind Energy, Esbjerg, Denmark, 2010.
- Vorpahl, F., Popko, W., and Kaufer, D.: *Description of a basic model of the “UpWind reference jacket” for code comparison in the OC4 project under IEA Wind Annex 30*, Fraunhofer IWES, Bremerhaven, Germany, 2013.
- Zwick, D. and Muskulus, M.: *The simulation error caused by input loading variability in offshore wind turbine structural analysis*, *Wind Energy*, 18, 1421–1432, 2015.

4 Sensitivity analysis

In probabilistic analyses, the inherent physical uncertainty of inputs (e.g. ECs) but also model uncertainties, etc. are modelled as probabilistic variables. For complex models, the number of variables can be extremely high making full probabilistic analyses - treating all parameters probabilistically - nearly impossible. Therefore, in this context, a central issue is the determination of “significant” parameters. Here, “significant” means that the uncertainty of those variables influences relevant outputs, whereas “insignificant” parameters can be set to deterministic values without changing the outcomes. The selection of significant parameters being modelled probabilistically can either be based on expert knowledge or - more objectively - on sensitivity analyses. Here, a new stepwise sensitivity method being a good compromise of accuracy and computing time is developed and applied to a coupled time-domain model for OWTs.

4.1 Research context

Today, normally, OWTs are simulated using deterministic inputs. In case of probabilistic approaches, the number of statically distributed inputs has to be limited. Although there are objective methods to identify those parameters that are to be modelled probabilistically (sensitivity analyses), parameters are mostly selected based on expert knowledge. While this procedure might be sufficient for well-known applications, where expert knowledge has been built up over decades, for a relatively new industry like OWTs, the use of expert knowledge can lead to disadvantageous parameter selections. Therefore, sensitivity analyses should be used.

In this context, three different types of sensitivity analyses can be differentiated: parameter studies, local approaches, and global methods. For parameter studies, various parameter combinations are tested. This is the most straightforward approach. It is used regularly for OWTs [23, 31, 131]. However, it does not yield any objective measure of sensitivity. Local methods are mainly useful, if sensitivities in a specific region of the data space are needed, but for parameter selections, the entire data space can be relevant. Hence, global methods are most expedient. Still, there are only a few examples which use global sensitivity methods for OWTs [187, 219]. The main reason for this limited use of global methods are high computing times. Recently, it has been shown that the application of stepwise global methods or meta-model-based ones can reduce computing times significantly [77]. Hence, it can be concluded that there is a need for efficient global sensitivity methods for OWTs that enable an objective parameter selection for subsequent probabilistic analyses.

4.2 Methods

Due to the described need for efficient and objective parameter selections for probabilistic analyses, in this thesis, a new global sensitivity analysis is developed, and subsequently,

applied to OWTs. Only global methods are considered, since OWT models are fairly non-linear and, a priori, the area of interest (i.e. the input subdomain leading to the highest sensitivities and/or critical outputs like structural failures) is unknown. Both facts disqualify local approaches. In the field of global sensitivity methods, there is a wide range of methods from simple OAT sampling with low computing times to sophisticated variance-based approaches that include all non-linearities and parameter interactions at the expense of an increased computational effort. To find a compromise between accuracy and computing time, a stepwise approach is developed. This approach consists of an OAT sampling in the first step, a linear regression in the second one, and finally, a variance-based analysis. Since the number of probabilistic parameters is reduced by the first two steps, there are less uncertain parameters included in the variance-based analysis. Thus, the computing time, which highly correlates with the number of uncertain parameters, can be limited, while the high accuracy of the final, variance-based analysis is preserved. The presented idea of a stepwise parameter reduction is quite flexible, since the three steps are interchangeable. For example, Hübler et al. [77] use the approach of this thesis, but replace the second step by a meta-model-based sensitivity analysis.

As ULS and FLS can be design-driving for OWTs and since significant parameters for both limit states do not have to be the same, the developed stepwise approach is applied to ULS and FLS independently.

4.3 Results

Regarding the results, two aspects have to be distinguished: first, results concerning the sensitivity methods (methodological findings), and second, outcomes regarding the parameter selection for OWTs (applied findings).

For the sensitivity method, on the one hand, it is shown that simplified sensitivity approaches do not yield accurate results. They are not always capable of determining the same probabilistic subset as the reference (variance-based) method. The reason for the lack of performance is mainly that interactions are not covered properly. However, especially for soil parameters and other parameters that are related to eigenfrequencies of the OWT, interactions are really important. On the other hand, compared to pure variance-based analyses, computing times can be reduced to approximately a third. Hence, the stepwise approach is a suitable compromise between accuracy and computational effort.

Regarding the parameter selection, it becomes apparent that only a few parameters are influential. Especially for FLS, only about 25 % of the inputs have to be treated probabilistically. The most important parameters are wind and wave conditions, while soil conditions are partly influential, and production tolerances of the steel components can be neglected.

4.4 Outlook

In this thesis, it is shown that the new sensitivity analysis outperforms some simplified approaches and that it is computationally more efficient than pure variance-based approaches. However, a comprehensive assessment of advantages and shortcomings is not done. Such an assessment can be found in Hübler et al. [77]. There, it is also recommended to interchange the second step of the analysis by a meta-model-based variance-based analysis in order to increase the accuracy. Further developments regarding the most suitable second step and

meta-model-based approaches are advisable.

Moreover, in this thesis, parameters are modelled as uncorrelated. Since parameters that are highly correlated in reality are, in the end, not analysed here (e.g. wind speed and wave height), this simplification is acceptable. Still, the inclusion of correlated parameters - as in Hübler et al. [77] - in future analyses is recommended. Sensitivity methods for correlated parameters can be found, for example, in Xu and Gertner [215] or Jacques et al. [88].

Furthermore, the types of parameters that are considered in sensitivity analyses have been limited so far. Only wind, wave, soil, material, and geometric (manufacturing tolerances) inputs with aleatory uncertainty are taken into account, whereas inputs on the resistance side (e.g. parameters of Miner's rule, etc.) and epistemic uncertainty (e.g. vaguely known model uncertainties or statistical uncertainties due to limited data) are neglected. An extension of the sensitivity analysis regarding these types of variables could lead to a broader knowledge of relevant uncertainties/parameters. Furthermore, the inclusion of the resistance side would allow an assessment of uncertainty with respect to the reliability of the structure (i.e. reliability analysis).

Apart from that, the present sensitivity analyses neglect the stochastic behaviour of the OWT models. Hence, future research could address this problem by applying sensitivity methods for stochastic systems [34, 113].

Finally, using present findings, for future probabilistic simulations, a relatively large number of inputs can already be fixed to deterministic values, which will lead to significantly reduced computing times and more stable, more robust solutions.

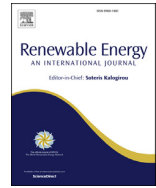
4.5 Paper C: Hierarchical four-step global sensitivity analysis of offshore wind turbines based on aeroelastic time domain simulations

The following paper is published in *Renewable Energy*, Volume 111 (2017), pages 878-891 (<https://doi.org/10.1016/j.renene.2017.05.013>). The main work was done by the author of this thesis. Cristian Gebhardt and Raimund Rolfes contributed with advisory and supporting work.



Contents lists available at ScienceDirect

Renewable Energy

journal homepage: www.elsevier.com/locate/renene

Hierarchical four-step global sensitivity analysis of offshore wind turbines based on aeroelastic time domain simulations



Clemens Hübler*, Cristian Guillermo Gebhardt, Raimund Rolfes

Institute of Structural Analysis, Leibniz Universität Hannover, Appelstr. 9a, D-30167, Hannover, Germany

ARTICLE INFO

Article history:

Received 8 August 2016
 Received in revised form
 1 March 2017
 Accepted 2 May 2017
 Available online 4 May 2017

Keywords:

Global sensitivity
 Offshore substructures
 Wind energy
 FAST
 Time domain simulations

ABSTRACT

Although uncertainties are present in all real parameters, numerical calculations of the structural behaviour of offshore wind turbines are usually conducted with deterministic values. However, with this approach, optimisation processes can be misleading and reliability levels cannot be calculated. The reasons for deterministic calculations are high computing times of probabilistic approaches and the lack of knowledge about the scatter of data. For deterministic approaches, more complex models with higher computing times are possible, although they, are less generally valid. Therefore, it is useful to identify the most influential parameters that have to be treated in a probabilistic manner using sensitivity analyses is valuable. Contrary to rudimentary sensitivity approaches being used in offshore wind energy so far, this paper presents a new four-step sensitivity analysis reducing the probabilistic parameter subset step by step and aiming to achieve a compromise between computing time and complexity. It can be shown that for different substructures and different load cases, only a small parameter subset is influential and many other inputs can be regarded as deterministic without losing accuracy. However, attention must be paid to the slight differences among substructures. Therefore, it must be highlighted that not all results are general.

© 2017 Elsevier Ltd. All rights reserved.

1. Introduction

Over the past decades, wind energy in general and recently offshore wind energy in particular have become more and more important for global energy production. However, the costs for offshore wind energy are still too high compared with energy based on coal to be really competitive [1]. For offshore wind turbines (OWTs), substructures and foundations account for a significant part of these costs [2]. Therefore, both the probabilistic analysis and the optimisation of substructures of offshore wind turbines become necessary. Since the design of OWTs has to be based on holistic time domain simulations, as stated in current standards [3], the calculations are fairly time-consuming. Furthermore, for an optimisation or a probabilistic analysis, a high amount of calculations is necessary which leads to computing time issues. Hence, apart from the development of suitable time domain models, the identification of the most relevant input parameters is crucial to treat non-influential inputs as deterministic. In this context, non-influential

inputs means that the scattering and uncertainty of these parameters do not influence the outputs significantly.

Current time domain models are based on finite elements (FE), multi-body systems (MBS) and modal approaches. Aerodynamics and hydrodynamics are coupled with the elastic behaviour of the turbine and its controller, which makes the overall system highly non-linear and quite complex. Turbulent wind fields, irregular waves as well as geometric non-linearities due to large rotations or shortening/lengthening are taken into account as well. The complexity of existing time domain codes allows only considering of a limited number of probabilistic input values. Some of the most important aero-elastic codes are GH BLADED, FAST, FLEX5 and HAWC2. An example of an even more sophisticated code with computing times of several days, and therefore not suitable for probabilistic calculations, can be found in Ref. [4]. Overviews of the most common codes and details concerning the differences of the codes are given by Passon and Kühn [5] and Böker [6] for example. FAST occupies a special position, as the whole source code is open. Hence, FAST can be adopted and enhanced by everyone for ad hoc applications.

It is current practice to assume the input parameters for these time domain models to be deterministic. However, in reality almost

* Corresponding author.

E-mail address: c.huebler@isd.uni-hannover.de (C. Hübler).

all inputs are uncertain in some way. Therefore, the determination of statistical distributions for input parameters either from expert knowledge or from statistical measurement or experimental data is indispensable for probabilistic analyses. In this paper, the focus is on environmental and geometrical inputs (cf. Table 1), as these inputs cannot be influenced by the numerical model itself or the turbine design. Cheng [7] and Veldkamp [8] use their expertise to state ranges and distributions for wind and wave parameters. Ernst and Seume [9] and Schmidt et al. [10] derive statistical distributions for wind parameters from data of the German research platform FINO1. Morgan et al. [11] analyse different wind speed distributions based on measurements in the US. Work on combined wind and wave distributions is conducted by Schmidt et al. [12] on the basis of FINO1 measurements. Distributions for soil properties based on expert knowledge and a literature research are stated for example by Zaajier [13]. The reliability analysis of Kim and Lee [14] is based on differently distributed soil properties. Sørensen and Toft [15] give, inter alia, some guidance on material parameters. Wei et al. [16] state some information on material scattering as well. Information on geometrical inputs can be found for example in Ref. [17]. Ziegler et al. [18] use statistical distributions for all kinds of parameters for a probabilistic fatigue load estimation. Toft et al. [19] analyse the influence of uncertain wind parameters on fatigue loads. In this context, statistical distributions for the uncertainties in wind and fatigue model parameters are given.

Sensitivity analyses to determine the most relevant inputs are quite infrequent in the field of structural offshore wind turbine modelling. If used, they are mainly applied to turbine parts. In most cases, the investigation of different input combinations is already called sensitivity analysis [20–22], though this approach cannot detect global phenomena. Some recent approaches fill this gap of global sensitivity analyses. Goretzka and Rolfes [23] analyse the most influential parameters for turbine eigenfrequencies with the aid of a linear regression. Ziegler et al. [24] conduct a sensitivity analysis concerning different site conditions for fatigue loads. In addition to simple one-at-a-time variations, they use scatter plots to qualitatively analyse randomly generated samples. Stieng and Muskulus [25] analyse the global sensitivity of the failure probability of the whole OWT. A simplified, uncoupled time domain model is applied and the sensitivity of four parameters is investigated using a rank correlation. However, all this recent work is based on simplified models and the global sensitivities are either based on qualitative, linear or monotonic approaches without interactions (cf. [26]). Therefore, they are not suitable for an adequate analysis of non-linear models with interaction effects, as it can be done with variance-based methods and an aero-hydro-servo-elastic simulation code.

Due to the lack of sensitivity analyses for OWTs, this paper focuses, firstly, on the investigation of fundamental parameters and, secondly, on non-influential parameters by means of a sensitivity analysis. The challenge in this context is that aero-elastic turbine models are highly non-linear and at the same time computing times are high. Therefore, neither standard sensitivity approaches

for linear models nor plain variance-based methods can be used. This is why in this paper, a global four-step sensitivity algorithm is developed and shown in Fig. 1. The approach is based on the idea of a stepwise parameter selection of Mokhtari et al. [27] to reduce the computing time of a final variance-based analysis. The first step is a parameter selection based on expert knowledge just to get a starting subset. A one-at-a-time analysis in the second step is used to check whether a more sophisticated sensitivity analysis can possibly reduce the number of influential parameters. Subsequently, a regression reduces the probabilistic subset for the fourth step. The regression is globally valid, but in the present case, it does only cover bilinear effects and no higher order terms. The last step is a time-consuming variance-based sensitivity analysis which includes all non-linearities and interactions between the parameters. This four-step algorithm reduces the computational effort significantly compared to plain variance-based methods. At the same time, the final parameter selections are still based on the full non-linear time domain model and not on approximations as it is the case for meta-models. This meets the requirements of the complex turbine models better.

The paper is organised as follows: Firstly, the time domain model used is presented and the deviation of statistical distributions is explained concisely. Subsequently, an introduction to the different global sensitivity methods as part of the four-step algorithm is given. After having introduced the general methodology, results of an application of this sensitivity scheme to offshore wind turbines are presented. Finally, the methodology and outcomes are discussed in the last section.

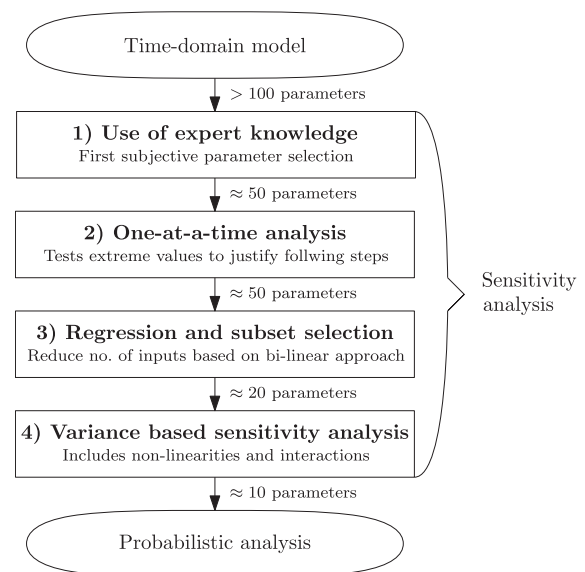


Fig. 1. Scheme of four-step sensitivity analysis for the substantial reduction of probabilistic input parameters in time domain offshore wind turbine models.

Table 1
Classification of input parameters.

Category	Main Application	Examples
Algorithm	Numerical optimisation	Time step sizes, integration method
Model	Model development	Cut-off frequency of wave spectrum, no. of modes for Craig-Bampton reduction
Control	Turbine design/optimisation	Blade pitch algorithm, nacelle yaw algorithm
Configuration	Turbine design/optimisation	Turbine height, wall thickness of design pile, no. of legs of the jacket
Environmental	Probabilistic analysis	Wind speed, soil density, wave height, wave direction
Geometrical	Probabilistic analysis	Deviations in pile wall thickness or pile diameter
Material	Probabilistic analysis	Young modulus or Poisson ratio of the steel

2. Methodology

There are several time domain simulation codes. Theoretically, all of them could be used for the present sensitivity analyses. However, due to the open source character of FAST, the code is easily adaptable to the specific needs. Therefore, the FAST code is used in this study. The code considers aero-hydro-servo-elastic coupling and includes, inter alia, non-linear effects of large rotations which are due to rigid body motions, non-linearities of the control system and due to geometrical stiffening. The structural model of an onshore wind turbine in FAST comprises up to 23 DoFs. This limited number of DoFs makes probabilistic calculations possible within adequate simulation times. Since offshore sub-structures are commonly computed by FE methods using beam elements with hundreds of nodes and often thousands DoFs, a reduction method called Component-Mode-Synthesis has been implemented in FAST [28], which is based on the work of Craig and Bampton [29]. This reduction method allows an appropriate structural representation with about 5–15 DoFs [30], but the turbine is modelled clamped to the seabed [31]. Since the uncertainties in the soil are considered to be significant, this is a massive simplification in the current context. Hence, to overcome this drawback, an adequate soil model by Häfele et al. [32] based on linearised mass and stiffness matrices is added to the FAST model.

2.1. Statistical distributions

It is common practice to assume parameters in time domain simulation as deterministic, although in reality, there are different kinds of uncertainties in all parameters. Examples for uncertainties are model uncertainties, measurement errors, lack of knowledge, physically stochastic inputs and human errors. Probabilistic models try to take some of these uncertainties into account by assuming statistical distributions for the input parameters. Therefore, in order to conduct profound sensitivity analyses, statistical distributions for the input parameters have to be derived. This can, firstly, be based on expert knowledge and secondly, on statistical measurement data. Expert knowledge based distributions are quite unreliable, as they only rely on experience. However, often there is insufficient data to derive distributions directly. In these cases, the use of expertise, frequently based on literature reviews, is the only alternative. If sufficient measurement data is available, substantiated statistical distributions can be derived. The deviation consists of three main steps. In the first step, different, potentially suitable distributions are selected. Here, the symmetry or the number of peaks of the data distribution can be used as an aid. Secondly, the distributions chosen are fitted to the data using methods like the maximum likelihood estimation (MLE), the least mean square error or methods of moments. In this paper, the fit is performed using the MLE method, because its estimates are mostly more precise compared to other fitting methods. The MLE is based on the maximisation of the likelihood:

$$\mathcal{L}(\mathbf{q}, \mathbf{x}) = \prod_{i=1}^n f(x^{(i)} | \mathbf{q}), \quad (1)$$

where \mathcal{L} is the likelihood, \mathbf{q} is the vector of distribution parameters that are varied, \mathbf{x} is the sample vector with the samples $x^{(1)}$ to $x^{(n)}$, $f(\dots)$ is the assumed distribution and n is the number of samples. Finally, the goodness of the fits of the different distributions can be evaluated with goodness tests. Some of the most common tests being used here as well are the Kolomogorow-Smirnow (KS) test and the Chi-squared test.

2.2. Sensitivity analysis

The objective of sensitivity analyses is, inter alia, to quantify the significance of all uncertain input parameters for a considered model output [33]. This means that sensitivity analyses investigate the effect of variations in inputs (\mathbf{x}) on the outputs (\mathbf{y}). Parameters that turn out to be non-influential can be treated deterministically in further analyses. Sensitivity analyses can be performed qualitatively or quantitatively and on a local or global level. Local approaches, based on derivatives $\partial y_k / \partial x_l$ at one specific point in the full data space, are only locally valid and general statements are only possible, if the model is linear. Global methods can either give better linearisations of non-linear models over the whole data space or are capable of globally analysing non-linear models. On the other hand, global methods are much more time-consuming. Nevertheless, this study focuses on global approaches. In the area of global sensitivity analyses, there is a wide range from rudimentary and straightforward approaches to sophisticated ones that are suitable for different kinds of problems and models. In this paper, a new four-step sensitivity analysis is conducted in order to stepwise reduce the amount of input parameters in a model that have to be considered in a probabilistic manner. Exemplarily, the FAST model is used here, but the scheme can be applied to all kinds of models and applications. The four steps are shown in Fig. 1. The underlying theory of all four steps is summarised in the following.

The first step is a significant reduction of parameters by the use of expert knowledge and decision making. This step is highly subjective, but it is necessary to get a starting subset and to focus on specific parameters. In this context, the parameters can be classified into different categories according to Table 1. This sensitivity study is not meant to be an evaluation of the robustness of the models used, e.g. the model for the wave loads. Therefore, algorithm, model and control parameters are treated deterministically. Furthermore, the design of the turbine shall neither be investigated nor optimised here. Hence, the configuration parameters remain unchanged as well and the focus is on parameters of statistical nature. The decision, whether some environmental, material or geometrical inputs are considered to be treated deterministically, is based on the expert knowledge of the authors and a broad literature research. Additionally, the aspect of missing probabilistic data for certain parameters is taken into account. Nevertheless, an isolated consideration of the probabilistic parameters is not possible, as there are always interactions with the deterministic values as well. For example, depending on the deterministic control algorithm, the effect of statistically distributed wind speeds can be different.

With this starting set of probabilistic parameters, the second step is the one-at-a-time (OAT) analysis which is one of the most frequently used approaches in structural engineering. This step is to clarify whether subsequent steps are useful or the probabilistic subset cannot be reduced significantly. However, this step does not reduce the probabilistic subset itself. Depending on the algorithm, the OAT analysis can be regarded as a local and a global analysis. The general concept is to vary one parameter while keeping all others fixed. In most cases, only the maximum and the minimum of the parameters are tested. If many parameters have to be varied, the implementation of a probabilistic preprocessor, that automatically changes the input files, starts the simulations and reads the output files, is beneficial. The OAT procedure has the advantage that the model has to be evaluated only a few times. Hence, it can be used to identify those parameters that are influential [26] and it never detects non-influential inputs as significant [34] which makes it suitable for the second step in this scheme. Only if some, but not nearly all, parameters are detected to be influential, further steps are valuable. A significant index for the OAT method can be

defined as follows:

$$S_{OAT,k} = \frac{f(x_1, \dots, x_k + \Delta x_k, \dots, x_m) - f(x_1, \dots, x_k - \Delta x_k, \dots, x_m)}{2\Delta x_k}, \quad (2)$$

where $S_{OAT,k}$ is the OAT sensitivity index corresponding to the k th input factor, $f(\dots)$ is the model function, x_1 to x_m are the m input factors and Δx_k is the variation in the k th input factor. A normalisation of the indices is valuable, if different parameters with heterogeneous variations are compared.

After having clarified that the probabilistic subset can be reduced, the third step is a regression analysis that is combined with an automated subset selection. The whole data space is analysed using a regression. However, this approach gives only a (bilinear) approximation of the real model which is subsequently used for the parameter reduction. Higher order effects are neglected in this step. For regression analyses, the input parameters are correlated with the considered output. For this purpose, Monte-Carlo sampling (MCS) is conducted. This means that the model is evaluated n times with m independent input parameters randomly generated according to their statistical distributions:

$$\mathbf{X}_{n \times m} = \begin{pmatrix} x_1^{(1)} & x_2^{(1)} & \dots & x_m^{(1)} \\ x_1^{(2)} & x_2^{(2)} & \dots & x_m^{(2)} \\ \vdots & \vdots & \ddots & \vdots \\ x_1^{(n)} & x_2^{(n)} & \dots & x_m^{(n)} \end{pmatrix}. \quad (3)$$

For a better coverage of the full data space and/or less correlations between the sampled inputs, latin hypercube sampling (LHS) or other more advanced sampling methods can replace the MCS, as the sampling method is freely selectable. The outcomes of the n model evaluations ($y^{(i)}$) are fitted with the n sample vectors ($\mathbf{x}^{(i)}$) by means of a least square algorithm. In case of a linear regression, only the first two terms of Eq. (4) are used for the fitting, which is a line of best fit in case of one input factor. If interaction effects or higher order terms are taken into account, the third and fourth term in Eq. (4) respectively are utilised as well. In this paper, a bilinear approach with the first three terms is used. The fitted outcomes ($\hat{y}^{(i)}$) are:

$$\hat{y}^{(i)} = \underbrace{b^{(0)} + \sum_{k=1}^m (b_k^{(1)} x_k^{(i)})}_{\text{Linear regression terms}} + \underbrace{\sum_{k=1}^m \sum_{l=k+1}^m (b_{k,l}^{(1)} x_k^{(i)} x_l^{(i)})}_{\text{Additional first order interactions}} + \underbrace{\sum_{k=1}^m (b_k^{(2)} (x_k^{(i)})^2)}_{\text{Additional quadratic terms}} \approx y^{(i)}, \quad (4)$$

with $b^{(0)}$, $b_k^{(1)}$, $b_k^{(2)}$, $b_{k,l}^{(1)}$ being the constant regression parameter and the regression parameters for the linear, quadratic and first order interaction terms respectively. Whether higher order terms improve the fit or not, highly depends on the nature of the non-linearity. Since all non-linearities are covered within the fourth step of this sensitivity scheme, in this step only interactions are taken into account. The goodness of the fit can be evaluated with the coefficient of determination (COD) and the with aid of the mean outcome (\bar{y}):

$$COD = R^2 = \frac{\sum_{i=1}^n (\hat{y}^{(i)} - \bar{y})^2}{\sum_{i=1}^n (y^{(i)} - \bar{y})^2} \quad (5)$$

The COD represents the proportion of the variance in the output

which can be explained by the input variables. However, the COD always increases with the number of model term m . Therefore, it tends to significantly overfit the model. The adjusted coefficient of determination takes the number of model terms m into account reducing the problem of overfitting:

$$R_{adjusted}^2 = 1 - \left(1 - R^2\right) \frac{n-1}{n-m}. \quad (6)$$

By fitting only one input variable to the output data, a single parameter COD for all inputs (R_k^2) can be computed which is simply the square of the correlation coefficient in the linear case. Higher CODs indicate more significant influences of this input. Furthermore, the effect on the overall coefficient of determination of adding or removing inputs from the overall model can be analysed. If the removal of a specific input from the model does not reduce or even increases the adjusted coefficient of determination, this input can be regarded as not influential. An automation of this process is the subset selection which is part of the third step. There are various methods of selecting the best subset and additionally different criteria for estimating the best subset. In this paper, two selection methods are used. Firstly, a straightforward approach of a forward selection is used. Here, the starting point is a constant model without any significant model parameters. Subsequently, parameters are added to the model one after the other as long as the model is getting better. The parameter that improves the model most is added first. One simple approach of evaluating the goodness of the model is the adjusted COD. Other criteria approximate the information that is lost by applying a specific meta-model (in this case multiple regressions with different number of model terms). This is performed by judging the goodness of the model fit using the likelihood function and penalising the number of model terms (e.g. with $+2m$ for the AIC). Such criteria are the Akaike Information Criterion (AIC) [35]

$$AIC = -2 \log \mathcal{L}(\mathbf{y}, \mathbf{X}_{n \times m}, \mathbf{b}) + 2m \quad (7)$$

and the Bayesian Information Criterion (BIC) [36]

$$BIC = -2 \log \mathcal{L}(\mathbf{y}, \mathbf{X}_{n \times m}, \mathbf{b}) + m \ln(n), \quad (8)$$

where m and n are the number of model parameters and samples respectively and $\log \mathcal{L}(\mathbf{y}, \mathbf{X}_{n \times m}, \mathbf{b})$ is the log-likelihood of the model with the parameters as above. There are different definitions of these criteria, especially other constant factors that do not change the overall behaviour. All different criteria have their advantages and shortcomings. For example, the BIC tends to underfit (keeps to few model parameters) the model, whereas the AIC and the adjusted COD overfit the model. Furthermore, the BIC will, if possible, result in the true model for $n \rightarrow \infty$, but, on the other hand, the AIC is asymptotically optimal which means that the squared error is as small as possible. The strengths of all criteria cannot be combined in one and the same index [37]. Therefore, for varying applications different criteria or even the simultaneous use of several ones can be valuable.

Selection methods like the forward selection do not always find

the best model. Therefore, another approaches called “shrinkage methods” can be used to find the best model. These methods reduce the parameter coefficients (b) in the regression model towards zero instead of only keeping or removing them. This procedure does not guarantee to find the best model as well, but it reduces the variance in the parameter coefficients and hence, leads to better model fits. Classical shrinkage methods are not appropriate for a subset selection, as all parameters are kept in the model and only their influence is reduced by “shrinking” the coefficients. However, there are further shrinkage methods, like the LASSO method [38], that combine the advantages of shrinking and reducing the set of parameters. This is achieved by reducing the coefficient of insignificant parameters down to zero. The linear LASSO method without interaction effects, which is used here, is based on the following equation with the definitions as before, \mathbf{b}^{LASSO} being the new vector of “shrunk” regression parameters and $t \geq 0$ a tuning parameter:

$$\mathbf{b}^{LASSO} = \arg \min_{\mathbf{b}^{(1)}} \left[\sum_{i=1}^n \left(y^{(i)} - b^{(0)} - \sum_{k=1}^m b_k^{(1)} x_k^{(i)} \right)^2 \right] \quad (9)$$

subject to $\sum_{k=1}^m |b_k^{(1)}| \leq t.$

It can be understood as a minimisation of the l^2 norm of the difference between the fitted outcomes ($\hat{y}^{(i)}$) and the real outcomes ($y^{(i)}$) with a secondary condition keeping the sum of regression parameters small in order to reduce insignificant parameters down to zero.

It is apparent that there are different regression and subset selection methods that can be used in the third step. Here, four approaches are combined. A forward selection with the adjusted COD, the AIC and the BIC are utilised. Additionally, the LASSO method is applied. If a parameter is selected by one of these approaches, it is further investigated in step four.

The fourth and last step of the sensitivity analysis is a global variance-based sensitivity analysis [39]. This analysis includes all non-linear high order effects and interactions between all input parameters. Hence, if no meta-model is used, this analysis conserves the whole complexity of the time domain model. On the other hand, it needs a large number of model evaluations, because conditional variances are analysed. This means, the influence on the total variance of keeping one factor fixed is investigated, which needs $n \times (m + 2)$ model evaluations. The total effects S_{Tk} that include all higher order and interaction effects can be calculated as follows:

$$S_{Tk} = \frac{E_{\mathbf{x}_{\sim k}}(V_{x_k}(y|\mathbf{x}_{\sim k}))}{V(y)} = 1 - \frac{V_{\mathbf{x}_{\sim k}}(E_{x_k}(y|\mathbf{x}_{\sim k}))}{V(y)}. \quad (10)$$

here, $V(y)$ is the unconditional variance of the output $y = f(x_1, x_2, \dots, x_k, \dots, x_m)$, $E_{\mathbf{x}_{\sim k}}(V_{x_k}(y|\mathbf{x}_{\sim k}))$ can be interpreted as the expected variance that would be left, if all factors except the k th factor are fixed and $V_{\mathbf{x}_{\sim k}}(E_{x_k}(y|\mathbf{x}_{\sim k}))$ is the expected reduction of the variance, if all factors except the k th factor are fixed. The first order

effects S_k can also be calculated without any additional model evaluations:

$$S_k = \frac{V_{x_k}(E_{\mathbf{x}_{\sim k}}(y|x_k))}{V(y)}. \quad (11)$$

here, $V_{x_k}(E_{\mathbf{x}_{\sim k}}(y|x_k))$ can be understood as the expected reduction of the variance, if the k th factor is fixed. For the mathematical background and a good overview of the sampling and numerical computation of the conditional variances and expectation and consequently of the sensitivity measures, the interested reader is referred to Saltelli et al. [40].

Finishing this section, Table 2 summarises the four steps included in the sensitivity scheme. The number of simulations is an approximate which will be explained later. It is included here to give an idea of the numerical cost. It has to be mentioned that this scheme is quite flexible and the methods in each step can be replaced by alternatives, if the general character of the stepwise parameter reduction is kept.

3. Sensitivity results

In this section, the results of the four-step sensitivity analysis are presented. It is divided into four subsections according to the steps performed. First of all, some general information about the simulation procedure is given. The time domain simulations of the turbine are conducted with the FASTv8 code [41] of the “National Renewable Energy Laboratory” (NREL). This code has been enhanced by a soil model described in Refs. [32] and [42]. The soil matrices required are based on the axial CPT method of FUGRO [43] and the lateral model of Thieken et al. [44]. The decision for these two soil models is based on experimental and numerical comparisons of different soil models ([44] and [45]). In all cases, the operating point is considered according to [42]. The consideration of the operating point is important as, especially the model by Thieken et al., leads to highly load-dependent soil stiffnesses. The wind fields are computed externally using TurbSim [46], which is capable of generating turbulent wind fields. Two substructures are investigated. Firstly, the OC3 monopile [47] and secondly, the OC4 jacket [48] are investigated in this study in order to apply the proposed four-step methodology to significantly different offshore wind energy applications. The choice of these two turbines is based on the scarcity of data, especially of the turbine controller, of real offshore wind turbines. Therefore, the use of cross-verified simulation turbines is probably the best and most common alternative. All simulations have a simulation time of 10 min as proposed in current standards. Additional 60 s at the beginning of each simulation are used to account for transient start-ups. The choice of 60 s for the start-ups should be sufficient, as in common code comparisons (e.g. Ref. [47]) only 30 s are used. For the OAT analysis, simulations of 10 min are quite short. A simulation of 1 h length or six 10-min simulations might be more reliable. However, the OAT analysis is only the first, non-selective step, and for the other approaches (regression and variance-based), several simulations are conducted as part of the procedure. Therefore, the usage of 10-min simulations is justified.

Table 2
Steps of the multi-step sensitivity analysis.

No.	Method	Approach	Aim	No. of simulations
1	Expert knowledge	Subjective selection	Get a starting subset and focus on desired parameter categories	0
2	One-at-a-time	“Local” variation of one parameter	Clarification if further steps are valuable	$2 \times m$
3	Regression	Global approximation of all parameters	Reduction of the parameter subset based on a (bilinear) approximation	$20 \times m$
4	Variance-based	Global and non-linear approach	Final parameter selection with all non-linearities and interactions	$1000 \times (m + 2)$

Table 3
List of all parameters that are treated as non-deterministic (MG: marine growth, SS: substructure).

Wind	Wave	Soil	Material	Geometry
Wind speed (v_s)	Water depth (L_{water})	Unit weight (γ'_i)	Young mod. ($E_{steel,SS}$)	Hub mass (m_{hub})
Power law exp. (α_{PL})	Water density (ρ_{water})	Friction angle (ϕ'_i)	Pois. ratio ($\nu_{steel,SS}$)	Nacelle mass (m_{nac})
Wind direction (θ_{wind})	Wave height (H_s)	Embedded length (L_{in})	Density ($\rho_{steel,SS}$)	Platform mass (m_{plat})
Air density (ρ_{air})	Wave direction (θ_{wave})	Relative density ($D_{r,i}$)	Young mod. ($E_{pile,foundation}$)	Pile diam. ($d_{pile,SS,i}$)
Turb. intensity (TI)	Wave period (T_p)	Cone tip resistance ($q_{c,i}$)	Pois. ratio ($\nu_{pile,foundation}$)	Wall thckn. ($t_{pile,SS,i}$)
Yaw error (Ψ)	MG thckn. (t_{MG})	Soil layer thckn. ($t_{soil\ layer,i}$)	Density ($\rho_{pile,foundation}$)	Pile diam. ($d_{pile,foundation}$)
Vertical flow angle (θ_v)	MG density (ρ_{MG})	Shear modulus ($G_{s,i}$)		Wall thckn. ($t_{pile,foundation}$)

3.1. Parameter selection and statistical distributions

In this paper, the first step of the sensitivity analysis in this paper is a reduction of the parameter set using expert knowledge. The focus of the present sensitivity analysis is on environmental conditions like wind, wave and soil conditions, material parameters of the substructure and local geometrical parameters of the substructure and foundation. Local geometrical parameters are, e.g., small changes in inputs, like pile diameters or wall thicknesses resulting from fabrication tolerances. Global or larger changes of the geometry resulting from different designs are not investigated here. The same applies to algorithm, model and control parameters. All parameters that are selected in the first step are summarised in Table 3. Here, E , ν , ρ , d and t are the Young's modulus, Poisson's ratio, density, diameter and (wall) thickness, respectively. The index i indicates that there are several values for this parameter. This is the case for soil properties, since the soil is modelled with three layers (cf. Fig. 3(a)), and for substructure components, as the substructure consists of piles with different wall thicknesses and diameters. This subdivision could be further expanded, so that each component of the substructure would have its own uncorrelated parameters which would be closer to reality, since fabrication tolerances are mainly uncorrelated. However, it has been decided to limit the number of independent values to an adequate level to avoid unnecessary complications. Furthermore, in order to keep the model "simple" and because of a lack of information, it is abstained from using correlations between the different input parameters. It is important to mention that especially for the soil parameters their effects are restricted to the models applied. In Table 3, for all inputs, statistical distributions have been derived either from literature research or from real data. Some distributions and the source of information are given in Table 4. In the introduction of this work, there is an overview of common statistical distributions in offshore wind energy (e.g. Refs. [9–15]). For the selection of distributions to be utilised for the fitting of the real data, these sources are used, inter alia.

As indicated in Table 4, several distributions have been derived from data of the FINO3 research platform. This platform is located

in the North Sea, 80 km to the west of the island Sylt. Wind and wave conditions have been measured continuously since 2009. Further data of the FINO1 platform, also located in the North Sea, is used for comparison, as for FINO1 more data (since 2003) is available. The FINO-WIND research programme is funded under the "Wind Energy Initiative" of the German Federal Ministry for Economic Affairs and Energy (BMWi) and "Projekträger Jülich". After some data cleansing (e.g. range constraints, cross-field validation), different distributions are fitted to the data with an MLE. The goodness of the fits is evaluated with KS and Chi-squared tests. For the choice of distributions that are fitted, existing distributions in offshore wind turbine literature (e.g. Refs. [9–15]), expert knowledge and the shape of the data distribution are taken into account. Two examples are presented in Fig. 2(a) and (b). For the air density at FINO1, the importance of bimodal distributions becomes obvious. For FINO3 (not shown here), the two peaks are less distinct. However, on the basis of the FINO1 data fit, bimodal distributions are fitted to the FINO3 data with best accordance as well. Fig. 2(b) clarifies the challenges of directional distributions. Several peaks are present and no tails develop, as there are no maximum or minimum angles. Therefore, classical parametric distributions can hardly fit directional data. The Kernel distribution as a non-parametric distribution realises an adequate fit as shown. However, dependencies between different parameters should be taken into account. As shown here, the fit of the wind direction is only valid for wind speeds between 12 m s^{-1} and 14 m s^{-1} . Therefore, for wind and wave parameters, correlations are assumed.

It has to be mentioned that the choice of the distributions includes some subjective decisions, as different distributions for one and the same parameter are proposed in literature, and especially the distribution parameters vary significantly between different turbine sites. However, this paper focuses on the sensitivity of the inputs. Therefore, it is sufficient to assume realistic distributions mainly being derived from real measurement data. For even more profound results, the influences of different distributions and/or statistical parameters should be analysed with the aid of robustness analyses. However, robustness analyses are beyond the scope of the present study.

Table 4
Parameter distributions for OC3 monopile.

Parameter	Unit	Distribution	Mean	CoV	Source	Notes
L_{water}	m	Normal (N)	20	0.04	[17]	Adjusted μ
v_s	m s^{-1}	Weibull	10.94	2.32	FINO3 data	Values are Weibull parameters a and b
ρ_{air}	kg m^{-3}	Bimodal Gumbel	1.21	0.022	FINO3 data	$\mu_2 = 1.25$, $\text{CoV}_2 = 0.016$ and $p = 0.87$
θ_{wind}	°	Kernel	–	–	FINO3 data	No parametric fit possible
t_{MG}	m	Uniform	–	–	[49]	0 m – 0.2 m
$t_{soil\ layer,1}$	m	Uniform	–	–	[13]	$14\text{ m} \pm 5\text{ m}$
$E_{steel,SS}$	N m^{-2}	Log-Normal (LN)	2.1×10^{11}	0.02	[15]	–
ϕ'_1	°	Truncated LN	33	0.15	[17]	Adjusted μ ; 29° and 45° as boundaries
θ_v	°	Normal (N)	0	1	[8]	–
$t_{pile,SS}$	m	Truncated N	0.06	0.1	[17]	0.0587 m and 0.0613 m as boundaries

884

C. Hübler et al. / Renewable Energy 111 (2017) 878–891

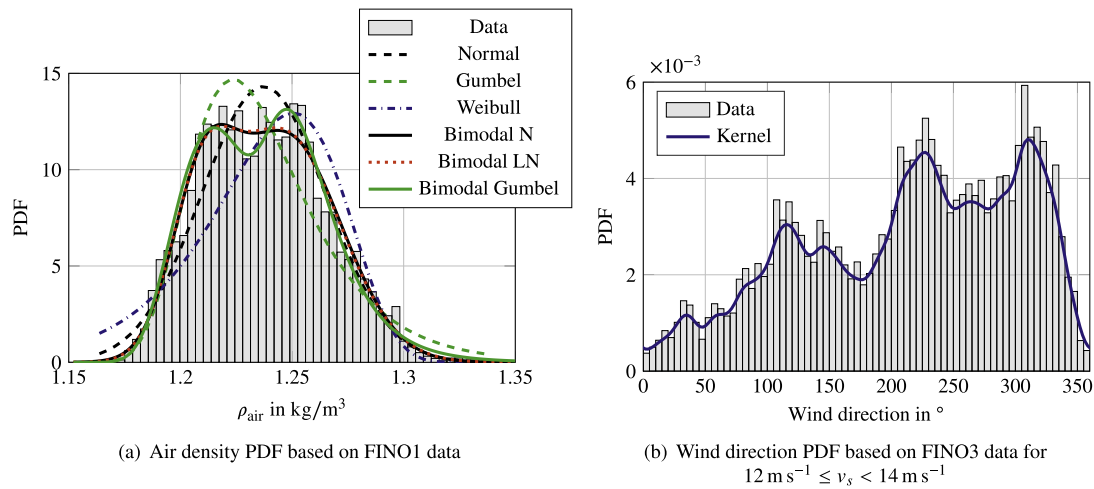


Fig. 2. Probability density functions (PDFs) for different parameters based on FINO data with fitted distributions.

3.2. One-at-a-time sampling

The input parameters that shall be analysed in the present sensitivity analysis have been identified in the previous section. Now, the results of the second step of the four-step methodology are presented. This step consists of an OAT analysis. As explained in section 2.2, this step is intended to clarify whether subsequent steps are useful, as a subset reduction is only possible if some, but not almost all, inputs are influential. For all m parameters, three values are chosen. The first one is the deterministic (“mean”) value. The other two are maxima and minima or $4\text{-}\sigma$ intervals for non-bounded distributions. Then, the $2 \times m$ full time domain calculations are conducted with all parameters fixed to their “mean” value, except for one which either takes its “minimum” or its “maximum”. The maximum values of the overturning moment, the shear force and in case of a jacket the axial force at mudline are chosen as outputs, since these forces and moments are frequently decisive for the reliability of the substructure. The forces and moments are

shown in Fig. 3 and the nomenclature is explained in Table 6. By analysing the change in these outputs, the significant indices $S_{OAT,k}$ can be calculated. In order to calculate comparable significant indices for all m inputs, the change in the input Δx_k has to be normalised. Here, the maximal range of the input is used to normalise the changes which leads to $\Delta x_k = 1 \forall k$. For two outputs, the ten most influential parameters for the monopile and the jacket are illustrated in Fig. 4(a) to (d). It becomes apparent that quite similar parameters, mainly wind and wave parameters, are most influential. Furthermore, in most cases only very few parameters have a major impact which is in particular obvious in Fig. 4(b). Here, the effect of the first input (H_s) is already more than ten times higher than the effect of the fifth input (θ_{wind}). This suggests that it is generally possible to reduce the probabilistic subset significantly and further steps are valuable. The least influential parameters are not shown here, but again there are some parameters that are not influential for both substructure and all outputs (maximum and fatigue loads at mudline, cf. Table 6 and Fig. 3). Examples are the

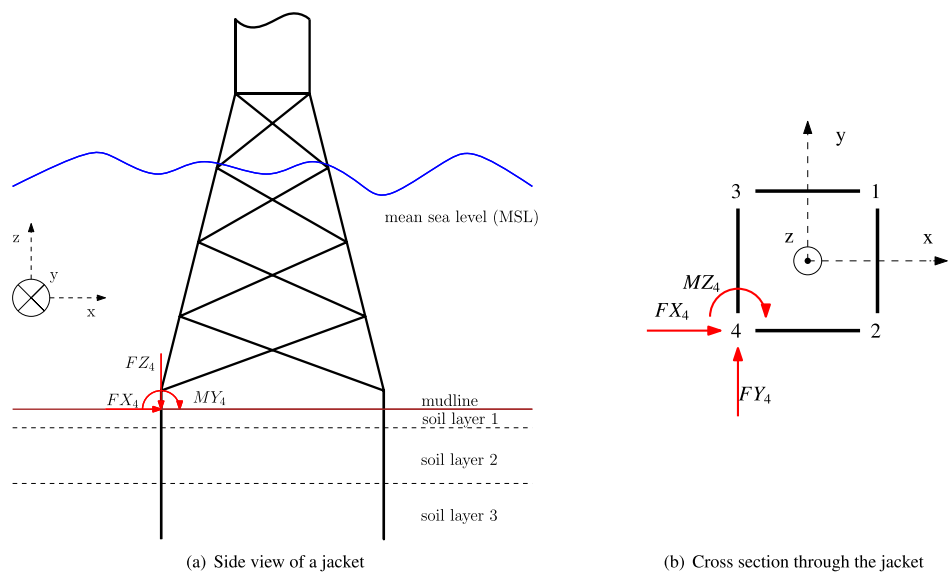


Fig. 3. Visualisation of the soil layer, forces and moments and leg numbering using an exemplary jacket.

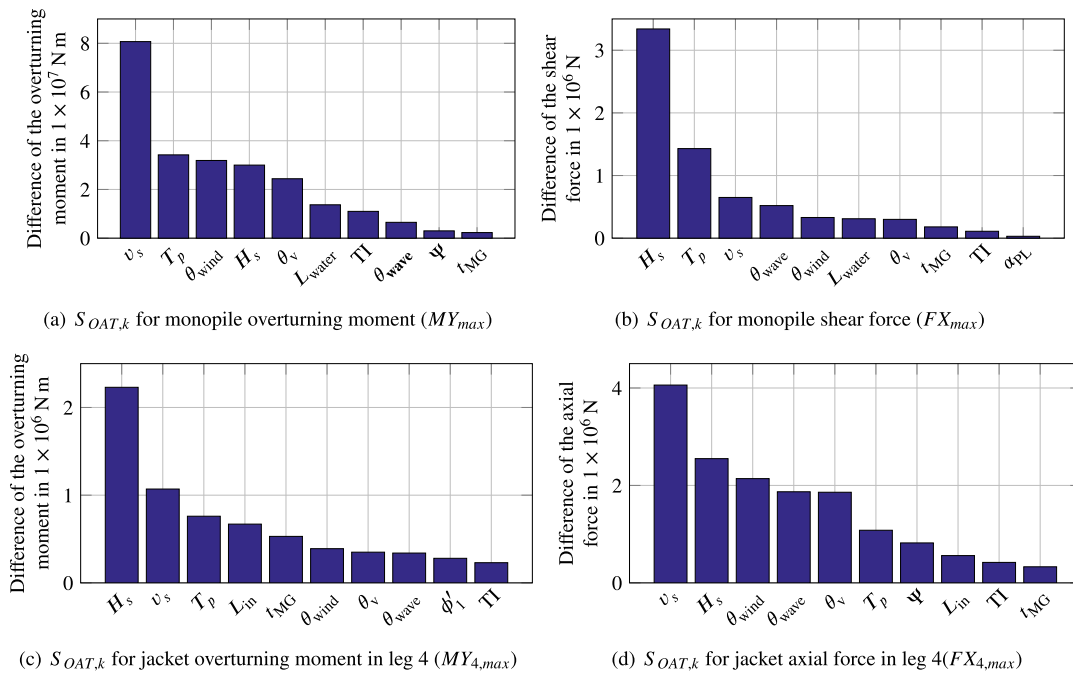


Fig. 4. Significant indices $S_{OAT,k}$ for the most important parameters (Step 2).

density and the Poisson's ratio of the foundation piles and the shear modulus ($G_{s,i}$) of the soil. The lack of influence of the shear modulus of the soil is due to the soil model applied [32]. It is only needed for the torsional stiffness, and torsional stiffness is insignificant.

Only extreme situations without interaction effects are considered with this kind of OAT analysis. Extreme parameters do not necessarily lead to extreme outputs. Especially for soil, material and geometrical parameters, non-extreme parameters and combinations of parameters can lead to resonance and therefore, to maximum responses. This shall be illustrated shortly with the aid of an exemplary oscillator having an eigen frequency of $\omega_0^2 = \frac{k}{m}$. Its mass (m) varies between 1 and 3 and its stiffness (k) is between 1 and 3. The oscillator is excited with a frequency of $\Omega^2 = 2.5$. Hence, it is obvious that neither an extreme value of k nor of m can lead to resonance, while the other value is fixed to 2 ($\rightarrow \omega_0^2 \leq 2$). Only a combination of high (not maximum) values for k and small (not minimum) ones for m (for example $m = 1.1$ and $k = 2.75$) will lead to maximum responses. It is obvious that wind turbine systems are not that simple, but similar combined effects occur. Therefore, it is inappropriate to select parameters only on the basis of these results. This step only clarifies that a further step by means of a

regression analysis including global and first-order coupling effects is needed. The number of significant parameters has not been reduced in this step, as the OAT analysis does not cover any interaction effects. Therefore, for a subset reduction based only on an OAT analysis, the risk of reducing the probabilistic subset too much and of neglecting influential, highly interactive parameters is very high. An example in the present context is the soil parameter ϕ_3 . By taking extremes in the OAT analysis, it is not detected to be influential (cf. Fig. 4), but if the full four-step approach is applied, it is one of the significant inputs (cf. Table 8).

3.3. Regression analysis and subset selection

For the regression analysis, $30 \times m$ samples for the monopile and $20 \times m$ samples for the jacket are generated with an LHS algorithm that reduces the correlations between the uncorrelated inputs. m is the number of inputs. This amount of samples should be sufficient [50] as also indicated in Fig. 5, which shows the coefficient of variation (CoV) of the maximum shear force for several calculations with different numbers of samples. It can be recognised that above 10 samples per input the variation of the CoVs tends to zero which means that each regression with this number of samples will have nearly the same outcome. The number of samples for the jacket calculations is smaller, as more samples are more challenging because of the high computing times. The distributions derived in the previous section are applied for the sampling. As indicated for the wind direction, some inputs are not independent of each other. θ_{wind} , α_{PL} , TI , H_s depend on the wind speed, T_p is correlated with the wave height and θ_{wave} depends on the wind direction and the wave height. Why this fact is of minor importance and all inputs are considered to be uncorrelated will be explained in the next sections.

At first, some qualitative and quantitative results of preliminary considerations are discussed. Scatter plots are presented in Fig. 6. These results are not used for the subset selection but are intended to assist the reader in understanding the general behaviour. For v_s

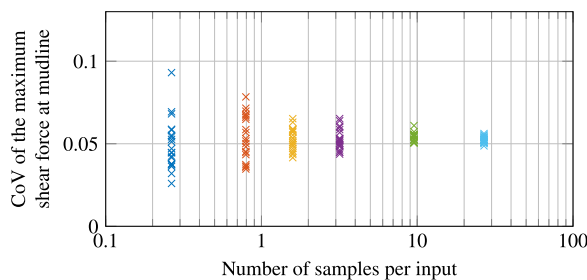


Fig. 5. Convergence of the coefficient of variation of the maximum shear force at mudline in wind direction (FX_{max} to investigate the no. of samples needed for step 3).

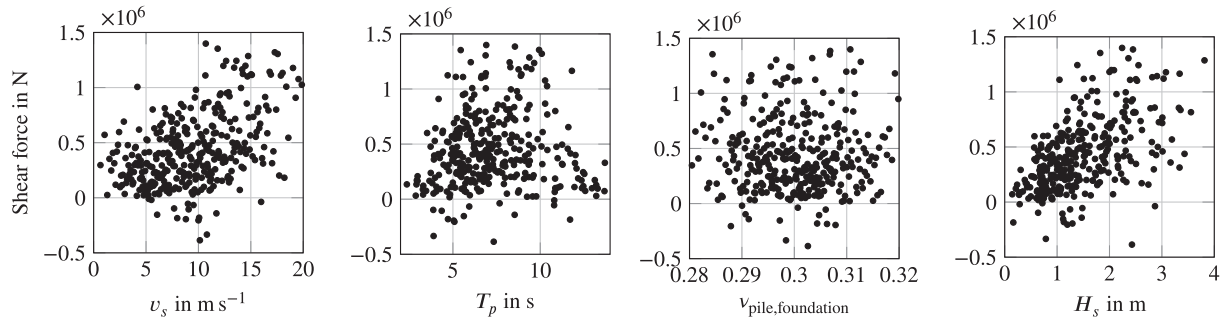


Fig. 6. Scatter plots for different inputs and the maximum monopile shear force at mudline (FX_{max}) as output (qualitative, preliminary considerations for step 3).

and H_s , a linear tendency becomes apparent, whereas for T_p , a non-linear relationship with the shear force can be recognised. For other parameters, like the Poisson's ratio, the scatter is totally random. Still, the tendencies are not very clear which is the reason why these qualitative outcomes are supported by preliminary, quantitative results. A linear regression is performed, and the single-parameter adjusted CODs and the overall adjusted COD, in case all parameters are taken into account, are calculated for different outputs and the two substructures. An exemplary result is shown in Fig. 7. For the main forces at mudline, the overall adjusted CODs are between 0.3 and 0.6, whereas for the moments only values between 0.05 and 0.3 are achieved. Furthermore, besides the five “main inputs” v_s , T_p , H_s , θ_{wind} and θ_{wave} no other parameters can be clearly identified to be influential. For other outputs that are not shown here, the “main inputs” are ranked differently and the influence of, for example, T_p or v_s is clearer. The fact that no other parameters can be identified is due to the regression model and not to the unimportance of all other parameters. Therefore, the importance of the other parameters is investigated subsequently.

After these preliminary considerations, step three starts with two additional regressions. For these regressions, the “main inputs” are fixed to specific values covering a wind state at rated wind speed, which is decisive for fatigue calculations, and an ultimate limit state (ULS). Here, the wind state is defined as a fixed environmental condition for the wind speed, its direction and the sea state. On the one hand, fixing the “main inputs” reduces non-linearities by removing the directional influences (e.g. $FX_{max} = f(\cos(\theta_{wave}), \dots)$) and on the other hand, effects of other parameters can be identified, since they are no longer dominated

by the “main effects”. Furthermore, the correlated inputs are fixed now. Therefore, it is no longer a simplification to consider the inputs as uncorrelated. Hence, a first outcome of the preliminary considerations in step three is that v_s , T_p , H_s , θ_{wind} and θ_{wave} have to be treated in a probabilistic way (cf. Fig. 7; further results of regressions for different outputs underlining this outcome are not shown here). From here on, only different wind states are considered, but no variations in these parameters themselves. Both wind states are chosen in accordance with the FINO3 data and the derived statistical distributions. The fixed values are summarised in Table 5, where 0° indicates north wind and 90° east wind. For both states, $20 \times m$ or $30 \times m$ samples, depending on the substructure, are generated and linear regressions are conducted. Here, m is reduced by 5, as the “main inputs” are fixed. The overall adjusted CODs and the highest single-parameter CODs are displayed in Fig. 8(a) – (d). Results of the monopile and the jacket for maximal loads and damage equivalent loads (DELs) as outputs are presented. The DELs are calculated using a rainflow algorithm, linear damage accumulation according to the Palmgren-Miner rule and a Goodman correction for loads with mean values unequal to zero. The wind state $v_s = 11 \text{ ms}^{-1}$ is used for the DELs, since this wind state corresponds with the rated wind speed. It has been shown that in many cases the highest fatigue damages result from rated wind speed, although higher DELs can occur at higher wind speeds, as the occurrence probability is much higher at rated wind speed compared to wind speeds close to cut-off [51]. For ULS loads, the $v_s = 35 \text{ ms}^{-1}$ wind state, which is derived using extrapolation analysis based on FINO3 data, is decisive which is the reason why this wind state is utilised for maximum loads. It has to be mentioned that the chosen ULS load case is a fairly moderate one, but the general trends of the sensitivity analysis should not be significantly influenced by this choice. The nomenclature of the outputs is summarised in Table 6.

From Fig. 8, it is apparent that the use of fixed “main inputs”, firstly, leads to a more appropriate use of the linear regression, as the adjusted CODs achieve values closer to 1 compared to the preliminary considerations including the “main inputs” (cf. Figs. 7 and 8). Furthermore, the effects of other parameters can be identified. In this context, mainly two further parameters become significant: t_{MG} and ϕ'_3 . It depends on the output, substructure and wind state which parameters are most influential. Not all influential parameters can be easily identified in Fig. 8. For example L_{water}

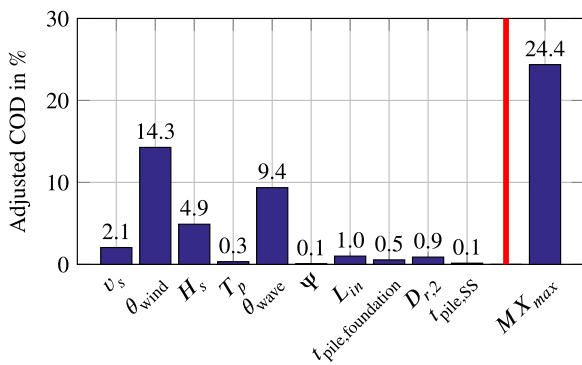


Fig. 7. Overall adjusted CODs (to the right of the red bars) and single-parameter CODs (to the left of the red bars) for maximum monopile overturning moment at mudline and perpendicular to the wind direction (quantitative, preliminary considerations for step 3 including “main inputs”). (For interpretation of the references to colour in this figure legend, the reader is referred to the web version of this article.)

Table 5
Values of the “main inputs” for the two wind states.

v_s in m s^{-1}	H_s in m	T_p in s	θ_{wind} in $^\circ$	θ_{wave} in $^\circ$
11	1.5	6	270	315
35	8	13	310	270

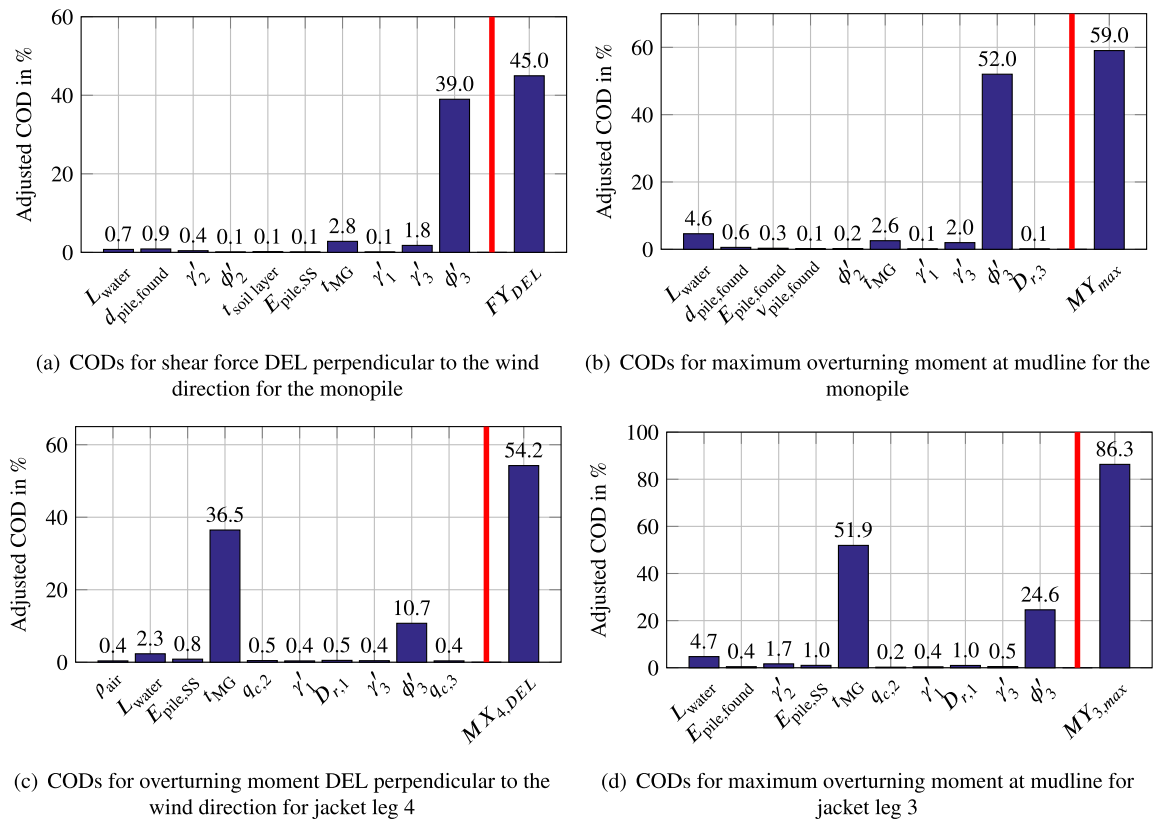


Fig. 8. Overall adjusted CODs (to the right of the red bars) and single-parameter CODs (to the left of the red bars) for different outputs, wind states and substructures (step 3 - part 1; without "main inputs"). (For interpretation of the references to colour in this figure legend, the reader is referred to the web version of this article.)

in Fig. 8(b) can be regarded as influential as well. For a clear and objective identification, an automated subset selection is performed next. However, some general statements are already possible. For example, the thickness of the marine growth (t_{MG}) is more decisive for jackets than for monopiles. Jackets have more braces where marine growth can occur, and as the diameters of the braces are smaller, the percentage increase because of marine growth is higher. Still it has to be kept in mind that the wave load effects are non-linear. Therefore, for different jackets (e.g. with three legs), the sensitivity of the marine growth might not be that pronounced. On the other hand, the internal friction angle ϕ_3 influences monopiles more than jackets. The reason is that ϕ_3 affects the lateral soil stiffness and not the axial one (for the applied soil model) and monopiles mainly experience lateral loading, whereas jackets are subjected to combined axial and lateral loads. These results show that not only one output can be considered for the

variable selection, as parameters having no influence on a certain output can still have significant influence on other important outputs. Nevertheless, it is obvious from Fig. 8 that some outputs seem to be not influential for all outputs.

So far, in step three, five "main inputs" have been identified in preliminary considerations. The first part of step three consists of regressions without the "main inputs" (cf. Fig. 8) making clear that slightly different parameters are most influential for different substructures and outputs. The second part of step three is the selection of the influential inputs using automated subset selections as described in section 2.2 (Step 3). Several outputs are investigated. For the jacket substructure, eight outputs are considered that have been identified to be the decisive loads. The outputs are $FX_{2,max}$, $MY_{2,max}$, $FZ_{1,min}$, $FZ_{1,max}$, $FZ_{1,DEL}$, $FZ_{2,DEL}$, $FY_{3,DEL}$ and $MX_{4,max}$ according to the nomenclature in Table 6. For DELs, generally, the loads perpendicular to the wind direction are less

Table 6
Nomenclature of the outputs.

Symbol	Output	Load case	Substructure
FX_{max}	Maximum shear force at mudline in wind direction	$v_s = 35 \text{ ms}^{-1}$	Monopile
FY_{max}	Maximum shear force at mudline perpendicular to the wind direction	$v_s = 35 \text{ ms}^{-1}$	Monopile
MX_{max}	Maximum overturning moment at mudline perpendicular to the wind direction	$v_s = 35 \text{ ms}^{-1}$	Monopile
MY_{max}	Maximum overturning moment in wind direction	$v_s = 35 \text{ ms}^{-1}$	Monopile
FY_{DEL}	DEL of the shear force at mudline perpendicular to the wind direction	$v_s = 11 \text{ ms}^{-1}$	Monopile
$FZ_{1,max}$	Maximum tensile axial force at mudline in leg 1	$v_s = 35 \text{ ms}^{-1}$	Jacket
$FZ_{1,min}$	Maximum compressive axial force at mudline in leg 1	$v_s = 35 \text{ ms}^{-1}$	Jacket
$FY_{3,DEL}$	DEL of the shear force at mudline perpendicular to the wind direction in leg 3	$v_s = 11 \text{ ms}^{-1}$	Jacket

888

C. Hübler et al. / Renewable Energy 111 (2017) 878–891

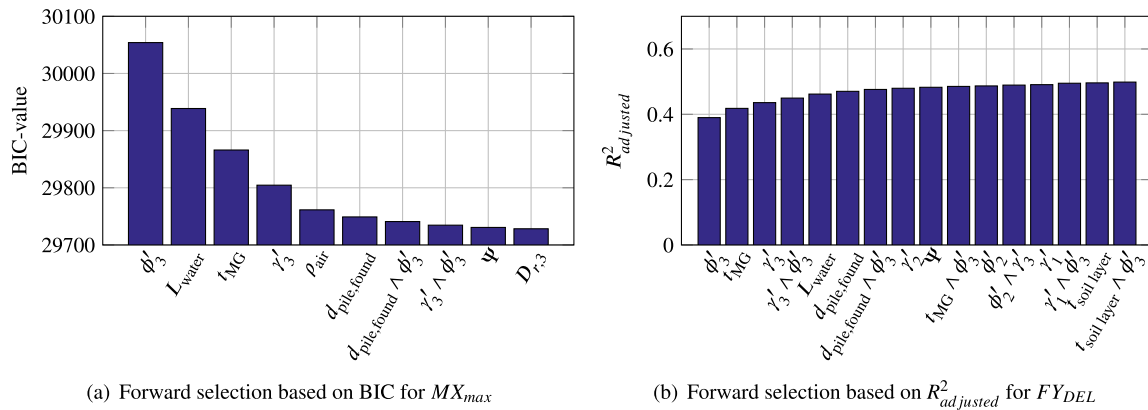


Fig. 9. Forward selections for monopile substructures based on different selection criteria and for different outputs (step 3 - part 2; without “main inputs”).

damped. At the same time, the excitation loads parallel to the wind directions are higher. Still, for the analysed system, it was found that the mean DELs in side-to-side direction are slightly higher than in fore-aft direction. This outcome is not generally valid and might be due to not aligned wind and wave directions and applied yaw errors, both increasing side-to-side excitation loads. For the monopile, four main outputs have been identified. These outputs are: FX_{max} , MX_{max} , FY_{DEL} and MX_{DEL} . For all outputs, a subset selection based on a forward selection with the adjusted COD, AIC value and the BIC value as selection criterion and one selection based on the LASSO method are performed. Here, the criteria for the jacket model are stricter compared to the monopile, as computing times for the jacket are much higher and a greater reduction of parameters is necessary. A subset selection based on the forward selection and the BIC for MY_{max} as well as a forward selection based on the adjusted COD with FY_{DEL} as the output are exemplarily shown in Fig. 9(a) and (b). The abscissa displays the added input parameter in each step. Parameters connected with the \wedge sign represent first-order interaction effects that are taken into account as well. The selection stops, if the BIC value no longer decreases (no model improvement) or the adjusted COD increases less than 0.001 (insignificant model improvement).

The subset selections with the four different criteria or methods lead to similar but slightly different results. For the final selection before variance-based sensitivity methods are used, the results of all four subset selections types are taken into account. When a parameter is selected for any output by one of the selection types, it is kept for this type of substructure. For this reason, the criteria are fairly strict. For example, the small improvements of the adjusted COD are not further considered, as it can be seen in Fig. 9(b) and from the boundary of 0.001 which is chosen based on expert knowledge. For the monopile, 14 parameters are selected as

influential plus the five fixed “main inputs” (14 + 5). Because of high computing times for jacket substructures, the criteria are stricter and only 9 + 5 parameters are chosen here. The parameters, including the “main inputs”, for both substructures can be found in Table 8 on the left hand side. More frequently selected and thus more influential parameters are listed first.

It is possible to reduce the size of the probabilistic subset and to create a linearised meta-model, as it is frequently used for variance-based sensitivity analyses, using a bilinear regression analysis. However, non-linearities have not been considered, and even if higher order terms are included in the regression, it remains an approximation. Hence, the fully non-linear time domain turbine model and not a meta-model is analysed with a variance-based approach in the next step. This enables the consideration of all kinds of non-linearities and also interactions of higher order. However, adequate simulation times of the variance-based approach applied to the turbine model are, especially for the jacket substructure, only possible because of the reduced probabilistic subset (cf. Table 7).

3.4. Variance-based sensitivity analysis

The final step of the presented multi-step sensitivity analysis is a variance-based sensitivity analysis that covers all interactions between inputs and all higher order effects. The variance-based method is applied to the reduced probabilistic subset (cf. Table 8, left), as computing times are only manageable for a small amount of parameters for the underlying time domain simulations. Just like for the regression analysis, two load cases ($v_s = 11 \text{ ms}^{-1}$ and 35 ms^{-1}) for the two considered substructures are analysed. Even for a reduced probabilistic subset, computing times are challenging, as $n \times (m + 2)$ samples have to be calculated. Therefore, the choice

Table 7
Approximate total computing times for the different substructures for both (2x) load cases.

No.	Method	No. of parameters	No. of simulations	Substructure	Computing time
1	Expert knowledge	> 100	0	Both	none
2	One-at-a-time	40	$2 \times (35 + 5)$	Monopile	1 h
		48	$2 \times (43 + 5)$	Jacket	30 h
3	Regression	35	$2 \times 30 \times 35$	Monopile	18 h
		43	$2 \times 20 \times 43$	Jacket	3 weeks
4	Variance-based	14	$2 \times 2000 \times (14 + 2)$	Monopile	3 weeks
		9	$2 \times 750 \times (9 + 2)$	Jacket	30 weeks
–	Plain var.-based	40	$2 \times 2000 \times (40 + 2)$	Monopile	8 weeks
		48	$2 \times 750 \times (48 + 2)$	Jacket	136 weeks

Table 8 List of the influential parameters for jacket and monopile selected using a regression-based subset selection (left) in the third step and a variance-based method (right) in step four. The “main inputs” are in bold. Parameters not selected in the fourth step are in grey.

Third step		Fourth step	
Monopile	Jacket	Monopile	Jacket
v_s	v_s	v_s	v_s
T_p	T_p	T_p	T_p
H_s	H_s	H_s	H_s
θ_{wind}	θ_{wind}	θ_{wind}	θ_{wind}
θ_{wave}	θ_{wave}	θ_{wave}	θ_{wave}
ϕ'_3	ϕ'_3	ϕ'_3	t_{MG}
t_{MG}	t_{MG}	γ_3	L_{water}
L_{water}	L_{water}	t_{MG}	ϕ'_3
γ_3	$q_{c,2}$	$d_{pile,found}$	$q_{c,3}$
ρ_{air}	γ'_2	$D_{r,3}$	$q_{c,2}$
$d_{pile,found}$	$D_{r,1}$	γ'_2	γ_2
γ_2	α^{PL}	L_{in}	
Ψ	γ'_1	L_{water}	
$D_{r,3}$	$q_{c,3}$	$D_{r,2}$	
L_{in}			
ϕ_2			
$D_{r,2}$			
$t_{soil\ layer}$			
γ'_1			

of sample size (n) is of high importance. Saltelli et al. propose $n \geq 500$ [40]. However, if $n = 500$ is chosen, the results are insufficient and inconsistent, if different methods for the calculation of the sensitivity indices are applied. Therefore, in this paper $n = 2000$ for the monopile analysis and $n = 750$ for the CPU-intensive jacket analysis are chosen. Table 7 summarises the approximate computing times for the different approaches used in this paper on

a “2× Intel Haswell Xeon E5-2630 v3 (8-cores, 2.40 GHz, 20 MB Cache, 85 W)” computer node, several nodes being used in parallel which is not taken into account in the table. The computing times of plain variance-based analysis (only step one and four) are given for comparison. This explains that the proposed four-step analysis reduces the computation cost by more than a factor of 4 (for the jacket). A first approximation of the reduction factor is the quotient

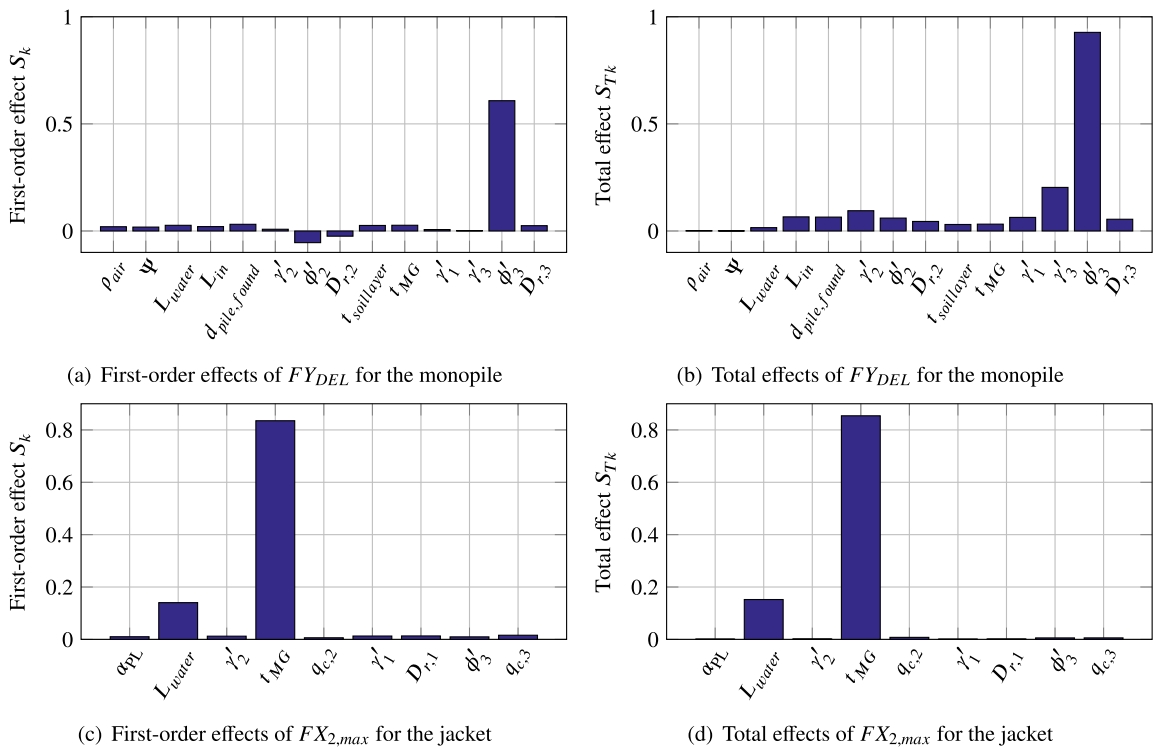


Fig. 10. Total and first-order effects for different outputs, wind states and substructures calculated with a variance-based sensitivity analysis (step 4; without “main inputs”).

of the number of initial input parameters to the number of inputs in the fourth step.

In Fig. 10(a) – (d), total and first-order sensitivity indices for different outputs, load cases and substructures are shown that are calculated with algorithms according to [52]. It becomes apparent that the sample size is still fairly small, as first-order effects are sometimes slightly higher than total effects, some sensitivity indices are slightly negative and different calculation algorithms (see Ref. [40]) give marginally varying results (not shown here). These problems are less severe for the jacket compared to the monopile, if the same number of samples is used. This can be explained by the smaller amount of inputs in the probabilistic subset (m) for the jacket. Therefore, the reduction of the probabilistic subset with the first three steps is even more important. Although these problems indicate that the convergence is not complete but just below a certain limit, the results are still much better than for $n = 500$, and larger sample sizes can hardly be realised because of limited computing power. Furthermore, this sensitivity analysis is “only” supposed to identify those parameters that have to be treated in a probabilistic manner. Therefore, the precise values of the sensitivity indices are of minor importance, and an incomplete convergence is acceptable.

The variance-based analysis enables some general conclusions concerning non-influential and the most important parameters. For both substructures, only a very limited number of parameters is really influential. Some parameters, like ϕ_3 or γ_3 for the monopile, influence all outputs, whereas others only influence either maximum or fatigue loads. Resonance is highly influenced by the effects of soil and geometrical parameters. This can be seen by comparing the total and first-order indices of soil and geometrical parameters. The total effects are much higher than the first-order indices which means that they exhibit high interactions effects. For other parameters, like L_{water} or ρ_{air} , this is not the case. Hence, these parameters do not interact that much. Furthermore, interaction effects are more relevant for the fatigue loads. After all, the parameters in Table 8 on the right hand side are the most influential ones for the monopile and the jacket, respectively. The most influential parameters are listed first, but the first five “main inputs” (in bold) are unranked as they are not studied in detail. It becomes apparent that the order of the selected parameters is different from the results of the regression in Table 8 on the left hand side. Soil and geometrical parameters are ranked higher, whereas other parameters are not selected (in grey) at all or are ranked lower. This can be explained by a more precise consideration of interactions and high-order terms. Hence, the final variance-based analysis has additional benefits compared to the previous steps.

4. Conclusion and outlook

In this paper, a multi-step global sensitivity analysis scheme is developed and results for two offshore wind turbine applications are presented. The idea of the multi-step approach is to identify the most influential parameters with a minimum amount of computing time, but by considering non-linear and interaction effects at the same time, requiring fully coupled time domain simulations. This is achieved by a stepwise reduction of the probabilistic subset of parameters. Such an approach is especially valuable, when every single simulation is time-consuming and meta-modelling is either not expedient or not desired. Therefore, the approach presented is especially adequate for offshore wind turbine calculations which have to be conducted in time domain. The CPU-intensive calculations one reason why practically no sophisticated or global sensitivity analyses for wind turbines have been conducted so far. This deficit is resolved with the current sensitivity analysis.

The four-step method has proved to be an adequate alternative, in case plain variance-based methods are too time-consuming. A comparison of both sides of Table 8 shows that a regression without subsequent variance-based analysis leads to a different variable selection, as interaction and high-order effects are not covered properly. Hence, the higher computing time of the presented method compared to regressions is compensated by more accurate results. For this reason, the approach can be regarded as a compromise between variance-based and less precise sensitivity analyses. The general concept of the multi-step approach is very flexible. Each step has its own purpose, but the methods that fulfil this aim are not fixed. For example, it is possible to replace the OAT method by “Elementary Effects”, the bilinear regression by rank or quadratic regressions and the variance-based method by the “Fourier Amplitude Sensitivity Test”.

The results of the sensitivity analysis make clear that only a few parameters are influential, and these parameters are mainly the same independent of the substructure. Hence, the results are of some general character. Nevertheless, this statement has to be examined by investigating more different substructures, and attention has to be paid to the small but not insignificant differences. Furthermore, it is important to notice that for fatigue loads different parameters have to be considered compared to ultimate loads. Therefore, it is not adequate to limit sensitivity analyses either to ultimate loads or to fatigue loads. On the other hand, if for both cases the influential parameters are known, the probabilistic subset can be optimised for each output. This means that it does not necessarily have to be the same for each output which can help to reduce computing times.

In this study, the convergence of the variance-based step is neither examined in detail nor is it totally completed. Such an investigation should be conducted in a further analysis together with a comparison of the results of a plain variance-based analysis with those of the present multi-step analysis. However, these considerations are beyond the scope of this paper, and for jacket substructures the computing times are hardly manageable (cf. Table 7).

As this study shows that soil parameters have large interactions effects, it can be assumed that the consideration of correlations between the soil parameters may change the results. For this reason, it is worthwhile to repeat this study with correlated inputs, if correlations are known which is generally not the case. Additionally, different soil models should be investigated, as it is known that there are significant differences between the models commonly used.

Acknowledgements

We gratefully acknowledge the financial support of the European Commission (research project IRPWIND, funded from the European Union’s Seventh Framework Programme for research, technological development and demonstration under grant agreement number 609795) that enabled this work. This work was supported by the compute cluster which is funded by Leibniz Universität Hannover, the Lower Saxony Ministry of Science and Culture (MWK), and the German Research Foundation (DFG).

References

- [1] C. Kost, J.N. Mayer, J. Thomson, N. Hartmann, C. Senkpiel, S. Philipps, S. Nold, S. Lude, T. Schlegl, Stromgestehungskosten erneuerbare Energien, Tech. rep., Fraunhofer-Institut für solare Energiesysteme ISE, 2013.
- [2] P.E. Morthorst, H. Auer, A. Garrad, I. Blanco, Wind Energy - the Facts - Part III - the Economics of Wind Power, Tech. rep., European wind energy association, 2009.
- [3] International Electrotechnical Commission, Wind Turbines – Part 3: Design

- Requirements for Offshore Wind Turbines, 2009.
- [4] C.G. Gebhardt, B.A. Rocca, Non-linear aeroelasticity: an approach to compute the response of three-blade large-scale horizontal-axis wind turbines, *Renew. Energy* 66 (2014) 495–514.
 - [5] P. Passon, M. Kühn, State-of-the-art and development needs of simulation codes for offshore wind turbines, in: *Copenhagen Offshore Wind 2005 Conference and Expedition Proceedings*, 2005.
 - [6] C. Böker, Load Simulation and Local Dynamics of Support Structures for Offshore Wind Turbines (Ph.D. thesis), Leibniz Universität Hannover, 2010.
 - [7] P.W. Cheng, A Reliability Based Design Methodology for Extreme Responses of Offshore Wind Turbines (Ph.D. thesis), Technische Universiteit Delft, 2002.
 - [8] D. Veldkamp, Chances in Wind Energy - a Probabilistic Approach to Wind Turbine Fatigue Design (Ph.D. thesis), Technische Universiteit Delft, 2006.
 - [9] B. Ernst, J.R. Seume, Investigation of site-specific wind field parameters and their effect on loads of offshore wind turbines, *Energies* 5 (10) (2012) 3835–3855.
 - [10] B. Schmidt, B. Ernst, M. Wilms, A. Hildebrandt, M. Hansen, Messdatenbasierte Empfehlungen von Wind- und Wellenparametern für die Auslegung von Offshore-Windenergieanlagen, *Bautechnik* 91 (8) (2014) 533–542.
 - [11] E.C. Morgan, M. Lackner, R.M. Vogel, L.G. Baise, Probability distributions for offshore wind speeds, *Energy Convers. Manag.* 52 (1) (2011) 15–26.
 - [12] B. Schmidt, M. Hansen, S. Marx, Directional dependence of extreme load parameters for offshore wind turbines, in: *The Twenty-fifth International Offshore and Polar Engineering Conference, International Society of Offshore and Polar Engineers*, 2015.
 - [13] M.B. Zaaijer, Foundation modelling to assess dynamic behaviour of offshore wind turbines, *Appl. Ocean Res.* 28 (1) (2006) 45–57.
 - [14] D.H. Kim, S.G. Lee, Reliability analysis of offshore wind turbine support structures under extreme ocean environmental loads, *Renew. Energy* 79 (2015) 161–166.
 - [15] J.D. Sørensen, H.S. Toft, Probabilistic design of wind turbines, *Energies* 3 (2) (2010) 241–257.
 - [16] K. Wei, S.R. Arwade, A.T. Myers, S. Hollowell, J.F. Hajjar, E.M. Hines, W. Pang, Toward performance-based evaluation for offshore wind turbine jacket support structures, *Renew. Energy* 97 (2016) 709–721.
 - [17] M. Hansen, B. Schmidt, B. Ernst, J. Seume, M. Wilms, A. Hildebrandt, T. Schlurmann, M. Achmus, K. Schmoor, P. Schaumann, S. Kelma, J. Goretzka, R. Rolfes, L. Lohaus, M. Werner, G. Poll, R. Böttcher, M. Wehner, F. Fuchs, S. Brenner, Probabilistic Safety Assessment of Offshore Wind Turbines, Tech. rep., Leibniz Universität Hannover, 2015.
 - [18] L. Ziegler, S. Voormeeren, S. Schafhirt, M. Muskulus, Design clustering of offshore wind turbines using probabilistic fatigue load estimation, *Renew. Energy* 91 (2016) 425–433.
 - [19] H.S. Toft, L. Svenningsen, J.D. Sørensen, W. Moser, M.L. Thøgersen, Uncertainty in wind climate parameters and their influence on wind turbine fatigue loads, *Renew. Energy* 90 (2016) 352–361.
 - [20] M. Damgaard, L.V. Andersen, L.B. Ibsen, Dynamic response sensitivity of an offshore wind turbine for varying subsoil conditions, *Ocean. Eng.* 101 (2015) 227–234.
 - [21] W. Carswell, S.R. Arwade, D.J. DeGroot, M.A. Lackner, Soil-structure reliability of offshore wind turbine monopile foundations, *Wind Energy* 18 (3) (2015) 483–498.
 - [22] M. Muskulus, S. Schafhirt, Reliability-based design of wind turbine support structures, in: *Symposium on Reliability of Engineering System, SRES2015, Hangzhou, China*, 2015.
 - [23] J. Goretzka, R. Rolfes, Modal and sensitivity analysis of the support of an offshore wind turbine under scattered soil parameters, in: *Proceedings of 8th PhD Seminar on Wind Energy in Europe, ETH Zurich, Switzerland*, 2012.
 - [24] L. Ziegler, S. Voormeeren, S. Schafhirt, M. Muskulus, Sensitivity of wave fatigue loads on offshore wind turbines under varying site conditions, *Energy Procedia* 80 (2015) 193–200.
 - [25] L.E.S. Stiang, M. Muskulus, A broad sensitivity analysis of uncertainties for offshore wind turbine support structures, in: *11th EAWE PhD Seminar on Wind Energy in Europe, Stuttgart, Germany*, 2015.
 - [26] B. Iooss, P. Lemaître, A Review on Global Sensitivity Analysis Methods, *Uncertainty Management in Simulation-Optimization of Complex Systems*, 2015, pp. 101–122.
 - [27] A. Mokhtari, H.C. Frey, J. Zheng, Evaluation and recommendation of sensitivity analysis methods for application to stochastic human exposure and dose simulation models, *J. Expo. Sci. Environ. Epidemiol.* 16 (6) (2006) 491–506.
 - [28] H. Song, R. Damiani, A. Robertson, J. Jonkman, A new structural-dynamics module for offshore multimember substructures within the wind turbine computer-aided engineering tool fast, in: *The Twenty-third International Offshore and Polar Engineering Conference, International Society of Offshore and Polar Engineers*, 2013.
 - [29] R.R. Craig Jr., M.C.C. Bampton, Coupling of substructures for dynamic analyses, *AIAA J.* 6 (7) (1968) 1313–1319.
 - [30] R. Damiani, J. Jonkman, A. Robertson, H. Song, Assessing the importance of nonlinearities in the development of a substructure model for the wind turbine CAE Tool FAST, in: *32nd International Conference on Ocean, Offshore and Arctic Engineering, Nantes*, 2013.
 - [31] W. Popko, F. Vorpahl, A. Zuga, M. Kohlmeier, J. Jonkman, A. Robertson, T.J. Larsen, A. Yde, K. Sætertrø, K.M. Okstad, J. Nichols, T.A. Nygaard, Z. Gao, D. Manolas, K. Kim, Q. Yu, W. Shi, H. Park, A. Vsquez-Rojas, J. Dubois, D. Kaufer, P. Thomassen, M.J. de Ruyter, T. van der Zee, J.M. Peeringa, H. Zhiwen, H. von Waaden, Offshore code comparison collaboration continuation (oc4), phase i - results of coupled simulations of an offshore wind turbine with jacket support structure, *J. Ocean Wind Energy* 1 (1) (2014) 1–11.
 - [32] J. Häfele, C. Hübler, C.G. Gebhardt, R. Rolfes, An improved two-step soil-structure interaction modeling method for dynamical analyses of offshore wind turbines, *Appl. Ocean Res.* 55 (2016) 141–150.
 - [33] T. Homma, A. Saltelli, Importance measures in global sensitivity analysis of nonlinear models, *Reliab. Eng. Syst. Saf.* 52 (1) (1996) 1–17.
 - [34] A. Saltelli, P. Annoni, How to avoid a perfunctory sensitivity analysis, *Environ. Model. Softw.* 25 (12) (2010) 1508–1517.
 - [35] H. Akaike, Information theory and an extension of the maximum likelihood principle, in: B.N. Petrov, F. Csaki (Eds.), *Second International Symposium on Information Theory, Akademiai Kiado, Budapest*, 1973, pp. 267–281.
 - [36] G. Schwarz, Estimating the dimension of a model, *Ann. Stat.* 6 (2) (1978) 461–464.
 - [37] Y. Yang, Can the strengths of aic and bic be shared? a conflict between model identification and regression estimation, *Biometrika* 92 (4) (2005) 937–950.
 - [38] R. Tibshirani, Regression shrinkage and selection via the lasso, *J. R. Stat. Soc. Ser. B Methodol.* 58 (1) (1996) 267–288.
 - [39] A. Saltelli, M. Ratto, T. Andres, F. Campolongo, J. Cariboni, D. Gatelli, M. Saisana, S. Tarantola, *Global Sensitivity Analysis: the Primer*, John Wiley & Sons, 2008.
 - [40] A. Saltelli, P. Annoni, I. Azzini, F. Campolongo, M. Ratto, S. Tarantola, Variance based sensitivity analysis of model output. design and estimator for the total sensitivity index, *Comput. Phys. Commun.* 181 (2) (2010) 259–270.
 - [41] J. Jonkman, The new modularization framework for the FAST wind turbine CAE tool, in: *51st AIAA Aerospace Sciences Meeting, Including the New Horizons Forum and Aerospace Exposition, No. NREL/CP-5000-57228, Dallas, TX*, 2013.
 - [42] C. Hübler, J. Häfele, A. Ehrmann, R. Rolfes, Effective consideration of soil characteristics in time domain simulations of bottom fixed offshore wind turbines, in: *The Twenty-sixth International Offshore and Polar Engineering Conference*, 2016.
 - [43] *Recommended Practice for Planning, Designing and Constructing Fixed Offshore Platforms - Working Stress Design - Errata and Supplement 3. API Recommended Practice 2A-WSD*, American Petroleum Institute, 2007.
 - [44] K. Thieken, M. Achmus, K. Lemke, A new static p-y-approach for piles with arbitrary dimensions in sand, *Geotechnik* 38(4).
 - [45] M. Achmus, M. Müller, Evaluation of pile capacity approaches with respect to piles for wind energy foundations in the north sea, in: *2nd International Symposium on Frontiers in Offshore Geotechnics, University of Western Australia, Perth*, 2010.
 - [46] J. Jonkman, L. Kilcher, *Turbsim User's Guide: Version 1.06.00*, Tech. rep., National Renewable Energy Laboratory, 2012.
 - [47] J. Jonkman, W. Musial, Offshore Code Comparison Collaboration (OC3) for IEA Task 23 Offshore Wind Technology and Deployment, Tech. Rep., NREL/TP-5000-48191, National Renewable Energy Laboratory, 2010.
 - [48] F. Vorpahl, W. Popko, D. Kaufer, Description of a Basic Model of the 'UpWind Reference Jacket' for Code Comparison in the OC4 Project under IEA Wind Annex 30, Tech. rep., Fraunhofer IWES, 2013.
 - [49] D. Oldfield, *Appraisal of Marine Fouling on Offshore Structures*, Offshore Technology Paper, Department of Energy.
 - [50] G.P. Brooks, R.S. Barcikowski, The pear method for sample sizes in multiple linear regression, *Mult. Linear Regres. Viewpoints* 38 (2) (2012) 1–16.
 - [51] D. Zwick, M. Muskulus, Simplified fatigue load assessment in offshore wind turbine structural analysis, *Wind Energy* 19 (2) (2016) 265–278.
 - [52] M.J. Jansen, Analysis of variance designs for model output, *Comput. Phys. Commun.* 117 (1) (1999) 35–43.

5 Long-term extrapolation

To certify OWTs, aero-elastic time-domain simulations are required by current standards [53, 84]. However, due to computational limits, it is not possible to simulate the entire turbine lifetime of normally 20 years. Therefore, some kind of long-term extrapolation is needed to extrapolate ULS and FLS values of some limited simulations to the entire lifetime. In this thesis, the focus is on FLS long-term extrapolation, since dominating failure modes of OWT substructures are FLS failures. Improved sampling techniques for the long-term extrapolation are developed and validated.

5.1 Methodologies for fatigue assessment of offshore wind turbines

5.1.1 Research context

The fatigue assessment of OWT substructures consists of two parts. First, the short-term damage (fatigue damage of a 10-minute simulation) has to be determined. This procedure is fairly normalised. Second, the short-term damage has to be extrapolated to a long-term or lifetime damage. Here, procedures are not standardised. This extrapolation is subject of the present section of this thesis.

Nevertheless, some remarks regarding the standard short-term damage calculation are given: For the considered case (e.g. load case and EC combination), an aero-elastic time-domain simulation is used to compute stress time series for all relevant locations (i.e. hot spots like welded connections). Rainflow counting and time series are used to determine the number of stress cycles for different stress amplitudes. Since there are stress concentrations at various hot spots, SCFs are applied. Finally, Miner's rule and S-N curves according to standards [38, 48] are applied to calculate the resulting short-term fatigue damage of this time series. The uncertainty of the short-term damage depends significantly on model uncertainties of Miner's rule and S-N curves. This uncertainty is not further considered here, as this work focuses on the long-term extrapolation.

For the long-term extrapolation, only vague recommendations are given by standards resulting in various extrapolation concepts. One of the most common ones in academia, used, for example, by Zwick and Muskulus [220], is the following: The entire wind speed range is split up into bins of 2 m s^{-1} or less. In each bin, all other ECs are set to constant values, while they can differ between the various bins. For example, for higher wind speeds, wave heights increase, but within a wind speed bin, the wave height is constant. Subsequently, for each wind speed bin, six simulations are conducted to reflect different realisations of turbulent wind and irregular waves. In the end, mean damages of all bins are weighted according to their occurrence probability and are extrapolated to the desired lifetime.

This procedure has several shortcomings that are pointed out, for example, by Müller and Cheng [126], Zwick and Muskulus [220], or Häfele et al. [61]. First, the assumption of constant ECs in all wind speed bins cannot reproduce the scattering of real offshore fatigue

measurements [126]. Therefore, probabilistic simulations are required. Second, even if constant ECs in each bin are assumed, six simulations lead to fairly high uncertainties due to limited sampling [220]. And third, if probabilistic simulations are conducted, the challenge of small uncertainties (due to finite sampling) is intensified [61].

Thus, there is a recent research focus on new long-term extrapolation techniques. In industry, normally bins for more ECs (e.g. wave heights) and a finer binning are used. This plain increase of the sampling effort while using the standard grid-based approach is also applied by Stewart as his reference approach [185]. Although such a procedure can lead to relatively low uncertainties due to finite sampling, this uncertainty reduction is only achieved at the expense of a high computational effort. This means that it is a quite inefficient concept, as shown, for example, by Graf et al. [55]. For industry, this inefficiency implies higher costs, and for academia - frequently having limited computational resources - it even might not be applicable. Hence, other concepts are valuable. One concept is the use of meta-models for fatigue damages [79, 185, 199, 221]. While this approach can reduce computing times significantly, the use of meta-models always adds some additional model uncertainty to the results. A second approach is the use of other sampling techniques. For example, one possibility is to determine the number of samples according to the occurrence probability of each bin (c.f. MCS) instead of a constant number of samples per bin [61, 185]. This means that there are no longer six (or another fixed number of) samples per bin, but less samples for rarely occurring high wind speeds and more samples for frequently occurring wind speeds close to rated wind speed. After all, there is still the need for further research to improve the extrapolation procedure which has been the reason for the development of two new extrapolation methods proposed in this thesis.

5.1.2 Methods

Due to the insufficient accordance of scattering of simulated fatigue damages and measured ones, if constant ECs are assumed [126], and due to the thematic focus of this thesis, a probabilistic approach is utilised here for the long-term extrapolation. Short-term fatigue damages are calculated according to the previously described standard approach. For the long-term extrapolation, two new advanced sampling techniques are developed: damage distribution based Monte Carlo simulation (DMCS) and reduced bin Monte Carlo simulation (RBMCS).

The idea of DMCS is to conduct more simulations where they are needed (c.f. importance sampling). In this context, this means that the number of simulations per bin is weighted according to the damage distribution (weighted lifetime damage). For example, if the wind speed bin 9 to 11 m s^{-1} accounts for 10 % of the overall lifetime damage, 10 % of the samples are generated in this bin. This has the advantage that uncertainties of “important” bins are reduced. The main challenge is that the damage distribution is not known a priori. This problem is handled by an initial “guess” of the damage distribution - using some equally distributed samples - and subsequent updates of it.

The concept of RBMCS is to reduce the number of bins by merging bins of similar damage behaviour. If, for example, the bins 3 to 5 m s^{-1} and 5 to 7 m s^{-1} are merged, more simulations can be conducted in all other bins. If the damage behaviour in merged bins is similar, the increase in uncertainty in these bins is small compared to the decrease in uncertainty in all other bins. Here, the main challenge is to decide which bins should be merged.

5.1.3 Results

The present investigation yields two results. First, if probabilistic approaches are used, the use of six simulations per bin leads to really high uncertainties due to limited sampling. This underpins results of Häfele et al. [61]. Second, neither the standard approach of equally distributed samples over all wind speed bins nor sampling according to the occurrence probability [61, 185] are suitable for reducing the uncertainty due to limited sampling. RBMCS outperforms both other approaches and is quite robust, for example, towards the overall sampling size. In most cases, DMCS yields even better results. However, care has to be taken, if damage values of one and the same bin are scattering a lot and overall samples sizes are fairly small. Hence, this is only relevant in academia with small sample sizes. Furthermore, DMCS has to be modified if parallelised simulations are used.

5.1.4 Outlook

In this first step, the two long-term extrapolation methodologies for fatigue damages are only tested for one type of substructure, one site (set of ECs), and simulated data using the aero-elastic simulation code FAST. This means that a general validity has not been shown yet. This is done in Section 5.2.

Furthermore, it should be noted that these improved sampling techniques can be combined with meta-models for fatigue - addressed in Section 1.2.8 and 5.1.1 - to further reduce computing times and/or uncertainties.

A parallelised version of DMCS could help to increase computational efficiency.

5.1.5 Paper D: Methodologies for fatigue assessment of offshore wind turbines considering scattering environmental conditions and the uncertainty due to finite sampling

The following paper is published in *Wind Energy*, Volume 21 (2018), pages 1092-1105 (<https://doi.org/10.1002/we.2216>). The main work was done by the author of this thesis. Cristian Gebhardt and Raimund Rolfes contributed with advisory and supporting work.

RESEARCH ARTICLE

Methodologies for fatigue assessment of offshore wind turbines considering scattering environmental conditions and the uncertainty due to finite sampling

Clemens Hübler¹ | Cristian G. Gebhardt | Raimund Rolfes

Institute of Structural Analysis, Leibniz Universität Hannover, Appelstr. 9a, D-30167 Hannover, Germany

Correspondence

Clemens Hübler, Institute of Structural Analysis, Leibniz Universität Hannover, Appelstr. 9a, D-30167 Hannover, Germany.
Email: c.huebler@isd.uni-hannover.de

Funding information

European Commission, Grant/Award Number: 609795; Lower Saxony Ministry of Science and Culture (MWK), Grant/Award Number: FKZ ZN3024; Leibniz Universität Hannover; German Research Foundation (DFG)

Abstract

For substructures of offshore wind turbines, the fatigue limit state is in most cases a decisive design factor. However, to calculate the fatigue lifetime of wind turbines, numerous time domain simulations for different load cases with changing environmental conditions are necessary. According to the state of the art, wind speed bins (of 2 m s^{-1}) are employed, while keeping all other environmental states constant. However, assuming constant parameters in each wind speed bin is an unfounded simplification. Therefore, in this study, methodologies for fatigue assessment considering scattering environmental conditions are investigated by assuming statistical distributions for environmental conditions for all wind speeds that are derived using real data measured at the North Sea research platform FINO3. These statistical distributions are used to conduct time domain simulations of an OC3 monopile—with a 5-MW wind turbine—using the aero-servo-hydro-elastic simulation framework FAST. The fatigue lifetime is calculated, and its uncertainty due to finite sampling is assessed. It is shown that if scattering environmental states in each wind speed bin are applied, the uncertainty due to finite sampling is significant. Furthermore, only some wind speed bins contribute to the overall fatigue damage. Based on these findings, in a last step, different Monte Carlo sampling concepts are investigated to reduce the number of simulations needed to calculate the fatigue lifetime with a defined uncertainty. By combining several wind speed bins and by sampling according to the damage distribution, it is proved that the number of simulations can be reduced by more than 30% without increasing the uncertainty.

KEYWORDS

fatigue limit state, offshore wind energy, scattering environmental conditions, simulation error, uncertainty

1 | INTRODUCTION

The share of offshore wind energy in overall energy production has grown over the last years. However, the cost of offshore wind energy is still high compared with other renewable energies.¹ As it is forecast that substructure improvements can potentially reduce the overall turbine cost by more than 5%,² an accurate and reliable simulation of offshore wind turbine substructures is beneficial. For substructures made of steel, mainly the fatigue limit state is decisive.³ To calculate the fatigue lifetime of wind turbines, numerous time domain simulations are necessary. Current standards⁴ define that these simulations should mirror the changing environmental conditions at the precise site of a wind turbine. However, for research purposes, these data are scarcely available, and even in industrial projects, the data quality is frequently poor because information on some parameters or long-term data is missing. This is why several research projects characterized environmental conditions at specific sites or entire areas and published statistical distributions as a reference. Examples for data bases of main conditions (wind speeds, wave height, wave period, and wind and wave directions) are the UPWIND design basis,⁵ the work of Stewart et al,⁶ the PSA-OWT project,⁷ Häfele et al,⁸ or Hübler et al.⁹ In this work, the data basis of Hübler et al⁹ is utilized, as it is—beside other advantages—the only one where additional environmental conditions, like the turbulence intensity or the wind shear, are considered in a statistical manner (see Table 2 for considered environmental conditions).

If for a specific site, data are available, it is state of the art to simplify the fatigue lifetime calculation roughly as follows¹⁰⁻¹²: The range of wind speeds in power production (eg, 3 m s^{-1} to 25 m s^{-1}) is divided into several bins of 2 m s^{-1} or less. All other environmental conditions are assumed to be constant within these wind speed bins, although Müller and Cheng¹³ recently showed that constant environmental conditions in each wind speed bin cannot reproduce the scattering observed in offshore fatigue measurements. Only the stochastic process of turbulent wind and irregular waves is considered in each bin by conducting 6 simulations (random seeds) per bin, as it is proposed by the standards.⁴ Although this is a state-of-the-art procedure, Zwick and Muskulus¹⁰ show that using only 6 simulations (random seeds) per wind speed bin leads to highly uncertain approximations of the lifetime damage. The reason for this uncertainty is the limited number of samples. Other types of uncertainty like errors of the aeroelastic model, the probability distributions, or the S-N curves are not taken into account, although they can be significant as well. For the remainder of this work, the expression “uncertainty” always refers to the uncertainty due to finite sampling. The effect of finite sampling is even intensified, if scattering of other environmental conditions within each bin is included, as it is done by Häfele et al.⁸ The authors show that even for 2048 overall simulations, distributed to the bins according to the statistical occurrence distribution of the wind speed, the error in the damage at an X-joint of the OC4 jacket due to finite samples is more than 10% with a probability of 5% (95th percentile). This high error results from the inclusion of stochastic effects (random seeds) and probabilistic effects (scattering environmental conditions).

Even for the simplified procedure, neglecting the scattering of environmental conditions in each wind bin and conducting only 6 simulations per bin, numerous time domain simulations are still necessary. That is why there exist several approaches to decrease the computing time by using meta models for fatigue damages. Examples are Zwick and Muskulus,¹⁴ Müller et al,¹⁵ Toft et al,¹⁶ or Stewart.¹⁷ Zwick and Muskulus reduced the number of simulations by a factor of 7 without adding a significant amount of additional uncertainty by applying a multivariate linear regression. Müller et al also use a linear regression, but it is based on a Box-Behnken design. Toft et al utilize, *inter alia*, a central composite design as meta model for the fatigue damage. Linear regressions and genetic programming are applied by Stewart, while generic programming shows better results.

Although a lot of work was done recently to enable reliable fatigue damage calculations within adequate computing times, there are still some major shortcomings. Three existing drawbacks according to the state of the art are treated in this study. Firstly, environmental conditions are no longer treated as constant within each wind speed bin, as Müller et al¹⁵ found out that variable environmental conditions can reproduce measurement variability more precisely. Secondly, so far, mainly jacket and floating substructures were investigated. Here, monopiles—widely neglected in uncertainty analyses—are investigated. And lastly, reduction concepts based on efficient sampling are developed. This differs from meta model-based approaches, as no approximation errors due to the meta model are added. Therefore, the following unanswered questions are addressed in the present work:

1. How high is the uncertainty of fatigue damages due to finite sampling for monopiles, if realistic, scattering environmental conditions in all wind speed bins are assumed?
2. To what extent is it possible to reduce the number of time domain simulations without adding additional simulation errors?

To address these topics, firstly, the utilized data basis for all significant environmental conditions, further settings, and the applied structural and fatigue model are presented. Secondly, a study of convergence for the number of simulations to assess the uncertainty in fatigue damages is conducted. Having determined the potential error in the lifetime damage, 3 sampling concepts for reducing the number of simulations without increasing the simulation error are presented and evaluated. It is abstained from applying meta models in this study, as these models add at least some model error. Lastly, the benefits and limitations of the current approach are summarized, and a conclusion is drawn.

2 | SIMULATION SET-UP

2.1 | Scattering environmental conditions

For various turbine sites, the environmental conditions can be fairly different. As these states significantly affect the fatigue damage of offshore wind energy plants, precise data of the specific turbine location are valuable. However, real site data are scarce, which is the reason for the formerly mentioned approaches of reference data bases.⁵⁻⁹ Although these data bases define conditional, statistical distributions for some environmental conditions, others are considered to be constant in each wind speed bin or even in all of them. The constant states of the frequently used UPWIND design basis are exemplarily summarized in Table 1.

TABLE 1 Environmental conditions of the K13 shallow water site (UPWIND design⁵ basis)^a

$v_s, \text{m s}^{-1}$	2	4	6	8	10	12	14	16	18	20	22	24	26
H_s, m	1.07	1.10	1.18	1.31	1.48	1.70	1.91	2.19	2.47	2.76	3.09	3.42	3.76
T_p, s	6.03	5.88	5.76	5.67	5.74	5.88	6.07	6.37	6.71	6.99	7.40	7.80	8.14
TI, %	29.2	20.4	17.5	16.0	15.2	14.6	14.2	13.9	13.6	13.4	13.3	13.1	13.0

^aThe wind shear exponent is considered to be constant ($\alpha = 0.14$), and wind and wave directions are usually set to zero but can be taken from scatter plots as well.

TABLE 2 Dependencies, statistical distributions, and bin widths for environmental conditions derived from FINO3 data

Parameter	Statistical distribution	Mean value	Dependencies	Bin sizes	Bin ranges
Wind speed (v_s)	Weibull	9.8 m s ⁻¹	None	None	-
Wind direction (θ_{wind})	Nonparametric KDE	207°	Wind speed	2 m s ⁻¹	0-34 m s ⁻¹
Turbulence intensity (TI)	Weibull	5.4%	Wind speed	2 m s ⁻¹	0-34 m s ⁻¹
Wind shear exponent (α_{PL})	Bimodal normal	0.088	Wind speed	2 m s ⁻¹	0-32 m s ⁻¹
Significant wave height (H_s)	Gumbel	1.6 m	Wind speed	2 m s ⁻¹	0-28 m s ⁻¹
Wave peak period (T_p)	Bimodal log-normal	7.3 s	Wave height	0.5 m	0-7 m
Wave direction (θ_{wave})	Nonparametric KDE	252°	Wave height	1.0 m	0-7 m
			Wind direction	36°	0-360°

In this study, an adopted version of the data basis of Hübler et al.⁹ is used. For 13 environmental parameters and 3 sites, conditional distributions, derived from offshore measurement data from FINO platforms, are available. The FINO platforms are measurement masts in the North and Baltic Sea, which are operated on behalf of the German Federal Ministry for the Environment, Nature Conservation, Building and Nuclear Safety (BMUB)*. In this work, the focus is on the 7 conditions in Table 2 that were measured at the FINO3 site, which is located 80 km west of the island Sylt near to the wind farm DanTysk and measures since 2009. For further details concerning the platform and the data, it is referred to the original source.⁹

According to Hübler et al.,⁹ distributions for all 7 environmental conditions are fitted to the data. The best fitting distributions—evaluated with Kolmogorov-Smirnov and χ^2 tests—are chosen, while keeping distributions as simple as possible (eg, multimodal distributions are only used, if the distribution of the raw data clearly exhibits several peaks). The resulting distributions and mean values are summarized in Table 2. As the parameters are not independent of each other, conditional distributions are defined. Hence, the data of the dependent parameters are split up into several bins of the independent parameters. To illustrate this approach, for example, the wave direction is fitted in several bins of 1 m wave height and 36° wind direction, eg, $p(\theta_{wave}) = p(\theta_{wave} | 1m \leq H_s < 2m, 36^\circ \leq \theta_{wind} < 72^\circ)$, where p is the probability density function. The dependencies, bin widths, and overall bin ranges for the dependent parameters are summarized in Table 2 as well. Bin ranges mark the limits for which sufficient data were available to fit distributions. For the statistical parameters of the distributions and more detailed explanations, it is referred to the data basis.⁹

2.2 | Further settings

In this study, the scattering of the previously mentioned 7 environmental conditions is taken into account, although variations of other conditions might be influential as well.¹⁸ However, for other parameters, either no data are available or they are assumed to be less significant. The following assumptions are made for all simulations:

- The turbulent wind field is calculated with the Kaimal model using the software TurbSim.¹⁹
- The JONSWAP spectrum according to IEC 61400-3 Annex B⁴ is used to compute irregular waves.
- The soil conditions of the OC3 phase II model²⁰ are assumed.
- Current, second-order and breaking waves, wave spreading effects, marine growth, and local vibration and degradation effects are neglected.

2.3 | Simulation prerequisites

For the calculation of fatigue lifetimes, numerous numerical simulations in time domain are necessary. In contrast to the deterministic, design load case-based approach recommended by the standards,⁴ a probabilistic simulation approach is applied here. Therefore, in this subsection, firstly, the probabilistic approach is explained. Secondly, the time domain simulation model and the utilized substructure are described. And lastly, the fatigue calculation is clarified.

2.3.1 | Probabilistic simulation approach

According to the standards,⁴ for the fatigue design of offshore wind turbines, several design load cases (eg, DLC1.2 or 2.4) have to be simulated. These load cases cover fatigue loads during power production, idling and fault conditions, and several special cases like rotor stops. Although stochastic inputs for turbulent wind and irregular wind are included, the DLCs remain quasi deterministic, as environmental conditions like wave heights and turbulence intensities do not scatter. For example, for DLC1.2 (power production), several wind speed bins have to be used, while other environmental conditions shall be selected together with the associated wind speed (ie, $H_s = f(v_s)$). Although the deterministic design aims to cover all critical events, it can be problematic, as some nonobvious fatigue driving conditions—like a wind-wave misalignment of 90° in combination with wave periods close to the eigenfrequency—might not be analysed. Especially for fatigue in side-side direction being significantly influenced by the wave induced turbine reaction, the deterministic wind focused approach might not always be conservative.

* Raw data of FINO platforms are freely available for research purposes. See www.fino-offshore.de/en/ for details.

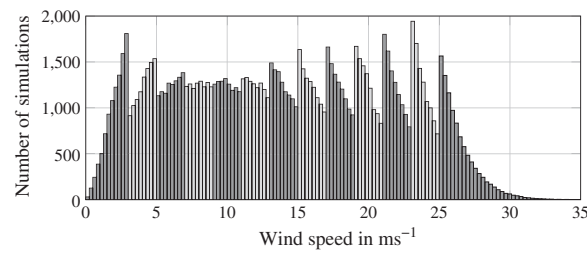


FIGURE 1 Number of simulation for different wind speeds using 130 000 overall simulations. Fairly homogeneous sampling due to applied bins, but in each bin, samples are generated using Monte Carlo simulation (shading illustrates the bins)

One possibility to overcome the shortcomings of the standard approach and to take scattering conditions at least partly into account is to apply several bins for the other environmental conditions, as it is done by Stewart.¹⁷ However, even if only 4 environmental conditions are used, this approach results—as discussed by Stewart—in an enormous computational effort with more than 100 000 bins (number of v_s bins multiplied by number of H_s bins multiplied by ...). For the 7 probabilistic environmental conditions of this work, millions of simulations would be necessary.

Therefore, in this work, a probabilistic simulation approach based on Monte Carlo simulation (MCS) and taking statistically scattering environmental conditions into account is applied. To be in accordance with the deterministic wind speed bins, the whole wind speed range is split up into bins, before applying MCS in each bin. For N overall samples, this means:

1. Split up the wind speed range into several (M) bins of, eg, 2 m s^{-1} . In each bin, $N_{\text{bin}} = N/M$ samples are generated to guarantee fairly homogeneous sampling over all wind speeds.
2. For each sample, the wind speed is determined according to a truncated version of the corresponding Weibull distribution (cf Table 2), for example, $p(v_s) = p(v_s|0 \text{ m s}^{-1} \leq v_s < 3 \text{ m s}^{-1})$ for the first bin.
3. If the wind speed is below cut-in or above cut-off, idling conditions are assumed. Otherwise, an operating turbine is simulated. Start-up or shutdown are not simulated.
4. Wind direction, turbulence intensity, wind shear exponent, and significant wave height are calculated using their statistical distributions, while the distributions themselves depend on the wind speed.
5. Wave peak period and wave direction are determined, while their statistical distributions depend on the previously calculated wave heights and wind directions (cf Table 2).

This bin-based approach—being an equally distributed Monte Carlo simulation (EMCS)—has the advantage that although all environmental conditions are computed according to their statistical distribution, it guarantees a fairly homogeneous sampling over all wind speeds (same number of simulations in each wind speed bin, but no completely uniform sampling, as the probability distribution of the wind speeds remains unchanged within each wind speed bin). Hence, rarely occurring wind speeds (eg, storm events) are simulated as well. If the simulation results of each wind speed bin are weighted using the occurrence probabilities, the EMCS still converges to the “real” value for a sufficient amount of samples. For a better understanding, in Figure 1, the occurrence probability of wind speeds using the EMCS approach is illustrated.

In this study, only power production (at different wind speeds) and idling conditions (below cut-in and above cut-off) are simulated. This is comparable to DLC 1.2.⁴ Fault cases (eg, DLC 2.4), start-up (DLC 3.1), etc, are not taken into account, as these load cases are very controller and design dependent making general conclusion nearly impossible. Furthermore, for highly transient conditions, like rotor stops, the widely linearized state-of-the-art simulations models (eg, FAST or HAWC2) are only limitedly valid. Since these special events account for a significant amount of fatigue damage, the overall lifetime damages being calculated here cannot directly be used for design purposes. Additional damage due to start-ups, installation, etc—all having their own uncertainty—have to be added.

2.3.2 | Time domain model

The time domain simulations are conducted using the aero-servo-hydro-elastic simulation framework FASTv8²¹ of the “National Renewable Energy Laboratory” (NREL). By including a soil model²² that applies soil-structure interaction matrices at the base node (cf Figure 2), this code is enhanced. The required soil matrices are based on non-linear spring models. In axial direction, the Fugro-05 method, recommended in the standards,²³ is used, and in lateral direction, the model of Thieken et al²⁴ is applied. Based on experimental comparisons²⁵ and the numerical results of Thieken et al,²⁴ the decisions for the soil models were made. Soil stiffnesses for operating conditions are assumed.²⁶

The NREL 5-MW reference wind turbine²⁷ with the OC3 monopile²⁰ as substructure is investigated (see Figure 2). The choice of this turbines is influenced by the scarcity of real data, especially of the turbine controller. Therefore, the use of a reference simulation turbine and its corresponding control algorithm²⁷ is a proper and quite common alternative. The substructure incorporates 1% critical structural damping²⁰ being important for the idling load cases with reduced aerodynamic damping. The simulation length is set to 10 minutes according to current standards⁴ and findings of Hübler et al⁹. A merge of several 10-minute simulations to improve the accuracy of the fatigue damage calculation^{9,10} is not performed due to increasing computing times. The “run-in” time or length of initial transients (ie., the time that has to be removed from each time series to exclude

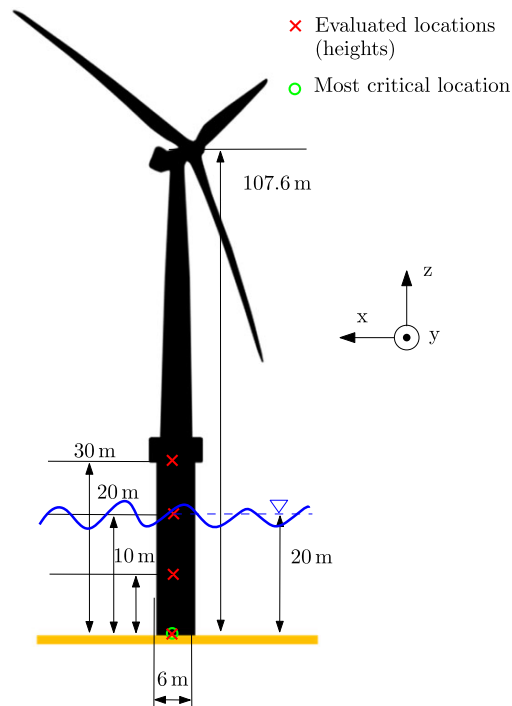


FIGURE 2 Visualization of the OC3 monopile and the 5-MW turbine. Inertial frame coordinate system: x pointing downwind, y pointing to the left when looking downwind, z pointing vertically upward opposite to gravity [Colour figure can be viewed at wileyonlinelibrary.com]

TABLE 3 Recommended “run-in” times for fatigue simulations with an OC3 monopile and for different wind speeds to achieve errors below 5%

v_s in m s^{-1}	< 3	3-5	5-7	7-9	9-11	11-13	13-15	15-17	17-19	19-21	21-23	23-25	> 25
Monopile	720 s	240 s	240 s	240 s	240 s	240 s	240 s	150 s	120 s	60 s	60 s	60 s	360 s

initial transients resulting from starting a calculation with a set of initial turbine conditions) depends, *inter alia*, on the wind speed. Therefore, varying “run-in” times determined by Hübler et al⁹ and summarized in Table 3 are applied.

2.3.3 | Fatigue assessment

The outcomes of the FAST time domain simulations are, *inter alia*, time series of forces and moments for each element of the monopile. Using these time series, it is either possible to calculate damage equivalent loads or the real lifetime fatigue damage. Both quantities have different uncertainties. Throughout this paper, the lifetime fatigue damage being a function of the stresses amplitude is used.

The welds of the monopile are exposed to higher fatigue damages, as stresses are concentrated in these hot spots (welds). Therefore, hot spot stresses have to be calculated according to Eurocode 3, part 1-9.²⁸ For transversal welds, the stress concentration is more critical (a detail of 71 MPa according to Eurocode 3) than for longitudinal welds (detail of 90 MPa). Hence, here, only transversal welds are investigated, and an additional stress concentration factor due to the size effect of the monopile wall thickness ($t > 25$ mm) is applied.²⁸

In most cases, for monopiles, shear stresses (τ) are significantly lower than direct stresses (σ). Therefore, the normal stress transverse to the weld can be approximated as follows:

$$\sigma_{\perp} = \frac{F_z}{A} + \frac{\sqrt{M_x^2 + M_y^2}}{S}, \quad (1)$$

where F and M are forces according to the coordinate system in Figure 2, A is the cross section area, and S is the section modulus. This procedure is a simplification and slightly conservative, as for each evaluated location of the monopile (cf Figure 2), always the maximum normal stress is assumed. This means that a directional dependence in each location for different load cases is neglected ($M = \sqrt{M_x^2 + M_y^2}$). This conservative approach is similar to the use of the highest hot spot stresses for jackets.¹⁴

For the normal stress in all elements, a rainflow counting evaluates the stress cycles. The conservative linear damage accumulation according to the Palmgren-Miner rule is assumed, as it is recommended by current standards. The damage for each time series (j) and each location (k) in each wind speed bin (m) is calculated as follows:

$$D_{TS,j,m}^{(k)} = \sum_{i=1}^l \frac{n_i}{N_i}, \quad (2)$$

where n_i is the number of cycles associated with the stress amplitude $\Delta\sigma_{\perp,i}$, N_i is the endurance (number of cycles) for the same stress amplitude, and l is the number of considered stress amplitudes. The slope of the S-N curve is set to 3 before and to 5 after the fatigue limit. This differs slightly from the Eurocode approach, where an additional cut-off limit at $N = 10^8$ is presumed.

The lifetime damage of each element ($D_U^{(k)}$) is the weighted sum of the damages of all time series in all wind speed bins:

$$D_U^{(k)} = \sum_{m=1}^M \sum_{j=1}^{J(m)} \left(D_{TS,j,m}^{(k)} \frac{J_{\text{total}} Pr(m)}{J(m)} \right), \quad (3)$$

where M is the number of wind speed bins, $J(m)$ is the number of time series depending on the wind speed bin, $Pr(m)$ is the occurrence probability of the wind speed bin, and J_{total} is the number of total time series during the lifetime (eg, $6 \times 24 \times 365.25 \times 20$ for 20 years lifetime and 10-min simulations).

Finally, the overall lifetime damage of the substructure (D) being considered in the following is the maximum lifetime damage of all K locations:

$$D = \max \left(D_U^{(1)}, \dots, D_U^{(K)} \right). \quad (4)$$

For the present monopile with its purely cylindrical shape the critical location is at mudline (cf Figure 2; locations below mudline are not considered), and therefore, $D = D_U^{\text{mudline}}$. However, the critical location might differ between different designs. Hence, the approach of using the location with the maximum damage is more generally valid.

3 | STUDY OF CONVERGENCE

The determination of lifetime damages is a time-consuming process, which has to be reliable at the same time. Therefore, the investigation of the number of simulations needed to enable a robust lifetime assessment in an adequate computing time is a challenge. This problem is even intensified by the use of several scattering environmental conditions, as additional uncertainties are introduced. Therefore, this section focuses on the determination of the number of simulations needed for the EMCS approach in Section 2.3.1. A compromise between computing time and remaining uncertainty has always to be made. However, this study is, firstly, supposed to give guidance for well-founded decisions, and secondly, to quantify the resulting errors.

For constant environmental conditions in each wind speed bin and a jacket substructure, Zwick and Muskulus¹⁰ already showed that following the recommendations in the standards of using six 10-minute simulations, the error in fatigue damages with a probability of occurrence of 1% (1% error ($\epsilon_{1\%}$); cf Equation 5) is up to 29%. As environmental conditions are set to constant values, this uncertainty is solely due to the stochastic nature of turbulent wind and irregular waves.

In this work, more realistic environmental states, scattering in each wind speed bin, are assumed. This leads to more strongly scattering fatigue damages in each wind speed bin, since the stochastic nature of turbulent wind and irregular waves is considered together with the scattering of environmental conditions. The increased uncertainty of the damage values is indicated in Figure 3A. Here, the normalized fatigue damages of 10 000 simulations with wind speeds of 15 to 17 m s⁻¹ are shown. For reasons of clarity, the horizontal axis ends at a normalized fatigue damage of 4, while some rare cases (less than 3%) exhibit values up to 215. In the following, a study of convergence is conducted to determine the number of simulations (N) that is necessary to achieve a certain reliability of the damage calculation. For this purpose, 10 000 simulations are conducted in each wind speed bin. These simulations have not only different random seeds, but scattering environmental conditions as well. Subsequently, 10 000 random combinations of $N_{\text{min}} = 6$ up to 10 000 simulations are selected with replacement using a bootstrap (BT) procedure.²⁹ The bootstrap approach allows to approximate the uncertainty in the fatigue damage for different combination sizes that is introduced by using a limited number of samples. The uncertainty in each samples (eg, due to model errors and uncertainties in the S-N curve) is not investigated, as discussed in Section 1. The resulting distributions of mean fatigue damages for different combination sizes (normalized with the mean value of N_{max}) are shown in Figure 3B for a wind speed of 15 to 17 m s⁻¹. It can be seen that the uncertainty reduces with increasing combination sizes. The 99th percentiles are marked, as this value can be used to calculate the 1% error ($\epsilon_{1\%}$):

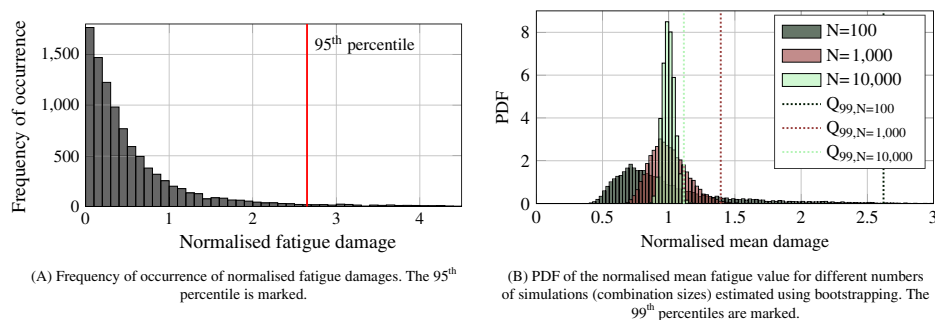


FIGURE 3 Illustration of the scattering and uncertainty of fatigue damages for $v_s = 15 - 17$ m s⁻¹. Normalization with to the mean value of 10 000 simulations [Colour figure can be viewed at wileyonlinelibrary.com]

$$\epsilon_{1\%} = \frac{Q_{99} - \mu_{N_{max}}}{\mu_{N_{max}}} \tag{5}$$

As the 1% error varies for different numbers of simulations, it is shown in Figure 4A as a function of N . Since the simulation error depends on the wind speed as well, Figure 4B displays the 1% error for all wind speeds and several combination sizes.

The most conspicuous feature is the enormous amount of simulations needed to reach small simulation errors. This increases overall computing times significantly. Therefore, the reasons for this high uncertainty are investigated in detail. Firstly, the scattering of the lifetime damage in one wind speed bin is analysed. For the wind speed of 15 to 17 m s^{-1} , for example, 95% of the fatigue damages are in the range of zero to 2.65 times the mean value (cf Figure 3A). However, there are some rare values exceeding the mean by a factor of 200 and more. Therefore, it is important to know the reason for these outliers, as they dominate the convergence behaviour, lead to high uncertainties, and influence the overall fatigue damage significantly. The main physical reason for these high damages is resonance. Monopile substructures are heavily influenced by wave loads. If waves excite the eigenfrequency of a wind turbine and the damping is low, high damage values occur. The first eigenfrequency of the monopile is about 0.25 Hz.²⁰ In general, wave peak frequencies are lower with 0.1 to 0.2 Hz (cf Table 1). However, as the environmental conditions scatter, higher wave peak frequencies occasionally occur as well. Figure 5A shows the distribution of the wave peak periods for $v_s = 15\text{--}17\text{ms}^{-1}$. The rare occurrence of waves with $T_p \approx 4\text{s}$ (0.25 Hz) is obvious. Figure 5B illustrates that these rare cases of resonance lead to the outliers of the fatigue damage, as the highest damages occur for $T_p \approx 4\text{s}$. This analysis makes clear that this effect is absent in case of constant environmental conditions. In this study, the relatively low design value for the structural damping of 1% is used.²⁰ However, damping values are fairly uncertain, especially the soil damping. Various standards recommend values between 1% and 5%,³⁰ and measured overall damping values during idling conditions can be about 2%.³¹ Hence, higher damping values are realistic as well. In this case, resonance effects would be much less pronounced. Some other reasons for outlier—not being further discussed, as less significant than the wave resonance and since a detailed discussion of all reasons is out of the scope of this work—are sea states with high waves or “extreme” turbulence, wind shear at lower wind speeds, or the stochastic nature of turbulent wind and irregular waves.¹⁰

After having clarified this main feature, another aspect shall be addressed. The uncertainty reduces with higher wind speeds (see Figure 4B). Wave peak periods increase with the wind speed. Therefore, the probability of wave periods close to the eigenfrequency of the structure decreases significantly, and the probability of resonance effects diminishes. In addition, but less significant, up to rated wind speed, wind loads increase leading to reduced uncertainties for higher wind speeds as well.

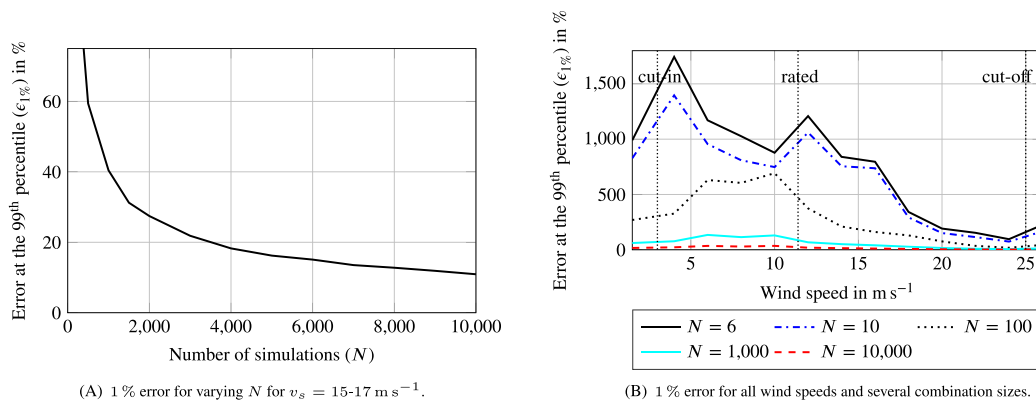


FIGURE 4 Lifetime damage 1% error ($\epsilon_{1\%}$) for different wind speeds and numbers of simulations per wind speed evaluated using 10 000 bootstrap samples (with replacement) [Colour figure can be viewed at wileyonlinelibrary.com]

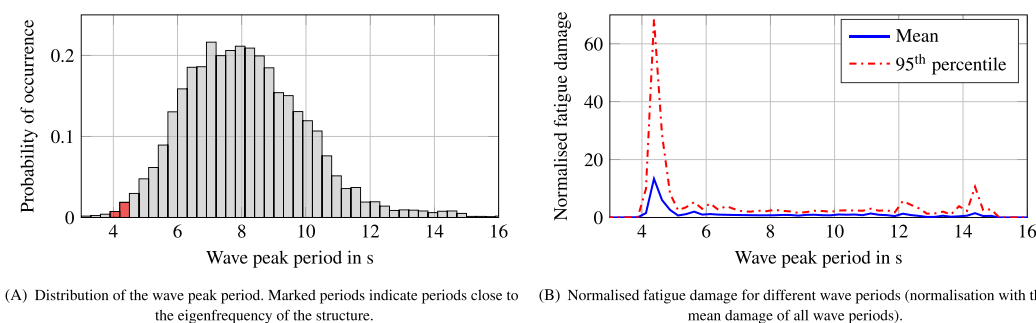


FIGURE 5 Investigation of the high uncertainties in fatigue damages by analysing resonance effects (exemplary for $v_s = 15\text{--}17 \text{ m s}^{-1}$) [Colour figure can be viewed at wileyonlinelibrary.com]

Finally, it is of interest to know how many simulations per wind speed bin are needed to achieve an “acceptable” error (eg, a 1% error of 25%). Figure 4A indicates that for $v_s = 15\text{--}17\text{ m s}^{-1}$, about 2500 simulations are needed. However, the uncertainties for different wind speed bins vary (cf Figure 4B), and according to Equation 3, the overall lifetime damage consists of the damages of all time series and wind speed bins. If the lifetime damages of all wind speed bins are summed up, a 1% error of 25% is achieved for about 1000 simulations per bin.

This result leads to 2 implications. Firstly, the assumption of constant environmental conditions might lead to unreliable results, as the rare cases of high loads (eg, resonance cases) are neglected, which might lead to nonconservative designs. It cannot be guaranteed that the high scattering of damage values is covered sufficiently by current safety factors, especially because resonance cases are not considered by the DLCs defined in current standards. Secondly, as an enormous amount of simulations is needed, reduction techniques are essential. That is why the next section gives an insight into the distribution of fatigue damages over wind speed, which is subsequently used in Section 5 to develop such reduction techniques.

4 | DISTRIBUTION OF FATIGUE DAMAGES

The convergence and uncertainty studies in the last section show that about 1000 simulations per bin are required. That is why a reduction of the number of simulations by preserving a constant level of accuracy at the same time is valuable. To be able to develop well-founded reduction schemes, a better knowledge of the lifetime damage is helpful. If conditions leading to a high proportion of the overall damage and those resulting in nearly no damage are known, it is possible to concentrate sampling on regions of the design space (here, only the wind speed design space) resulting in high damages to reduce the number of required samples. Therefore, in this section, 2 questions concerning the fatigue damage are answered:

- Do idling load cases (below cut-in and above cut-off) have significant influence on the fatigue lifetime?
- To which extent is the fatigue damage correlated to the wind speed?

The first question aims at a possible exclusion of (or a special focus on) idling load cases. The second one targets identifying the most relevant wind speeds for well-founded (importance) sampling.

To address these 2 problem statements, the lifetime damage for each wind speed bin is calculated separately. Physically, this means that lifetime damages are calculated, while it is assumed that only a single wind speed (bin) occurs for the whole lifetime. Mathematically, the mean fatigue damage for each wind speed bin is calculated separately using Equation 3 with one bin ($M = 1$), 10 000 simulations in this bin ($J(m)=10\ 000$) and a probability of this bin of one ($Pr(m) = 1$). The results are presented in Figure 6A. It is apparent that the highest fatigue damages occur below cut-in and above cut-out (values > 1 are possible, as the occurrence probability is not taken into account). In both cases, the turbine is idling and aerodynamic damping is reduced. Similar results of a significant amount of damage for idling conditions was shown, for example, by Aasen et al.³² However, it has to be mentioned that, as discussed before, higher damping values (eg, due to a significant amount of soil damping) would reduce the damage proportion being produced below cut-in. Furthermore, many real control algorithms start to pitch in for wind speeds below cut-in. In this case, the aerodynamic damping is increased and low wind speed fatigue becomes less significant.

So far, the probability of occurrence of each wind speed bin is set to one ($Pr(m) = 1$). This helps to assess the damage caused by single events or time series (eg, storm events with $v_s > 25\text{ m s}^{-1}$ lead to high damages). However, Figure 6A does not give any information on the contribution of each wind speed bin to the overall lifetime damage (eg, storm events are so rare that their contribution to the lifetime damage is small). To take the probability of occurrence of each wind speed bin into account, Figure 6B shows the weighted lifetime damage, where $Pr(m) = f(v_s) < 1$.

The damage distribution (weighted lifetime damage versus wind speed bins for the most critical section; $D(m)$) in Figure 6B helps to answer the 2 questions concerning the relevance of idling load cases and the D - v_s correlation. Firstly, it is apparent that, although idling conditions are relatively rare ($Pr(v_s < 3\text{ m s}^{-1}) + Pr(v_s > 25\text{ m s}^{-1}) < 0.03$), idling load cases still produce significant damage (cf Figure 6A). The main reason is a reduced aerodynamic damping for idling conditions. Still, for low wind speeds, the mean wave height is only about 1 m (cf Hübler et al.⁹ or Table 1), and therefore, the energy input is quite low. However, due to the scattering wave heights, for those load cases, values above 2 m are possible as well leading to a significant amount of energy input, which is marginally damped. Secondly, low wind speeds ($v_s < v_{rated}$) have a significant influence on the overall damage (here, nearly 40%). For small wind speeds, the scattering of the wave peak period is higher and more resonance cases occur.⁹ For high wind

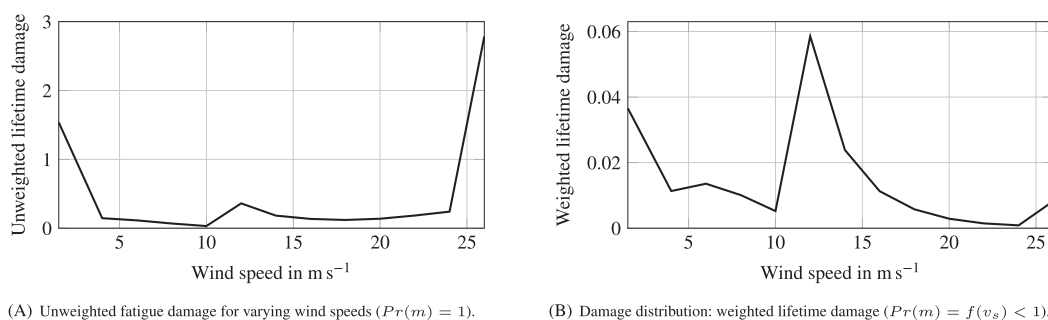


FIGURE 6 Mean fatigue damage for all wind speed bins based on 10 000 simulations per bin

speeds, the increase of aerodynamic loads—slightly visible in Figure 6A—is totally compensated by decreasing occurrence probabilities. Therefore, wind speeds above 18 m s^{-1} do not contribute significantly to the overall damage. Thus, it can be deduced that there is a significant, but non-linear relationship between wind speed and fatigue damages. In accordance with Figure 6B, high wind speeds are less relevant due to their low occurrence probabilities. Wind speeds around rated wind speed result in the highest fatigue damages. Low wind speeds—especially below cut-in—are still quite relevant. This specific distribution of damages is not generally valid but mainly accounts for the considered site and substructure. Still, maximum fatigue damages around rated wind speed are typical. Anyhow, the reduction concepts in the next section can be used independently of the precise shape of the damage distribution.

The sum of the weighted lifetime damages over all wind speed bins in Figure 6B is below one ($D \approx 0.2$). This can be explained by several facts. Firstly and most important, the design of the OC3 monopile was not conducted for this specific site. For example, the turbulence intensity at the FINO3 site⁹ is significantly lower than the recommended value in standards. Secondly, the absence of marine growth reduces fatigue, as hydrodynamic loads are decreased. Thirdly, for the damage calculation, no Goodman correction is applied. The usage of a Goodman correction would increase fatigue, as fatigue limits are reduced for cycles with nonzero mean values. And lastly, relatively long “run-in” times are used (cf Table 3). For too short “run-in” times, fatigue damages are overestimated, as not all initial transients are damped out and artificial damage is introduced.⁹

5 | REDUCTION STUDY

With the gained knowledge of the lifetime damage distribution, it is possible to conduct a preliminary assessment of several concepts to decrease the number of simulations using efficient sampling. At the same time, the simulation error should not be increased, which differs from other approaches that introduce additional errors by their approximations (meta models) of the fatigue damage.^{8,10,16} It has to be mentioned that further in-depth investigations of these concepts are still necessary and forthcoming, as here only one site and one substructure are investigated. Three different concepts are studied in addition to the equally distributed bin-based Monte Carlo simulation (EMCS):

1. Pure Monte Carlo simulation (PMCS): Samples are generated according to probability distributions (cf Table 2). No bins are applied.
2. Damage distribution-based Monte Carlo simulation (DMCS): The number of samples in each wind speed bin is in accordance with the damage distribution (cf Figure 6B). In each bin, MCS—based on (truncated versions of) the probability distributions in Table 2—is applied.
3. Reduced bin Monte Carlo simulation (RBMCS): Samples are equally distributed over the wind speed bins, but several bins with similar general behaviour are merged. Again, in each bin, MCS—based on (truncated versions of) the probability distributions in Table 2—is applied.

For all these concepts, only the first step in Section 2.3.1 (the binning) is changed. The realistic wind speed dependent sampling of the other environmental conditions remains unchanged. All concepts have their advantages and shortcomings that are evaluated in the following before applying them to the simulation results.

5.1 | Reduction concepts

5.1.1 | Pure Monte Carlo simulation

The idea of PMCS is that some wind speeds rarely occur. The question is: Why should we aim at a homogeneous sampling as strived by EMCS? Why should the same amount of simulations for these rarely happening load cases (wind speed bins) be conducted as for others? If it is sampled according to the probability distribution of the wind speed (PMCS), more results of frequently occurring load cases are available, which makes the approximation of these conditions more reliable. PMCS is also used by Häfele et al⁸ and is similar to the “probability sorting method” of Stewart,¹⁷ but does not rely on previously defined bins, and includes some random effects.

The great advantage of this approach is that the wind speed distribution is generally known, and as the EMCS, it convergences for a sufficient number of samples to the “true” value. On the downside, low occurrence probabilities do not mean low percental damages, eg, $v_s < 3 \text{ m s}^{-1}$. Therefore, PMCS reduces uncertainties for wind speeds around rated wind speed. However, it might lead to a really uncertain approximation of the not negligible damages produced by rarely occurring wind speeds.

5.1.2 | Damage distribution-based Monte Carlo simulation

DMCS aims at conducting many simulations for those load cases leading to high damages by applying the damage distribution (cf Figure 6B; $D(m)$) for the sampling (comparable to importance sampling). For example, if 20% of the damage is produced by one bin, 20% of all samples should be in this bin. Theoretically, DMCS leads to a far more accurate approximation, as more data are available where it has significant influence. However, the damage distribution is generally not known. Hence, in a first step, an approximated damage distribution (prior function) has to be determined by conducting, for example, $N_{\text{approx}} = 20$ simulations in all wind speed bins (ie, $20 \times 13 = 260$ EMCS cases). However, an approximation based on only 20 simulations per bin is not precise enough (5% error of about 100% depending on the wind speed). Therefore, Bayesian statistics is applied to update the initially approximated damage distribution after each new sample. The procedure is the following:

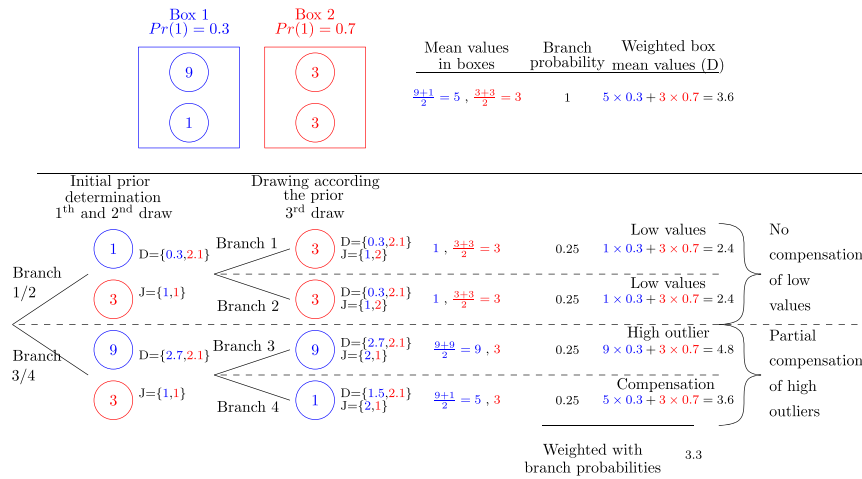


FIGURE 7 Tree diagram: example to illustrate damage distribution-based Monte Carlo simulation and its possible bias [Colour figure can be viewed at wileyonlinelibrary.com]

1. Conduct $N_{\text{approx}} \times M$ simulations (eg, 260 EMCS).
2. Calculate the prior function (ie, initial damage distribution; $D(m)$) being the weighted mean damage of $N_{\text{approx}} = 20$ cases in each bin.
3. The next sample ($j + 1$) is generated according to the damage distribution (ie, prior function). This means that it is sampled from the bin (m_{j+1}) where quotient of the number of samples and the number of samples required by the prior is minimal: $m_{j+1} = \arg \min \left(\frac{J(m) \sum_{m=1}^M D(m)}{D(m) \sum_{m=1}^M J(m)} \right)$.
4. Calculate the damage of the sample ($D_{TS,j+1,m_{j+1}}^{(k)}$) and update the damage distribution using Equations 3 and 4, as $D(m_{j+1})$ has changed.
5. Continue with steps 3 and 4 until the desired number of samples (eg, 1000) is generated.
6. Calculate the overall lifetime damage (D) using all generated samples.

For an illustration of the DMCS procedure, Figure 7—showing a simple example—can be used: There are 2 boxes (wind speed bins) with 2 coins each (2 possible simulation outcomes). The values of the coins (fatigue damages of the simulations ($D_{TS,j,m}^{(k)}$)) in the first box are 1 and 9 (9 represents an outlier, for example, due to wave resonance), and 3 and 3 in the second box. The occurrence probability of the boxes are $Pr(1) = 0.3$ and $Pr(2) = 0.7$. We are interested in weighted mean value (D). For infinite sampling (see upper part of Figure 7), the mean values of the 2 boxes will converge to $D(1) = 5$ and $D(2) = 3$, and therefore, the weighted mean value is $D = 3.6$. Now, not infinite sampling is applied, but only 3 samples are used, and these samples are generated according to the DMCS procedure (see lower part of Figure 7). Hence, in step 1, $N_{\text{approx}} \times M$ samples are needed. There are 2 boxes ($M = 2$), and we decide to use $N_{\text{approx}} = 1$. This means that one sample in each box is drawn (initial prior determination). For this simple example, there are only 2 possible outcomes for these 2 samples (branch 1/2 or branch 3/4). In step 2, the prior function is calculated. For probability branch 3/4, it is $D = \{9 \times 0.3, 3 \times 0.7\} = \{2.7, 2.1\}$. Step 3 requires that the next (3rd draw) sample is generated according to the damage distribution. Hence, $m_{j+1} = \arg \min \left(\frac{J(m) \sum_{m=1}^M D(m)}{D(m) \sum_{m=1}^M J(m)} \right) = \arg \min \left(\left\{ \frac{1 \times 4.8}{2.7 \times 2}, \frac{1 \times 4.8}{2.1 \times 2} \right\} \right) = \arg \min (\{0.84, 1.14\}) = 1$. This means that, for branch 3/4, the 3rd draw is taken from box 1. Possible outcomes of this 3rd draw are 9 and 1 (branches 3 and 4, respectively). Assuming that a 1 was drawn (branch 4), the damage distribution is now updated in step 4: $D = \{0.5 \times (9 + 1) \times 0.3, 3 \times 0.7\} = \{1.5, 2.1\}$. As we reached the desired number of samples, a repetition of steps 3 and 4 is not necessary. Still, a 4th draw (in branch 4) would be taken from box 2, as $m_{j+1} = \arg \min \left(\left\{ \frac{2 \times 3.6}{1.5 \times 3}, \frac{1 \times 3.6}{1.5 \times 3} \right\} \right) = \arg \min (\{1.6, 0.8\}) = 2$. In step 6, D is calculated. For branch 4, it follows: $D = 5 \times 0.3 + 3 \times 0.7 = 3.6$. The other branches and possible compensation effects of biased results are discussed in Section 5.2.2.

The advantage of applying Bayesian statistics to update the approximated damage distribution is that the initial approximation can be fairly rough. Therefore, step 1 is not very time-consuming. However, there are 2 drawbacks. Firstly, a significantly biased estimation of the damage distribution can lead to biased results (see Section 5.2.2). Secondly, the postprocessing of each simulation has to be conducted directly in order to update the damage distribution. This is problematic, if parallelized simulations are used.

5.1.3 | Reduced bin Monte Carlo simulation

RB MCS does not rely on an approximated damage distribution but reduces the number of bins, as also conducted by Stewart.¹⁷ However, while Stewart increases bin sizes equally, here, the idea is to merge bins with similar physical and generalized damage behaviour. Hence, for the investigated monopile, with its wave and wind dominated behaviour, the division in wind speed bins can follow more or less the controller actions (idling, no pitch, around rated, pitching, idling). An additional focus is on low wind speeds with more pronounced wave-resonance effects. Thence, the wind speed bins are the following: $<3 \text{ m s}^{-1}$, 3 to 7 m s^{-1} , 7 to 11 m s^{-1} , 11 to 13 m s^{-1} , 15 to 25 m s^{-1} , and $>25 \text{ m s}^{-1}$.

Therefore, RB MCS consists of fewer bins with more cases in each bin. As in each bin MCS is conducted, the RB MCS also converges to the “correct” value. Since there are more cases in bins with similar behaviour, the uncertainty in each bin can be reduced. Nevertheless, a challenge is the determination of the optimal combination of merged bins.

5.2 | Concept evaluations

To evaluate the different concepts, the lifetime fatigue damage (D) is calculated according to Section 2.3.3. For this calculation, $N_{\text{high}} = 10000$ or $N_{\text{low}} = 1000$ overall samples are generated using the different sampling concepts. Two different number of cases are chosen, as the number of simulations influences the performance of the concepts. To estimate the statistical variation in D , $N_{\text{BT}} = 10,000$ random combinations of the N_{high} or N_{low} simulated samples are selected with replacement (bootstrapping). Finally, the normalized lifetime damage distribution (\hat{D}) is computed. For this normalization, ideally the “real” lifetime damage should be used. As all concepts use MCS in each bin and the bins are weighted using their occurrence probability, for a sufficient number of samples, all concepts converge to the “real” value. Here, all $13 \times N_{\text{max}} = 130,000$ simulations of the EMCS concept are used as reference. For this number of samples, the convergence is sufficient with errors at the 5th and 95th percentile (determined using bootstrapping) of about 5%:

$$\hat{D} = \frac{D_{N,\text{concept}}}{D_{N_{\text{max}},\text{EMCS}}} \quad (6)$$

For the 3 concepts and the standard case (EMCS), Tables 4 and 5 present the mean value of \hat{D} , the coefficient of variation, and the errors of \hat{D} at the 95th and 99th percentile (cf Equation 5). The coefficient of variance is introduced, as for a reduced (biased) mean value, the 95th and 99th percentile are closer to the overall mean by definition. Hence, the errors at high percentile values have less informative value. For DMCS, the number of simulations used for the approximation of the damage distribution ($N_{\text{approx}} \times M$) is given as well.

5.2.1 | Evaluation PMCS

The results in Tables 4 and 5 show that PMCS does not have any advantages over the EMCS approach. In this study, for small sample sizes (Table 5), PMCS performs slightly better than EMCS, whereas for more simulations (Table 4), EMCS has lower uncertainties than PMCS. In both cases, the differences are negligible. The explanation for the lack of improvement is that PMCS reduces uncertainties for wind speeds around rated but increases errors for rarely occurring wind speeds. Both effects cancel each other out.

5.2.2 | Evaluation DMCS

On the one hand, DMCS reduces the 1% error by more than 50% compared with the EMCS concept (cf Table 4). The reduction is even more pronounced, if less cases are used (>80%). On the other hand, DMCS highly depends on the estimation of the damage distribution. Hence, on the downside, the reduction in uncertainty can come along with a biased mean value (see Tables 4 and 5). As discussed before, having a biased mean leads to less informative values of the errors at percentiles, but the coefficient of variation can still clarify that DMCS actually reduces the uncertainty. Although the uncertainty is reduced, the mean value is not accurately determined. To understand the reason for this bias, the short example, illustrated in Figure 7, is helpful. In Section 5.1.2, the general procedure of DMCS is discussed by exemplary using branch 4. To understand the possible bias of DMCS, all branches (possible outcomes of 3 draws) are discussed. For branch 3/4, the selected value of box 1 is a “high outlier,” as it

TABLE 4 Errors and uncertainties in fatigue damage using different concepts and $N_{\text{high}} = 10000$ simulations in total (recommended concept in bold)

	EMCS	PMCS	DMCS	RB MCS
Cases for approximation	-	-	20 × 13	-
Normalized mean	1.00	1.00	0.95	1.00
Coefficient of variation	0.110	0.111	0.071	0.086
Error at the 95th percentile in %	19.77	20.24	6.40	15.15
Error at the 99th percentile in %	30.41	32.25	12.90	22.18

Abbreviations: DMCS, damage distribution-based Monte Carlo simulation; EMCS, equally distributed MCS; PMCS, pure MCS; RB MCS, reduced bin MCS.

TABLE 5 Errors and uncertainties in fatigue damage using different concepts and $N_{\text{low}} = 1000$ simulations in total (recommended concept in bold)

	EMCS	PMCS	DMCS	RB MCS
Cases for approximation	-	-	20 × 13	-
Normalized mean	1.00	1.00	0.80	1.00
Coefficient of variation	0.350	0.346	0.194	0.271
Error at the 95th percentile in %	61.30	60.51	7.71	51.70
Error at the 99th percentile in %	131.25	129.99	25.33	89.30

Abbreviations: DMCS, damage distribution-based Monte Carlo simulation; EMCS, equally distributed MCS; PMCS, pure MCS; RB MCS, reduced bin MCS.

significantly exceeds the mean value of this box ($9 > 5$). Due to this overestimation of the outcomes of box 1, further sampling is concentrated on this box, ie, the 3rd draw is taken from it. If another “high outlier” is drawn (branch 3), the weighted mean value remains biased ($D_{\text{branch } 3} = 4.8$). However, if the 3rd draw is a low value (branch 4), the outlier is compensated and the bias is reduced or even removed ($D_{\text{branch } 4} = 3.6$). More problematic are “low outliers” for the initial prior determination (branch 1/2). Here, due to the low value, further sampling is concentrated on other boxes (wind speed bins) and a compensation is nearly not possible ($D_{\text{branch } 1} = D_{\text{branch } 2} = 2.4$). Combining all possible outcomes (branches), the weighted mean value is biased ($D_{\text{DMCS}} = 3.3 < 3.6 = D_{\text{real}}$).

Having this simple example in mind, the bias in DMCS becomes clear. For high numbers of overall simulations, the compensation works better and the bias is less significant and diminishes for an infinite number of cases. Therefore, the concept still performs well. However, for fewer overall cases, it is not suitable, as the approximation becomes significantly biased. It should be noted that the more pronounced the outliers are, as it is the case for the monopile, the more the bias increases. It can be assumed that for substructures with less pronounced outliers (eg, wind dominated jackets), DMCS is less biased.

5.2.3 | Evaluation RBMCS

RBMCS does not need an a priori approximation of the damage distribution. Therefore, its performance is relatively independent of the number of overall simulations and it is unbiased. For small numbers of cases, it is recommended to use RBMCS, although the errors are significantly higher than for DMCS (see Table 5). However, due to the significant bias of DMCS in this case, RBMCS is the best alternative. One challenge is the determination of the best combination of merged bins that is partly based on experience. An interesting observation is that RBMCS outperforms PMCS, whereas Stewart¹⁷ concluded that his “probability sorting method” (roughly comparable with PMCS) performs better than his bin reduction, which has certain similarities with RBMCS. One reason for this difference is the fact that the current RBMCS does not increase bin sizes purely systematically, but based on physical damage behaviour.

5.2.4 | Summary concept evaluations

After all, it has to be pointed out that a reduction of the errors in fatigue damage of more than 30% compared to EMCS and PMCS is possible without any extra work by applying efficient sampling. According to this study, DMCS is the best choice, if many simulations are conducted. For fewer simulations, the approximation of the damage distributions gets significantly biased, which finally results in biased lifetime damages. Therefore, in this case, RBMCS being the most stable one is recommended. Still, the error reduction of RBMCS is less pronounced, and it needs expert knowledge of the user to define the merged bins.

For both concepts, optimizations concerning the bin selection (RBMCS) or the number of simulations for the prior function (DMCS) are possible. For this study, for both parameters, several values were tested, and the current settings reduce the fatigue damage errors significantly. However, using optimized settings, both concepts might be even more beneficial.

6 | BENEFITS AND LIMITATIONS

At least for steel parts of offshore wind turbines, the fatigue damage lifetime is of major importance. Therefore, this study focuses on an efficient and accurate way to determine fatigue lifetimes for realistic, scattering environmental conditions. Exemplary, a monopile substructure was investigated. Different types of substructures or varying designs were not taken into account being the major limitation of this work, as a general validity of the proposed methodology was not tested so far. Furthermore, as discussed before, a quite low structural damping is assumed. This leads to increased fatigue damages in idling conditions, where aerodynamic damping is missing. Although different designs and damping values might change the damage distribution and turbine behaviour, the authors expect the reduction methods still being valid due to their application independent approaches.

To overcome the state-of-the-art simplification of constant environmental conditions and to simulate more realistic ones, statistical distributions for 7 scattering environmental conditions, derived from real data, were applied. Only other, less significant conditions were set constant. Taking into account these scattering environmental states, an assessment of the distribution of fatigue damage over all wind speeds including the resulting uncertainty due to finite sampling was carried out. Other types of uncertainty like the error in Miner's rule are not taken into account, although both types can have the same order of magnitude of about 50% error at the 95th percentile.³³ It was shown that the use of scattering environmental conditions is essential. The uncertainty in fatigue damages is much higher than predicted by deterministic approaches.¹⁰ Therefore, the use of deterministic damage calculations and state-of-the-art safety factors might be nonconservative, as safety factors are not calibrated for these high uncertainties. Only some wind speeds contribute significantly to the overall lifetime damage. This fact enables a reduction of the needed simulations. It has to be pointed out that this study is limited to operating and idling conditions. Start-up or maintenance cases are excluded, for example, as it is discussed by Jonkman and Buhl.³⁴ Still, so far even idling conditions are rarely taken into account in academia.^{10,14}

Based on the damage distribution, several concepts of reducing the amount of simulations and maintaining the same uncertainty were developed. It was proved that it is possible to reduce the error by more than 30% without adding an additional approximation error (being the case for meta model-based approaches) or to decrease the number of simulations by more than 30% and keeping the error constant. A more detailed analysis of the

influence of concept parameters, eg, the number of simulations used for the approximation of the prior function, is still forthcoming. Furthermore, the great potential of the application of Bayesian statistics to reduce the uncertainty was shown (cf Tables 4 and 5). However, Bayesian updated damage distributions can lead to significantly biased results, and their use is restricted, if parallel computing is utilized. Therefore, an intensive study of Bayesian updating could be valuable. For example, an update of the damage distribution after several samples—so far, it is updated after each new sample—is a possibility. A consideration of not only the mean damage but also the variance of the damage in each wind speed bin could be another starting point. Moreover, the general validity for different substructures should be checked, as up to now, the results are exemplary and general conclusions concerning the number of simulations needed to capture fatigue damage are only restrictedly possible.

7 | CONCLUSION

The main objective of this study is to answer the following 2 questions concerning the fatigue damage calculation stated in the introduction: How high is the uncertainty of fatigue damages due to finite sampling for monopiles, if realistic, scattering environmental conditions in all wind speed bins are assumed? To what extent is it possible to reduce the number of time domain simulations without adding additional simulation errors? For the first one, it was shown that realistic environmental conditions cannot be ignored, as calculation errors of fatigue damages are much higher than expected. Concerning the second one, this work demonstrates that, although a case reduction is not straightforward, the error in fatigue lifetime calculation occurring with a probability of 1% can be reduced by more than 30% when efficient sampling techniques are applied.

Further work should especially address the general validity of this work by investigating the effect of other substructures, designs, and realistic conditions of other offshore sites. Moreover, the combination of the presented reduction concepts with meta models or other simplification techniques (eg, aligned wind and wave direction) is a valuable starting point for a further reduction of the fatigue damage computing time. Lastly, an interesting concept is the use of correlations with environmental conditions. The example of the wave peak period shows that specific environmental conditions lead to high fatigue damages. If unfavourable conditions can be identified, a weighting in the sampling using stochastic importance sampling could be beneficial. Lastly, this work only addresses fatigue damages due to idling and operating conditions. Since start-ups can lead to a significant amount of damage, a probabilistic analysis and an uncertainty assessment of starting and stopping turbines could be valuable.

ACKNOWLEDGEMENTS

We gratefully acknowledge the financial support of the Lower Saxony Ministry of Science and Culture (research project VENTUS EFFICIENS, FKZ ZN3024) and the European Commission (research project IRPWIND, funded from the European Union's Seventh Framework Programme for research, technological development, and demonstration under grant agreement number 609795) that enabled this work. This work was supported by the compute cluster which is funded by Leibniz Universität Hannover, the Lower Saxony Ministry of Science and Culture (MWK), and the German Research Foundation (DFG).

ORCID

Clemens Hübler  <http://orcid.org/0000-0001-7191-4369>

REFERENCES

1. Energy Information Administration. *Levelized Cost and Levelized Avoided Cost of New Generation Resources in the Annual Energy Outlook 2017*. Washington, DC: U.S. Energy Information Administration (IEA); 2017.
2. Prognos AG, Fichtner. *Kostensenkungspotenziale der Offshore-Windenergie in Deutschland*. Stiftung Offshore-Windenergie; 2013.
3. Moriarty PJ, Holley WE, Butterfield C. P. *Extrapolation of extreme and fatigue loads using probabilistic methods*. National Renewable Energy Laboratory; 2004.
4. International Electrotechnical Commission. *Wind turbines - part 3: Design requirements for offshore wind turbines*. International standard IEC 61400-3; 2009.
5. Fischer T, de Vries W, Schmidt B. *Upwind design basis*; 2010.
6. Stewart GM, Robertson A, Jonkman J, Lackner M. A. The creation of a comprehensive metocean data set for offshore wind turbine simulations. *Wind Energy*. 2015;19:1151-1159.
7. Hansen M, Schmidt B, Ernst B, et al. *Probabilistic safety assessment of offshore wind turbines*. Technische Informationsbibliothek u. Universitätsbibliothek: Hannover. 2015.
8. Häfele J, Hübler C, Gebhardt CG, Rolfes R. A comprehensive fatigue load set reduction study for offshore wind turbines with jacket substructures. *Renew Energy*. 2018;118:99-112.
9. Hübler C, Gebhardt CG, Rolfes R. Development of a comprehensive database of scattering environmental conditions and simulation constraints for offshore wind turbines. *Wind Energy Sci*. 2017;2:491-505.
10. Zwick D, Muskulus M. The simulation error caused by input loading variability in offshore wind turbine structural analysis. *Wind Energy*. 2015;18:1421-1432.
11. Muskulus M, Zwick D. Reliability-based design of wind turbine support structures. Symposium on Reliability of Engineering System, SRES2015.
12. Bilonis DV, Vamvatsikos D. Fatigue analysis of an offshore wind turbine in Mediterranean Sea under a probabilistic framework. 6th MARINE International Conference on Computational Methods in Marine Engineering, MARINE2015.

13. Müller K, Cheng PW. Validation of uncertainty in IEC damage calculations based on measurements from alpha ventus. *Energy Procedia*. 2016;94:133-145.
14. Zwick D, Muskulus M. Simplified fatigue load assessment in offshore wind turbine structural analysis. *Wind Energy*. 2016;19:265-278.
15. Müller K, Reiber M, Cheng PW. Comparison of measured and simulated structural loads of an offshore wind turbine at alpha ventus. *Int J Offshore Polar Eng*. 2016;26:209-218.
16. Toft HS, Svenningsen L, Moser W, Sørensen JD, Thøgersen ML. Assessment of wind turbine structural integrity using response surface methodology. *Eng Struct*. 2016;106:471-483.
17. Stewart GM. Design load analysis of two floating offshore wind turbine concepts. *PhD-thesis*: University of Massachusetts; 2016.
18. Hübler C, Gebhardt CG, Rolfes R. Hierarchical four-step global sensitivity analysis of offshore wind turbines based on aeroelastic time-domain simulations. *Renew. Energy*. 2017;111:878-891.
19. Jonkman BJ. *TurbSim User's Guide: Version 1.50*. Golden, Colo.: National Renewable Energy Laboratory; 2009.
20. Jonkman JM, Musial W. *Offshore Code Comparison Collaboration (OC3) for IEA Task 23 Offshore Wind Technology and Deployment*. Golden, CO: National Renewable Energy Laboratory; 2010.
21. Jonkman J. The new modularization framework for the FAST wind turbine CAE tool. In: 51st AIAA Aerospace Sciences Meeting including the New Horizons Forum and Aerospace Exposition; 2013; Dallas, Texas. 25-26.
22. Häfele J, Hübler C, Gebhardt CG, Rolfes R. An improved two-step soil-structure interaction modeling method for dynamical analyses of offshore wind turbines. *Appl Ocean Res*. 2016;55:141-150.
23. American Petroleum Institute. Recommended practice for planning, designing and constructing fixed offshore platforms—working stress design—Errata and supplement 3. API Recommended practice 2A-WSD; 2007.
24. Thieken K, Achmus M, Lemke K. A new static py approach for piles with arbitrary dimensions in sand. *Geotechnik*. 2015;38:267-288.
25. Achmus M, Müller M. Evaluation of pile capacity approaches with respect to piles for wind energy foundations in the North Sea. In: 2nd International Symposium on Frontiers in Offshore Geotechnics; 2010; Perth. 8-10.
26. Hübler C, Häfele J, Gebhardt CG, Rolfes R. Experimentally supported considerations of operating point dependent soil properties in coupled dynamics of offshore wind turbines. *Mar Struct*. 2018;57:18-37.
27. Jonkman J, Butterfield S, Musial W, Scott G. *Definition of a 5-MW Reference Wind Turbine for Offshore System Development*. Golden, CO: National Renewable Energy Laboratory; 2009.
28. European Committee for Standardization. Eurocode 3: Design of steel structures Part 1-9: Fatigue. EN 1993-1-9; 2010.
29. Efron B. Bootstrap methods: another look at the jackknife. *Ann Stat*. 1979;7:1-26.
30. Van Der Tempel J. Design of support structures for offshore wind turbines. *PhD-thesis*: TU Delft; 2006.
31. Weijtjens W, Noppe N, Verbelen T, Helsen J, de Sitter G, Devriendt C. Monitoring of offshore turbines for design and O&M: an overview of the activities of OWI-Lab. In: Analysis of Operating Wind Farms 2014 - EWEA Technology Workshop; 2014; Malmö - Sweden. 1-32.
32. Aasen S, Page AM, Skau KS, Nygaard TA. Effect of foundation modelling on the fatigue lifetime of a monopile-based offshore wind turbine. *Wind Energy Sci*. 2017;2:361-376.
33. Sørensen JD. Reliability analysis of wind turbines exposed to dynamic loads. In: 9th International Conference on Structural Dynamics EURO-DYN 2014; 2014; Portugal. 39-46.
34. Jonkman JM, Buhl ML Jr. Loads analysis of a floating offshore wind turbine using fully coupled simulation. In: Wind Power Conference and Exhibition; 2007; Los Angeles, California. 1-32.

How to cite this article: Hübler C, Gebhardt CG, Rolfes R. Methodologies for fatigue assessment of offshore wind turbines considering scattering environmental conditions and the uncertainty due to finite sampling. *Wind Energy*. 2018;21:1092-1105. <https://doi.org/10.1002/we.2216>

5.2 Validation of improved sampling concepts for offshore wind turbine fatigue design

5.2.1 Research context

In the previous section, it was shown that the long-term extrapolation of fatigue damages of OWT substructures is a fairly uncertain process due to finite sampling. There are various concepts that try to enable accurate approximations of lifetime damages in combination with moderate computing times, but all of them have their shortcomings. Therefore, two new concepts were introduced. Both perform well for the presented setting. However, a general validity of the concepts for different substructures, simulation codes, wind turbine sites, sample sizes, etc. has not been proved yet. Furthermore, all recent research approaches focus on numerical data. This is not surprising, as measurement data is typically not available during the design phase. Nevertheless, numerical data can include purely numerical anomalies. Moreover, not all sources of uncertainty that are present in reality are covered by state-of-the-art simulations (e.g. breaking waves). In addition, for measurement data, normally, extensive data sets of up to several years are available and enable analyses of the convergence of the approaches for large sample sizes. That is why the use of measurement data - being treated like “realistic simulation data” - is a promising approach to prove the general applicability of the two concepts.

5.2.2 Methods

To investigate the validity of the two previously developed sampling concepts for long-term extrapolation, first, a test function that mimics real fatigue behaviour is investigated. Second, real offshore measurement data is used. The measurement data is treated like “realistic simulation data”. This has the advantage that numerical effects are excluded and an extensive validation data set of more than 120 000 samples for two structures is available. Strain gauge data at the transition piece of two OWTs sampled for several years and provided by the Belgian partners is utilised here.

Strain gauge data is post-processed to calculate short-term damages for all 10-minute measurement intervals (cf. Fig. 1-10). Then, the uncertainty due to finite sampling and reasons for it are analysed. Subsequent, the convergence of several standard and both advanced sampling algorithms - RBMCS and DMCS - for increasing sample sizes is investigated. Since a test function, measurement and simulation data are used and turbines, substructures, and site conditions are different, it is possible to draw general conclusions, i.e. to validate the sampling concepts.

5.2.3 Results

Using a test function and strain measurements of offshore wind turbines and treating them as “realistic simulation data”, it is possible to validate the previously developed fatigue uncertainty reducing sampling techniques. The performance of both concepts is relatively independent of the system (turbine, substructure, site, etc.) and of simulation code specifications. While RBMCS is also independent of the sample size (academic and industry approaches), the performance of DMCS is influenced by the number of samples. The more samples are used, the more pronounced is the benefit of DMCS. This is especially relevant for industry applications with classically large sample sizes.

RBMCS reduces 1% errors¹² by about 10-20% compared to MCS and DMCS achieves reductions of up to 50% compared to MCS. A reduction of the 1% error by 25% is synonymous with halving the required samples while keeping the uncertainty constant.

Regarding uncertainty due to finite sampling in general, it is shown that it is high (in the same order of magnitude as other important types of uncertainty like the model uncertainty of Miner's rule), that it depends significantly on the substructure and turbine, and that it is considerably influenced by controller actions. Hence, although quantitative conclusions concerning the uncertainty are difficult, commonly applied approaches in academia should perhaps be reconsidered.

5.2.4 Outlook

In this section, measurement data being treated as “realistic simulation data” is used to determine long-term damages. Nevertheless, extrapolation methods are still intended to be used for simulation data, since it is assumed that the designer can decide how many samples are needed in each bin. If long-term extrapolations are to be based on measurements only, different extrapolation techniques have to be used. For measurement data, limited data is normally not problematic (thousands of 10-minute measurements in one year), but representative data is challenging (e.g. rare occurrence of storm events). Such a measurement-based lifetime estimation can be a valuable addition to simulations, as, for example, proposed by the current lifetime extension standard [39]. Therefore, long-term extrapolation techniques for measurement-based lifetime estimations are an important field of future research. First approaches can be found in Hübler et al. [78] or Loraux and Brühwiler [108].

5.2.5 Paper E: Validation of improved sampling concepts for offshore wind turbine fatigue design

The following paper is published in *Energies* (<https://doi.org/10.3390/en12040603>), Volume 12 (2019), article number 603. The main work was done by the author of this thesis. All other authors contributed with advisory and supporting work. Special thanks go to the partners from OWI-lab (Offshore Wind Infrastructure Application Lab), Vrije Universiteit Brussel for providing the raw data.

¹²The 1% error is a measure of the uncertainty and is defined as the deviation of the lifetime at the 1st percentile to the “real”, reference lifetime. Here, the reference lifetime is calculated using the full measured data set of three years. For more information, it is referred to Section 5.2.5.



Article

Validation of Improved Sampling Concepts for Offshore Wind Turbine Fatigue Design

Clemens Hübler ^{1,*} , Wout Weijtjens ² , Cristian G. Gebhardt ¹, Raimund Rolfes ¹ 
and Christof Devriendt ²

¹ Institute of Structural Analysis, Leibniz Universität Hannover, ForWind, Appelstr. 9a, D-30167 Hannover, Germany; c.gebhardt@isd.uni-hannover.de (C.G.G.); r.rolfes@isd.uni-hannover.de (R.R.)

² OWI-lab, Vrije Universiteit Brussel, Pleinlaan 2, 1050 Brussel, Belgium; wout.weijtjens@avrg.be (W.W.); Christof.Devriendt@vub.ac.be (C.D.)

* Correspondence: c.huebler@isd.uni-hannover.de

Received: 21 January 2019; Accepted: 11 February 2019; Published: 14 February 2019



Abstract: Fatigue damage is a design-driving phenomenon for substructures of offshore wind turbines. However, fatigue design based on numerical simulations is quite uncertain. One main reason for this uncertainty is scattering offshore conditions combined with a limited number of simulations (samples). According to current standards, environmental conditions are sampled using a deterministic grid of the most important environmental conditions (e.g., wind speed and direction, significant wave height, and wave period). Recently, there has been some effort to reduce the inherent uncertainty of damage calculations due to limited data by applying other sampling concepts. Still, the investigation of this uncertainty and of methods to reduce it is a subject of ongoing research. In this work, two improved sampling concepts—previously proposed by the authors and reducing the uncertainty due to limited sampling—are validated. The use of strain measurement data enables a realistic estimate of the inherent uncertainty due to limited samples, as numerical effects, etc., are excluded. Furthermore, an extensive data set of three years of data of two turbines of the Belgian wind farm Northwind is available. It is demonstrated that two previously developed sampling methods are generally valid. For a broad range of model types (i.e., input dimensions as well as degrees of non-linearity), they outperform standard sampling concepts such as deterministic grid sampling or Monte Carlo sampling. Hence, they can reduce the uncertainty while keeping the sampling effort constant, or vice versa.

Keywords: offshore wind energy; fatigue; uncertainty; monitoring; strain measurements; sampling concepts

1. Introduction

The share of offshore wind energy in overall energy production is growing rapidly. Even though the first subsidy-free offshore wind auction bids have been made recently, costs are still relatively high compared to other renewable energies such as onshore wind energy [1]. On the one hand, the waiver of subsidies is provoked by the expected increase in electricity prices. On the other hand, it is forecast that the levelized cost of energy (LCOE) will decrease [2]. Hence, to enable subsidy-free offshore wind energy, optimizations of the whole structure are needed. Here, the improvement of the substructure—in most cases monopile substructures/foundations—is an important possibility to reduce costs.

For substructures made of steel, in most cases, the fatigue lifetime is decisive for the design. To calculate fatigue damages of substructures in the design phase, numerous time-domain simulations are needed. Commonly, these simulations are conducted with state-of-the-art aero-hydro-servo-elastic

codes such as FAST [3] or HAWC2 [4]. Current standards [5] define that these simulations should mirror changing environmental conditions (EC) at the precise site of a wind turbine. Commonly, this is achieved by sampling EC using a deterministic grid. In academia, mostly, one-dimensional grids (only wind speed) are applied, leading to a “quasi-deterministic” fatigue damage calculation, which is roughly done as follows [6–8]: The range of wind speeds in power production (e.g., 3 m s^{-1} to 25 m s^{-1}) is split up into steps (so-called bins) of 2 m s^{-1} or less. All other EC are set to constant values within these wind speed bins. Turbulent wind and irregular waves are considered in a stochastic process in each bin by conducting simulations of an overall length of one hour (normally divided into six 10 min simulations) per bin, as it is proposed by standards [5]. In industry and some academic studies [9–11], the same approach but with finer binning and bins for more EC (e.g., wind direction, wave height and period) is used to increase the accuracy and to reduce the uncertainty at the cost of higher computing times [9].

For the simplified one-dimensional academic approach, it was shown by Müller and Cheng [12] that it cannot reproduce the scattering observed in offshore fatigue measurements. Moreover, it leads to highly uncertain approximations of the lifetime damage due to a very limited number of samples [6]. In the present contribution, we only investigate the uncertainty introduced by so-called finite sampling (i.e., limited cases/samples) and the selection of these samples during the design phase. Other sources of uncertainty, for example the error in Miner’s rule or the uncertainty of stress concentration factors, are not the topic of this investigation. The multi-dimensional grid-based approach—used in industry—leads to more accurate approximations of the long-term fatigue damage. However, it was repeatedly shown that it is numerically inefficient [10,11]. Therefore, either meta models [9,13,14], replacing time-domain simulations and reducing the computing time of each model evaluation significantly, are applied or alternative sampling concepts, improving the computational efficiency by reducing the number of model evaluations while conserving the same level of uncertainty, are needed. In this work, the latter approach is investigated.

Two different types of improved sampling concepts can be differentiated. First, there are those approaches that still consider a deterministic grid, but only use the most important grid points. Stiang and Muskulus [15,16] determine the most important grid points in a computationally expansive preliminary study using a full grid. Velarde and Bachynski [17] estimate the relevant grid points by applying a simple sea state-damage correlation. While Stewart [9] assumes in his “probability sorting method” that “important” is equivalent to “probable”.

The second type of improved sampling concepts are probabilistic approaches taking scattering EC into account, which makes simulations more realistic and deals with the deviations to measurement results [12]. The most frequently applied probabilistic sampling concept is Monte Carlo sampling (MCS). In the context of fatigue design of offshore wind turbine substructures, MCS has recently been investigated by various authors [10,11,16,18,19]. On the one hand, probabilistic approaches can reproduce measurement results more precisely [20] and MCS is more suitable for high-dimensional input spaces [10,11]. On the other hand, fatigue damage approximations using probabilistic approaches and limited samples are quite uncertain [18,19] and MCS becomes inefficient (i.e., converges slowly) for highly non-linear model functions [10]. Therefore, to limit computing times while uncertainties are kept on an adequate level, improved sampling techniques are needed. For example, Hübler et al. [18] and Stiang and Muskulus [16] concentrate their sampling on the input subspace leading to high damages or Müller and Cheng [21] apply quasi-random sampling based on Sobol’ sequences.

One shortcoming of all previously mentioned studies is the fact that they are all based on pure simulation results. Although the use of simulated data for design purposes is not surprising, since measurement data is not available at this stage, still, the general validity of these numerical findings is not warranted. Are these sampling methods valid independent of the considered system (i.e., turbine, substructure, site, etc.), used simulation code, dimension of the input space, etc.? This is the reason the objective of this study is to validate two sampling concepts that were previously developed by Hübler et al. [18]. In this context, “validation” does not mean that their benefit is proven mathematically,

but their performance is assessed using a broad range of wind turbine specific applications. For this purpose, first, a generic test function is applied, and second, real offshore strain measurements are used. The measurements are treated like simulation results for fatigue design. This may seem slightly odd in the first place, since in the design phase, measurements are not available. Nevertheless, this has two major advantages. First, although measurement data is not perfect due to measurement errors, purely numerical effects and simulation/model errors are excluded by using “realistic simulation data” (i.e., measurement data). Second, using measurement data, an extensive number of samples (144 samples per day and several years of measurements) for different turbines is available. This enables an assessment of these concepts not only for small sample sizes—as it is common in academia—but also for large data sets—as done in industry approaches, so that the convergence of the approaches can be analyzed. Convergence studies through simulations would hardly be feasible in an academic context. After all, this enables an assessment of the general validity of numerical approaches for different systems, sample sizes, and independent of simulation code specifics.

After a general introduction to damage calculation and extrapolation (Section 2) and a brief presentation of different sampling concepts (Section 3), a test example is analyzed (Section 4). This test example mimics the real fatigue behavior and helps to get a first insight in the performance of the various sampling concepts for changing input space dimensions and degrees of non-linearity. Subsequently, real offshore measurement data of the Belgian wind farm Northwind is taken as “realistic simulation data” (Section 5). Damage calculations using this data are conducted and the uncertainty of this calculation is analyzed. For this purpose, bootstrapping in combination with different numbers of samples and various sampling concepts is used for the damage extrapolation. Therefore, it is possible to assess the general validity of reduction concepts, proposed in literature.

2. Damage Calculation

The fatigue damage calculation procedure for offshore wind turbine substructures is a two-stage process. First, the short-term damage of a single short (normally 10 min) measurement or simulation is determined. Second, the long-term or lifetime damage is calculated by extrapolating short-term damages of several samples (i.e., measurements or simulations) to the entire lifetime. Here, the choice of the samples, and therefore the sampling concept, is essential. Improved sampling concepts are the focus of this work and are discussed in the following sections. In this section, the general procedure of calculating and extrapolating fatigue damages—being applied in this work and being mostly independent of the sampling concept—is presented. Some shortcomings and alternatives are briefly discussed. While the short-term fatigue damage calculation procedure is relatively standardized, there is no consensus on how to extrapolate short-term values to long-term lifetime damages.

2.1. Short-Term Damage

An overview of the standard short-term damage calculation procedure is given in Figure 1.

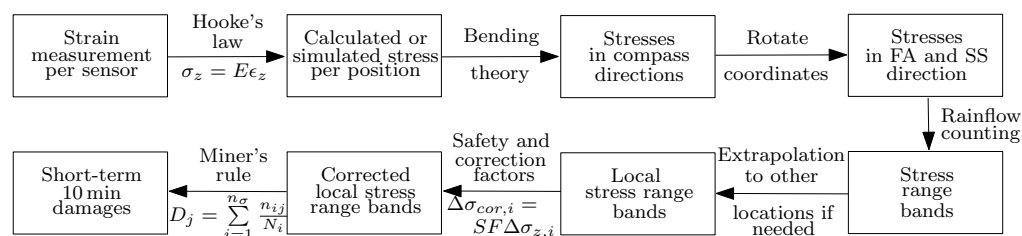


Figure 1. Flowchart presenting the short-term damage calculation procedure based on strain measurements or stress simulation (FA: fore-aft, SS: side-to-side). Explicitly stated methods such as Hooke’s law are common examples but could also be replaced by more accurate methods.

If the damage calculation is based on strain measurements, as in this work (c.f. Section 5.1), the measured axial strain signals (ϵ_z) are used to calculate tensile stresses (σ_z) according to Hooke's law:

$$\sigma_z = E\epsilon_z. \quad (1)$$

Here, E is the Young's modulus of steel, and for measurement positions above mean sea level, it is assumed that longitudinal and radial stresses are negligible, as hydrostatic loads do not act. In case of simulation data, normally, stresses are directly available, so that this first step is not necessary. With three sensors around the circumference of the monopile (substructure), the tensile stresses of all sensors can be used to calculate the bending moments in two perpendicular directions (M_{north} and M_{west}) and the normal force (F_N) using the following equation:

$$\sigma_z(\theta_{i_s}) = \frac{M_{north}}{S} \cos(\theta_{i_s}) - \frac{M_{west}}{S} \sin(\theta_{i_s}) + \frac{F_N}{A} \quad \forall \quad i_s = \{1, 2, 3\}, \quad (2)$$

with θ_{i_s} being the angle of the i_s th sensor to the northern direction and A and S being the cross-section area and section modulus, respectively. For a cylindrical monopile, the section modulus is defined as follows:

$$S = \frac{\pi (r_{out}^4 - r_{in}^4)}{4r_{out}}, \quad (3)$$

where r_{out} and r_{in} are the outer and inner radius of the monopile, respectively.

Subsequently, the stresses parallel (fore-aft (FA)) and perpendicular (side-to-side (SS)) to the wind direction can be computed by rotating the moments (M_{north}) and (M_{west}) by an angle ϕ to the wind direction.

Knowing FA and SS stresses, a rainflow cycle counting of stress ranges ($\Delta\sigma_{z,i}$) is performed for both directions. Here, $\Delta\sigma_{z,i}$ is the stress range of the i th band (also called block or bin) in the factored stress spectrum (cf. Annex A of Eurocode 3 [22]). The number of required stress bands (n_σ) was determined in a preliminary convergence study. Fulfilling the requirements by current standards [23,24], $n_\sigma = 500$ bands—logarithmically spaced between 10 kPa and 1 GPa—are used. A conservative approach of using the higher cycle count of the FA and SS direction, i.e., this is equivalent to a single dominant wind direction, is applied. More sophisticated approaches, taking the wind direction into account, can reduce conservatism, but should not influence the performance of the sampling concepts, and therefore, are not investigated in this work.

Subsequently, an extrapolation of the loads to other positions (i.e., heights) can be performed for all stress bands. Extrapolations are needed, if measurements at critical positions are not possible or have not been done. In this case, for example, the so-called "virtual sensing concept" of Maes et al. [25] that is based on a modal approach can be applied. In this work, we do not apply any load extrapolation, but evaluate the fatigue damage at the precise measurement position. This position might not be the design-driving location (e.g., the most critical weld). However, for the present analysis, this is not essential, since we do not analyze the design itself.

For nominal stresses at the position of interest (here: the measurement position), an overall safety factor (SF) consisting of several sub-factors is applied to get a representative value for the concentrated stresses at the specific detail. First, a stress concentration factor for the present detail is used (here: $SCF = 1.0$ according to a recommended practice of Det Norske Veritas [23]). Second, a correction for high wall thicknesses—the so-called size effect (SE) correction—is applied [23]. Third, a material safety factor (here: $MSF = 1.25$ due to limited accessibility, and therefore, no inspections [26]) is used. In this work, these three factors are taken from the original industry design of the monopiles. Additionally, when measuring with welded—instead of glued—fiber Bragg gratings (FBG), a correction of the reduced sensitivity of welded FBG ($FSF = 0.9$) [27] is needed. In addition, last, an additional safety factor (ASF) covering unexpected behavior, etc., and being easily adjustable is introduced. All these factors can be regarded as uncertain themselves. However, since—as stated in

the introduction—only the uncertainty due to limited sampling is topic of the investigation, this is not relevant here. The corrected stress ranges—for the stress concentration at the present detail—can be calculated using:

$$\Delta\sigma_{cor,i} = \Delta\sigma_{z,i} \times SF = \Delta\sigma_{z,i} \times SCF \times SE \times FSF \times MSF \times ASF. \quad (4)$$

The last step to calculate the damage of each sample (10 min measurement) is the application of a linear damage accumulation according to the Palmgren-Miner rule, and the application of S-N curves according to the standards [23] and the state of the art [6,9,12]. Here, DNV S-N curve D in air is applied. The fatigue damage for each measurement time series (D_j) according to the Palmgren-Miner rule can be calculated as follows:

$$D_j = \sum_{i=1}^{n_\sigma} \frac{n_{ij}}{N_i}, \quad (5)$$

where i and j are indices for the stress band and the time series, respectively, and n_{ij} is the number of cycles associated with the stress range $\Delta\sigma_{cor,ij}$. The endurance (N_i ; number of maximum cycles) for the same stress range is obtained from the corresponding S-N curve.

2.2. Long-Term Damage

Having calculated the short-term damages, one of the most uncertain and most unreliable aspects of the lifetime damage calculation, which has not been sufficiently investigated so far, follows next: the extrapolation to the long-term. Here, only one method of extrapolating damages D_j to a lifetime damage D_{LT} in combination with different sampling concepts presented in the next section is applied. Alternative extrapolations are mentioned, but for details, it is referred to, for example, Hübler et al. [28], who investigate the effect of alternative approaches on extrapolated lifetimes for service life extensions. To extrapolate fatigue damages, all damages (D_j) are sorted into several (M) bins of EC. Depending on the sampling concept, the dimension of the binning (d_g) can differ. For example, for pure MCS, no bins are applied ($d_g = 0$), while for a deterministic grid approach, one (wind speed; $d_g = 1$) or more (wind direction, significant wave height, and wave period; $d_g = 4$) dimensions of the binning are possible. For each of these bins, the mean value of all $J(m)$ corresponding damage values is calculated. Alternatively, the 90th percentile can be used for a more conservative estimate (c.f. Hübler et al. [28]). Each bin has a certain occurrence probability ($Pr(m)$) that is either given in design documents (as it is for this work) or must be determined by using environmental measurement data (e.g., SCADA wind data of several years). The mean damage of each bin is now weighted with the corresponding occurrence probability. Finally, to get the lifetime damage (D_{LT}), the weighted mean damages of all $M_t = \prod_{i_d=1}^{d_g} M_{i_d}$ bins must be summed up and multiplied by a time factor. From this, it follows:

$$D_{LT} = \frac{20 \text{ years}}{10 \text{ min}} \sum_{m=1}^{M_t} \left(Pr(m) \frac{1}{J(m)} \sum_{j=1}^{J(m)} D_j(m) \right). \quad (6)$$

Finally, the overall lifetime L in years is the inverse of the lifetime damage multiplied by the design lifetime of 20 years:

$$L = \frac{20 \text{ years}}{D_{LT}}. \quad (7)$$

2.3. Damage Uncertainty

It has been shown how fatigue damages can be calculated (c.f. Section 2.1) and extrapolated (c.f. Section 2.2) using a specific number of samples (i.e., damage values D_j). As offshore conditions are scattering, some uncertainty of the extrapolated design lifetimes that depends on the number of used samples is introduced. In literature, the number of simulations required to achieve acceptable uncertainty levels was investigated in various computational studies [6,18,19]. However, first,

this number depends significantly on the sampling concept [10,18]. In addition, second, all these studies are limited to simulation data. Therefore, an isolated investigation of the performance of the sampling concepts regarding fatigue damage uncertainties without including purely numerical effects or model errors has not been done before. That is why in this work, various sampling concepts (see Section 3) are assessed and validated using measurement data. For this purpose, the convergence of the sampling concepts for increasing numbers of samples is analyzed. The methodology to determine the resulting uncertainty of the different sampling concepts using measurement data is the following:

1. Measure strain values at real offshore wind turbine substructures.
2. Calculate hot spot stresses for a relevant position using Equations (1) to (4).
3. Calculate damages of all 10 min measurements using Equation (5).
4. Sample short-term damages using the chosen sampling concept (Section 3).
5. Extrapolate short-term damages to a lifetime value using Equations (6) and (7).
6. Repeat steps 4 and 5 $N_{BT} = 10,000$ times using bootstrapping (i.e., sampling from all available data (here: about 120,000 usable samples) with replacement).

3. Sampling Concepts

3.1. Deterministic Grid (DG)

The standard sampling approach proposed by the standards is a uniform, deterministic rectangular grid of EC (variables). For all d variables, the design space is separated into M bins (e.g., the wind speed range is split up into bins of 2 m s^{-1} or less). For all M^d combinations of variables (i.e., each bin), at least one sample is needed. In each bin, all EC are kept constant at their mean value making the approach quasi-deterministic. This means that for example in the wind speed bin $6.5\text{--}8.5 \text{ m s}^{-1}$, the wind speed is always 7.5 m s^{-1} . DG becomes very inefficient for high input dimensions (d), as M^d samples are required.

3.2. Monte Carlo sampling (MCS)

MCS is a standard approach for probabilistic simulations that generates all samples (J_{Σ}) by applying the (dependent/joint) statistical distributions of all variables. For linear systems, this has the advantage of a constant convergence rate of $J_{\Sigma}^{-0.5}$ independent of the input dimension. However, for highly non-linear systems, MCS becomes inefficient, since rarely occurring events determine the converge behavior [10].

3.3. Equally Distributed Monte Carlo Sampling (EMCS)

EMCS is a probabilistic version of DG. Just as for DG, a grid of EC is set up. However, the grid dimension (d_g) is chosen to be smaller than the input dimension d . Normally, it is set to one. In contrast to DG, in each bin, EC are not kept constant, but MCS is applied. Hence, in the wind speed bin $6.5\text{--}8.5 \text{ m s}^{-1}$, wind speed values between 6.5 m s^{-1} and 8.5 m s^{-1} are possible and other EC are sampled from their (dependent) distributions. For $d_g = 0$, EMCS becomes MCS, and for $d_g = d$, it is DG. For more details regarding EMCS, it is referred to Hübler et al. [18].

3.4. Damage Distribution-Based Monte Carlo Sampling (DMCS)

DMCS by Hübler et al. [18] is based on EMCS, but its idea is to focus samples on load cases leading to high damages by applying the damage distribution (i.e., weighted lifetime damage versus wind speed) to the sampling. This is comparable to importance sampling. For example, if 15% of the damage is produced by a bin, 15% of the samples should be drawn from this bin. In theory, DMCS improves the accuracy significantly, as more data is available where it is influential. However, since the damage distribution is normally not known in advance, in a first step, an approximated damage distribution (prior function) must be determined by sampling, for example, $N_{\text{approx}} = 20$ cases in $M = 14$ bins (e.g., $20 \times 14 = 280$ EMCS cases). As an approximation based on only 20 samples per

bin is not precise enough, Bayesian statistics is applied to update the initially approximated damage distribution after each new sample. It becomes apparent that DMCS is more suitable for larger sample sizes being typical for industry applications, since the estimation of the damage distribution improves with every additional sample. The DMCS procedure is the following:

1. Sample $N_{\text{approx}} \times M$ cases (e.g., 280 EMCS cases).
2. Calculate the prior function (i.e., initial damage distribution), being the weighted mean damage of N_{approx} cases in each bin.
3. The next sample ($j + 1$) is generated according to the damage distribution (i.e., prior function). This means that it is sampled from the bin (m_{j+1}) where the quotient of the number of samples and the number of samples required by the prior is minimal: $m_{j+1} = \arg \min \left(\frac{J(m) \sum_{m=1}^M D(m)}{D(m) \sum_{m=1}^M J(m)} \right)$.
4. Calculate the damage of the sample (D_{j+1}) and update the damage distribution.
5. Continue with steps 3 and 4 until the desired number of overall samples (e.g., $J_{\Sigma} = 1000$) is generated.

3.5. Reduced Bin Monte Carlo Sampling (RBMCS)

To be independent of an approximated damage distribution, another concept is RBMCS of Hübler et al. [18]. It is also based on EMCS and reduces the number of bins by merging bins with similar physical and generalized damage behavior. For example, for small monopiles with a wind-dominated behavior and highest loads around rated wind speed, low wind speed bins can be merged, and for high wind speed bins, the bin sizes are slightly increased: $<4.5 \text{ m s}^{-1}$, $4.5\text{--}6.5 \text{ m s}^{-1}$, $6.5\text{--}8.5 \text{ m s}^{-1}$, $8.5\text{--}10.5 \text{ m s}^{-1}$, $10.5\text{--}12.5 \text{ m s}^{-1}$, $12.5\text{--}14.5 \text{ m s}^{-1}$, $14.5\text{--}18.5 \text{ m s}^{-1}$, $18.5\text{--}22.5 \text{ m s}^{-1}$, and $>22.5 \text{ m s}^{-1}$. RBMCS reduces the number of bins and leads to more cases in each bin. As in each bin random sampling (MCS) is conducted, RBMCS converges to the “correct” value for a sufficient number of samples. Since there are more cases in bins with similar behavior, the uncertainty in each bin can be reduced. Nonetheless, it can be a challenge to determine the optimal combination of merged bins.

4. Test Example

To gain a better insight in the performance of the various sampling techniques, a test function is analyzed in a first step, before measurement data is used for the validation (c.f. Section 5).

4.1. Theory

The test function is based on the test function of Graf et al. [10]. It mimics real fatigue behavior by representing a damage distribution and is capable of modelling different input space dimensions as well as degrees of non-linearity. The test function is defined as:

$$f(x) = \left[\sum_{i_d=1}^d \left(\left(\frac{1}{2} \right)^{i_d-1} x_{i_d}^{m_{\text{mat}}} \right) \right]^{\frac{1}{m_{\text{mat}}}}, \quad (8)$$

where x is the d -dimensional input vector and m_{mat} mimics the real fatigue behavior by introducing a “material” (Wöhler) exponent. All inputs are sampled from independent, truncated Weibull distributions (scale parameter $a = 3$, shape parameter $b = 1.12$, $x_{\text{max}} = 24$) and are weighted with the factor $\left(\frac{1}{2} \right)^{i_d-1}$. The decreasing importance of the inputs while the dimension increases also mimics real fatigue behavior, as the influence of the first random inputs (e.g., wind speed) is more pronounced than of others (e.g., wind direction). For all five sampling concepts (c.f. Section 3), this function is evaluated for dimensions up to six and exponents up to 20. Increasing dimensions represent a growing number of influential EC and higher exponents lead to a more pronounced non-linear model behavior. The grid of DG is equidistant between zero and x_{max} . For EMCS, $d_g = 1$ and $M = 15$ are used. For DMCS, $d_g = 1$, $N_{\text{approx}} = 5$, and $M = 15$ are applied. The merging of the bins for RBMCS

($d_g = 1$) depends on m_{mat} , since the overall behavior changes with an increasing exponent. $M = 15$ bins are merged to eight bins. For small m_{mat} , higher bins are merged, and vice versa.

4.2. Results

The performance of the five sampling concepts for different dimensions and degrees of non-linearity is displayed in Figure 2.

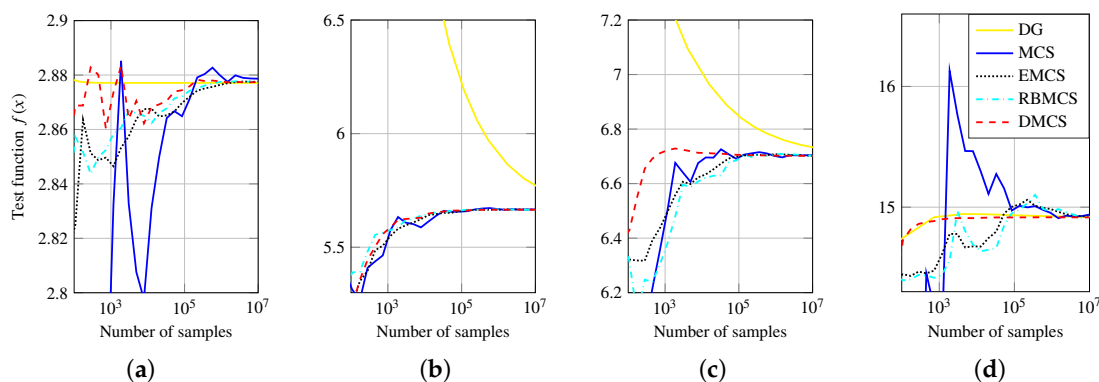


Figure 2. Convergence of the five sampling concepts using the test function $f(x)$ and different input dimensions d and exponents m_{mat} . For non-deterministic concepts, several runs were conducted and a “representative” one is shown here. (a) $d = 1, m_{\text{mat}} = 1$; (b) $d = 6, m_{\text{mat}} = 1$; (c) $d = 6, m_{\text{mat}} = 4$; (d) $d = 6, m_{\text{mat}} = 20$.

Graf et al. [10] have already shown that for linear systems and low dimensions (Figure 2a), DG performs tremendously well, since it converges with J_{Σ}^{-1} . MCS requires the highest number of samples to converge. However, for higher dimensions, DG becomes very inefficient (Figure 2b), as its convergence rate reduces to $J_{\Sigma}^{-1/d}$, while MCS still converges with $J_{\Sigma}^{-1/2}$. The challenge of fatigue damage extrapolations is that the dimension of the input space is high, and in addition that single events (samples) can determine the whole fatigue behavior. Hence, the model is high-dimensional and non-linear (Figure 2c,d). The problem of DG for high dimensions has already been discussed and is also visible for non-linear models, although it becomes less relevant. Increasing d are uncritical for MCS, but high m_{mat} reduce the convergence rate, so that MCS is not efficiently applicable to highly non-linear models (Figure 2d). Alternatives to DG and MCS are the probabilistic bin-based approaches. EMCS and RBMCS combine advantages of DG and MCS. Therefore, they perform similar to MCS for high dimensions, where DG is not applicable. If DG is performing better than MCS (e.g., low dimensions) or the damage distribution (here: $f(x)$) does not resemble the sampling distributions (here: Weibull), as it is the case for high m_{mat} , EMCS and RBMCS outperform MCS. DMCS has the advantage of concentrating samples in “important” bins. Its convergence is comparable to the other bin-based approaches for linear models, as in this case, its importance sampling does not differ significantly from uniform sampling in EMCS. For non-linear models, DMCS outperforms all other approaches.

To summarize, as the performance of DG and MCS depends on the dimension of the input space and the degree of non-linearity of the model, both cannot generally be applied efficiently. EMCS leads to similar results as MCS, while—for a direct comparison—the similarity of the sampling and the damage distribution is relevant. In most cases, RBMCS is quite similar to EMCS. However, when equipped with well-founded expert knowledge to merge bins appropriately, RBMCS can be quite beneficial as demonstrated in Hübler et al. [18]. Finally, DMCS always converges relatively fast and can be regarded as the most appropriate sampling concept for this test function.

5. Validation

In the previous section, sampling concepts were tested using a test function. That yields a better insight in their performance. However, for a profound validation, measurement data is needed.

5.1. Measurement Set-Up

In this work, measurement data of a large measurement campaign in the Belgian Northwind offshore wind farm is used. Data of this measurement campaign was used in several previous investigations. For detailed information regarding raw data and data quality, it is referred, for example, to Weijtjens et al. [29].

Northwind is located about 37 km off the Belgium coast (see Figure 3a), and has moderate water depths of 16 m to 29 m. The wind farm consists of 72 Vestas V112-3 MW turbines. For all turbines, monopile foundations with diameters of 5.2 m are used.

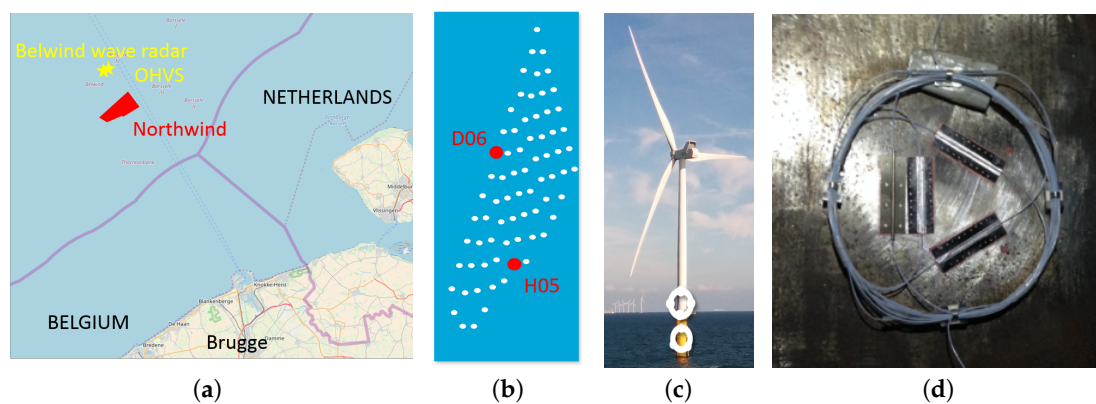


Figure 3. Illustration of the investigated turbines, the metocean stations, and the measurement set-up. (a) Location of the wind farm Northwind and the used metocean stations (©OpenStreetMap contributors (openstreetmap.org) Copyright: CCBY-SA). (b) Northwind layout with both instrumented turbines marked. (c) Vestas V112 turbine. (d) Fiber Bragg gratings welded to the transition piece.

Since October 2014, strain measurements of two instrumented turbines are available. In this work, we use three years of data from 1st November 2014 to 31st October 2017. The two turbines, instrumented by OWI-lab, are marked in Figure 3b. The positions of the turbines on both sides of the wind farm enable an analysis of slightly different wind conditions, as free inflow conditions are given for different wind directions. Moreover, both turbines are located at different water depths. This leads to slightly different designs of the two monopiles, and therefore, to varying eigenfrequencies (see Table 1). Both turbines are instrumented, inter alia, with seven FBG as strain gauges spread over two different levels (see Figure 3c,d). The strain gauges are positioned at the interface between tower and transition piece (TP) and the interface between TP and monopile. Here, the lower measurement layer between TP and monopile is used. For this layer, FBG are welded to the wall making a correction due to reduced sensitivities necessary [27]. The chosen configuration of the strain gauges (spread around the circumference) and a temperature compensation enable a determination of bending moments at these interface levels.

Table 1. Main properties of the considered turbines (eigenfrequencies according to Weijtjens et al. [30]).

Turbine	Location	Type	Hub Height	Water Depth	Eigenfrequency	Diameter Monopile
H05	South	Vestas V112	71 m	18.9 m	0.30 Hz	5.2 m
D06	North	Vestas V112	71 m	26.9 m	0.27 Hz	5.2 m

In addition to the strain data, metocean data of various sources is available. In the first instance, wind data (e.g., wind speeds or turbulence intensities) can directly be derived using SCADA data of the turbines. Wave conditions are measured at several locations around the wind farm. High-frequency wave data (sampling frequency of 1 Hz) is available from a wave radar in Belwind. The position of the wave radar is marked in Figure 3a. However, as the wave radar was not measuring during the whole measurement period (it was removed in June 2016), additional information of the offshore high voltage substation (OHVS) on “Bligh Bank” (also marked in Figure 3a) has to be used, if no data of the wave radar is available. SCADA data is also used to exclude time periods with a curtailed turbine and down-times.

5.2. Resulting Uncertainty

Short-term damages of all measured strain signals are calculated using the procedure in Section 2.1. If 10 min damages of wind speed bins are analyzed separately, the scattering of these values shows qualitatively the amount of uncertainty in short-term damages. Figure 4a displays for a wind speed of $16.5 \text{ m s}^{-1} < v_s < 18.5 \text{ m s}^{-1}$ and 3 years of data (about 5000 samples for this wind speed bin) the occurrence frequency of fatigue damages (D_j). All damages are normalized with the mean value of all damages of these wind speeds. Damages scatter significantly and reach values of more than 2.5 times the mean value with a probability of 5%. High outliers, reaching values of more than 100 times the mean value, are not shown, but can significantly influence the overall fatigue damage behavior and demonstrate a non-linear model behavior comparable to the analyzed test function.

The uncertainty in lifetime damages can be assessed by calculating the probability density function (PDF) of the fatigue lifetime. It can be determined by using the long-term extrapolation in Section 2.2 and the bootstrapping in Section 2.3. Exemplary PDF for different numbers of samples and EMCS are presented in Figure 4b. Due to reasons of confidentiality, lifetimes are normalized with the mean lifetime of using the whole 3-year data ($\mu_{3\text{years}}$).

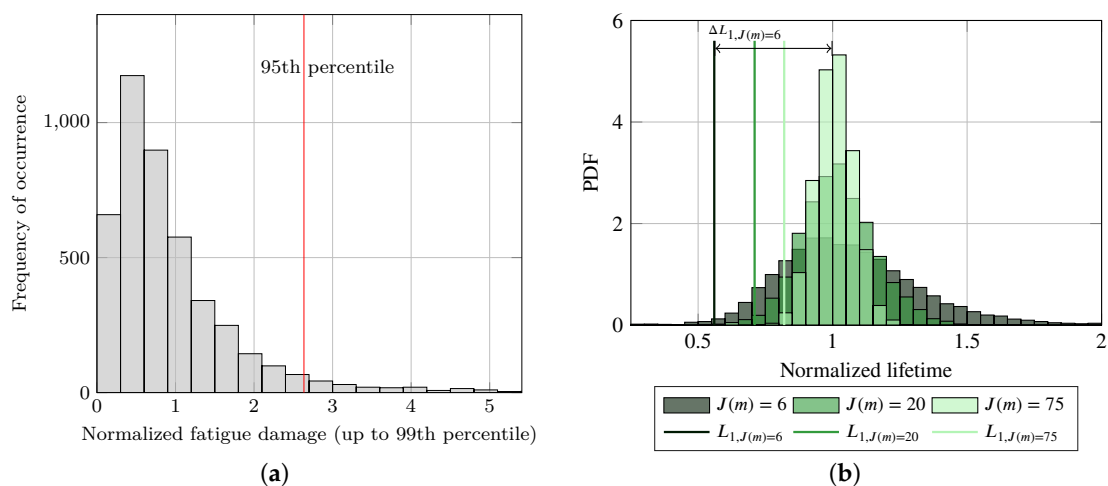


Figure 4. Illustration of the scattering and uncertainty of fatigue damages based on measured strain data for turbine H05. (a) Frequency of occurrence of normalized fatigue damages for a wind speed of $16.5 \text{ m s}^{-1} < v_s < 18.5 \text{ m s}^{-1}$. The 95th percentile is marked. (b) Lifetime PDF for three different numbers of samples ($J(m)$) in each bin (EMCS). The 1st percentiles are marked.

It is demonstrated that using only a few samples (commonly done in academia [6,12]) leads to high uncertainties. At the expense of higher computing times, the uncertainty can be reduced by increasing the number of samples, as it is done in industry. This trade-off is the reason improved sampling concepts are investigated in this work.

In most cases, the full lifetime PDF (see Figure 4b) is not the focus, as the main interest is to guarantee safe designs. Hence, the lowest lifetime approximations (e.g., the 1st percentile) are more relevant. Therefore, the 1% error (ΔL_1) is defined as the deviation of the lifetime at the 1st percentile (marked in Figure 4b) to the “real” lifetime (estimated using the whole three years of strain data):

$$\Delta L_1 = \frac{\mu_{3\text{years}} - L_1}{\mu_{3\text{years}}}. \quad (9)$$

For EMCS and six samples per bin, the 1% error is about 40% ($\Delta L_{1,J(m)=6} = \frac{1-0.61}{1} = 0.39$; see Figure 4b). Hence, a higher number of samples and/or another sampling concept are recommended. The number of samples per bin is not the best comparative value, as it does not incorporate the number of bins. Therefore, in the remainder of this work, we always relate to the overall number of samples (J_Σ).

To gain a deeper understanding of the uncertainty due to finite sampling for the present measurement data, the reasons for it are determined in the next section.

5.3. Reasons for High Uncertainty

In general, relatively rare but highly damaging events are the reason for high uncertainties due to finite sampling (i.e., slow convergence with increasing number of samples). These events are only covered, if a high number of samples is used. On the one hand, highly damaging single events (with low occurrence probabilities, for example, a 100-year storm) do not contribute a lot to the overall damage [21]. On the other hand, a relatively small amount of load situations leads to a high proportion of the overall damage. Hence, it is important to determine reasons for highly damaging but not too unlikely situations for the Northwind monopiles. Figure 5 gives an insight in scattering and the EC that are responsible for the damage. High wind speeds lead to high mean damages. However, these values do not scatter significantly, and furthermore, are not responsible for the highest damage values. The highest “outliers” occur for high turbulence intensities and wind speeds around rated wind speed (cf. Figure 5b). For these wind speeds, the maximum thrust loads occur, as blades have not been pitched out yet. Furthermore, for high turbulence intensities, fluctuations in the wind speed are more pronounced and cannot always be covered by relatively slow pitch controller actions. However, normal operation is not responsible for maximum damages. Rotor stops, shown in Figure 6, increase damages dramatically, as at least one very large cycle is introduced by the rotor stop event. These rare stopping events at rated wind speed drive the uncertainty for the present measurement data. Other conditions increasing the uncertainty are, for example, highly scattering (significant) wave heights or turbulence intensities (cf. Figure 5a).

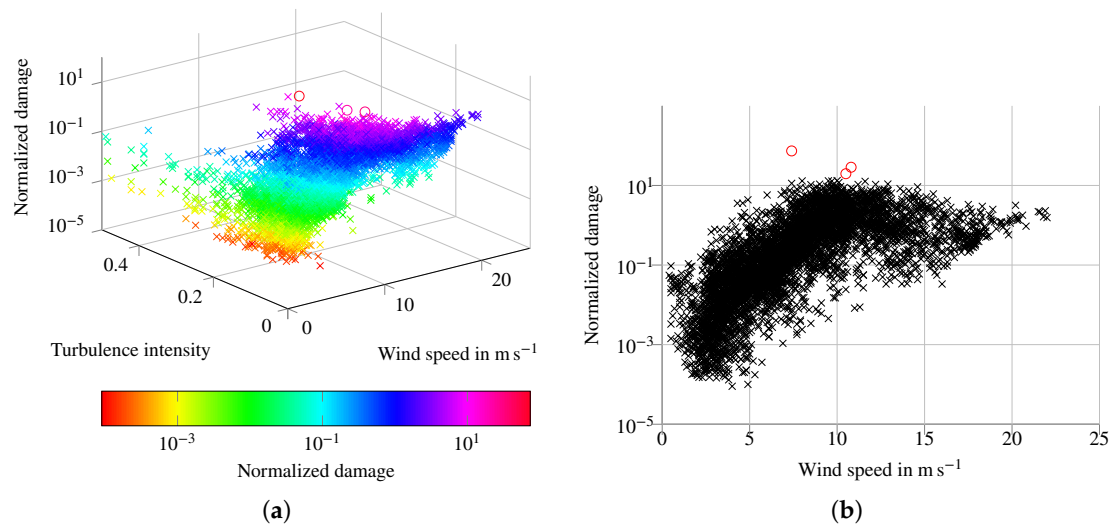


Figure 5. Investigation of the reasons for high uncertainty. (a) Scatter plot showing damages depending on wind speed and turbulence intensity (representative 1-month measurement data of D06). “Outliers” are marked with circles. (b) Scatter plot showing damages depending on the wind speed (representative 1-month measurement data of D06). “Outliers” are marked with circles.

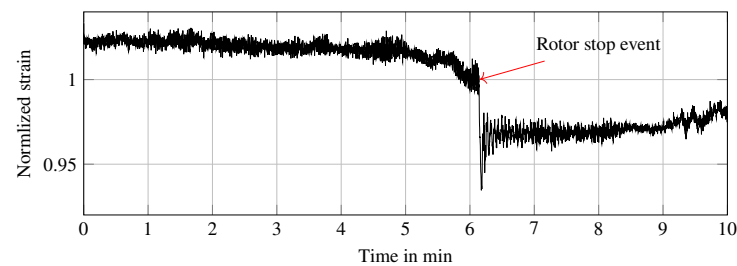


Figure 6. 10 min time series of a rotor stop event around rated wind speed: Normalized measured strains (FBG) versus time.

Hence, current results make clear that there can be various reasons for sampling induced uncertainty. In Hübler et al. [18], the main reason is wave resonance. In contrast, for the present measurement data, controller actions are decisive. If the reason for the high uncertainty is known, these rare cases can be excluded from the standard load case (DLC 1.2 in IEC 61400-3 [5]) and be treated separately. For normal shut downs, etc., this is usually done. They are not included in DLC 1.2, but have their own (deterministic) load cases (DLC 4.1, etc.). However, it is not possible to exclude all rare, highly damaging cases. Therefore, sampling concepts such as RBMCS and DMCS that are designed to reduce the uncertainty compared to standard approaches are needed to keep the sampling effort small. In the next section, the previously developed probabilistic bin-based approaches by Hübler et al. [18] (RBMCS and DMCS) are validated and compared to DG, MCS, and EMCS.

5.4. Convergence of Improved Sampling Concepts

For an assessment of the different concepts, the lifetime (L) is calculated according to Section 2. For this calculation, different numbers of overall samples (J_{Σ}) are generated using the various sampling concepts and the available 3-year data (about 120,000 usable samples). The bootstrap procedure is repeated 10,000 times to estimate the statistical variation in L . Last, the lifetime distribution is normalized by the “real” lifetime (using 3 years of data):

$$\hat{L} = \frac{L_{J_{\Sigma}, \text{concept}}}{\mu_{3\text{years}}} \quad (10)$$

To evaluate the performance of RBMCS and DMCS, the same procedure is conducted for samples that are generated using DG, MCS, and EMCS. For EMCS, RBMCS, and DMCS, $d_g = 1$ and $M = 14$ is used. For RBMCS, the applied merging of the bins to $M = 9$ is explained in Section 3.5. For DMCS, $N_{\text{approx}} = 20$ is applied. DG uses a grid dimension of $d_g = 5$ (i.e., wind speed and direction, (significant) wave height and period, and turbulence intensity). However, for high-dimensional grids, using measurement data, data is not available for all grid points. Very unlikely EC combinations—not occurring during the three years of measurements and making up more than 50% of all grid points for $M \geq 3$ —are not taken into account. Hence, the applied (sparse) DG approach for measurement data is only partly comparable to the (full) standard DG for simulation data.

To illustrate the general performance of the two improved concepts, Figure 7 shows the lifetime PDF that are generated using RBMCS and DMCS compared to EMCS. As in Hübler et al. [18], EMCS serve as reference here. The uncertainty is significantly reduced, and more reliable lifetime approximations are achieved, while the number of samples remains constant. Especially for DMCS, it becomes apparent that the lowest lifetimes are much less uncertain. As samples are concentrated on bins with high damages, low lifetime outliers are effectively removed.

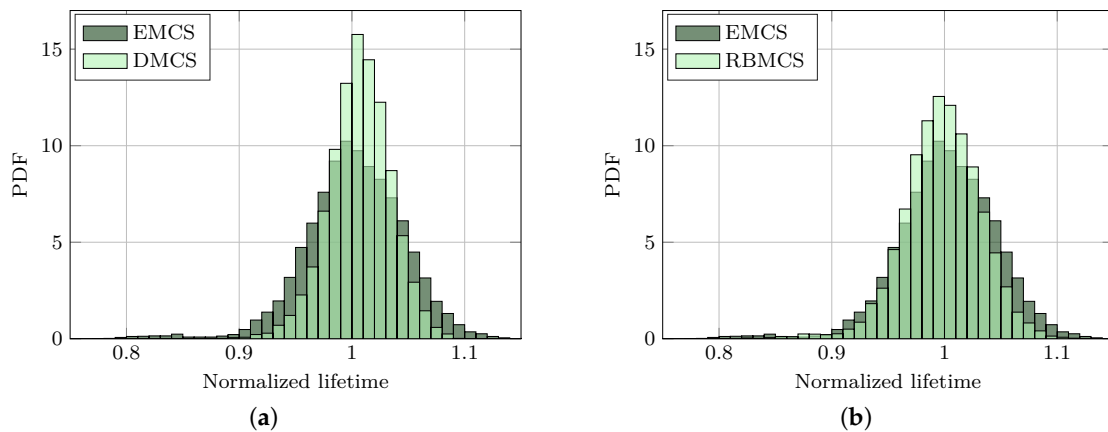


Figure 7. Illustrative assessment of the performance of the two improved sampling concepts for turbine H05: normalized lifetime PDF (normalized with the mean lifetime using 3 years of data ($\mu_{3\text{years}}$) for reasons of confidentiality). (a) Lifetime PDF for $J_{\Sigma} = 2800$ and EMCS compared to DMCS. (b) Lifetime PDF for $J_{\Sigma} = 2800$ and EMCS compared to RBMCS.

For an objective assessment of the concepts, the convergence of three evaluation criteria— \hat{L} (or rather its deviation from $\mu_{3\text{years}}$; $\Delta\mu$), ΔL_1 , and the coefficient of variation (CV)—for an increasing number of overall cases for all concepts and both turbines is illustrated in Figures 8 and 9. The coefficient of variation is defined as the ratio of the standard deviation (σ) to the mean value (μ):

$$CV = \frac{\sigma}{\mu}. \quad (11)$$

It is introduced, as for a reduced (biased) mean value, the 1st percentile is closer to the “real” mean by definition. Here, a biased mean value can have two reasons. First, if the sample size is relatively low, it might not have been converged yet. Second, the binning procedure can influence the mean value, if measurement data is used in combination with long-term design EC distributions for the bin probabilities (cf. Section 2.2). In this case, bin probabilities do not correspond completely to the occurrence probability of the samples in each bin. Therefore, errors at high percentiles can have less informative value. In addition to the illustration of the convergence in Figures 8 and 9, some quantitative results are given in Table 2.

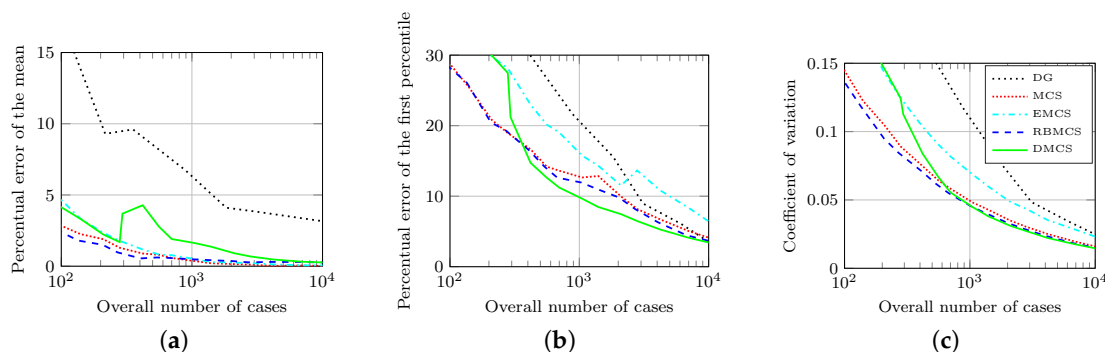


Figure 8. Convergence of the five sampling concepts using measurement data of H05. (a) Lifetime mean value errors ($\Delta\mu$). (b) Lifetime 1% error (ΔL_1). (c) Lifetime coefficient of variation (CV).

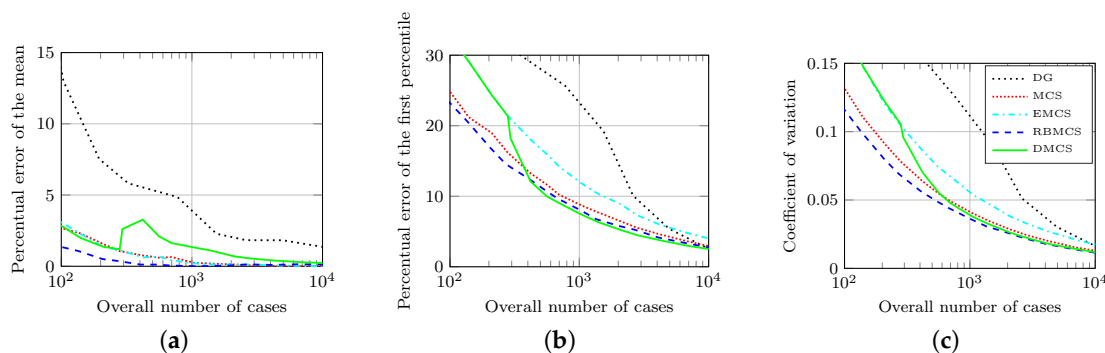


Figure 9. Convergence of the five sampling concepts using measurement data of D06. (a) Lifetime mean value errors ($\Delta\mu$). (b) Lifetime 1% error (ΔL_1). (c) Lifetime coefficient of variation (CV).

Table 2. Errors and uncertainties in lifetime using different concepts and 1000 as well as 10,000 overall samples; measurement data of H05. Changes (of CV and ΔL_1) refer to the reference approach (EMCS).

	EMCS	DMCS	RBMCS	MCS	EMCS	DMCS	RBMCS	MCS
Overall cases (J_Σ)	1050	1050	1035	1050	10,010	10,010	10,035	10,010
Cases for approximation	–	20×14	–	–	–	20×14	–	–
Normalized mean ($E(\hat{L})$)	1.01	1.02	1.00	1.00	1.00	1.00	1.00	1.00
Coefficient of variation (CV)	0.069	0.045	0.045	0.048	0.023	0.015	0.015	0.016
CV change in %	–	–34.8	–34.5	–29.8	–	–36.8	–34.6	–30.7
Error (ΔL_1) in %	15.75	9.66	11.94	12.65	6.43	3.43	3.66	4.12
ΔL_1 change in %	–	–38.7	–24.2	–19.7	–	–46.7	–43.1	–35.9

First, it becomes apparent that the increase of the number of cases is a possible but not very effective way to reduce uncertainties. Then, for both turbines, uncertainties and possible reductions of the two improved concepts are quite similar. Although the sparse version of DG theoretically improves the performance of DG, as “impossible” EC combinations are not taken into account, DG requires a much higher number of samples to achieve adequate uncertainties. Furthermore, it converges to a different mean value due to the varied binning procedure. This biased mean value only occurs for measurement data, where the occurrence probability of each bin does not completely match the long-term EC distributions. As postulated before [10,11], MCS outperforms DG. The good performance of MCS is supported by similar sampling and damage distributions (see Figure 10a). For such similar distributions, it has already been shown with the help of the test function (cf. Figure 2c) that MCS can outperform EMCS and RBMCS. Hence, EMCS still converges faster than DG, but does not perform as good as MCS. RBMCS is an improvement of EMCS and performs better than MCS for the present measurement data. Improvements of ΔL_1 of about 10% and 30% compared to MCS and EMCS,

respectively, are achieved. DMCS shows the best convergence behavior. It reduces ΔL_1 by around 20% and 40% compared to MCS and EMCS, respectively. This may not sound that much. However, having in mind that for plain MCS, a reduction of ΔL_1 of 25% means doubling the sampling effort, these are considerable reductions. Furthermore, the slower convergence of the mean value (bias of the mean value for small sample sizes described by Hübler et al. [18]) is not that relevant. It is mainly apparent for samples sizes just above $N_{\text{approx}} \times M = 280$, where only a few samples are generated according to the damage distribution. The main disadvantage of DMCS is that it requires some samples to generate an initial prior. For sample sizes smaller than $J_{\Sigma} = N_{\text{approx}} \times M$, DMCS is equal to EMCS.

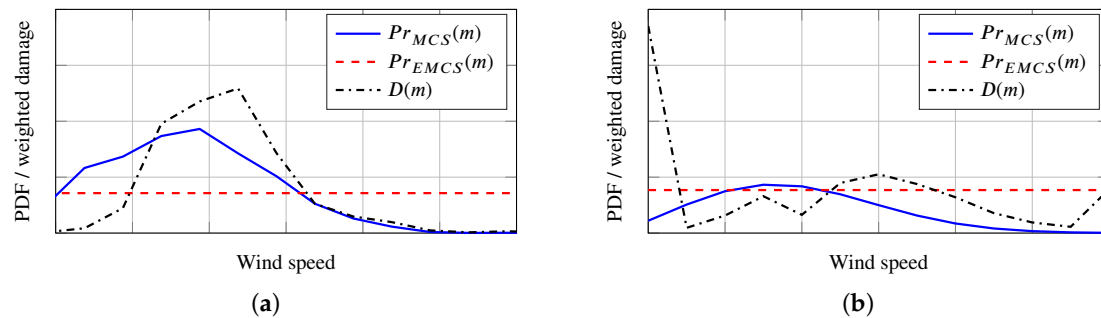


Figure 10. Qualitative comparison of the sampling distributions of EMCS ($Pr_{EMCS}(m)$) and MCS ($Pr_{MCS}(m)$) with the actual damage distribution ($D(m)$). (a) Measurement data. (b) Simulation data of Hübler et al. [18].

5.5. Comparison of the Performance for Simulation and Measurement Data

Finally, the performance of MCS, EMCS, RBMCS, and DMCS is evaluated for previously published simulation results [18] and the present measurement data (treated as “realistic simulation data”) and for the different designs (OC3 monopile and different Northwind designs). DG is not taken into account, as first, no simulation data is available. Second, DG is hardly applicable to measurement data. In addition, third, DG features a poorer performance compared to all other concepts. The variety of applications can demonstrate the general performance of the concepts. Table 3 gives an overview of the reduction concepts based on the previous computational analysis [18]. Two different sample sizes (academia and industry) are shown.

Table 3. Errors and uncertainties in lifetime using different concepts and 1000 as well as 10,000 overall samples; simulation data [18]. Changes (of CV and ΔL_1) refer to the reference approach (EMCS).

	EMCS	DMCS	RBMCS	MCS	EMCS	DMCS	RBMCS	MCS
Overall cases (J_{Σ})	1000	1000	1000	1000	10,000	10,000	10,000	10,000
Cases for approximation	–	20×13	–	–	–	20×13	–	–
Normalized mean ($E(\hat{L})$)	1.00	1.25	1.00	1.00	1.00	1.05	1.00	1.00
Coefficient of variation (CV)	0.259	0.162	0.213	0.257	0.099	0.066	0.079	0.100
CV change in %	–	–37.5	–17.8	–0.8	–	–33.3	–20.2	+1.0
Error (ΔL_1) in %	56.76	20.21	47.10	56.52	23.32	11.43	18.15	24.39
ΔL_1 change in %	–	–64.4	–17.0	–0.4	–	–51.0	–22.2	+4.6

In contrast to measurement data, for simulation data, MCS does not perform better than EMCS. This clarifies the relevance of sampling distributions in comparison with the damage distribution, and therefore, the missing general applicability of MCS. For the simulation data, the distributions are shown in Figure 10b, where $D(m)$ is more similar to $Pr_{EMCS}(m)$.

For RBMCS, the results are quite consistent again. Reductions of the 1% error of about 20% compared to EMCS and MCS are achieved without introducing any bias.

For DMCS, the reductions of ΔL_1 are above 50% independent of the sample size. This approximately matches the measurement results for high numbers of samples (e.g., $J_\Sigma > 500$). The “poorer” performance for measurement data, if a small number of samples is chosen (e.g., $J_\Sigma = 300$), is a result of the previously mentioned disadvantage of DMCS (i.e., it needs some samples for the prior creation). For simulation data and DMCS, there is a pronounced bias of the mean value especially for low numbers of samples. To understand the bias for simulation data, its reason is briefly explained. As DMCS concentrates its sampling on bins with high damages, it cannot represent damages correctly, if there are high outliers in bins with low median damages. In this case, too low damages are estimated by the prior, and therefore, only a few samples are generated for these bins. This leads to an insufficient coverage of high outliers (see Hübler et al. [18] for more information). For the simulation data of the OC3 monopile, there are such outliers—due to wave resonance—in bins of low median damages (e.g., low wind speeds). For the measurement data of the wind-dominated Northwind monopiles, this is not the case. Hence, the reason for the bias of DMCS is not the simulation data itself, but the wave resonance. In any case, the bias diminishes for a sufficient number of samples.

To conclude: The performance of RBMCS is robust by decreasing the 1% error by about 20–30% compared to EMCS independent of other conditions. DMCS can achieve significantly higher error reductions of 40–50% compared to EMCS and 20–50% in comparison with MCS. Hence, it achieves the best results for the test function, simulation data, as well as measurement data. However, for very small sample numbers, the performance is limited. For wave resonance-dominated structures, biased results can occur, if the number of cases is chosen too small to guarantee a convergence of the mean value. Both problems are not relevant for large sample sizes that are common in industry.

6. Benefits and Limitations

As the fatigue design of substructures of offshore wind turbines is a time-consuming process that must be accurate at the same time, the present study focuses on the validation of previously developed sampling methods that reduce the uncertainty due to finite sampling. For this validation, no actual simulation data is used but, first, a test function, and second, real offshore strain measurements that are considered to be “realistic simulations”. The test function helps to demonstrate the general performance for different types of problems. It is shown that the concepts perform well for a broad range of input dimensions as well as degrees of non-linearity. Measurement data has, on the one hand, the advantage that purely numerical effects (e.g., errors of the aero-elastic model) are excluded. Furthermore, a very extensive number of samples for two different structures is available, which would not have been feasible through simulations in an academic context. Hence, the current work can assess the proposed methods for different systems (turbines, substructures, sites, etc.) and sample sizes (convergence study) and independent of any simulation code specifications. On the other hand, measurement errors occur and must be treated carefully. For example, spikes in strain signals due to measurement errors must be filtered or removed manually.

The present outcomes underpin the recently repeatedly formulated presumption [6,12,18] that standard recommendations concerning lifetime extrapolations (in academia) lead to unacceptable uncertainties due to finite sampling (cf. $J(m) = 6$ in Figure 4b) that are in the same order of magnitude as other important types of uncertainty that are not the topic of this investigation (e.g., the error of Miner’s rule [31]).

Regarding sampling methods that reduce the uncertainty in the damage approximation without increasing the number of samples (i.e., computing time), two concepts are validated. Previously, they performed well for simulation data and one set-up. Here, they are tested for measurement data, different turbine designs, and a test function and are compared to standard approaches such as MCS or deterministic grid sampling. It is shown that these two concepts are generally valid independent of the structure (e.g., OC3 or Northwind monopile) and reason of the uncertainty (e.g., wave resonance or rotor stops). They lead to 1% error reductions of about 30% and 40% compared to EMCS for RBMCS and DMCS, respectively. A reduction of the 1% error of 25% is tantamount to halving the required

samples while keeping the 1% error constant. DMCS enables higher uncertainty reductions compared to RBMCS, but it can be slightly biased for smaller sample sizes. An important factor for industry is that the benefit of DMCS compared to other sampling concepts grows with increasing sampling effort.

7. Conclusions

The main objective of this study is the validation of sampling concepts that reduce the uncertainty due to finite sampling. This validation is performed by assessing the concept performance for a broad range of applications and data types. For this purpose, real offshore measurement data is used and treated as “realistic simulation data”. This enables an assessment of previously developed methods while simulation errors, etc. are excluded and by using a large data set for the validation.

It is shown that uncertainties are high, depend significantly on the design of (monopile) substructure and turbine, and are considerably influenced by controller actions. Therefore, quantitative conclusions concerning the uncertainty are difficult. However, commonly applied approaches in academia should be reconsidered, as deterministic approaches cannot reproduce the real uncertainty due to rare, highly damaging situations. A possibility to reduce the sampling effort is to exclude rare, highly damaging events from probabilistic analyses and to add them as additional deterministic damages. For normal shut-down events, etc. this is commonly done. For wave resonance, this is unusual and more challenging.

To overcome the problem of uncertain damage extrapolations, in industry, the number of simulated load situations is much higher than in academia at the expense of high computational costs. Alternatives to the plain increase of sampling are valuable. Such an alternative are advanced sampling concepts. Without adding additional computation effort, it is possible to increase the reliability of the damage extrapolation (error reductions of up to 50% or reducing the sampling effort to approximately a fifth) by applying advanced sampling concepts. Here, the relatively general validity of such concepts was proven. It is recommended to use DMCS—especially for larger sample sizes in industry. RBMCS can be an alternative for smaller sample sizes, for example in academia. In future, such concepts could replace the inefficient grid-based approach that is recommended by the standards.

After all, based on present findings and previous simulation-based results, it can be concluded that lifetimes of designs—relying on very limited simulation data—can be relatively uncertain. Therefore, the consideration of measurement-based fatigue lifetime calculations is valuable. Certainly, it is hardly possible to use measurements during the design phase before having built a turbine. However, for lifetime extension, current standards [32] already recommend to use measurement data, if possible. Hübler et al. [28] show that measurement-based lifetime approximations are not completely certain as well. Still, if available, strain measurements for lifetime approximations are definitely a valuable addition to design simulations and should be further investigated.

Author Contributions: Conceptualization, C.H. and W.W.; Formal analysis, C.H.; Funding acquisition, R.R.; Investigation, C.H. and W.W.; Methodology, C.H.; Project administration, C.H. and R.R.; Software, C.H.; Supervision, W.W., C.G.G. and C.D.; Validation, C.H.; Visualization, C.H.; Writing—original draft, C.H.; Writing—review & editing, W.W., C.G.G., R.R. and C.D.

Funding: We gratefully acknowledge the European Commission (research project IRPWIND, grant agreement number 609795) that enabled this work. The publication of this article was funded by the Open Access Fund of the Leibniz Universität Hannover.

Acknowledgments: The authors gratefully thank the people of Northwind for their continuous support.

Conflicts of Interest: The authors declare no conflict of interest.

Nomenclature

The following nomenclature is used in this manuscript:

a	Scale parameter of the truncated Weibull distribution
A	Cross-section area
ASF	Additional safety factor

b	Shape parameter of the truncated Weibull distribution
CV	Coefficient of variation
d	Input dimension (i.e., number of variables)
d_g	Dimension of the binning
D	(Short-term) Damage
D_{LT}	Lifetime damage
E	Young's modulus or expected value
f	Test function
F_N	Normal force
FSF	Correction factor for reduced sensitivity of welded FBG
i	Index for the stress band
i_d	Index for the (binning) dimension
i_s	Index for the sensor
j	Index for the time series/sample
J	Number of time series/samples in a bin
J_Σ	Number of overall samples (in all bins)
L	Lifetime
$L_{1,J(m)}$	Lifetime at the 1st percentile for $J(m)$ samples in each bin (EMCS)
\hat{L}	Normalized lifetime distribution
m	Index for the bins
m_{mat}	(Material) Exponent of the test function
M	Number of bins of one input
M_{north}	Bending moment in northern direction
MSF	Material safety factor
M_t	Total number of bins of all inputs
M_{west}	Bending moment in western direction
n_i	Number of cycles associated with the stress range $\Delta\sigma_{cor,i}$
n_σ	Number of stress bands
N_{approx}	Number of samples per bin for the prior creation in DMCS
N_{BT}	Number of bootstrap evaluations
N_i	Endurance (number of maximum cycles) for $\Delta\sigma_{cor,i}$ obtained from an S-N curve
Pr	Occurrence probability of a bin
r_{in}	Inner radius of the monopile
r_{out}	Outer radius of the monopile
S	Section modulus
SCF	Stress concentration factor
SE	Factor for the size effect
SF	(Overall) Safety factor
v_s	Wind speed
x	d -dimensional input vector
x_{max}	Upper limit of the truncated Weibull distribution
ΔL_1	Lifetime error at the 1st percentile
$\Delta\mu$	Deviation of \hat{L} from μ_{3years}
$\Delta\sigma_{cor}$	Corrected stress range
$\Delta\sigma_z$	Stress range
ϵ_z	Axial strain
θ	Angle between sensor and northern direction
μ	Mean value
μ_{3years}	Mean lifetime of using the whole 3-year data
σ	Standard deviation
σ_z	Tensile stress
ϕ	Angle between northern and actual wind direction

Abbreviations

The following abbreviations are used in this manuscript:

DG	Deterministic grid
DLC	Design load case
DMCS	Damage distribution-based Monte Carlo sampling
EC	Environmental condition
EMCS	Equally distributed Monte Carlo sampling
FA	Fore-aft
FAST	Fatigue, aerodynamics, structures, and turbulence
FBG	Fiber Bragg grating
HAWC2	Horizontal axis wind turbine code 2nd generation
MCS	Monte Carlo sampling
LCOE	Levelized cost of energy
OC3	Offshore Code Comparison Collaboration
OHVS	Offshore high voltage substation
OWI	Offshore Wind Infrastructure Application
PDF	Probability density function
RBMCS	Reduced bin Monte Carlo sampling
SCADA	Supervisory control and data acquisition
SS	Site-to-side
TP	Transition piece

References

1. Energy Information Administration (IEA). *Levelized Cost and Levelized Avoided Cost of New Generation Resources in the Annual Energy Outlook 2017*; Technical Report; 2017. Available online: http://www.dnrec.delaware.gov/energy/Documents/Offshore%20Wind%20Working%20Group/Briefing%20Materials/2017_EIA_Levelilized%20Cost%20and%20Levelized%20Avoided%20Cost%20of%20New%20Generation%20Resources_Annual%20Energy%20Outlook%202017.pdf (accessed on 14 February 2019).
2. Valpy, B.; Hundleby, G.; Freeman, K.; Roberts, A.; Logan, A. *Future Renewable Energy Costs: Offshore Wind*; Technical Report; InnoEnergy: Eindhoven, The Netherlands, 2017; ISBN 978-84-697-756.
3. Jonkman, J.M.; Buhl, M.L., Jr. *FAST User's Guide*; Technical Report: EL-500-38230; National Renewable Energy Laboratory (NREL): Golden, CO, USA, 2005.
4. Larsen, T.J.; Hansen, A.M. *How 2 HAWC2, the User's Manual*; Technical Report: Risø-R-1597(ver. 3-1)(EN); Technical University of Denmark (DTU): Lyngby, Denmark, 2007.
5. International Electrotechnical Commission. *Wind Turbines—Part 3: Design Requirements for Offshore Wind Turbines*; Standard IEC 61400-3; International Electrotechnical Commission: Geneva, Switzerland, 2009.
6. Zwick, D.; Muskulus, M. The simulation error caused by input loading variability in offshore wind turbine structural analysis. *Wind Energy* **2015**, *18*, 1421–1432. [[CrossRef](#)]
7. Muskulus, M.; Schafhirt, S. Reliability-based design of wind turbine support structures. In Proceedings of the Symposium on Reliability of Engineering System, Hangzhou, China, 15–17 October 2015.
8. Bilonis, D.V.; Vamvatsikos, D. Fatigue analysis of an offshore wind turbine in Mediterranean Sea under a probabilistic framework. In Proceedings of the 6th International Conference on Computational Methods in Marine Engineering, Rome, Italy, 15–17 June 2015.
9. Stewart, G.M. Design Load Analysis of Two Floating Offshore Wind Turbine Concepts. Ph.D. Thesis, University of Massachusetts, Amherst, MA, USA, 2016.
10. Graf, P.A.; Stewart, G.; Lackner, M.; Dykes, K.; Veers, P. High-throughput computation and the applicability of Monte Carlo integration in fatigue load estimation of floating offshore wind turbines. *Wind Energy* **2016**, *19*, 861–872. [[CrossRef](#)]
11. Chian, C.Y.; Zhao, Y.Q.; Lin, T.Y.; Nelson, B.; Huang, H.H. Comparative Study of Time-Domain Fatigue Assessments for an Offshore Wind Turbine Jacket Substructure by Using Conventional Grid-Based and Monte Carlo Sampling Methods. *Energies* **2018**, *11*, 3112. [[CrossRef](#)]

12. Müller, K.; Cheng, P.W. Validation of uncertainty in IEC damage calculations based on measurements from alpha ventus. *Energy Procedia* **2016**, *94*, 133–145. [[CrossRef](#)]
13. Zwick, D.; Muskulus, M. Simplified fatigue load assessment in offshore wind turbine structural analysis. *Wind Energy* **2016**, *19*, 265–278. [[CrossRef](#)]
14. Müller, K.; Dazer, M.; Cheng, P.W. Damage Assessment of Floating Offshore Wind Turbines Using Response Surface Modeling. *Energy Procedia* **2017**, *137*, 119–133. [[CrossRef](#)]
15. Stieng, L.E.S.; Muskulus, M. Reducing the number of load cases for fatigue damage assessment of offshore wind turbine support structures using a simple severity-based sampling method. *Wind Energy Sci.* **2018**, *3*, 805–818. [[CrossRef](#)]
16. Stieng, L.E.S.; Muskulus, M. Sampling Methods for Simplified Offshore Wind Turbine Support Structures Load Case Assessment. In Proceedings of the 28th International Ocean and Polar Engineering Conference, Sapporo, Japan, 10–15 June 2018.
17. Velarde, J.; Bachynski, E.E. Design and fatigue analysis of monopile foundations to support the DTU 10 MW offshore wind turbine. *Energy Procedia* **2017**, *137*, 3–13. [[CrossRef](#)]
18. Hübler, C.; Gebhardt, C.G.; Rolfes, R. Methodologies for fatigue assessment of offshore wind turbines considering scattering environmental conditions and the uncertainty due to finite sampling. *Wind Energy* **2018**, *21*, 1092–1105. [[CrossRef](#)]
19. Häfele, J.; Hübler, C.; Gebhardt, C.G.; Rolfes, R. A comprehensive fatigue load set reduction study for offshore wind turbines with jacket substructures. *Renew. Energy* **2018**, *118*, 99–112. [[CrossRef](#)]
20. Müller, K.; Reiber, M.; Cheng, P.W. Comparison of measured and simulated structural loads of an offshore wind turbine at alpha ventus. *Int. J. Offshore Pol. Eng.* **2016**, *26*, 209–218. [[CrossRef](#)]
21. Müller, K.; Cheng, P.W. Application of a Monte Carlo procedure for probabilistic fatigue design of floating offshore wind turbines. *Wind Energy Sci.* **2018**, *3*, 149–162. [[CrossRef](#)]
22. European Committee for Standardization. *Eurocode 3: Design of Steel Structures—Part 1–9: Fatigue*; EN 1993-1-9; European Committee for Standardization: Brussels, Belgium, 2010.
23. Det Norske Veritas. *Fatigue Design of Offshore Steel Structures*; Recommended Practice DNV-RP-C203; Det Norske Veritas: Hovik, Norway, 2010.
24. International Electrotechnical Commission. *Wind Turbine Generator Systems—Part 13: Measurement of Mechanical Loads*; Standard IEC 61400-13; International Electrotechnical Commission: Geneva, Switzerland, 2015.
25. Maes, K.; Iliopoulos, A.; Weijtjens, W.; Devriendt, C.; Lombaert, G. Dynamic strain estimation for fatigue assessment of an offshore monopile wind turbine using filtering and modal expansion algorithms. *Mech. Syst. Signal Process.* **2016**, *76–77*, 592–611. [[CrossRef](#)]
26. DNV GL AS. *Support Structures for Wind Turbines*; Standard DNVGL-ST-0126; 4C Offshore: Lowestoft Suffolk, UK, 2016.
27. Weijtjens, W.; Noppe, N.; Verbelen, T.; Devriendt, C. Fleet-wise structural health monitoring of (offshore) wind turbine foundations. In Proceedings of the 8th European Workshop on Structural Health Monitoring, Bilbao, Spain, 5–8 July 2016.
28. Hübler, C.; Weijtjens, W.; Rolfes, R.; Devriendt, C. Reliability analysis of fatigue damage extrapolations of wind turbines using offshore strain measurements. *J. Phys. Conf. Ser.* **2018**, *1037*, 032035. [[CrossRef](#)]
29. Weijtjens, W.; Iliopoulos, A.; Helsen, J.; Devriendt, C. Monitoring the consumed fatigue life of wind turbines on monopile foundations. In Proceedings of the EWEA Offshore Conference, Copenhagen, Denmark, 10–12 March 2015.
30. Weijtjens, W.; Noppe, N.; Verbelen, T.; Iliopoulos, A.; Devriendt, C. Offshore wind turbine foundation monitoring, extrapolating fatigue measurements from fleet leaders to the entire wind farm. *J. Phys. Conf. Ser.* **2016**, *753*, 092018. [[CrossRef](#)]
31. Sørensen, J.D. Reliability analysis of wind turbines exposed to dynamic loads. In Proceedings of the 9th International Conference on Structural Dynamics, Porto, Portugal, 30 June–2 July 2014.
32. DNV GL AS. *Lifetime Extension of Wind Turbines*; Standard DNVGL-ST-0262; 2016. Available online: <http://rules.dnvgl.com/docs/pdf/DNVGL/ST/2016-03/DNVGL-ST-0262.pdf> (accessed on 14 February 2019).



6 Economic effects

While previously presented work in this thesis is intended to build up a framework for probabilistic structural analyses of OWTs, this last section focuses on the effects of probabilistic modelling. Economic effects are investigated by combining the developed probabilistic structural OWT model with an economic viability model for offshore wind farms. This enables an evaluation of the influences of scattering (due to aleatory uncertainty of ECs) and variable (due to different designs) OWT lifetimes as well as variable capital expenditures (e.g. substructure costs) on the profitability of wind farm projects.

6.1 Research context

In contrast to most structures in classical civil engineering (e.g. bridges), for OWTs, reliability is not related to public safety, since practically no human lives are directly endangered by potentially failing OWTs. Therefore and due to the need for competitive wind energy, structural optimisations of OWTs with respect to the economic efficiency are an important field of research. However, economic effects of structural changes are not trivial and coupling economic and engineering models is a challenging task. Hence, for most engineering approaches, the structural mass is used as a cost indicator [96, 105]. This procedure does not always lead to optimal structures with regard to economic efficiency. For example, a lightweight structure with a complicated manufacturing process might have higher overall costs than a heavier structure that can easily be produced at a low price. As an alternative, costs or capital expenditures (CAPEX) can be used [49, 111]. Although, CAPEX are a better measure for the economic viability of OWT projects, some important aspects are still neglected. These are, for example, costs during the project lifetime due to operation and maintenance or interest payments. Furthermore, state-of-the-art approaches utilise constant (not uncertain and not variable) lifetimes. Fixed lifetimes can lead to non-optimal designs. For example, Ziegler et al. [218] show the effect of lifetime extensions. This points out that economic effects are not sufficiently considered in engineering approaches of OWTs.

Surely, there are complex economic wind farm models that are capable of investigating the previously discussed effects. However, on the economic side, the engineering aspects are widely simplified. Common simplifications are the use of constant lifetimes or bundled cost inputs for substructures and foundations [154].

Neither pure engineering nor pure economic approaches can yield optimal designs. Combined approaches are needed, but to the author's knowledge, there exist no combined probabilistic approaches so far.

6.2 Methods

In this thesis, the presented probabilistic engineering approach is combined with an economic viability model being developed by the partners of this work [143]. The engineering model

is the proposed FAST model with probabilistic inputs. Using this simulation approach, variable lifetimes (lifetime distributions) can be computed for various designs. Furthermore, a simplified cost model for the substructure is used to approximate the CAPEX of different substructure designs. Lifetime distributions and substructure costs are used as inputs for the economic model.

The economic viability model is not a simplified model for engineering purposes, but a sophisticated economic model whose details might be hard to understand without a profound economic background. The general idea is to simulate an economic agent to represent real-world investment decisions. The model calculates the minimum price per unit of generated electricity (marginal cost) that is sufficient to fulfil two requirements. First, the mean adjusted present value (APV) has to be positive to get equity capital (e.g. of investors). Second, with a probability of 75 %, the project has to be able to repay its debts during the entire project duration to get debt capital (e.g. of banks).

Using this combined model, a realistic wind farm project in the North Sea is simulated. Seven slightly different designs of the substructure are analysed. More durable designs with higher lifetimes but increased substructure costs and cheaper designs (low costs but reduced lifetimes) are created. This enables an analysis of the trade-off between lifetime and initial costs.

6.3 Results

The first important feature revealed by the combined analysis is that even small changes of the substructure affect the overall viability of a wind farm project. Hence, it is important to take all aspects of the project and all components of the OWT into account.

In accordance with current initiatives to extend wind turbine lifetimes, this study shows that in most cases, the effect of increased lifetimes outweighs the influence of higher initial costs. However, it has to be kept in mind that this effect can reverse, if the overall lifetime is limited. This means that an increase of the substructure lifetime is not valuable, if an overall lifetime extension is not possible, since for example, the rotor blade lifetime cannot be increased. Nevertheless, the trade-off in favour of lifetime clarifies that lifetime extensions or higher design lifetimes in general can be valuable.

Finally, in contrast to state-of-the-art approaches, it has to be remarked that fixed design lifetimes hinder optimal designs. The lifetime itself should be regarded as a stochastic variable that has to be optimised with respect to economic efficiency.

6.4 Outlook

The present combined structural and economic analysis is intended to be a first step showing the potential of probabilistic structural analyses and of the consideration of complex economic effects. However, a comparative study demonstrating the benefits compared to pure structural weight or CAPEX considerations is missing so far. Nonetheless, in this field of research, there is a large potential for promising work. At first, real structural optimisations are needed, as only different designs are analysed here. For this purpose, a two-way coupled techno-economic model has to be developed. The present approach is a mere combination of a structural and an economic model, i.e. it is one-way coupled. So, the economic model has no retroactive effect on the structural model, as needed, for example, for optimisation tasks.

Furthermore, design changes are limited to wall thicknesses and diameters. Design variables - like the number of legs, joint geometries, etc. - are kept constant so that significantly different designs are not considered.

Apart from that, the present analysis focuses on the substructure. Design variations and variable lifetimes of other important components would result in even more significant effects on the wind farm viability. Moreover, the consideration of the lifetime of all relevant components would solve the challenge of judging whether lifetime extensions are possible or unrealistic.

In addition, only monopiles have been investigated so far. Other types of substructures, like jackets or floating substructures, have higher initial costs which might influence the trade-off between lifetimes and initial costs.

6.5 Paper F: Influence of Structural Design Variations on Economic Viability of Offshore Wind Turbines: an Interdisciplinary Analysis

The following paper is under review (minor revision) for Renewable Energy. The version printed here is the submitted “author’s version”. The work was conducted in cooperation with partners from the “Information Systems Institute” of “Leibniz Universität Hannover”. The partners mainly worked on economic aspects, while engineering parts were conducted by the author of this thesis. Cristian Gebhardt, Raimund Rolfes, and Michael Breitner contributed with advisory and supporting work.

Influence of Structural Design Variations on Economic Viability of Offshore Wind Turbines: an Interdisciplinary Analysis

Clemens Hübler^a, Jan-Hendrik Piel^b, Chris Stetter^b, Cristian G. Gebhardt^a, Michael H. Breitner^b, Raimund Rolfes^a

^a*Institute of Structural Analysis, Leibniz Universität Hannover, ForWind, Appelstr. 9a, D-30167 Hannover, Germany*

^b*Information Systems Institute, Leibniz Universität Hannover, Königsworther Platz 1, D-30167 Hannover, Germany*

Abstract

Offshore wind energy is a seminal technology to achieve the goals set for renewable energy deployment. However, today's offshore wind energy projects are mostly not yet sufficiently competitive. The optimization of offshore wind turbine substructures with regard to costs and reliability is a promising approach to increase competitiveness. Today, interdisciplinary analyses considering sophisticated engineering models and their complex economic effects are not widespread. Existing approaches are deterministic. This research gap is addressed by combining an aero-elastic wind turbine model with an economic viability model for probabilistic investment analyses. The impact of different monopile designs on the stochastic cost-efficiency of an offshore wind farm is investigated. Monopiles are varied with regard to diameters and wall thicknesses creating designs with increased lifetimes but higher capital expenditures (durable designs) and vice versa (cheaper designs). For each substructure, the aero-elastic wind turbine model yields distributions for the fatigue lifetime and electricity yield and different capital expenditures, which are applied to the economic viability model. For other components, e.g. blades, constant lifetimes and costs are assumed. The results indicate that the gain of increased stochastic lifetimes exceeds the benefit of reduced initial costs, if the overall lifetime is not governed by other turbine components' lifetimes.

Keywords: Offshore wind energy, Substructure design, Economic viability, Stochastic cost-efficiency, Lifetime distribution

List of abbreviations

APV Adjusted present value	KPI Key performance indicator
BT Bootstrap	IRR Internal rate of return
CAPEX Capital expenditures	LCOE Levelized cost of electricity
CDF Cumulative density function	MCS Monte Carlo simulation
DECEX Decommissioning expenses	NREL National Renewable Energy Laboratory
DEP Depression	NPV Net present value
DLC Design load case	NOH Net operating hours
DSCR Debt service cover ratio	OPEX Annual operating expenditures
DSC Debt service capacity	OW Offshore wind
EBIT Earnings before interest, and taxes	OWT Offshore wind turbine
EBITDA Earnings before interest, taxes, depreciation, and amortization	PDC Decommissioning provisions
EC Environmental conditions	PDF Probability density function
EMCS Equally distributed Monte Carlo simulation	TAX Taxes on EBIT
FCF Free cash-flow	WACC Weighted average cost of capital
INT Annual interest payment	

1. Introduction

Although offshore wind energy is a steadily growing market [1] and a promising technology to achieve the long-term goals set for renewable energy deployment, its LCOE is still high compared to other energy supply types [2, 3]. Today, OW energy is - apart from some rare and special examples - not yet competitive without financial support mechanisms [4], as compensation according to current electricity market prices does not enable a profitable and financially viable construction and operation of OW farms. Consequently, increasing the cost-efficiency of this technology is one of the major objectives of current research. As OWT substructures and foundations account for nearly 20 % of the overall OW farm CAPEX (including planning, installation, and component costs, but excluding OPEX) and represent a significant cost reduction opportunity [2, 5], their optimal design with regard to costs and reliability is a promising approach. This means that a change in paradigm for optimal designs is required. In contrast to state-of-the-art optimization approaches, not only costs need to be minimized, but the trade-off between variable lifetimes and component costs needs to be analyzed in interdisciplinary approaches to find the most cost-efficient structural design. Nevertheless, such interdisciplinary approaches, considering both the complex engineering and economic aspects of OWT structural designs, are still unusual.

On the part of engineering analyses, most optimization approaches minimize the structural weight as a cost indicator [6–9]. Muskulus and Schafhirt [10] give a comprehensive review of these optimization approaches. Even if cost models are applied instead of mass considerations, the costs are, in general, approximated by empirical formulations taking into account material, production, and installation costs [11, 12]. The effects of reduced masses or costs on the economic viability of entire projects are not evaluated, as economic aspects, like risk-adjusted discount rates, etc., are not taken into account. Furthermore, lifetimes are set to deterministic, constant values. This disables an analysis of the trade-off between lifetime and costs. A first approach to take variable lifetimes in engineering models for OWT into account is conducted by Ziegler et al. [13]. However, they focus on the trade-off between variable lifetimes and mass, and - as typical for engineering approaches - do not consider complex economic effects.

On the part of economic analyses, substructures and foundations are, in general, considered as a bundled cost input within the CAPEX of an OW farm. Furthermore, as with the engineering analyses, the operating OWT lifetime is typically treated as a deterministic, constant value commonly set to 20 years [14–16]. In addition, several economic studies conduct simple deterministic sensitivity analyses regarding the lifetime, but do not consider any dependencies of the lifetime on other model inputs [17–19]. A first approach to analyze the effects of lifetime extension measures for onshore wind turbines on the LCOE is developed by Rubert et al. [20]. They link the lifetime to model inputs, like retrofits of different components, and also conduct deterministic sensitivity analyses. However, due to the significant variability of offshore conditions, economic effects of structural design variations are different, if probabilistic approaches are applied. Nevertheless, comprehensive probabilistic economic analyses of OW farms that take into account the complex economic effects of structural designs on the trade-off between operating lifetime and the cost of OWT cannot be found.

This research gap is addressed by combining an aero-elastic OWT model with an economic viability model. The combined model can deal with probabilistic inputs based on real offshore measurements and OW investment characteristics. An overview of the combined approach is illustrated in Fig. 1. This concept enables analyzing the effects of substructure design variations on the cost-efficiency of OW farms. Therefore, it is possible to assess the trade-off between substructure lifetime - being modeled using a probability distribution - and substructure CAPEX with regard to the cost-efficiency of each design. To this end, both models are outlined in the following and are then applied to a concise OW farm case study.

2. Aero-elastic wind turbine model

2.1. Time domain model

The dynamic OWT behavior is very complex due to several reasons: nonlinearities, transient load cases, scattering environmental conditions, highly coupled subsystems, etc. Hence, aero-hydro-servo-elastic simulations in the time domain are required by the standards [21]. One software being capable of simulating

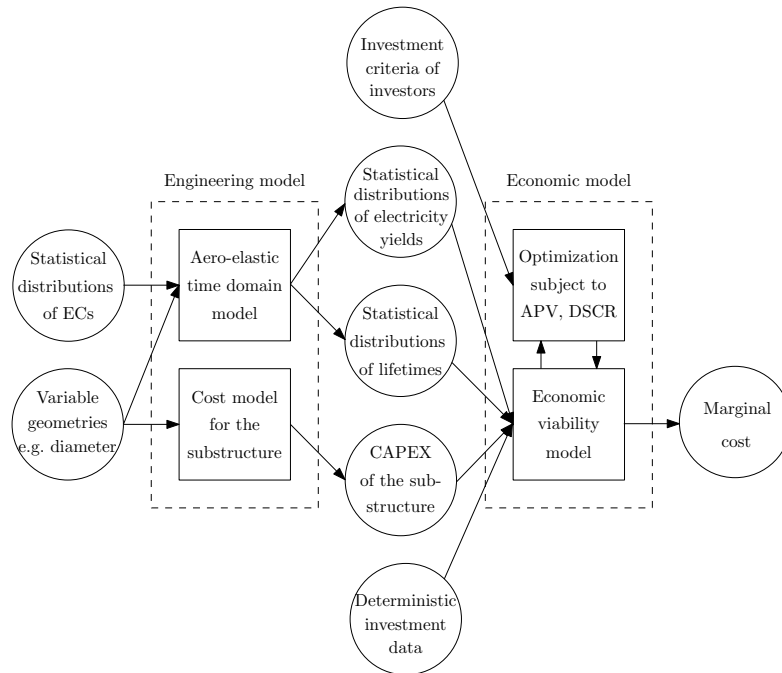


Figure 1: Visualization of the combined engineering and economic model.

50 these coupled systems in approximately real time and being used in this study is the FASTv8 software code
 51 by the NREL [22]. Using FAST, in this study, the NREL 5 MW reference wind turbine [23] is investigated.
 52 Well-founded reference turbines are only available for 5 MW [23] and 10 MW [24]. Since a wind farm with
 53 a commission date of 2020 - where normally 6-8 MW turbines are used - is considered (cf. Section 3.1), the
 54 use of a relatively small 5 MW turbine is justified. The corresponding OC3 phase I monopile (cf. Fig. 2) is
 55 used as substructure [25]. Slight design changes of the OC3 monopile are applied to analyze the effect of
 56 design variations on the economic viability of an entire OW farm.

57 Using the aero-elastic model and various EC that mirror the changing EC at the offshore site as inputs, it
 58 is possible to calculate time series of forces and moments acting on all structural components. The focus
 59 is on the design of steel substructures, so that fatigue damages are most critical. Therefore, time series are
 60 post-processed to approximate the fatigue lifetime, as described in Section 2.3. At this point, the limitation
 61 of this work to the substructure is highlighted. Constant lifetimes and costs for all other turbine parts (e.g.
 62 blades) are assumed. This approach is unproblematic as long as the substructure has a lifetime below 20
 63 years. In this case, the lifetime of other components is not completely exploited. For substructure lifetimes
 64 above the 20-year design lifetime, this concept is questionable. A lifetime extension of other components
 65 is not always possible without significantly increasing the costs. This drawback of the present approach and
 66 some possible workarounds are discussed in Section 4.

67 For all simulations, the simulation length is set to 10 minutes according to current standards and previous
 68 research [21, 26]. The “run-in” time (i.e. the time that has to be removed from each time series to exclude
 69 initial transients) is set to values between 60 and 720 seconds according to Hübler et al. [26]. The turbulent
 70 wind field is calculated using the Kaimal model and the software TurbSim [27]. The JONSWAP spectrum
 71 is applied to compute irregular waves. To keep the simulation setup as simple as possible and to be in ac-
 72 cordance with the OC3 study [25], currents, second-order and breaking waves, local vibrations, degradation
 73 effects, and soil conditions are not taken into account. These common assumptions might affect the precise
 74 lifetimes values, but do not limit the general conclusions.

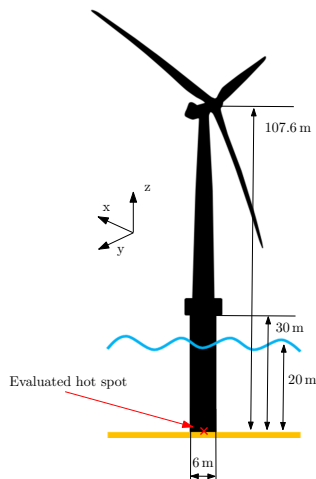


Figure 2: Visualization of the OC3 monopile and the NREL 5 MW reference wind turbine. Inertial frame coordinate system: x downwind direction, y to the left when looking downwind, and z vertically upwards.

75

76 2.2. Probabilistic simulation approach

77 FAST is capable of simulating time series of forces and moments for a given set of EC. Ideally, the entire
 78 (20 year) design lifetime of a wind turbine would be simulated. However, due to computational limitations,
 79 this is hardly possible. Hence, to get well-founded lifetime approximations, it is not only necessary to
 80 calculate the resulting damages of each simulation (see Section 2.3), but also to use a representative set of
 81 load cases. These load cases should mirror the entire OWT lifetime. This can either be done by applying a
 82 deterministic, DLC based approach, as proposed by current standards [21] or a probabilistic approach [28].
 83 In any case, the damage extrapolation is based on a limited number of simulations so that fatigue damage
 84 designs become relatively uncertain. Here, a probabilistic bin based approach is utilized: the EMCS [28].
 85 This means: The wind speed range is split up into several bins of 2 m s^{-1} . In each wind speed bin, the
 86 same number of $N_{\text{bin}} = 100$ simulations is conducted. The use of a relatively high number of simulations
 87 in each bin (current standards recommend at least six simulations per bin) is required, since simulation
 88 results within each bin scatter significantly. Reasons for these highly uncertain loads within one and the
 89 same bin are, first, random realizations of the turbulent wind and the sea state (i.e. random seeds) [29],
 90 and second, other statistically distributed EC (e.g. wave heights or turbulence intensities) [28]. The EC for
 91 each simulation are determined by sampling from given statistical distributions. Hence, in each bin, MCS
 92 is applied. The difference to plain MCS is that more simulations are conducted for high wind speeds having
 93 very low occurrence probabilities, but leading to relatively high damages. Therefore, depending on the
 94 damage-wind speed correlation, the intensified sampling for high wind speeds by EMCS reduces the error
 95 due to limited sampling. To illustrate the EMCS approach, Fig. 3 shows the applied sampling distribution
 96 for wind speeds, being a piecewise defined Weibull distribution and no longer the real wind speed Weibull
 97 distribution (F_{Wbl}). For a detailed description, it is referred to the original source [28].

98 Dependent statistical distributions for seven EC (wind speed (F_{Wbl}) and direction, turbulence intensity,
 99 wind shear and wave height, period and direction) are taken from the database in Hübler et al. [26]. For
 100 this database, measurement data of the FINO3 measurement mast in the North Sea is used.

101 2.3. Lifetime calculation

102 To approximate the substructure lifetime, the lifetime fatigue damage has to be calculated. Therefore,
 103 the forces and moments for the most critical location are needed. The applied lifetime calculation procedure

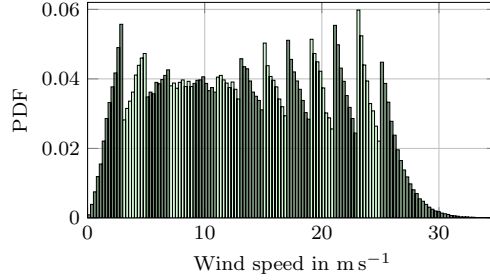


Figure 3: EMCS sampling distribution for wind speeds. Fairly homogeneous sampling due to applied bins, but in each bin samples are generated using truncated Weibull distributions and MCS leading to discontinuities at the boundaries of bins. Shading illustrates the bins.

104 [28] is briefly explained in the following: The monopile welds are exposed to higher fatigue damages compared to the rest of the monopile (e.g. plain steel plates), as stresses are concentrated in these hot spots (welds).
 105 Hence, in a first step, hot spot stresses are calculated according to Eurocode 3, part 1-9 [30]. As the stress concentration at transversal welds is more critical (a detail of 71 MPa according to Eurocode 3) than at
 106 longitudinal welds, only transversal welds are investigated. An additional stress concentration factor due to the size effect of the monopile wall thickness ($t > 25$ mm) is applied [30]. Since the considered monopile has
 107 a pure cylindrical shape and hot spots below mudline are not taken into account, the design driving location - being exposed to the highest bending moments - is at mudline. For this location marked in Fig. 2, the
 108 lifetime calculation is conducted.

109 In most cases, for monopiles, shear stresses (τ) are negligible compared to direct stresses (σ). Thence, the normal stress transverse to the weld can be approximated as follows:
 110
 111
 112

$$\sigma_{\perp} = \frac{F_z}{A} + \frac{\sqrt{M_x^2 + M_y^2}}{S}. \quad (1)$$

115 Here, F and M are forces and moments (cf. Fig. 4), A is the cross section area, and S is the section modulus.
 116 This procedure is a simplification, as the maximum normal stress is assumed and a directional dependence for different load cases is neglected ($M = \sqrt{M_x^2 + M_y^2}$).

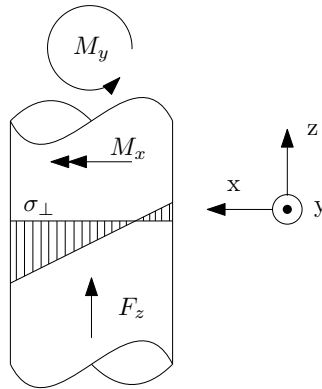


Figure 4: Illustration of relevant forces and moments acting on the monopile cross section.

117 For the normal stress, a rainflow counting evaluates the stress cycles and the linear damage accumulation
 118 according to the Palmgren-Miner rule is applied. The damage for each time series (j) in each wind speed
 119

120 bin (m) is calculated as follows:

$$D_{TS,j,m} = \sum_{i=1}^I \frac{n_i}{N_i}; \quad \forall j \in J(m), m \in M, \quad (2)$$

121 where n_i is the cycle number associated with the stress amplitude $\Delta\sigma_{\perp,i}$, N_i is the endurance (cycle number)
122 for the same stress amplitude, and I is the number of considered stress amplitudes. M and $J(m)$ are the
123 bin number and the number of time series depending on the bin, respectively. Since EMCS with 13 bins
124 and 100 samples per bin is applied, it follows $M = 13$ and $J(m) = 100$. The slope of the S-N curve is set to
125 three before and to five after the fatigue limit.

126 In general, the extrapolated lifetime damage (D_{LT}) is the weighted sum of the damages of all time series in
127 all wind speed bins:

$$D_{LT} = \sum_{m=1}^M \sum_{j=1}^{J(m)} \left(D_{TS,j,m} \frac{J_{\text{total}} Pr(m)}{J(m)} \right), \quad (3)$$

128 where J_{total} is the number of total time series during the lifetime (e.g. $6 \times 24 \times 365.25 \times 20$ for a 20-year
129 lifetime and 10-minute simulations). $Pr(m) = F_{Wbl}(b_m) - F_{Wbl}(a_m)$ is the occurrence probability of the
130 m th wind speed bin according to the real wind speed Weibull distribution (F_{Wbl}) and decreases for high
131 wind speeds. a_m and b_m are the minimum and maximum wind speeds of the m th bin, respectively. $Pr(m)$
132 is not related to the EMCS sampling distribution (piecewise defined Weibull distribution, cf. Fig. 3) that is
133 only relevant for the sampling.

134 However, since yearly realizations of the EC are needed for the economic model, here, yearly damages for
135 each year (t) are calculated first:

$$D_{\text{year},t} = \sum_{m=1}^M \sum_{j=1}^{J_y(m)} \left(D_{TS,j,m} \frac{J_{\text{total},y} Pr(m)}{J_y(m)} \right), \quad (4)$$

136 where $J_y(m)$ is the number of time series per year depending on the bin (assuming a lifetime of 20 years
137 $J_y(m) = 100/20 = 5$) and $J_{\text{total},y} = 6 \times 24 \times 365.25$ is the number of total time series during one year. Using
138 the same EC realizations, the annual electricity yield (Y_t) is calculated:

$$Y_t = \sum_{m=1}^M \sum_{j=1}^{J_y(m)} \left(P(v) \frac{J_{\text{total},y} Pr(m)}{J_y(m)} \right), \quad (5)$$

139 where $P(v)$ represents the realization of a cumulative power curve of all wind turbines of an OW farm at
140 wind speed v .

141 The damage after T years is the sum of the yearly damages:

$$D_{\text{sum}} = \sum_{t=1}^T D_{\text{year},t}. \quad (6)$$

142 If D_{sum} exceeds 1, the substructure lifetime (L) is reached. Hence, L can be determined by finding T^* being
143 the last value for T where $D_{\text{sum}} < 1$. Since the end of life will normally not be reached at the end of full
144 years, $D_{\text{sum}} = 1$ and therefore L is approximated by using partial years.

145 In this work, a probabilistic lifetime calculation is applied. Hence, Eqs. 4, 6, and the determination of L are
146 not evaluated once, but $N_{BT} = 10,000$ times using a bootstrap algorithm. This means: Having $N_{\text{bin}} = 100$
147 simulation results available in each bin, 5 samples per year - corresponding to 100 samples per 20 years design
148 lifetime - are drawn randomly with replacement from each bin. Therefore, for each bootstrap evaluation
149 (N_{BT}), different cases ($D_{TS,j,m}$) are randomly selected which leads to varying yearly damages ($D_{\text{year},t}$),
150 lifetimes (L), and electricity yields (Y_t). This bootstrap approach enables an uncertainty estimation due

151 to finite sampling in combination with varying EC and yields the lifetime PDF (cf. Fig. 5) as well as the
 152 electricity yield PDF. At this stage, it has to be clarified that the resulting variability of lifetime values
 153 is mainly due to the uncertain extrapolation process that is part of today's turbine designs. If the entire
 154 lifetime would be simulated, the variation would only be due to the long-term EC scattering, which is much
 155 smaller.

156 Since, for example, the reference design is not designed for the investigated OW farm site, quite damaging
 157 load cases for fault conditions are not taken into account, and safety factors - like the material safety factor
 158 - are not applied, the calculated lifetime does not match the 20-year design lifetime, but is significantly
 159 higher (by a factor of about 75). This is not problematic, since this is an exemplary study that does not
 160 intend to actually find the best design. However, to ensure reasonable results for the economic viability,
 161 substructural lifetimes have to be close to realistic project durations (typically 20 years). Therefore, all
 162 lifetimes are normalized using the 5th percentile of the lifetime of the reference design (i.e. it is assumed that
 163 the reference design lifetime is at least 20 years with a probability of 95 %).

164 2.4. Cost model for the substructure

165 The cost model for the substructure CAPEX is based on Häfele and Rolfes [8]. Some changes are made
 166 to adjust this model to monopiles. For example, welding costs are significantly lower for monopiles, as
 167 the welding is automated. It is assumed that the substructure CAPEX (C_{sub}) consists of costs for the
 168 monopile (C_{mono}), the transition piece (C_{TP}), the tower (C_{tower}), and secondary components (C_{add}) (e.g.
 169 boat landings, etc.):

$$C_{sub} = C_{mono} + C_{TP} + C_{tower} + C_{add}. \quad (7)$$

170 Since only slight design variations are carried out, it can be assumed that transition piece, tower, and
 171 secondary components are not significantly affected. Therefore, their costs per mass can be set to constant
 172 values (see Table 1). Monopile costs are further divided into raw material costs (C_{mat}), welding costs
 173 (C_{weld}), fixed production costs (C_{prod}), and coating costs (C_{coat}):

$$C_{mono} = C_{mat} + C_{weld} + C_{prod} + C_{coat}. \quad (8)$$

Table 1: CAPEX for various parts and aspects. Adapted using several sources.

Cost type	Cost	Adapted sources
C_{TP}	2600 EUR/t	[11]
C_{tower}	2500 EUR/t	[31]
C_{add}	5900 EUR/t	[11]
C_{mat}	920 EUR/t	[11, 32]
C_{weld}	0.33 MEUR/m ³	[11, 32]
C_{prod}	0.20 MEUR	[11, 32]
C_{coat}	200 EUR/m ²	[11, 33]

174 Here, the material costs are proportional to the mass, the welding costs to the weld volume, and the coating
 175 costs to the surface area. For the coating costs, an initial (onshore) coating (down to 5 m below mudline)
 176 and an additional (offshore) patch coating of 2% of the surface area are assumed. This leads to the relatively
 177 high costs per m².
 178

179 2.5. Design of substructures

180 To analyze the effect of substructural design variations on lifetimes and costs, and in the end on the eco-
 181 nomic viability, a reference structure is needed. As stated in Section 2.1, this reference is the well-established
 182 OC3 monopile substructure with the NREL 5 MW turbine. In this study, seven design variations are in-
 183 vestigated: the reference OC3 monopile, three more durable designs (with increased wall thicknesses and

diameters of the monopile) and three cheaper ones (decreased thicknesses and diameters). The design changes are summarized in Table 2.

Table 2: Analyzed substructures with small design changes.

Design	Abbreviation	Change in diameter	Change in wall thickness
Reference	Ref	–	–
Design 2	D+	+1 %	–
Design 3	D–	–1 %	–
Design 4	t+	–	+2 %
Design 5	t–	–	–2 %
Design 6	Dur	+1 %	+2 %
Design 7	Chp	–1 %	–2 %

3. Economic viability model

In order to measure the cost-efficiency of substructure designs, an economic viability model for financial analyses of wind farms is applied in a simulation study of a project located in the German Exclusive Economic Zone of the North Sea. The economic viability model is an extension of the model presented in Piel et al. [34]. It simulates an economic agent to depict the investment decisions of real-world corporations investing in OW farms. The economic viability model is reformulated as an optimization problem. It yields the required minimum sales price per unit of generated electricity - the marginal cost (in ct/kWh) - for which the analyzed OW farm would exactly meet the investment criteria of both debt (see Section 3.2) and equity (see Section 3.3) investors taking into account each substructure design separately (see Section 3.4). The marginal cost is comparable to the LCOE and has a similar meaning [34]. However, as it considers the specific project finance characteristics (see Sections 3.1-3.3). It allows for more precise financial analyses of OW farms. Consequently, the marginal cost is utilized as the competitiveness criterion for the comparison of substructure designs according to the following rationale: The lower the marginal cost of the OW farm, the higher the cost-efficiency of the analyzed substructure design.

3.1. Cash-flow simulation

The economic viability model combines a state-of-the-art cash-flow calculation for OW farms oriented towards Piel et al. [34] with the MCS approach of the aero-elastic OWT model. This enables the simulation of uncertain cash-flows using the $N_{BT} = 10,000$ realizations provided by the aero-elastic OWT model for the annual gross electricity yield and the turbine lifetime as well as CAPEX of the different substructure designs. For every turbine of the investigated OW farm, the cash-flows are simulated until the end of the corresponding lifetime realization (i.e. no electricity is produced by a turbine after reaching its end of life, $Y_t = 0 \forall t > T^*$). The cash-flow simulation is based on an income statement and a cash-flow statement, as shown in Table 3. Both statements are simulated for each year of the project life cycle and each MCS iteration. This yields PDF estimations of the unlevered FCF, which serve as the basis for the debt sculpting in Section 3.2 and the project valuation in Section 3.3.

Table 4 shows the project characteristics of the OW farm under investigation to which the cash-flow simulation is applied. The cost data is derived from Reimers and Kaltschmitt [35] using their experience curve theory model in consideration of an estimated total installed wind energy capacity of 741.70 GW (34 GW offshore [36]) in 2020 [37]. The financing data is oriented towards the cost of capital forecast for German OW farms commissioned in 2020 from Prognos and Fichtner [5]. The tax data refers to the German tax legislation. The annual revenues $R_{i,t} = p \cdot Y_{i,t} \cdot NOH$ are calculated by multiplying the sales price per unit of generated electricity p by the gross electricity yield $Y_{i,t}$ and the net operating hours NOH in each year

Table 3: Income and cash-flow statements.

Income statement	Cash-flow statement
Revenues	EBIT
– OPEX	– Taxes on EBIT
= EBITDA	+ Depreciation
– Depreciation	+ Decommissioning provision expenses
– Decommissioning provision expenses	– CAPEX
= EBIT	– Decommissioning expenses
	= Unlevered free cash-flow

Table 4: Project characteristics of the OW farm under investigation.

General data		Cost data	
Distance to shore	10 km	CAPEX	
Distance to port	20 km	-Project development	110 MEUR
Water depth	20 m	-Installation	2.4 MEUR/turb.
Commissioning date	01.01.2020	-Rotor, nacelle and tower	8.2 MEUR/turb.
Wind turbines	80 NREL 5 MW	-Substructure	Substructure costs
Total capacity	400 MW	-Insurance and financing	36 MEUR
OW farm efficiency	74 %	OPEX	
Net operating hours	6500 h/turb.	-Operation & maintenance	0.20 MEUR/turb.
Wind resource	Wind speed PDF	-Insurance	0.10 MEUR/turb.
Project duration	Lifetime PDF	Decommissioning expenses	0.51 MEUR/turb.
Tax data		Financing data	
Corporate tax	31 %	Unlevered cost of capital	5.6 %
Straight line depreciation	16 years	Cost of debt	3.5 %
Provision expenses	Discounted at 5.5 %	Debt service period	16 years

219 $t = (0, \dots, T_i)$, where T_i represents the total project life cycle length. The net operating hours are derived
220 from the OW farm efficiency stated in Prognos and Fichtner [5]. All probabilistic parameters are denoted
221 by the index $i = (1, \dots, N_{BT})$ with N_{BT} as the number of MCS iterations.

222 3.2. Debt sculpting

223 In recent years, OW farms were, to a large extent, funded via non-recourse project finance which typically
224 features high shares of debt [38]. The debt-to-equity ratio can be optimized by means of a debt sculpting
225 model based on the unlevered FCF resulting from the cash-flow simulation. Optimizing the debt-to-equity
226 ratio utilizes the leverage effect of debt financing, which increases the profitability from equity investors'
227 perspective, if the cost of debt is lower than the IRR [39]. In order to optimally utilize the leverage effect,
228 the debt sculpting model yields the maximum amount of debt capital that can be raised such that the
229 investment criteria of debt investors are exactly met. In project financing, debt investors typically consider
230 a certain DSCR target as their investment criteria. The DSCR measures the coverage of the contractual debt
231 service by the cash-flow available for debt service [40]. Based on the DSCR target, debt sculpting entails
232 calculating the repayment schedule of debt capital such that the debt service, including interest payments
233 and principal repayments, is tailored to the cash-flow available for debt service (here: unlevered FCF) [40].
234 Consequently, the debt sculpting ensures that a minimum DSCR is maintained in each year of the debt
235 service period.

236 The DSCR is calculated as follows:

$$DSCR_{i,t} = \frac{FCF_{i,t}}{INT_t + P_t}; \quad \forall i \in N_{BT}, t \in T_{Debt}, \quad (9)$$

237 where $FCF_{i,t}$ is the unlevered FCF, INT_t is the annual interest payment, $P_{i,t}$ is the annual principal
 238 repayment, and T_{Debt} is the length of the entire debt service period. Based on a predefined minimum DSCR
 239 target, the maximum debt service capacity is calculated as follows:

$$DSC_t = \frac{F_{FCF,t}^{-1}(\alpha)}{\beta}; \quad \forall t \in T_{Debt}, \quad (10)$$

240 where $F_{FCF,t}^{-1}$ is the inverse of the unlevered FCF CDF, α is a confidence level, and β is the predefined
 241 minimum DSCR target. Both α and β represent the investment requirements of debt investors. Debt
 242 investors of OW farms are typically willing to invest, if the DSCR is equal to $\beta = 1.2$ with a confidence of
 243 $1 - \alpha = 75\%$ throughout all debt service periods [40]. A DSCR greater than one implies that the project
 244 is able to cover the debt service in a specific period by the FCF generated in the same period, and thus,
 245 indicates the soundness of the project corporation. Given that the debt capital is raised in form of zero
 246 coupon bonds, the maximum amount of debt capital is derived from the debt service capacity as follows:

$$D = \sum_{t=1}^{T_{Debt}} \frac{DSC_t}{(1+r_d)^t}, \quad (11)$$

247 where r_d is the cost of debt. Zero coupon bonds do not pay any interest and their principal is the amount to
 248 be repaid at the time to maturity. Thus, with coupon-stripping any bond can be separated into individual
 249 securities each representing a zero coupon bond selling at different discounts depending on the time to
 250 maturity [41]. This property enables sculpting the debt to the debt service capacity in each individual
 251 debt service period such that the summed security values equal the maximum amount of debt capital to be
 252 raised. Based on the latter, the principal repayments (P_t) and interest payments (INT_t) can be calculated
 253 as follows:

$$P_t = \frac{DSC_t}{(1+r_d)^t}; \quad \forall t \in T_{Debt} \quad (12)$$

254 and

$$INT_t = DSC_t - P_t; \quad \forall t \in T_{Debt}. \quad (13)$$

255 Due to the debt sculpting, the sum of principal repayments and interest payments is equal to the debt
 256 service capacity in each year of the debt service period. This ensures that the minimum DSCR target of the
 257 debt investors is fulfilled and the maximum amount of debt capital is raised.

258 3.3. Valuation

259 In order to enable the evaluation of the OW farm profitability, the present economic viability model
 260 utilizes the APV method to estimate a PDF of the project value by discounting the unlevered FCF to the
 261 valuation date. Following Myers [42], the APV method is applied as follows:

$$APV_i = \sum_{t=0}^{T_i} \frac{FCF_{i,t}}{(1+r_e)^t} + \frac{\tau \cdot INT_t}{(1+r_d)^t}; \quad \forall i \in N_{BT}, \quad (14)$$

262 where τ is the corporate tax rate and r_e is the unlevered cost of equity. In market-oriented financing and
 263 industrialized economies, the alternative WACC method is widely used. The APV method is applied to
 264 valuing investments in economies of high uncertainty and scarce financial markets where stable debt-to-
 265 equity ratios are hard to obtain [43]. As the latter applies to OW farms, the use of the APV method is
 266 the best choice [44]. This is due to the explicit tax-shield consideration, which represents tax advantages
 267 arising from debt financing, in the second fraction of the APV equation. The APV method enables a
 268 straightforward tax-shield adjustment for changes in the debt-to-equity ratio during the project life cycle.
 269 However, if consistently applied, the alternative WACC method with the corresponding NPV would lead to
 270 the same project value [34].

3.4. Marginal cost calculation

The combination of cash-flow simulation, debt sculpting, and APV method yields several KPI in the form of PDF. These KPI are the basis for the optimization model that quantifies the marginal cost of the analyzed OW farm. As the implementation of wind farms depends on balancing the interests of both equity and debt investors, the optimization model considers an economic agent that represents the perspectives of both groups of decision-makers. By keeping the investment behavior of real-world corporations in the realm of wind farms, the economic agent measures the soundness of the analyzed project from debt investor perspective by way of the DSCR and utilizes the APV to analyze the profitability from equity investor perspective. A simple mathematical formulation of the optimization problem is as follows:

$$\text{Minimize } p \quad \text{subject to} \quad (15)$$

$$E(APV) \geq 0 \quad (16)$$

and

$$F_{DSCR,t}^{-1}(\alpha) \geq \beta; \quad \forall t \in T_{Debt}, \quad (17)$$

where $E(APV)$ is the expected APV and $F_{DSCR,t}^{-1}$ is the inverse of the DSCR CDF. The optimization model minimizes the sales price per unit of generated electricity p by accounting for the trade-off between APV and DSCR, which is strongly influenced by the debt share. The first constraint represents the general investment requirement of the equity investors. It determines that they are willing to invest, if the expected APV is nonnegative. This is equivalent to an expected (unlevered) IRR that is equal to or greater than the (unlevered) cost of capital - a typical investment rule of equity investors of OW farms [45]. Accordingly, the second constraint represents the investment requirement of the debt investors.

In order to find an analytical solution for the optimization problem, a derivative of the expected APV with respect to p is used:

$$\frac{dE(APV)}{dp} = (1 - \tau) \cdot \sum_{t=1}^T \frac{E(Y_t)}{(1 + r_e)^t} + \tau \cdot (1 - \tau) \cdot \sum_{t=1}^{T_{Debt}} \frac{\frac{F_{Y,t}^{-1}(\alpha)}{\beta}}{(1 + r_d)^t} \cdot (1 - (1 + r_d)^{-t}), \quad (18)$$

where T is the maximum total project life cycle length for all iterations, $E(Y_t)$ is the expected electricity yield, and $F_{Y,t}^{-1}(\alpha)$ with $1 - \alpha = 75\%$ is the 25th percentile of the electricity yield. The mathematical derivation of Eq. 18 using Eq. 14 is given in Appendix A. The first addend refers to the discounting of the unlevered FCF in the APV method. The second addend refers to the discounting of the tax-shields and is based on the second constraint. By means of the revenues, the sales price per unit of generated electricity p affects the unlevered FCF as well as the tax shield. The latter is based on p due to the debt sculpting, which maximizes the amount of debt financing, and thus, determines the interest payments considered in the tax shield calculation. The derivative measures the sensitivity of changes in the expected APV with respect to a change in p .

Since the APV in Eq. 14 is linear in the price p (cf. Appendix A), the exact solution of the optimization problem can be found by means of the derivative. The cash-flow simulation, debt sculpting, and APV method are conducted using an initial guess $p_{initial} \in \mathbb{R}^+ \setminus \{0\}$. Afterwards, the minimum sales price per unit of generated electricity is calculated as follows:

$$p^* = p_{initial} - \frac{E(APV)}{\frac{dE(APV)}{dp}}, \quad (19)$$

where the second subtrahend represents the change of the initial guess necessary to set the expected APV exactly to zero. As stated in Section 3, the resulting minimum sales price per unit of generated electricity p^* represents the marginal cost and thus the competitiveness criterion.

Table 5: Approximated substructure costs and lifetimes.

Design	Substructure costs in MEUR	Difference	Expected substructure lifetime in years	Difference	Coefficient of Variation of the lifetime
Ref	2.84	–	23.4	–	0.086
D+	2.87	+1.09 %	26.6	+13.9 %	0.091
D–	2.81	–1.09 %	22.7	–3.08 %	0.066
t+	2.88	+1.32 %	26.7	+14.2 %	0.076
t–	2.80	–1.30 %	21.0	–10.1 %	0.094
Dur	2.91	+2.46 %	30.2	+29.2 %	0.068
Chp	2.78	–2.33 %	17.3	–26.0 %	0.084

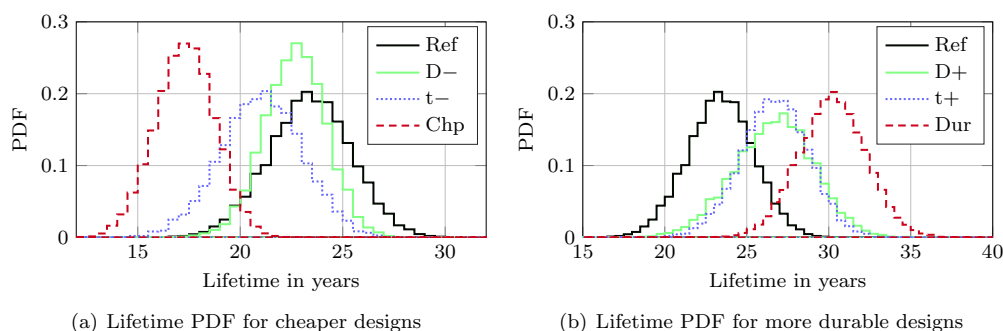


Figure 5: Lifetime PDF for different substructure designs.

4. Results

4.1. Lifetimes and substructure costs

State-of-the-art design investigations for OWT frequently focus on the structural mass. However, relevant outputs for investors rather concern the cost-efficiency. Consequently, the presented engineering and economic models are combined to focus on the relevant economic results. Nevertheless, as the outputs of the aero-elastic OWT model - substructure lifetimes and CAPEX - are needed for the financial analyses (cf. Fig. 1), first, these intermediate results are presented in brief.

The approximated costs of all seven substructures are summarized in Table 5. The lifetime distributions are shown in Fig. 5 and indicate the effect of design variations on the lifetime. On the one hand, decreased diameters and wall thicknesses result in lower costs. On the other hand, the mean lifetimes of these designs decrease as well. Analogical results are apparent for the durable designs, which have higher costs, but also higher mean lifetimes than the reference design. This trade-off between costs and lifetime leads to opposite effects concerning the profitability and soundness of the OW farm. It has to be further analyzed to assess the overall effect on the cost-efficiency of the substructure designs.

Before analyzing the cost-efficiency, the lifetime distributions are briefly discussed. Figure 5 shows that substructure lifetimes between about 12 and 40 years are possible. If substructure lifetimes are very low for cheap designs, the whole OWT can only be operated for this limited period. However, for durable designs, it is questionable whether the whole OWT can be run for the increased substructure lifetime. Lifetimes of other components (e.g. rotor blades) will limit the overall lifetime in this case. Hence, the positive effect of durable designs is overestimated. Since a lifetime extension of some years for other parts might be possible, while an extension of more than about 10 years is definitely unrealistic, in a second step, the overall lifetime is limited to 20, 25, and 30 years. Exemplary, for a limit of 30 years, the adjusted lifetime PDF are displayed in Fig. 6. Here, the difference to the unlimited lifetime is mainly visible for the durable design. However,

330 for a limitation of 20 years (not shown), the lifetime distributions of all design are significantly “truncated”
 331 and the more durable designs have constant lifetimes of 20 years.

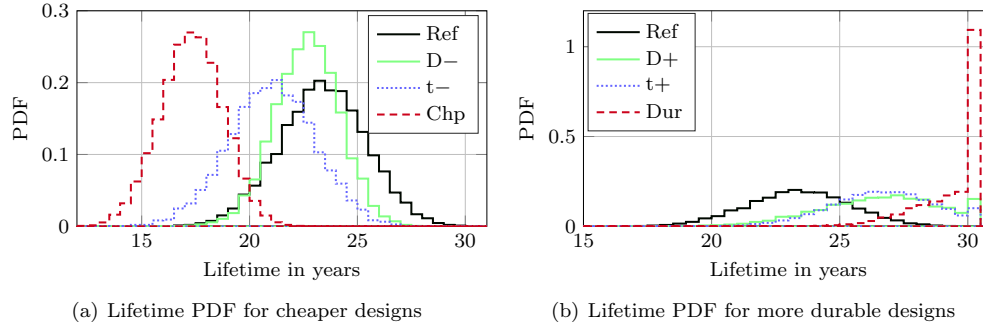


Figure 6: Lifetime PDF for different substructure designs using a maximum lifetime of 30 years.

331

332 4.2. Cost-efficiency

333 In consideration of the outputs of the aero-elastic OWT model, the economic viability model is applied
 334 to the project characteristics of the OW farm given each substructure design separately. Figure 7 shows the
 335 results of the optimization model for the reference substructure design. For a sales price of 8.57 ct/kWh,
 336 the following applies: $E(APV) = 0$ and $F_{DSCR,t}^{-1}(25\%) = 1.2$. The APV PDF mean value is nil (see
 337 Fig. 7(a)) and the 25th percentiles of the DSCR PDF are equal to the DSCR target of 1.2 (see Fig. 7(b)).
 338 Hence, the investment criteria of both equity and debt investors are exactly fulfilled, which means that the
 339 marginal cost is equal to the estimated sales price. The economic viability model is congruently applied
 340 to the other substructure designs. Table 6 shows the calculated marginal cost of all substructure designs
 341 and their percentage deviations from the marginal cost of the reference design. To enable an additional
 342 design comparison by means of the APV, the resulting APV PDF of the OW farm for each design given the
 343 marginal cost of the reference design are shown in Figs. 8 to 10. In addition, the corresponding expected
 344 APV and expected unlevered IRR are shown in Table 7. The unlevered IRR is used to compare the results
 345 for different substructures, as it is independent of a project’s individual leverage which changes for the
 346 considered substructure design. As the marginal cost for the reference design is used, the corresponding
 347 expected APV is equal to zero and the expected unlevered IRR is equal to the unlevered cost of capital.
 348 The results show that - for the unlimited lifetime (“unltd”) - the analyzed OW farm has the lowest marginal
 349 cost in consideration of the durable substructure design (Dur), which has the highest cost, but longest
 350 expected lifetime. Consequently, following the defined competitiveness criterion, the durable design is the
 351 most cost-efficient solution among all substructure designs. Accordingly, the cheapest substructure design
 352 (Chp) is least cost-efficient and has the highest marginal cost. Taking all substructure designs into account,
 353 the results indicate that the marginal cost decreases with increasing diameters and wall thicknesses. Hence,
 354 for the present setup (i.e. turbine, project characteristics, minor design variations, etc.), it holds true that
 355 the more durable a substructure design, the more competitive it is compared to the reference design, and
 356 vice versa.

357 As discussed before, an unlimited lifetime is not realistic, as other turbine parts are not considered. If a
 358 limitation of the lifetime to 25 or 30 years is introduced (“max25” and “max30”), the APV PDF of the more
 359 durable designs feature a negative skewness (see Fig. 9(b)), as they highly dependent on the lifetime PDF
 360 that are also skewed due to the “truncation”. The positive effects of increased durability decrease, as the
 361 total lifetime potential of these substructure designs is not fully used (i.e. the durable design cannot exploit
 362 its full lifetime of up to 40 years). This means that the cost-efficiency of the more durable design variations
 363 is overestimated for the unlimited case. Nevertheless, although the durable design is overdesigned in the
 364 limited cases (“max25” and “max30”), it is still the most cost-efficient one. Hence, for the investigated
 365 monopile, it is reasonable to slightly overdesign the substructure to guarantee the design lifetime and even

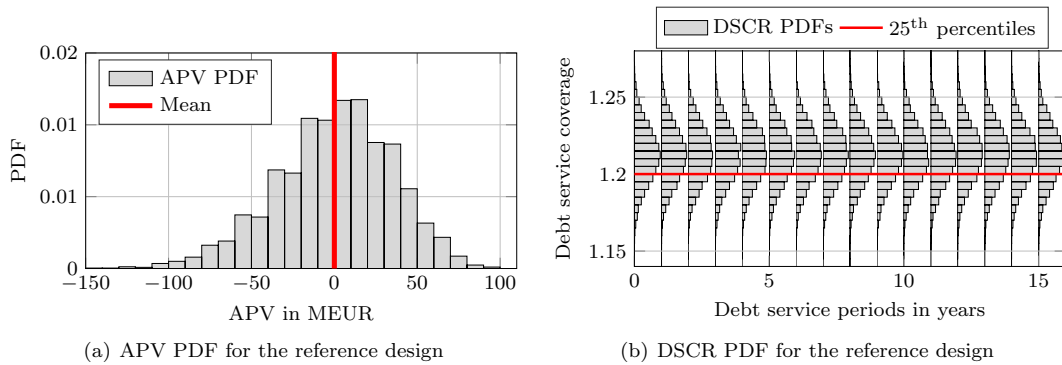


Figure 7: APV and DSCR PDF for the reference substructure design.

366 a lifetime extension of several years.

367 If it is assumed that the lifetime of other turbine parts cannot be extended and the overall lifetime is
 368 limited to 20 years (“max20”), it becomes clear that a significant overdesign (e.g. the durable design with
 369 an expected lifetime of more than 30 years, i.e. the substructure lifetime exceeds the fixed turbine lifetime
 370 by 50 % on average) will lead to less cost-efficiency. Table 6 shows that for this case, a cheaper design (D–)
 371 is the most cost-efficient solution. This means that in some cases, reduced lifetimes can even be beneficial.
 372 Furthermore, variances of the APV PDF decrease significantly given a lifetime limitation of 20 years (cf. Fig.
 373 10(b)), since then, for most designs, the lifetime is constant. Hence, the marginal cost of the substructure
 374 designs differs only slightly, except for the cheapest design that features lifetimes below 20 years with a
 375 significant probability. From this, it follows that cheap designs with expected lifetimes significantly lower
 376 than 20 years should be avoided and that longer lifetimes using more durable designs are promising in most
 377 cases.

378 The results for the expected APV and unlevered IRR shown in Table 7 confirm the findings from the
 379 comparison according to the marginal cost. The highest expected APV can be achieved with the most
 380 durable substructure design. The cheapest design results in the lowest expected APV. The same holds true
 381 for the unlevered IRR. A comparison of Figs. 8(b) and 9(b) makes clear that the advantage of the durable
 382 design decreases for more realistically limited maximum lifetimes. Although the lifetime restriction to 30
 383 years only affects more durable designs (cf. Fig. 6), these designs are still most competitive. In contrast,
 384 lifetimes are strictly limited to the design lifetime of 20 years, all designs are affected (cf. Fig. 10), since for
 385 all lifetime PDF, a significant part above 20 years is “truncated”. Given this lifetime limitation, the more
 386 durable designs lead to quite similar results, as they have nearly constant lifetimes of 20 years. Cheaper
 387 designs become much more competitive. In this case, the design with a reduced diameter (D–) is the most
 388 cost-efficient one, as it has lower substructure costs (cf. Table 5), but the lifetime still reaches the maximum
 389 of 20 years with a probability of about 95 % (cf. Fig. 5). The most durable design (Dur) - being the best
 390 design for less limited lifetimes - has even slightly lower expected APV and unlevered IRR than the reference
 391 case. The reason are higher CAPEX for the substructure, whereas the lifetime cannot be increased due to
 392 the limitation to 20 years.

393 5. Discussion, limitations and outlook

394 The effects of substructural design variations on the OW farm’s economic viability using an interdisci-
 395 plinary, probabilistic simulation approach that combines engineering and economic models are analyzed. It
 396 becomes apparent that even small changes in the designs can lead to significantly different marginal cost
 397 for OW farms. Results indicate that the effect of varying lifetimes exceeds the effect of changes in initial
 398 costs. This means that for the considered OW farm, more durable designs with higher lifetimes outperform
 399 cheaper designs. This implies strong incentives for investors to make rather sustainable investment decisions

Table 6: Marginal cost (in ct/kWh) given each substructure design and different maximum lifetimes (unltd: unlimited, max30: maximum of 30 years, max25: maximum of 25 years, max20: maximum of 20 years). Best designs in bold.

Design	Marginal cost (in ct/kWh)				Deviation from Ref			
	unltd	max30	max25	max20	unltd	max30	max25	max20
Ref	8.57	8.57	8.59	8.99	0.00 %	0.00 %	0.23 %	4.84 %
D+	8.28	8.28	8.44	8.99	-3.44 %	-3.39 %	-1.57 %	4.91 %
D-	8.64	8.64	8.64	8.97	0.76 %	0.76 %	0.79 %	4.68 %
t+	8.27	8.27	8.43	9.00	-3.50 %	-3.48 %	-1.71 %	4.94 %
t-	8.85	8.85	8.85	9.03	3.25 %	3.25 %	3.26 %	5.40 %
Dur	8.03	8.08	8.41	9.01	-6.29 %	-5.70 %	-1.87 %	5.08 %
Chp	9.50	9.50	9.50	9.51	10.9 %	10.9 %	10.9 %	10.9 %

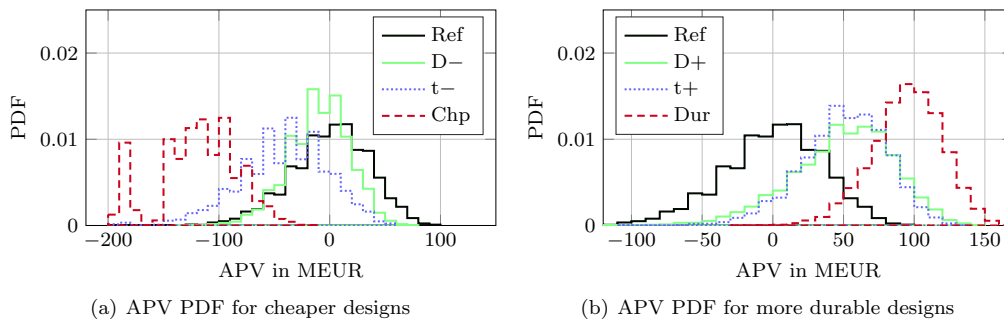


Figure 8: APV PDF for different substructure designs.

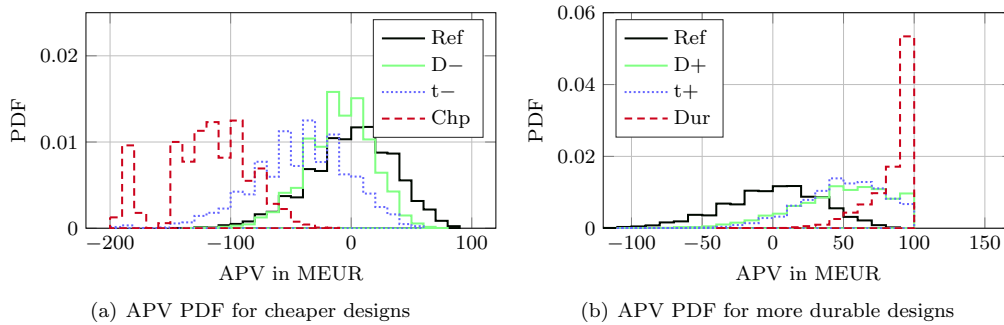


Figure 9: APV PDF for different substructure designs using a maximum lifetime of 30 years.

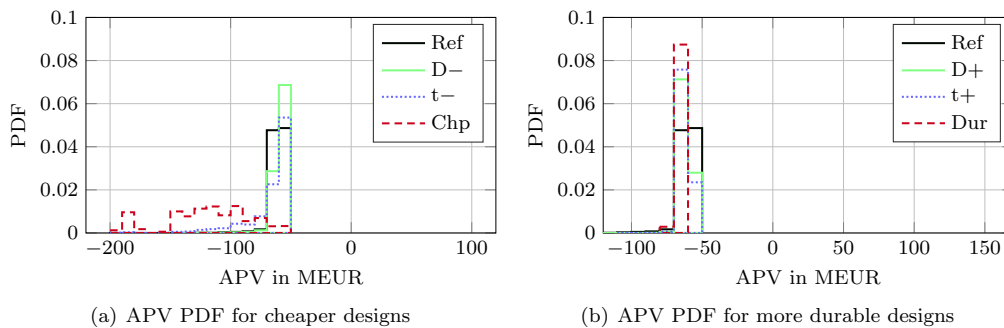


Figure 10: APV PDF for different substructure designs using a maximum lifetime of 20 years.

Table 7: APV and IRR given each substructure design. Best designs in bold.

Design	APV in MEUR				IRR in %			
	unltd	max30	max25	max20	unltd	max30	max25	max20
Ref	0	-0.00	-3.14	-61.0	5.56	5.56	5.52	4.54
D+	49.4	48.6	21.8	-61.9	6.25	6.24	5.91	4.53
D-	-10.1	-10.1	-10.6	-58.9	5.42	5.42	5.42	4.58
t+	50.4	50.0	23.8	-62.3	6.27	6.27	5.95	4.53
t-	-41.7	-41.7	-41.9	-67.2	4.84	4.84	4.84	4.39
Dur	95.1	85.4	26.3	-64.1	6.76	6.67	5.98	4.50
Chp	-125	-125	-125	-125	2.94	2.94	2.94	2.94

400 regarding turbine substructures.

401 The present analyses are limited to a single monopile design (including small design variations). Therefore,
 402 a general validity of these results is not given. Especially for other substructure types, the trade-off between
 403 lifetime and CAPEX might be differently valued. If the substructure CAPEX are higher, being the case for
 404 jackets or floating substructures, the economic advantage of longer lifetimes will be smaller or even diminish.
 405 The results of the “max20” case indicate that sometimes it might be even beneficial to reduce lifetimes, if
 406 this limits the CAPEX.

407 For the sake of simplicity, OPEX are considered to be constant for all designs and over time. For a more
 408 realistic representation, in future research, the influence of variable OPEX should be investigated as well.
 409 Normally, cheaper designs cause higher OPEX. Another limitation of the analyses refers to the constant
 410 unlevered cost of capital and the corresponding effect of discounting on the trade-off between lifetime and
 411 CAPEX. Higher unlevered cost of capital, as for example, caused by country risk premiums, significantly
 412 reduces the impact of cash-flows in later years due to a higher discounting such that the economic effect of
 413 lifetime extensions becomes less important, and vice versa.

414 Regardless the type of effect, the combined engineering and economic analysis clarifies that the lifetime
 415 should not be considered as a constant. It should be included as an important variable that has to be
 416 optimized relative to the corresponding CAPEX by analyzing the economic effect of their trade-off.

417 This leads to some open issues that should be addressed by upcoming work: First, so far, only the effect
 418 of different designs was analyzed. As noted before, in future optimizations, the OWT lifetime should be
 419 regarded as a variable. Hence, such an optimization of the substructure taking into account an optimal
 420 lifetime would be beneficial. It might lead to significantly different “optimal” structures compared to opti-
 421 mizations using constant lifetimes. Second, such future optimizations should also consider variable unlevered
 422 cost of capital, which depend on the risk inherent to the analyzed substructure design. For example, more
 423 durable designs decrease the overall project risk and should thus slightly reduce the unlevered cost of capital
 424 due to a lower beta factor (risk measure), and vice versa. This could further increase the cost-efficiency
 425 of durable substructure designs. Third, so far, only the design of the substructure was varied. The whole
 426 economic viability topic using probabilistic, interdisciplinary analyses can be applied to other turbine parts
 427 as well. Hence, upcoming work should also address other components (e.g. blades). The inclusion of other
 428 components will probably lead to even more pronounced differences in the marginal cost.

429 Appendix A

The purpose of this derivation is to show the derivative of the expected APV with respect to the sales price per unit of generated electricity (cf. Eq. 18):

$$\frac{dE(APV)}{dp} = (1 - \tau) \cdot \sum_{t=0}^T \frac{E(Y_t)}{(1 + r_e)^t} + \tau \cdot (1 - \tau) \cdot \sum_{t=0}^{T_{Debt}} \frac{F_{Y,t}^{-1}(\alpha)}{(1 + r_d)^t} \cdot (1 - (1 + r_d)^{-t}).$$

The starting point is the adjusted present value in Eq. 14. The APV can be split in two addends, the unlevered APV ($uAPV_t$) and the discounted tax shield (DTS_t):

$$\begin{aligned} APV &= \sum_{t=0}^T \frac{FCF_t}{(1+r_e)^t} + \frac{\tau \cdot INT_t}{(1+r_d)^t} \\ &= \sum_{t=0}^T uAPV_t + DTS_t. \end{aligned}$$

$$\frac{dE(APV)}{dp} = \frac{d}{dp} E \left[\sum_{t=0}^T uAPV_t \right] + \frac{d}{dp} E \left[\sum_{t=0}^{T_{Debt}} DTS_t \right].$$

Using Table 3, the first addend of the APV equation - the unlevered APV - can be rearranged as follows, where we denote depreciation as DEP , decommissioning expenses as $DECEX$, its provisions as PDC , and the taxes on EBIT as TAX_t :

$$\begin{aligned} \frac{d}{dp} E \left[\sum_{t=0}^T uAPV_t \right] &= \frac{d}{dp} E \left[\sum_{t=0}^T \frac{FCF_t}{(1+r_e)^t} \right] \\ &= \frac{d}{dp} E \left[\sum_{t=0}^T \frac{EBIT_t - TAX_t - CAPEX_t - DECEX_t + DEP_t + PDC_t}{(1+r_e)^t} \right]. \end{aligned}$$

It is assumed that $CAPEX_t$, $DECEX_t$, DEP_t , and PDC_t are independent of p and constant in our case. Therefore, we can simplify as follows:

$$\begin{aligned} \frac{d}{dp} E \left[\sum_{t=0}^T uAPV_t \right] &= \frac{d}{dp} E \left[\sum_{t=0}^T \frac{EBIT_t - TAX_t}{(1+r_e)^t} \right] \\ &= \frac{d}{dp} E \left[\sum_{t=0}^T \frac{EBIT_t - \tau \cdot EBIT_t}{(1+r_e)^t} \right] \\ &= \frac{d}{dp} E \left[\sum_{t=0}^T \frac{EBIT_t \cdot (1-\tau)}{(1+r_e)^t} \right] \\ &= \frac{d}{dp} E \left[\sum_{t=0}^T \frac{(R_t - (OPEX_t + DEP_t + PDC_t)) \cdot (1-\tau)}{(1+r_e)^t} \right]. \end{aligned}$$

DEP_t , and PDC_t are still independent of p and constant. The same holds true for $OPEX_t$. However, it is conceivable that specific contractual arrangements feature dependency on the revenues and thus on the price p . An example could be the land lease. As we assume turbine dependent $OPEX_t$, they are independent of p and constant in our case. It follows:

$$\begin{aligned} \frac{d}{dp} E \left[\sum_{t=0}^T uAPV_t \right] &= \frac{d}{dp} E \left[\sum_{t=0}^T \frac{R_t \cdot (1-\tau)}{(1+r_e)^t} \right] \\ &= \frac{d}{dp} E \left[\sum_{t=0}^T \frac{Y_t \cdot p \cdot (1-\tau)}{(1+r_e)^t} \right] \\ &= (1-\tau) \cdot \sum_{t=0}^T \frac{E(Y_t)}{(1+r_e)^t}. \end{aligned}$$

For the second addend - the tax shield (TSt), Eqs. 9 to 13 and Table 3 are used for the following rearrangements:

$$\begin{aligned}
\frac{d}{dp} E \left[\sum_{t=0}^{T_{Debt}} DTS_t \right] &= \frac{d}{dp} E \left[\sum_{t=0}^{T_{Debt}} \frac{TS_t}{(1+r_d)^t} \right] \\
&= \frac{d}{dp} E \left[\sum_{t=0}^{T_{Debt}} \frac{\tau \cdot INT_t}{(1+r_d)^t} \right] \\
&= \frac{d}{dp} E \left[\sum_{t=0}^{T_{Debt}} \frac{\tau \cdot (DSC_t - P_t)}{(1+r_d)^t} \right] \\
&= \frac{d}{dp} E \left[\sum_{t=0}^{T_{Debt}} \frac{\tau \cdot \left(DSC_t - \frac{DSC_t}{(1+r_d)^t} \right)}{(1+r_d)^t} \right] \\
&= \frac{d}{dp} E \left[\sum_{t=0}^{T_{Debt}} \frac{\tau \cdot DSC_t}{(1+r_d)^t} \cdot \left(1 - (1+r_d)^{-t} \right) \right] \\
&= \frac{d}{dp} E \left[\sum_{t=0}^{T_{Debt}} \frac{\tau \cdot \frac{F_{FCF,t}^{-1}(\alpha)}{\beta}}{(1+r_d)^t} \cdot \left(1 - (1+r_d)^{-t} \right) \right].
\end{aligned}$$

As before, FCF can be expressed as:

$$FCF = (Y_t \cdot p - OPEX_t + DEP_t + PDC_t)(1 - \tau) - CAPEX_t - DECEX_t + DEP_t + PDC_t$$

and $OPEX_t$, $CAPEX_t$, $DECEX_t$, DEP_t , and PDC_t are independent of p and in our case constant. Therefore, it holds:

$$F_{FCF,t}^{-1}(\alpha) = F_{Y,t}^{-1}(\alpha) \cdot p \cdot (1 - \tau) + c$$

where, $c = -(OPEX_t + DEP_t + PDC_t)(1 - \tau) - CAPEX_t - DECEX_t + DEP_t + PDC_t$. We can further rearrange the second addend:

$$\frac{d}{dp} E \left[\sum_{t=0}^{T_{Debt}} DTS_t \right] = \frac{d}{dp} E \left[\sum_{t=0}^{T_{Debt}} \tau \cdot \frac{F_{Y,t}^{-1}(\alpha) \cdot p \cdot (1 - \tau) + c}{\beta} \cdot \left(1 - (1+r_d)^{-t} \right) \right].$$

Since the previous term does not contain any random variable, the expected value of the term is the term itself, it follows:

$$\frac{d}{dp} E \left[\sum_{t=0}^{T_{Debt}} DTS_t \right] = \tau \cdot (1 - \tau) \cdot \sum_{t=0}^{T_{Debt}} \frac{F_{Y,t}^{-1}(\alpha)}{\beta} \cdot \left(1 - (1+r_d)^{-t} \right).$$

Finally, the full expression in Eq. 18 is:

$$\begin{aligned}
\frac{dE(APV)}{dp} &= \frac{d}{dp} E \left[\sum_{t=0}^T uAPV_t \right] + \frac{d}{dp} E \left[\sum_{t=0}^{T_{Debt}} DTS_t \right] \\
&= (1 - \tau) \cdot \sum_{t=0}^T \frac{E(Y_t)}{(1+r_e)^t} + \tau \cdot (1 - \tau) \cdot \sum_{t=0}^{T_{Debt}} \frac{F_{Y,t}^{-1}(\alpha)}{\beta} \cdot \left(1 - (1+r_d)^{-t} \right).
\end{aligned}$$

Acknowledgements

We gratefully acknowledge the financial support of the European Commission (research project IRPWIND, funded from the European Union’s Seventh Framework Programme for research, technological development and demonstration under grant agreement number 609795) that enabled this work.

This work was supported by the compute cluster, which is funded by Leibniz Universität Hannover, the Lower Saxony Ministry of Science and Culture (MWK) and the German Research Association (DFG).

References

- [1] J. K. Kaldellis, D. Apostolou, Life cycle energy and carbon footprint of offshore wind energy. comparison with onshore counterpart, *Renewable Energy* 108 (2017) 72–84.
- [2] C. Brown, R. Poudineh, B. Foley, Achieving a cost-competitive offshore wind power industry: What is the most effective policy framework?, Tech. rep., Oxford Institute for Energy Studies (2015).
- [3] Energy Information Administration, Levelized cost and levelized avoided cost of new generation resources in the annual energy outlook 2017, Tech. rep., U.S. Energy Information Administration (EIA) (2017).
- [4] A. Mbistrova, A. Nghiem, The value of hedging - new approaches to managing wind energy resource risk, Tech. rep., Wind Europe (2017).
- [5] Prognos AG and Fichtner, Kostensenkungspotenziale der Offshore-Windenergie in Deutschland, Tech. rep., Stiftung Offshore-Windenergie (2013).
- [6] Y. S. Lee, B. L. Choi, J. H. Lee, S. Y. Kim, S. Han, Reliability-based design optimization of monopile transition piece for offshore wind turbine system, *Renewable Energy* 71 (2014) 729–741.
- [7] D. Kallehave, B. W. Byrne, C. L. Thilsted, K. K. Mikkelsen, Optimization of monopiles for offshore wind turbines, *Philosophical Transactions of the Royal Society* 373 (2015) 20140100.
- [8] J. Häfele, R. Rolfes, Approaching the ideal design of jacket substructures for offshore wind turbines with a particle swarm optimization algorithm, in: ISOPE Conference, Rhodes, Greece, 2016, pp. 156–163.
- [9] J. Oest, R. Sørensen, L. C. T. Overgaard, E. Lund, Structural optimization with fatigue and ultimate limit constraints of jacket structures for large offshore wind turbines, *Structural and Multidisciplinary Optimization* 55 (3) (2017) 779–793.
- [10] M. Muskulus, S. Schafhirt, Design optimization of wind turbine support structures - a review, *Journal Ocean Wind Energy* 1 (1) (2014) 12–22.
- [11] M. Maness, B. Maples, A. Smith, Nrel offshore balance-of-system model, Tech. rep., National Renewable Energy Laboratory (2017).
- [12] J. Farkas, K. Jármai, Optimum design of steel structures, Springer, Heidelberg, 2013.
- [13] L. Ziegler, M. Rhomberg, M. Muskulus, Optimization of monopiles with genetic algorithms: How does steel mass increase if offshore wind monopiles are designed for a longer service life?, *Journal of Physics: Conference Series* 1104 (2018) 012014.
- [14] O. Salo, S. Syri, What economic support is needed for arctic offshore wind power?, *Renewable and Sustainable Energy Reviews* 31 (2014) 343 – 352.
- [15] N. Ederer, The right size matters: Investigating the offshore wind turbine market equilibrium, *Energy* 68 (2014) 910 – 921.
- [16] D. E. Gernaat, D. P. V. Vuuren, J. V. Vliet, P. Sullivan, D. J. Arent, Global long-term cost dynamics of offshore wind electricity generation, *Energy* 76 (2014) 663 – 672.
- [17] H. L. Raadal, B. I. Vold, A. Myhr, T. A. Nygaard, GHG emissions and energy performance of offshore wind power, *Renewable Energy* 66 (2014) 314 – 324.
- [18] S. Afanasyeva, J. Saari, M. Kalkofen, J. Partanen, O. Pyrhönen, Technical, economic and uncertainty modelling of a wind farm project, *Energy Conversion and Management* 107 (2016) 22 – 33, special Issue on Efficiency, Cost, Optimisation, Simulation and Environmental Impact of Energy Systems (ECOS)-2014.
- [19] M. Batchelor, Feasibility of offshore wind in australia, Ph.D. thesis, Murdoch University (2012).
- [20] T. Rubert, D. McMillan, P. Niewczas, A decision support tool to assist with lifetime extension of wind turbines, *Renewable Energy* 120 (2018) 423 – 433.
- [21] Wind turbines – Part 3: Design requirements for offshore wind turbines. IEC-61400-3 (2009).
- [22] J. Jonkman, The new modularization framework for the FAST wind turbine CAE tool, in: 51st AIAA Aerospace Sciences Meeting, including the New Horizons Forum and Aerospace Exposition, no. NREL/CP-5000-57228, Dallas, United States, 2013.
- [23] J. Jonkman, S. Butterfield, W. Musial, G. Scott, Definition of a 5-MW reference wind turbine for offshore system development, Tech. rep., National Renewable Energy Lab (2009).
- [24] C. Bak, F. Zahle, R. Bitsche, T. Kim, A. Yde, L. C. Henriksen, M. H. Hansen, J. P. A. A. Blasques, M. Gaunaa, A. Natarajan, The dtu 10-mw reference wind turbine, in: Danish Wind Power Research, 2013.
- [25] J. M. Jonkman, W. Musial, Offshore code comparison collaboration (OC3) for IEA task 23 offshore wind technology and deployment, Technical Report NREL/TP-5000-48191, National Renewable Energy Laboratory, Golden, CO (2010).
- [26] C. Hübler, C. G. Gebhardt, R. Rolfes, Development of a comprehensive database of scattering environmental conditions and simulation constraints for offshore wind turbines, *Wind Energy Science* 2 (2017) 491–505.
- [27] J. Jonkman, L. Kilcher, Turbsim user’s guide: Version 1.06.00, Tech. rep., National Renewable Energy Laboratory (2012).

- 489 [28] C. Hübler, C. G. Gebhardt, R. Rolfes, Methodologies for fatigue assessment of offshore wind turbines considering scattering
490 environmental conditions and the uncertainty due to finite sampling, *Wind Energy* 21 (11) (2018) 1092–1105.
- 491 [29] D. Zwick, M. Muskulus, The simulation error caused by input loading variability in offshore wind turbine structural
492 analysis, *Wind Energy* 18 (8) (2015) 1421–1432.
- 493 [30] Eurocode 3: Design of steel structures - part 1-9: Fatigue. EN 1993-1-9 (2010).
- 494 [31] C. Bjerkseter, A. Ågotnes, Levelised costs of energy for offshore floating wind turbine concepts, Master's thesis, Norwegian
495 University of Life Science (2013).
- 496 [32] W. de Vries, N. Vemula, P. Passon, T. Fischer, D. Kaufer, D. Matha, B. Schmidt, F. Vorpahl, Final report WP 4.2:
497 Support structure concepts for deep water sites: Deliverable d4.2.8, Tech. rep., Delft University of Technology (2011).
- 498 [33] E. de Vries, Foundations built on corrosion protection, *Windpower offshore*, 30 September 2014.
- 499 [34] J.-H. Piel, J. F. Hamann, A. Koukal, M. H. Breitner, Promoting the system integration of renewable energies: Toward a
500 decision support system for incentivizing spatially diversified deployment, *Journal of Management Information Systems*
501 34 (4) (2017) 994–1022.
- 502 [35] B. Reimers, M. Kaltschmitt, Kostenentwicklung der Offshore-Windstromerzeugung - Analyse mithilfe der Erfahrungskur-
503 ventheorie, *Zeitschrift für Energiewirtschaft* 38 (4) (2014) 217–234.
- 504 [36] Bloomberg New Energy Finance, *New energy outlook 2016*, Tech. rep. (2017).
- 505 [37] Global Wind Energy Council, *Global wind report 2016 – annual market update*, Tech. rep. (2017).
- 506 [38] B. Steffen, The importance of project finance for renewable energy projects, *Energy Economics* 69 (2018) 280–294.
- 507 [39] L. Lang, E. Ofek, R. Stulz, Leverage, investment, and firm growth, *Journal of financial Economics* 40 (1) (1996) 3–29.
- 508 [40] C. McInerney, D. W. Bunn, Optimal over installation of wind generation facilities, *Energy Economics* 61 (2017) 87–96.
- 509 [41] F. S. Mishkin, *The economics of money, banking, and financial markets*, 11th Edition, Pearson education, 2016.
- 510 [42] S. C. Myers, Interactions of corporate financing and investment decisions—implications for capital budgeting, *The Journal*
511 *of finance* 29 (1) (1974) 1–25.
- 512 [43] J. Sabal, Wacc or apv?, *Journal of Business Valuation and Economic Loss Analysis* 2 (2) (2007) 1–17.
- 513 [44] A. Koukal, M. H. Breitner, Offshore wind energy in emerging countries: A decision support system for the assessment of
514 projects, in: *Proceedings of the 47th HICSS*, Hawaii, United States, 2014, pp. 865–874.
- 515 [45] L. Werner, B. Scholtens, Firm type, feed-in tariff, and wind energy investment in germany: An investigation of decision
516 making factors of energy producers regarding investing in wind energy capacity, *Journal of Industrial Ecology* 21 (2) (2017)
517 402–411.

7 Summary and outlook

7.1 Summary

In this thesis, **a comprehensive probabilistic framework for the time-domain simulation of offshore wind turbines is developed and applied.** In contrast to previous probabilistic simulation approaches, the entire framework is based on time-domain simulations. This is only possible with adequate efficiency due to several innovations with respect to various aspects, e.g. sensitivity analyses or long-term extrapolations.

Primary intention of this work is to enable time-domain probabilistic simulations that model inherent physical uncertainties directly. There are manifold reasons why probabilistic simulations can outperform state-of-the-art deterministic approaches and simplified probabilistic approaches, being based on semi-analytical expressions. Some examples are the capability of calibrating and reducing safety factors, the possibility to compute failure probabilities, the chance to assess present uncertainties, a more realistic and accurate representation of the structure, and a more general validity compared to semi-analytical methods, since no calibration for different load cases is needed. Nevertheless, probabilistic approaches are not commonly used, since comprehensive and efficient methodologies are missing. Therefore, a probabilistic framework - consisting of the following steps - is built up in this work: At first, deterministic models for the structure and possible failures (failure modes) are needed. Second, the aleatory uncertainty in all inputs has to be quantified. Third, a probabilistic design of experiments is required that includes an objective selection of uncertain parameters. Fourth, efficient and accurate long-term extrapolations have to be conducted. Finally, relevant evaluation criteria, for example, the assessment of economic effects, are necessary. To set up such a framework, the aforementioned aspects are thoroughly investigated. Regarding the deterministic modelling, **an effective soil model is developed.** This soil model is incorporated in the state-of-the-art aero-elastic simulation code FAST and enables a more realistic representation of soil-structure interaction for OWTs. To quantify inherent physical uncertainties of some of the most important inputs, **a database containing statistical distributions of various wind and wave parameters is created.** For this purpose, raw data of offshore metocean measurements is analysed. Concerning the probabilistic design of experiments, **a methodology for an accurate but efficient identification of the most important uncertain parameters is developed.** The method is based on the objective, stepwise reduction of probabilistic parameters by means of several sensitivity analyses. Long-term extrapolations for OWT loads are challenging. Therefore, **two new sampling concepts for long-term extrapolations are proposed.** These concepts can help to reduce the uncertainty due to finite sampling. **Both concepts are proved to be generally valid,** since they perform well for different turbines, sites, and measurement and simulation data. Finally, **an innovative, combined techno-economic approach is tested** that is capable of assessing probabilistic economic effects of design changes of OWT substructures, if lifetimes are no longer set to constant values.

The achieved results of this work can be divided into three categories: general outcomes of the probabilistic framework, methodological developments, and application-specific interim findings.

Generally speaking, this thesis provides a framework for probabilistic OWT simulations. The framework can, for example, be used to improve designs using probabilistic methods or to calibrate safety factors for subsequent semi-probabilistic analyses. Nevertheless, it has to be mentioned that no ready-for-use software solution is provided. This means that the framework provides new methods and useful interim findings that can be used for probabilistic analyses, but each analysis still requires an extensive workload and some expert knowledge to combine the proposed steps as needed.

Regarding the methodological developments, the following outcomes can be quoted: The new soil-structure module for FAST is useful for all probabilistic analyses that are conducted with FAST. For other simulation codes, it should be possible to adapt the presented soil model. The stepwise sensitivity analysis is code- and application-independent and can be useful for all kinds of probabilistic analyses - not only for OWTs. However, sensitivity analyses are not essential for probabilistic analyses. Sometimes, it is sufficient to use findings of previous research - like outcomes of the present sensitivity analysis - to select the most important parameters. Sampling concepts for more efficient long-term extrapolations of fatigue loads are not only useful for probabilistic simulations but also for (quasi-)deterministic ones. Due to turbulent wind fields and irregular waves, even deterministic approaches require a relatively high number of simulations that can be reduced using the proposed sampling methods. It is shown that the sampling concepts are code-, structure-, and site-independent. A transfer to other applications needs major adaptations, but should be possible. Finally, on the one hand, the proposed combined techno-economic model is - just like sensitivity analyses - not essential for the framework. On the other hand, this model represents a relatively generally applicable model that can be used for all kinds of economic investigations of OWTs.

Lastly, some OWT-specific interim findings are achieved. These findings can be used directly, but they are hardly transferable to other applications. Distributions for probabilistic wind and wave parameters are now available for future work. This means that it is possible to conduct forthcoming probabilistic analyses without an a priori uncertainty quantification. The most important input parameters are identified and form a well-founded basis for upcoming probabilistic work that does include an own sensitivity analysis. Finally, it is shown that the lifetime of the substructure influences the economic viability of an OWT wind farm project significantly. So, even for deterministic approaches, this result suggests that longer lifetimes could be valuable and that the lifetime should be treated as a design variable that has to be optimised with respect to economic efficiency.

7.2 Limitations and outlook

Although benefits of probabilistic analyses are indisputable, for OWTs, deterministic approaches are still state of the art. Some of the main reasons are high computing times, seemingly unambiguous results, the lack of customised probabilistic methods for OWTs, and missing software solutions. Although this thesis focuses on the development of methods for a probabilistic simulation framework for OWTs and some of the developed methods help to limit the computational effort, a major limitation is that software solutions are not addressed.

This leads to future work that is needed to establish probabilistic analyses as standard approaches. To establish probabilistic approaches in industry, software solutions are needed in the first place. Of course, there are commercial software solutions for probabilistic analyses in general, e.g. *OptiSlang* [46]. However, the incorporation of such commercial probabilistic programmes into wind turbine modelling schemes is definitely not straightforward. Certainly, it is unrealistic that complete probabilistic simulations of wind turbines will be possible with just a few clicks. However, the various steps and methods in the present framework have to be coupled and automated to make the framework easier to use without deeper knowledge of probability theory or a high workload. The next point is that although the proposed concepts already reduce computing times significantly, the computational effort is still not manageable for many applications. Hence, research is required that deals with a more efficient simulation set-up. This could be, for example, the use of meta-models for fatigue calculations or advanced sampling methods (e.g. importance sampling) for the design of experiments. There are still many possibilities to improve probabilistic analyses in such a framework.

Independent of a faster and easier framework, further potential for improvement is that the performance of the present framework is not conclusively assessed. Such an assessment is started in Section 6, but should be continued in future work to demonstrate the real benefits of this probabilistic approach for industry and academia. Running holistic examples for various turbines, sites, etc., would reveal the benefits of probabilistic approaches. Moreover, existing shortcomings can be identified. In this context, it should be noted that previous examples (Section 5.1, 5.2, and 6) are limited to a probabilistic analysis that considers aleatory uncertainties of ECs over the lifetime. Design uncertainties (e.g. manufacturing tolerances or soil conditions) are not taken into account, since they are of secondary importance (cf. Section 4). Nonetheless, they would increase the value of the probabilistic analysis. Other important sources of uncertainty not considered in this work are statistical and model uncertainties. Although model uncertainties are hardly quantifiable, further research should address this important type of uncertainty by applying imprecise probability methods.

The topic “model uncertainty” leads to the next limitation. Regardless of probabilistic considerations, limitations concerning the deterministic “black box” model have to be mentioned. For OWT modelling, the coupled aero-hydro-servo-elastic simulation code FAST is used in this thesis. Although FAST is state of the art and is certified for wind turbine design certifications in industry, it is partly simplified. Many types of non-linearities are not considered, e.g. material and most geometric non-linearities. Hence, the accuracy, especially for wind turbines with growing dimensions that exhibit larger deformations, can be limited. So, future research should also address the question of the influence of the “black box” model. Here, this assessment is only done for the uncertainty reduction in Section 5 by validating the proposed models using measurement data.

Finally, focusing on the probabilistic analysis itself (i.e. not taking into account the complexity due to the coupled modelling in the time domain), there are several aspects that can be improved. In this respect, future work should address topics that are already state of the art, if semi-analytical models are used for the probabilistic analysis. However, these advanced probabilistic approaches, e.g. Bayesian approaches or system reliability, which cannot be applied to time-domain simulations directly, have to be adapted, and are out of the scope of this thesis.

Although individual outlooks for each step of the framework have already been given in the corresponding sections, a brief outlook for some steps is given here too. These outlooks

concentrate on implications on the overall framework. Starting with the uncertainty assessment: Probabilistic analyses get more realistic, if not only aleatory uncertainty but also epistemic uncertainty is taken into account. Second, sensitivity analyses do not have to be part of a probabilistic framework. It is also possible to select important parameters based on previous investigations. However, if sensitivity analyses are included, low computing times are essential. Therefore, for possible future software solutions, it is recommended to use meta-model-based sensitivity analyses. They are less accurate, but can be implemented into an automated framework more easily. Third, further improvements for long-term extrapolations are necessary. Based on achieved results, advancements of sampling concepts can limit computing times. It should be noted that the long-term extrapolation is the most time-critical part of probabilistic analyses. Lastly, although an economic analysis is included in the present framework and yields interesting and valuable results, for an automated framework, it is recommended to decouple economic analysis and probabilistic framework or at least to keep one-way coupling. The reason for this advice is the complexity of economics. For most engineers, it will be complicated or even impossible to assess economic analyses or to judge outcomes. Hence, it is advisable to separate the two analyses, and to run the downstream economic work together with economists using probabilistic results of the structural analysis.

Bibliography

- [1] ABDALLAH, I., NATARAJAN, A., AND SØRENSEN, J. D. Influence of the control system on wind turbine loads during power production in extreme turbulence: Structural reliability. *Renewable Energy* 87 (2016), 464–477.
- [2] ACHMUS, M., KUO, Y. S., AND ABDEL-RAHMAN, K. Behavior of monopile foundations under cyclic lateral load. *Computers and Geotechnics* 36, 5 (2009), 725–735.
- [3] AKAIKE, H. Information theory and an extension of the maximum likelihood principle. In *Proceedings of the 2nd International Symposium on Information Theory* (Budapest, Hungary, 1973).
- [4] ALATI, N., FAILLA, G., AND ARENA, F. Seismic analysis of offshore wind turbines on bottom-fixed support structures. *Philosophical Transactions of the Royal Society of London A* 373, 2035 (2015), 20140086.
- [5] AMAR BOUZID, D. Numerical investigation of large-diameter monopiles in sands: Critical review and evaluation of both API and newly proposed py curves. *International Journal of Geomechanics* 18, 11 (2018), 04018141.
- [6] AMERICAN PETROLEUM INSTITUTE. Recommended practice for planning, designing and constructing fixed offshore platforms - Working stress design. Recommended practice 2A-WSD, 2002.
- [7] ARANY, L., BHATTACHARYA, S., HOGAN, S. J., AND MACDONALD, J. Dynamic soil-structure interaction issues of offshore wind turbines. In *Proceedings of the 9th international conference on structural dynamics* (Porto, Portugal, 2014).
- [8] AUGUSTI, G., BARATTA, A., AND CASCIATI, F. *Probabilistic methods in structural engineering*. Chapman and Hall Ltd, London, UK, and New York, USA, 1984.
- [9] BACHAROUDIS, K. C., LEKOU, D. J., PHILIPPIDIS, T. P., AND RIO, P. Structural reliability analysis of rotor blades in ultimate loading. In *Proceedings of the European Wind Energy Conference and Exhibition* (Brussels, Belgium, 2011).
- [10] BAECHER, G., AND CHRISTIAN, J. B. *Reliability and statistics in geotechnical engineering*. John Wiley & Sons, London, UK, and New York, USA, 2003.
- [11] BARLTROP, N. D. P., AND ADAMS, A. J. *Dynamics of fixed marine structures*. Butterworth Heinemann Ltd, Oxford, UK, 1991.
- [12] BEER, M., FERSON, S., AND KREINOVICH, V. Imprecise probabilities in engineering analyses. *Mechanical systems and signal processing* 37, 1-2 (2013), 4–29.
- [13] BEUCKELAERS, W. Fatigue life calculation of monopiles for offshore wind turbines using a kinematic hardening soil model. *Ground Engineering* (June 2015), 26–29.
- [14] BIENEN, B., AND CASSIDY, M. J. Advances in the three-dimensional fluid-structure-soil interaction analysis of offshore jack-up structures. *Marine Structures* 19, 2-3 (2006), 110–140.
- [15] BIERBOOMS, W. A. A. M. Determination of wind and wave design conditions based

- on the NEXT database. In *Proceedings of the Offshore Wind Energy-Special Topic Conference* (Brussels, Belgium, 2001).
- [16] BÖKER, C. *Load simulation and local dynamics of support structures for offshore wind turbines*. PhD thesis, Leibniz-Universität Hannover, Institut für Stahlbau, Shaker-Verlag: 26, Germany, 2010.
- [17] BOSSANYI, E. A. GH Bladed - Version 3.51. Tech. Rep. 282/BR/010, Garrad Hassan and Partners Limited, 2003.
- [18] BOX, G. E., AND DRAPER, N. R. *Empirical model-building and response surfaces*. Wiley, New York, USA, 1987.
- [19] BREIMAN, L. Better subset regression using the nonnegative garrote. *Technometrics* 37, 4 (1995), 373–384.
- [20] BUCHER, C. G., AND BOURGUND, U. A fast and efficient response surface approach for structural reliability problems. *Structural safety* 7, 1 (1990), 57–66.
- [21] BUTTERFIELD, S., MUSIAL, W., AND SCOTT, G. Definition of a 5-MW reference wind turbine for offshore system development. Tech. Rep. TP-500-38060, National Renewable Energy Laboratory (NREL), Golden, USA, 2009.
- [22] CABONI, M., MINISCI, E., AND RICCARDI, A. Aerodynamic design optimization of wind turbine airfoils under aleatory and epistemic uncertainty. *Journal of Physics: Conference Series* 1037 (2018), 042011.
- [23] CARSWELL, W., ARWADE, S. R., DE GROOT, D. J., AND LACKNER, M. A. Soil-structure reliability of offshore wind turbine monopile foundations. *Wind Energy* 18, 3 (2015), 483–498.
- [24] CARSWELL, W., ARWADE, S. R., MYERS, A. T., AND HAJJAR, J. F. Reliability analysis of monopile offshore wind turbine support structures. In *Safety, Reliability, Risk and Life-Cycle Performance of Structures and Infrastructures* (New York, USA, 2014).
- [25] CHENG, P. W. *A reliability based design methodology for extreme responses of offshore wind turbines*. PhD thesis, DUWIND Delft University Wind Energy Research Institute, ISBN 90-79468-08-7, Netherlands, 2002.
- [26] CHIAN, C. Y., ZHAO, Y. Q., LIN, T. Y., NELSON, B., AND HUANG, H. H. Comparative study of time-domain fatigue assessments for an offshore wind turbine jacket substructure by using conventional grid-based and monte carlo sampling methods. *Energies* 11 (2018), 3112.
- [27] CHOE, Y., BYON, E., AND CHEN, N. Importance sampling for reliability evaluation with stochastic simulation models. *Technometrics* 57, 3 (2015), 351–361.
- [28] CHOE, Y., PAN, Q., AND BYON, E. Computationally efficient uncertainty minimization in wind turbine extreme load assessments. *Journal of Solar Energy Engineering* 138, 4 (2016), 041012.
- [29] CORNELL, C. A. Bounds on the reliability of structural systems. *Journal of the Structural Division* 93, 1 (1967), 171–200.
- [30] CRAIG JR., R. R., AND BAMPTON, M. C. C. Coupling of substructures for dynamic analyses. *AIAA Journal* 6, 7 (1968), 1313–1319.
- [31] DAMGAARD, M., ANDERSEN, L. V., AND IBSEN, L. B. Dynamic response sensitivity

- of an offshore wind turbine for varying subsoil conditions. *Ocean Engineering* 101 (2015), 227–234.
- [32] DAMGAARD, M., BAYAT, M., ANDERSEN, L. V., AND IBSEN, L. B. Assessment of the dynamic behaviour of saturated soil subjected to cyclic loading from offshore monopile wind turbine foundations. *Computers and Geotechnics* 61 (2014), 116–126.
- [33] DE VRIES, P. G. *Sampling Theory for Forest Inventory: A Teach-Yourself Course*. Springer-Verlag, Berlin and Heidelberg, Germany, 1986.
- [34] DEGASPERI, A., AND GILMORE, S. Sensitivity analysis of stochastic models of bistable biochemical reactions. In *International School on Formal Methods for the Design of Computer, Communication and Software Systems* (Berlin, Germany, 2008).
- [35] DENNY, M. Introduction to importance sampling in rare-event simulations. *European Journal of Physics* 22, 4 (2001), 403–411.
- [36] DET NORSKE VERITAS. Statistical representation of soil data. Recommended practice DNV-RP-C207, 2012.
- [37] DET NORSKE VERITAS. Design of offshore wind turbine structures. Offshore standard DNV-OS-J101, 2014.
- [38] DET NORSKE VERITAS - GERMANISCHER LLOYD. Fatigue design of offshore steel structures. Recommended practice DNVGL-RP-C203, 2014.
- [39] DET NORSKE VERITAS - GERMANISCHER LLOYD. Lifetime extension of wind turbines. Standard DNVGL-ST-0262, 2016.
- [40] DET NORSKE VERITAS - GERMANISCHER LLOYD. Floating wind turbine structures. Standard DNVGL-ST-0126, 2018.
- [41] DET NORSKE VERITAS - GERMANISCHER LLOYD. Support structures for wind turbines. Standard DNVGL-ST-0119, 2018.
- [42] DEUTSCHES INSTITUT FÜR NORMUNG. Baugrund - Sicherheitsnachweise im Erd und Grundbau - Ergänzende Regelungen zu DIN EN 1997-1. International standard DIN EN 1997-1, 2010.
- [43] DEUTSCHES INSTITUT FÜR NORMUNG. Eurocode 0: Grundlagen der Tragwerksplanung. International standard DIN EN 1990, 2010.
- [44] DOWNING, S. D., AND SOCIE, D. F. Simple rainflow counting algorithms. *International journal of fatigue* 4, 1 (1982), 31–40.
- [45] DUBOIS, J., THIEKEN, K., TERCEROS, M., SCHAUMANN, P., AND ACHMUS, M. Advanced incorporation of soil-structure interaction into integrated load simulation. In *Proceedings of the 26th International Ocean and Polar Engineering Conference* (Rhodes, Greece, 2016).
- [46] DYNARDO GMBH. Optislang - the optimizing structural language: Sensitivity analysis, multidisciplinary optimization, robustness evaluation, reliability analysis and robust design optimization. Tech. rep., Dynamic Software and Engineering GmbH (dynardo), Weimar, Germany, 2011.
- [47] ERNST, B., AND SEUME, J. R. Investigation of site-specific wind field parameters and their effect on loads of offshore wind turbines. *Energies* 5, 10 (2012), 3835–3855.
- [48] EUROPEAN COMMITTEE FOR STANDARDIZATION. Eurocode 3: Design of steel structures part 1-9. International standard EN 1993-1-9, 2010.

- [49] FARKAS, J., AND JÁRMAI, K. *Optimum design of steel structures*. Springer-Verlag, Heidelberg, Germany, 2013.
- [50] FIESSLER, B., RACKWITZ, R., AND NEUMANN, H. J. Quadratic limit states in structural reliability. *Journal of the Engineering Mechanics Division* 105, 4 (1979), 661–676.
- [51] FISCHER, T., DE VRIES, W., AND SCHMIDT, B. Upwind design basis (WP4: Offshore foundations and support structures). Tech. rep., Endowed Chair of Wind Energy (SWE) at the Institute of Aircraft Design Universität Stuttgart, Germany, 2010.
- [52] FRAILE, D., AND MBISTROVA, A. Wind in power 2017 - Annual combined onshore and offshore wind energy statistics. Tech. rep., WindEurope Business Intelligence, 2018.
- [53] GERMANISCHER LLOYD. Guideline for the certification of offshore wind turbines. Guideline, 2012.
- [54] GOODMAN, J. *Mechanics applied to engineering*. Longmans, Green, and Co., London, UK, 1899.
- [55] GRAF, P. A., STEWART, G., LACKNER, M., DYKES, K., AND VEERS, P. High-throughput computation and the applicability of Monte Carlo integration in fatigue load estimation of floating offshore wind turbines. *Wind Energy* 19, 5 (2016), 861–872.
- [56] GUDE, J. Statistisches Jahrbuch Deutschland und Internationales 2017. Tech. rep., Statistisches Bundesamt (Destatis), 2017.
- [57] GUYAN, R. J. Reduction of stiffness and mass matrices. *AIAA Journal* 3, 2 (1965), 380.
- [58] GUZMÁN, R. F., MÜLLER, K., VITA, L., AND CHENG, P. W. Simulation requirements and relevant load conditions in the design of floating offshore wind turbines. In *Proceedings of the ASME 2018, 37th International Conference on Ocean, Offshore and Arctic Engineering* (Madrid, Spain, 2018).
- [59] HÄFELE, J., HÜBLER, C., GEBHARDT, C. G., AND ROLFES, R. An improved two-step soil-structure interaction modeling method for dynamical analyses of offshore wind turbines. *Applied Ocean Research* 55 (2016), 141–150.
- [60] HÄFELE, J., HÜBLER, C., GEBHARDT, C. G., AND ROLFES, R. Reconsidering fatigue limit state load sets for jacket substructures utilizing probability distributions of environmental states. In *Proceedings of the 27th International Ocean and Polar Engineering Conference* (San Francisco, USA, 2017).
- [61] HÄFELE, J., HÜBLER, C., GEBHARDT, C. G., AND ROLFES, R. A comprehensive fatigue load set reduction study for offshore wind turbines with jacket substructures. *Renewable Energy* 118 (2018), 99–112.
- [62] HÄFELE, J., AND ROLFES, R. Approaching the ideal design of jacket substructures for offshore wind turbines with a particle swarm optimization algorithm. In *Proceedings of the 26th International Ocean and Polar Engineering Conference* (Rhodes, Greece, 2016).
- [63] HAID, L., STEWART, G., JONKMAN, J., ROBERTSON, A., LACKNER, M., AND MATHA, D. Simulation-length requirements in the loads analysis of offshore floating wind turbines. In *Proceedings of the 32nd International Conference on Ocean, Offshore*

- and Arctic Engineering* (Nantes, France, 2013).
- [64] HALD, T., MORCH, C., JENSEN, L., BAKMAR, C. L., AND AHLE, K. Revisiting monopile design using py curves. Results from full scale measurements on Horns Rev., In *Proceedings of the European Offshore Wind 2009 Conference* (Stockholm, Sweden, 2009).
- [65] HALTON, J. H. On the efficiency of certain quasi-random sequences of points in evaluating multi-dimensional integrals. *Numerische Mathematik* 2, 1 (1960), 84–90.
- [66] HANNUS, M. Numerical analysis of structural reliability. Tech. rep., Technical Research Centre of Finland, Helsinki, Finland, 1973.
- [67] HANSEN, M. *Zur Auswirkung von Überwachungsmaßnahmen auf die Zuverlässigkeit von Betonbauteilen*. PhD thesis, Leibniz-Universität Hannover, Institut für Massivbau, Fraunhofer-IRB-Verlag: 2, Germany, 2004.
- [68] HANSEN, M., SCHMIDT, B., ERNST, B., SEUME, J., WILMS, M., HILDEBRANDT, A., SCHLURMANN, T., ACHMUS, M., SCHMOOR, K., SCHAUMANN, P., BECHTEL, A., MEYERING, R., KOHLMEIER, M., GRIESSMANN, T., ROLFES, R., LOHAUS, L., WERNER, M., POLL, G., OTTO, S., WEHNER, M., FUCHS, F., AND BRENNER, S. Probabilistic safety assessment of offshore wind turbines - annual report 2010. Tech. rep., Leibniz Universität Hannover, Germany, 2011.
- [69] HANSEN, M., SCHMIDT, B., ERNST, B., SEUME, J., WILMS, M., HILDEBRANDT, A., SCHLURMANN, T., ACHMUS, M., SCHMOOR, K., SCHAUMANN, P., KELMA, S., GORETZKA, J., ROLFES, R., LOHAUS, L., WERNER, M., POLL, G., BÖTTCHER, R., WEHNER, M., FUCHS, F., AND BRENNER, S. Probabilistic safety assessment of offshore wind turbines. Tech. rep., Leibniz Universität Hannover, Germany, 2015.
- [70] HASOFER, A., AND LIND, N. An exact and invariant second-moment code format. *Journal of Engineering Mechanics Division* 100, 1 (1974), 111–121.
- [71] HO, A., AND MBISTROVA, A. The european offshore wind industry - key trends and statistics 2016. Tech. rep., WindEurope Business Intelligence, 2017.
- [72] HOMMA, T., AND SALTELLI, A. Importance measures in global sensitivity analysis of nonlinear models. *Reliability Engineering & System Safety* 52, 1 (1996), 1–17.
- [73] HONG, Y. J., XING, J., AND WANG, J. B. A second-order third-moment method for calculating the reliability of fatigue. *International Journal of Pressure Vessels and Piping* 76, 8 (1999), 567–570.
- [74] HU, W., CHOI, K. K., AND CHO, H. Reliability-based design optimization of wind turbine blades for fatigue life under dynamic wind load uncertainty. *Structural and Multidisciplinary Optimization* 54, 4 (2016), 953–970.
- [75] HÜBLER, C., GEBHARDT, C. G., AND ROLFES, R. Assessment of a standard state-of-the-art ULS design procedure for offshore wind turbine sub-structures. *Journal of Physics: Conference Series* 1104 (2018), 012013.
- [76] HÜBLER, C., HÄFELE, J., EHRMANN, A., AND ROLFES, R. Effective consideration of soil characteristics in time domain simulations of bottom fixed offshore wind turbines. In *Proceedings of the 26th International Ocean and Polar Engineering Conference* (Rhodes, Greece, 2016).
- [77] HÜBLER, C., MÜLLER, F., GEBHARDT, C. G., AND ROLFES, R. Global sensitivity

- analysis of offshore wind turbine substructures. In *Proceedings of the 15th International Probabilistic Workshop* (Dresden, Germany, 2017).
- [78] HÜBLER, C., WEIJTJENS, W., ROLFES, R., AND DEVRIENDT, C. Reliability analysis of fatigue damage extrapolation of wind turbines using offshore strain measurements. *Journal of Physics: Conference Series 1037* (2018), 032035.
- [79] HUCHET, Q., MATTRAND, C., BEAUREPAIRE, P., RELUN, N., AND GAYTON, N. Cost effective strategy using kriging surrogates to compute fatigue at multiple locations of a structure: Application to offshore wind turbine certification. In *Proceedings of the 12th International Fatigue Congress* (Poitiers, France, 2018).
- [80] HUCHET, Q., MATTRAND, C., BEAUREPAIRE, P., RELUN, N., AND GAYTON, N. A kriging based procedure for the certification of wind turbine structures: application to large scale models. In *Proceedings of the 54th European Safety, Reliability & Data Association Seminar* (Nantes, France, 2018).
- [81] HUCHET, Q., MATTRAND, C., BEAUREPAIRE, P., RELUN, N., AND GAYTON, N. AK-DA: An efficient method for the fatigue assessment of wind turbine structures. *Wind Energy* (2019).
- [82] ILAS, A., RALON, P., RODRIGUEZ, A., AND TAYLOR, M. Renewable power generation costs in 2017. Tech. rep., International Renewable Energy Agency (IRENA), Abu Dhabi, United Arab Emirates, 2018.
- [83] INTERNATIONAL ELECTROTECHNICAL COMMISSION. Wind turbines - part 1: Design requirements. International standard IEC 61400-1, 2005.
- [84] INTERNATIONAL ELECTROTECHNICAL COMMISSION. Wind turbines - part 3: Design requirements for offshore wind turbines. International standard IEC 61400-3, 2009.
- [85] INTERNATIONAL ELECTROTECHNICAL COMMISSION. Wind turbines - part 1: Design requirements. International standard IEC 61400-1 (Draft), 2015.
- [86] INTERNATIONAL ORGANIZATION FOR STANDARDIZATION. General principles on reliability for structures. International standard ISO 2394:2015(en), 2015.
- [87] IOOSS, B., AND LEMAÎTRE, P. A review on global sensitivity analysis methods. In *Uncertainty Management in Simulation-Optimization of Complex Systems - Algorithms and Applications* (2015), G. Dellino and C. Meloni, Eds., Springer, New York, USA.
- [88] JACQUES, J., LAVERGNE, C., AND DEVICTOR, N. Sensitivity analysis in presence of model uncertainty and correlated inputs. *Reliability Engineering & System Safety 91*, 10-11 (2006), 1126–1134.
- [89] JANG, Y. S., SITAR, N., AND DER KIUREGHIAN, A. Reliability analysis of contaminant transport in saturated porous media. *Water Resources Research 30*, 8 (1994), 2435–2448.
- [90] JANSEN, M. J. Analysis of variance designs for model output. *Computer Physics Communications 117*, 1 (1999), 35–43.
- [91] JIANG, Z., HU, W., DONG, W., GAO, Z., AND REN, Z. Structural reliability analysis of wind turbines: A review. *Energies 10*, 12 (2017), 2099.
- [92] JOINT COMMITTEE ON STRUCTURAL SAFETY. Probabilistic model code - part 1 - basis of design. Tech. Rep. JCSS-OSTL/DIA/VROU-10-11-2000, Joint Committee on Structural Safety, 2001.

- [93] JONKMAN, J. The new modularization framework for the FAST wind turbine CAE tool. In *Proceedings of the 51st AIAA aerospace sciences meeting, including the new horizonsforum and aerospace exposition* (Dellas, USA, 2013).
- [94] JONKMAN, J. M., AND BUHL JR., M. L. FAST User's Guide. Tech. Rep. EL-500-38230, National Renewable Energy Laboratory (NREL), Golden, USA, 2005.
- [95] JONKMAN, J. M., AND MUSIAL, W. Offshore code comparison collaboration (OC3) for IEA task 23 offshore wind technology and deployment. Tech. Rep. TP-5000-48191, National Renewable Energy Laboratory (NREL), Golden, USA, 2010.
- [96] KALLEHAVE, D., BYRNE, B. W., THILSTED, C. L., AND MIKKELSEN, K. K. Optimization of monopiles for offshore wind turbines. *Philosophical Transactions of the Royal Society of London A: Mathematical, Physical and Engineering Sciences* 373, 2035 (2015), 20140100.
- [97] KALLEHAVE, D., THILSTED, C. L., AND LIINGAARD, M. Modification of the API p-y formulation of initial stiffness of sand. In *Proceedings of the 7th International Conference Offshore Site Investigation and Geotechnics* (London, UK, 2012).
- [98] KARPA, O., AND NAESS, A. Extreme value statistics of wind speed data by the ACER method. *Journal of Wind Engineering and Industrial Aerodynamics* 112 (2013), 1–10.
- [99] KELMA, S., SCHMOOR, K. A., GORETZKA, J., AND HANSEN, M. Sicherheitsaspekte der Tragstruktur von Offshore-Windenergieanlagen. *Bautechnik* 91, 8 (2014), 543–553.
- [100] KIM, D. H., AND LEE, S. G. Reliability analysis of offshore wind turbine support structures under extreme ocean environmental loads. *Renewable Energy* 79 (2015), 161–166.
- [101] KOOLIJMAN, H. J. T., LINDENBURG, C., WINKELAAR, D., AND VAN DER HOOFT, E. L. DOWEC 6 MW Pre-Design: Aero-elastic modeling of the DOWEC 6 MW pre-design in PHATAS. Tech. Rep. F1W2-HJK-01-046/9, Energy Research Center of the Netherlands (ECN), 2003.
- [102] KRIEGESMANN, B. *Probabilistic design of thin-walled fiber composite structures*. PhD thesis, Leibniz-Universität Hannover, Institut für Statik und Dynamik: 15, Germany, 2012.
- [103] LARSEN, G., AND PETERSEN, S. Experimental investigation of ultimate loads. In *Proceedings of the European Wind Energy Conference* (Copenhagen, Denmark, 2001).
- [104] LARSEN, T. J., AND HANSEN, A. M. How 2 HAWC2, the user's manual. Tech. Rep. Risø-R-1597(ver. 3-1)(EN), Technical University of Denmark (DTU), Roskilde, Denmark, 2007.
- [105] LEE, Y. S., CHOI, B. L., LEE, J. H., KIM, S. Y., AND HAN, S. Reliability-based design optimization of monopile transition piece for offshore wind turbine system. *Renewable Energy* 71 (2014), 729–741.
- [106] LEMIEUX, C. *Monte Carlo and quasi-Monte Carlo sampling*. Springer Science & Business Media, New York, USA, 2009.
- [107] LESNY, K., AND WIEMANN, J. Finite-element-modelling of large diameter monopiles for offshore wind energy converters. In *Proceedings of the GeoCongress 2006: Geotechnical Engineering in the Information Technology Age* (Atlanta, USA, 2006).

- [108] LORAUX, C., AND BRÜHWILER, E. The use of long term monitoring data for the extension of the service duration of existing wind turbine support structures. *Journal of Physics: Conference Series* 753 (2016), 072023.
- [109] LOTT, S., AND CHENG, P. W. Load extrapolations based on measurements from an offshore wind turbine at Alpha Ventus. *Journal of Physics: Conference Series* 753, 7 (2016), 072004.
- [110] MADSEN, H., KRENK, S., AND LIND, N. *Methods of structural safety*. Prentice-Hall, New Jersey, USA, 1986.
- [111] MANESS, M., MAPLES, B., AND SMITH, A. NREL offshore balance-of-system model. Tech. Rep. TP-6A20-66874, National Renewable Energy Laboratory (NREL), Golden, USA, 2017.
- [112] MÁRQUEZ-DOMÍNGUEZ, S., AND SØRENSEN, J. D. Fatigue reliability and calibration of fatigue design factors for offshore wind turbines. *Energies* 5, 6 (2012), 1816–1834.
- [113] MARREL, A., IOOSS, B., DA VEIGA, S., AND RIBATET, M. Global sensitivity analysis of stochastic computer models with joint metamodels. *Statistics and Computing* 22, 3 (2012), 833–847.
- [114] MCKAY, M. D., BECKMAN, R. J., AND CONOVER, W. J. A comparison of three methods for selecting values of input variables in the analysis of output from a computer code. *Technometrics* 21, 2 (1979), 239–245.
- [115] MELCHERS, R. E. Importance sampling in structural systems. *Structural Safety* 6, 1 (1989), 3–10.
- [116] MELCHERS, R. E., AND BECK, A. T. *Structural reliability analysis and prediction*, third ed. John Wiley & Sons, New Jersey, USA, 2018.
- [117] METROPOLIS, N., AND ULAM, S. M. The Monte Carlo method. *Journal of the American Statistical Association* 44 (1949), 335–341.
- [118] MILLER, A. *Subset selection in regression*. CRC Press, Boca Raton, USA, 2002.
- [119] MIRZADEH, J., KIMIAEI, M., AND CASSIDY, M. J. Effects of irregular nonlinear ocean waves on the dynamic performance of an example jack-up structure during an extreme event. *Marine Structures* 49 (2016), 148–162.
- [120] MOKHTARI, A., FREY, H. C., AND ZHENG, J. Evaluation and recommendation of sensitivity analysis methods for application to stochastic human exposure and dose simulation models. *Journal of Exposure Science and Environmental Epidemiology* 16, 6 (2006), 491–506.
- [121] MONÉ, C., HAND, M., BOLINGER, M., RAND, J., HEIMILLER, D., AND HO, J. 2015 cost of wind energy review. Tech. Rep. TP-6A20-66861, National Renewable Energy Laboratory (NREL), Golden, USA, 2017.
- [122] MORATÓ, A., SRIRAMULA, S., AND KRISHNAN, N. Reliability analysis of offshore wind turbine support structures using kriging models. In *Risk, Reliability and Safety: Innovating Theory and Practice: Proceedings of ESREL 2016* (Glasgow, UK, 2016).
- [123] MORGAN, E. C., LACKNER, M., VOGEL, R. M., AND BAISE, L. G. Probability distributions for offshore wind speeds. *Energy Conversion and Management* 52, 1 (2011), 15–26.
- [124] MORIARTY, P. J., HOLLEY, W. E., AND BUTTERFIELD, S. P. Extrapolation of

- extreme and fatigue loads using probabilistic methods. Tech. Rep. TP-500-34421, National Renewable Energy Lab, Golden, USA, 2004.
- [125] MORRIS, M. D. Factorial sampling plans for preliminary computational experiments. *Technometrics* 33, 2 (1991), 161–174.
- [126] MÜLLER, K., AND CHENG, P. W. Validation of uncertainty in IEC damage calculations based on measurements from Alpha Ventus. *Energy Procedia* 94 (2016), 133–145.
- [127] MÜLLER, K., AND CHENG, P. W. Application of a Monte Carlo procedure for probabilistic fatigue design of floating offshore wind turbines. *Wind Energy Science* 3, 1 (2018), 149–162.
- [128] MÜLLER, K., DAZER, M., AND CHENG, P. Damage assessment of floating offshore wind turbines using response surface modeling. *Energy Procedia* 137 (2017), 119–133.
- [129] MURCHISON, J. M., AND O’NEILL, M. W. Evaluation of py relationships in cohesionless soils. In *Analysis and Design of Pile Foundations - A Symposium of ASCE Convention* (San Francisco, USA, 1984).
- [130] MURCIA, J. P., RÉTHORÉ, P.-E., DIMITROV, N., NATARAJANA, A., AND SØRENSEN, J. D. Uncertainty propagation through an aeroelastic wind turbine model using polynomial surrogates. *Renewable Energy* 119 (2018), 910–922.
- [131] MUSKULUS, M., AND SCHAFHIRT, S. Reliability-based design of wind turbine support structures. In *Proceedings of the Symposium on Reliability of Engineering System* (Hangzhou, China, 2015).
- [132] NAESS, A., AND GAIDAI, O. Monte Carlo methods for estimating the extreme response of dynamical systems. *Journal of Engineering Mechanics* 134, 8 (2008), 628–636.
- [133] NAESS, A., AND GAIDAI, O. Estimation of extreme values from sampled time series. *Structural Safety* 31, 4 (2009), 325–334.
- [134] NAESS, A., AND HAUG, E. Extreme value statistics of wind speed data by the POT and ACER methods. *Journal of Offshore Mechanics and Arctic Engineering* 132, 4 (2010), 041604.
- [135] NAESS, A., LEIRA, B. J., AND BATSEVYCH, O. System reliability analysis by enhanced Monte Carlo simulation. *Structural safety* 31, 5 (2009), 349–355.
- [136] NEGRO, V., LÓPEZ-GUTIÉRREZ, J. S., ESTEBAN, M. D., AND MATUTANO, C. Uncertainties in the design of support structures and foundations for offshore wind turbines. *Renewable Energy* 63 (2014), 125–132.
- [137] NIEŚŁONY, A. Determination of fragments of multiaxial service loading strongly influencing the fatigue of machine components. *Mechanical Systems and Signal Processing* 23, 8 (2009), 2712–2721.
- [138] OEST, J., SØRENSEN, R., OVERGAARD, L. C. T., AND LUND, E. Structural optimization with fatigue and ultimate limit constraints of jacket structures for large offshore wind turbines. *Structural and Multidisciplinary Optimization* 55, 3 (2017), 779–793.
- [139] PAPAIOANNOU, I., BETZ, W., ZWIRGLMAIER, K., AND STRAUB, D. MCMC algorithms for subset simulation. *Probabilistic Engineering Mechanics* 41 (2015), 89–103.

- [140] PASSON, P. Memorandum: derivation and description of the soil-pile-interaction models. Tech. Rep. IEA-Annex XXIII Subtask 2, Endowed Chair of Wind Energy (SWE) at the Universität Stuttgart, Germany, 2006.
- [141] PETERS, D., SHAW, C., GRANT, C., HEIDEMAN, J., AND SZABO, D. Modelling the North Sea through the north european storm study. In *Proceedings of the 25th Offshore Technology Conference* (Houston, USA, 1993).
- [142] PHOON, K.-K. *Reliability-based design in geotechnical engineering: Computations and applications*. Taylor and Francis, New York, USA, 2008.
- [143] PIEL, J.-H., HAMANN, J. F., KOUKAL, A., AND BREITNER, M. H. Promoting the system integration of renewable energies: Toward a decision support system for incentivizing spatially diversified deployment. *Journal of Management Information Systems* 34, 4 (2017), 994–1022.
- [144] POPKO, W., HUHN, M. L., ROBERTSON, A., JONKMAN, J., WENDT, F., MÜLLER, K., KRETSCHMER, M., VORPAHL, F., RUUD HAGEN, T., GALINOS, C., LE DREFF, J., GILBERT, P., AURIAC, B., NAVARRO VILLORA, F., SCHUNEMANN, P., BAYATI, I., BELLOLI, M., OH, S., TOTSUKA, Y., QVIST, J., BACHYNSKI, E., HØEGH SØRUM, S., THOMASSEN, P. E., SHIN, H., VITTORI, F., GALVAN, J., MOLINS, C., BONNET, P., VAN DER ZEE, T., BERGUA, R., WANG, K., FU, P., AND CAI, J. Verification of a numerical model of the offshore wind turbine from the alpha ventus wind farm within oc5 phase iii. In *Proceedings of the 37th International Conference on Ocean, Offshore and Arctic Engineering* (Madrid, Spain, 2018).
- [145] POPKO, W., VORPAHL, F., ZUGA, A., KOHLMEIER, M., JONKMAN, J., ROBERTSON, A., LARSEN, T. J., YDE, A., SÆTERTRØ, K., OKSTAD, K. M., NICHOLS, J., NYGAARD, T. A., GAO, Z., MANOLAS, D., KIM, K., YU, Q., SHI, W., PARK, H., VÁSQUEZ-ROJAS, A., DUBOIS, J., KAUFER, D., THOMASSEN, P., DE RUITER, M. J., VAN DER ZEE, T., PEERINGA, J. M., ZHIWEN, H., AND VON WAADEN, H. Offshore code comparison collaboration continuation (OC4), phase I-results of coupled simulations of an offshore wind turbine with jacket support structure. *Journal of Ocean and Wind Energy* 1, 1 (2014), 1–11.
- [146] RACKWITZ, R. Practical probabilistic approach to design. *Comité Européen du Béton Bulletin d'Information* 112 (1976), 13–71.
- [147] ROBERTSON, A., SETHURAMAN, L., JONKMAN, J., AND QUICK, J. Assessment of wind parameter sensitivity on ultimate and fatigue wind turbine loads. In *Proceedings of the AIAA SciTech Forum - Wind Energy Symposium* (Orlando, USA, 2018).
- [148] ROBERTSON, A. N., WENDT, F., JONKMAN, J. M., POPKO, W., DAGHER, H., GUEYDON, S., QVIST, J., VITTORI, F., AZCONA, J., UZUNOGLU, E., SOARES, C. G., HARRIES, R., YDE, A., GALINOS, C., HERMANS, K., DE VAAL, J. B., BOZONNET, P., BOUY, L., BAYATI, I., BERGUA, R., GALVAN, J., MENDIKOA, I., SANCHEZ, C. B., SHIN, H., OH, S., MOLINS, C., AND DEBRUYNE, Y. OC5 project phase II: validation of global loads of the deepcwind floating semisubmersible wind turbine. *Energy Procedia* 137 (2017), 38–57.
- [149] ROBERTSON, A. N., WENDT, F., JONKMAN, J. M., POPKO, W., STANSBERG, C. T., BACHYNSKI, E. E., BAYATI, I., BEYER, F., DE VAAL, J. B., HARRIES, R., YAMAGUCHI, A., SHIN, H., KIM, B., VAN DER ZEE, T., BOZONNET, P., AGUILO, B., BERGUA, R., QVIST, J., QIJUN, W., CHEN, X., GUERINEL, M., TU, Y., YUTONG,

- H., LI, R., AND BOUY, L. OC5 project phase I: validation of hydrodynamic loading on a fixed cylinder. In *Proceedings of the 25th International Ocean and Polar Engineering Conference* (Kona, USA, 2015).
- [150] ROHRIG, K. Windenergie Report Deutschland 2016. Tech. rep., Fraunhofer-Institut für Windenergie und Energiesystemtechnik (IWES), Kassel, Germany, 2017.
- [151] RONOLD, K. O., WEDEL-HEINEN, J., AND CHRISTENSEN, C. J. Reliability-based fatigue design of wind-turbine rotor blades. *Engineering structures* 21, 12 (1999), 1101–1114.
- [152] RUBINSTEIN, R. Y. *Simulation and the Monte Carlo method*. John Wiley and Sons, New York, USA, 1981.
- [153] SALB, C., GÜL, S., CUNTZ, C., MONSCHAUER, Y., AND BEYSCHLAG, L. Klimaschutz in Zahlen - Fakten, Trends und Impulse deutscher Klimapolitik - Ausgabe 2017. Tech. rep., Bundesministerium für Umwelt, Naturschutz, Bau und Reaktorsicherheit (BMUB), Berlin, Germany, 2017.
- [154] SALO, O., AND SYRI, S. What economic support is needed for arctic offshore wind power? *Renewable and Sustainable Energy Reviews* 31 (2014), 343–352.
- [155] SALTELLI, A., AND ANNONI, P. How to avoid a perfunctory sensitivity analysis. *Environmental Modelling & Software* 25, 12 (2010), 1508–1517.
- [156] SALTELLI, A., ANNONI, P., AZZINI, I., CAMPOLONGO, F., RATTO, M., AND TARANTOLA, S. Variance based sensitivity analysis of model output. Design and estimator for the total sensitivity index. *Computer Physics Communications* 181, 2 (2010), 259–270.
- [157] SALTELLI, A., CHAN, K., AND SCOTT, E. M. *Sensitivity analysis*. John Wiley & Sons., Chichester, UK, 2000.
- [158] SALTELLI, A., RATTO, M., ANDRES, T., CAMPOLONGO, F., CARIBONI, J., GATELLI, D., SAISANA, M., AND TARANTOLA, S. *Global sensitivity analysis: the primer*. John Wiley & Sons., Chichester, UK, 2008.
- [159] SCHEPERS, J. G., HEIJDR, J., FOUSSEKIS, D., ØYE, S., SMITH, R. R., BELESSIS, M., THOMSEN, K., LARSEN, T., KRAAN, I., VISSER, B., CARLEN, I., GANANDER, H., AND DROST, L. Verification of European wind turbine design codes, VEWTD: final report. Tech. Rep. ECN-C-01-055, Netherlands Energy Research Foundation (ECN), Petten, Netherlands, 2002.
- [160] SCHMIDT, B., ERNST, B., WILMS, M., HILDEBRANDT, A., AND HANSEN, M. Messdatenbasierte Empfehlungen von Wind- und Wellenparametern für die Auslegung von Offshore-Windenergieanlagen. *Bautechnik* 91, 8 (2014), 533–542.
- [161] SCHMIDT, B., AND HANSEN, M. Analyse mehrjähriger Messzeitreihen zur Ermittlung designrelevanter Lastparameter für Offshore-Windenergieanlagen. In *Proceedings of the DVW-Seminar “Zeitabhängige Messgrößen”* (Hannover, Germany, 2014).
- [162] SCHMIDT, B., HANSEN, M., AND MARX, S. Directional dependence of extreme load parameters for offshore wind turbines. In *Proceedings of the 25th International Offshore and Polar Engineering Conference* (Kona, USA, 2015).
- [163] SCHMIDT, B., MARX, S., AND HANSEN, M. Measurement based investigations of design load parameters for offshore wind turbines. In *Proceedings of the International*

- Wind Engineering Conference* (Hannover, Germany, 2014).
- [164] SCHMOOR, K., AND ACHMUS, M. On the influence of the variability of soil parameters on the behaviour of laterally loaded piles in sand. In *Proceedings of the 9th International Probabilistic Workshop* (Braunschweig, Germany, 2011).
- [165] SCHMOOR, K. A., ACHMUS, M., FOGLIA, A., AND WEFER, M. Reliability of design approaches for axially loaded offshore piles and its consequences with respect to the north sea. *Journal of Rock Mechanics and Geotechnical Engineering* (2018).
- [166] SCHWARZ, G. Estimating the dimension of a model. *The annals of statistics* 6, 2 (1978), 461–464.
- [167] SETT, K., AND JEREMÍC, B. Forward and backward probabilistic simulations in geotechnical engineering. *Contemporary Topics in In-Situ Testing, Analysis and Reliability of Foundations. Geotechnical Special Publication 186* (2009), 332–339.
- [168] SHEIKHOLESAMI, R., AND RAZAVI, S. Progressive latin hypercube sampling: An efficient approach for robust sampling-based analysis of environmental models. *Environmental Modelling & Software* 93 (2017), 109–126.
- [169] SOBOL', I. Sensitivity analysis for non-linear mathematical models. *Mathematical Modelling and Computational Experiment* 1, 4 (1993), 407–414.
- [170] SOBOL', I. M. On the distribution of points in a cube and the approximate evaluation of integrals. *USSR Computational Mathematics and Mathematical Physics* 7 (1967), 86–112.
- [171] SOBOL', I. M., ASOTSKY, D., KREININ, A., AND KUCHERENKO, S. Construction and comparison of high-dimensional Sobol' generators. *Wilmott* 2011, 56 (2011), 64–79.
- [172] SONG, H., DAMIANI, R., ROBERTSON, A., AND JONKMAN, J. A new structural-dynamics module for offshore multimember substructures within the wind turbine computer-aided engineering tool FAST. In *Proceedings of the 23rd International Ocean and Polar Engineering Conference* (Anchorage, USA, 2013).
- [173] SØRENSEN, J. D. Notes in structural reliability theory and risk analysis. Tech. rep., Aalborg University, Aalborg, Denmark, 2004.
- [174] SØRENSEN, J. D. Reliability assessment of wind turbines. In *Proceedings of the 12th International Conference on Applications of Statistics and Probability in Civil Engineering* (Vancouver, Canada, 2015).
- [175] SØRENSEN, J. D. Reliability analysis and risk-based methods for planning of operation & maintenance of offshore wind turbines. In *Proceedings of the 36th International Conference on Ocean, Offshore and Arctic Engineering* (Trondheim, Norway, 2017).
- [176] SØRENSEN, J. D., FRANDBSEN, S., AND TARP-JOHANSEN, N. J. Effective turbulence models and fatigue reliability in wind farms. *Probabilistic Engineering Mechanics* 23, 4 (2008), 531–538.
- [177] SØRENSEN, J. D., AND TARP-JOHANSEN, N. J. Reliability-based optimization and optimal reliability level of offshore wind turbines. *International Journal of Offshore and Polar Engineering* 15, 2 (2005).
- [178] SØRENSEN, J. D., AND TOFT, H. S. Probabilistic design of wind turbines. *Energies* 3, 2 (2010), 241–257.
- [179] SØRENSEN, J. D., AND TOFT, H. S. Safety Factors - IEC 61400-1 ed. 4 - background

- document. Tech. Rep. E-Report-0066, Technical University of Denmark (DTU), Copenhagen, Denmark, 2014.
- [180] SØRENSEN, S. *Soil-structure interaction for non-slender, large-diameter offshore monopiles*. PhD thesis, Aalborg University, Department of Civil Engineering: 37, Denmark, 2012.
- [181] SØRENSEN, S. P. H., IBSEN, L. B., AND AUGUSTESEN, A. H. Effects of diameter on initial stiffness of p-y curves for large-diameter piles in sand. In *Numerical Methods in Geotechnical Engineering: proceedings of the 7th european conference on numerical methods in geotechnical engineering* (Trondheim, Norway, 2010).
- [182] SPAETHE, G. *Die Sicherheit tragender Baukonstruktionen - 2.Auflage*. Springer-Verlag, Vienna, Austria, and New York, USA, 1992.
- [183] STAMATELATOS, M., APOSTOLAKIS, G., DEZFULI, H., EVERLINE, C., GUARRO, S., MOIENI, P., MOSLEH, A., PAULOS, T., AND YOUNGBLOOD, R. Probabilistic risk assessment procedures guide for NASA managers and practitioners. Tech. Rep. SP-2011-3421, National Aeronautics and Space Administration (NASA), Washington, USA, 2002.
- [184] STANDARDS NORWAY (NORSOK). Design of steel structures. Standard N-004, 2004.
- [185] STEWART, G. M. *Design Load Analysis of Two Floating Offshore Wind Turbine Concepts*. PhD thesis, University of Massachusetts - Amherst: 601, USA, 2016.
- [186] STEWART, G. M., ROBERTSON, A., JONKMAN, J., AND LACKNER, M. A. The creation of a comprehensive metocean data set for offshore wind turbine simulations. *Wind Energy* 19, 6 (2016), 1151–1159.
- [187] STIENG, L. E. S., AND MUSKULUS, M. A broad sensitivity analysis of uncertainties for offshore wind turbine support structures. In *Proceedings of the 11th EAWC PhD Seminar on Wind Energy in Europe* (Stuttgart, Germany, 2015).
- [188] STIENG, L. E. S., AND MUSKULUS, M. Reducing the number of load cases for fatigue damage assessment of offshore wind turbine support structures using a simple severity-based sampling method. *Wind Energy Science* 3 (2018), 805–818.
- [189] STIENG, L. E. S., AND MUSKULUS, M. Sampling methods for simplified offshore wind turbine support structures load case assessment. In *Proceedings of the 28th International Ocean and Polar Engineering Conference* (Sapporo, Japan, 2018).
- [190] TARP-JOHANSEN, N., MADSEN, P., AND FRANDBEN, S. Calibration of partial safety factors for extreme loads on wind turbines. In *Proceedings of the European wind energy conference and exhibition* (Brussels, Belgium, 2003).
- [191] TARP-JOHANSEN, N. J. Partial safety factors and characteristic values for combined extreme wind and wave load effects. *Journal of Solar Energy Engineering* 127, 2 (2005), 242–252.
- [192] THIEKEN, K., ACHMUS, M., AND LEMKE, K. A new static p-y-approach for piles with arbitrary dimensions in sand. *Geotechnik* 38, 4 (2015), 267–288.
- [193] THIEKEN, K., ACHMUS, M., LEMKE, K., AND TERCEROS, M. Evaluation of p-y approaches for large-diameter monopiles in sand. *International Journal of Offshore and Polar Engineering* 25, 2 (2015), 134–144.
- [194] TIAN, W. A review of sensitivity analysis methods in building energy analysis.

- Renewable and Sustainable Energy Reviews* 20 (2013), 411–419.
- [195] TIBSHIRANI, R. Regression shrinkage and selection via the LASSO. *Journal of the Royal Statistical Society. Series B (Methodological)* 58, 1 (1996), 267–288.
- [196] TOFT, H. S., NAESS, A., SAHA, N., AND SØRENSEN, J. D. Response load extrapolation for wind turbines during operation based on average conditional exceedance rates. *Wind Energy* 14, 6 (2011), 749–766.
- [197] TOFT, H. S., SØRENSEN, J. D., AND VELDKAMP, D. Assessment of load extrapolation methods for wind turbines. *Journal of Solar Energy Engineering* 133, 2 (2011), 021001.
- [198] TOFT, H. S., AND SØRENSEN, J. D. Reliability-based design of wind turbine blades. *Structural Safety* 33, 6 (2011), 333–342.
- [199] TOFT, H. S., SVENNINGSSEN, L., MOSER, W., SØRENSEN, J. D., AND THØGERSEN, M. L. Assessment of wind turbine structural integrity using response surface methodology. *Engineering Structures* 106 (2016), 471–483.
- [200] VAN BUREN, E., AND MUSKULUS, M. Improving pile foundation models for use in bottom-fixed offshore wind turbine applications. *Energy Procedia* 24 (2012), 363–370.
- [201] VAN BUSSEL, G., AND SCHÖNTAG, C. Operation and maintenance aspects of large offshore windfarms. In *Proceedings of the European Wind Energy Conference* (Dublin, Ireland, 1997).
- [202] VAN EIJK, S. F., BOS, R., AND BIERBOOMS, W. A. The risks of extreme load extrapolation. *Wind Energy Science* 2, 2 (2017), 377–386.
- [203] VELARDE, J., KRAMHØFT, C., AND SØRENSEN, J. D. Global sensitivity analysis of offshore wind turbine foundation fatigue loads. In *Proceedings of the 14th EAWE PhD Seminar on Wind Energy* (Brussel, Belgium, 2018).
- [204] VELDKAMP, D. *Chances in wind energy - A probabilistic approach to wind turbine fatigue design*. PhD thesis, DUWIND Delft University Wind Energy Research Institute, ISBN 90-76468-12-5, Netherlands, 2006.
- [205] VELDKAMP, D. A probabilistic evaluation of wind turbine fatigue design rules. *Wind Energy* 11, 6 (2008), 655–672.
- [206] VEMULA, N. K., DE VRIES, W., FISCHER, T., CORDLE, A., AND SCHMIDT, B. Design solution for the UpWind reference offshore support structure - deliverable D4.2.5 (WP4: Offshore foundations and support structures). Tech. rep., Rambøll Wind Energy, Esbjerg, Denmark, 2010.
- [207] VERMA, A. K., AJIT, S., AND KARANKI, D. R. *Reliability and safety engineering*. Springer-Verlag, London, UK, 2010.
- [208] VIANA, F. A. Things you wanted to know about the latin hypercube design and were afraid to ask. In *Proceedings of the 10th World Congress on Structural and Multidisciplinary Optimization* (Orlando, USA, 2013).
- [209] VOORMEEREN, S. N., VALK, P. L. C., NORTIER, B. P., MOLENAAR, D. P., AND RIXEN, D. J. Accurate and efficient modeling of complex offshore wind turbine support structures using augmented superelements. *Wind Energy* 17, 7 (2014), 1035–1054.
- [210] VORPAHL, F., AND POPKO, W. Description of the load cases and output sensors to be simulated in the OC4 project under IEA wind annex 30. Tech. rep., Fraunhofer Institute for Wind Energy and Energy System Technology (IWES), Bremerhaven,

Germany, 2013.

- [211] VORPAHL, F., POPKO, W., AND KAUFER, D. Description of a basic model of the “UpWind reference jacket” for code comparison in the OC4 project under IEA wind annex 30. Tech. rep., Fraunhofer Institute for Wind Energy and Energy System Technology (IWES), Bremerhaven, Germany, 2011.
- [212] VORPAHL, F., STROBEL, M., JONKMAN, J. M., LARSEN, T. J., PASSON, P., AND NICHOLS, J. Verification of aeroelastic offshore wind turbine design codes under IEA wind task XXIII. *Wind Energy* 17, 4 (2014), 519–547.
- [213] WEI, K., ARWADE, S. R., MYERS, A. T., HALLOWELL, S., HAJJAR, J. F., HINES, E. M., AND PANG, W. Toward performance-based evaluation for offshore wind turbine jacket support structures. *Renewable Energy* 97 (2016), 709–721.
- [214] WINKLER, E. *Die Lehre von der Elasticitaet und Festigkeit*. Verlag H. Dominicus, Prague, Czech Republic, 1867.
- [215] XU, C., AND GERTNER, G. Z. Uncertainty and sensitivity analysis for models with correlated parameters. *Reliability Engineering & System Safety* 93, 10 (2008), 1563–1573.
- [216] ZAAIJER, M., AND VUGTS, J. Sensitivity of dynamics of fixed offshore support structures to foundation and soil properties. In *Proceedings of the European Wind Energy Conference and Exhibition* (Copenhagen, Denmark, 2001).
- [217] ZAAIJER, M. B. Foundation modelling to assess dynamic behaviour of offshore wind turbines. *Applied Ocean Research* 28, 1 (2006), 45–57.
- [218] ZIEGLER, L., RHOMBERG, M., AND MUSKULUS, M. Design optimization with genetic algorithms: How does steel mass increase if offshore wind monopiles are designed for a longer service life? *Journal of Physics: Conference Series* 1104 (2018), 012014.
- [219] ZIEGLER, L., VOORMEEREN, S., SCHAFHIRT, S., AND MUSKULUS, M. Sensitivity of wave fatigue loads on offshore wind turbines under varying site conditions. *Energy Procedia* 80 (2015), 193–200.
- [220] ZWICK, D., AND MUSKULUS, M. The simulation error caused by input loading variability in offshore wind turbine structural analysis. *Wind Energy* 18 (2015), 1421–1432.
- [221] ZWICK, D., AND MUSKULUS, M. Simplified fatigue load assessment in offshore wind turbine structural analysis. *Wind Energy* 19 (2016), 265–278.

Curriculum vitae

Personal details

Name: Clemens Janek Hübler
Date of birth: 27.01.1989
Place of birth: Hannover
Nationality: German

Education

1995-2008: School education (Hannover, Germany)
2005-2006: Year abroad (Cambridge, UK)
2008-2009: Civil service
2009-2012: Bachelor of Science in “Mechanical engineering”, Leibniz Universität Hannover, Germany
2012-2014: Master of Science in “Aeronautics and astronautics”, Technische Universität Berlin, Germany
2014: Master thesis at the “Deutsches Zentrum für Luft- und Raumfahrt” (DLR) - Institute of Flight Systems, Braunschweig, Germany

Scientific career

2017: Research stay at the Vrije Universiteit Brussels, Belgium
since 2014: Research associate at the Institute of Structural Analysis, Leibniz Universität Hannover, Germany

Awards

2010: Scholarship of the “Studienstiftung des deutschen Volkes”
2014: “Dr.-Jürgen-Ulderup” award of the Faculty of Mechanical Engineering (Leibniz Universität Hannover)
2017: Research scholarship, International Office of the Leibniz Universität Hannover (sponsored by the DAAD and the BMBF)
2019: “Leibniz Young Investigator Grant” of the Leibniz Universität Hannover

